Zellwandquellung: Ursachen, Mechanismen und Konsequenzen für das Platzen von Süßkirschen

Von der Naturwissenschaftlichen Fakultät der

Gottfried Wilhelm Leibniz Universität Hannover

zur Erlangung des Grades

Doktorin der Gartenbauwissenschaften (Dr. rer. hort.)

genehmigte Dissertation von

Christine Schumann, M. Sc.

(2024)

Referent: Prof. Dr. agr. Moritz Knoche

Korreferentin: Prof. Dr. rer. hort. Traud Winkelmann

Tag der Promotion: 14. März 2023

Summary

Ripe sweet cherry fruit (*Prunus avium* L.) are susceptible to cracking during and after rainfall. Cracking is the final step in a series of events. According to the 'Zipper model', a localized bursting of cells causes swelling of cell walls. Swelling - in turn – reduces cell-to-cell adhesion thereby weakening the strained fruit skin. This – in turn - results in rupture of the skin and development of macroscopically visible cracks. Little is known about the mechanism of swelling and the factors affecting swelling. The objectives of the present study were to (1) identify the part of the cell wall that fails during formation of a crack, (2) establish methods to quantify cell wall swelling and identify the underlying mechanisms, (3) characterize cell wall swelling during fruit development and identify the cell wall fraction responsible for swelling, and (4) manipulate cell wall swelling using Ca salts. Light microscopy studies of macroscopically cracked fruit surfaces revealed, that cell wall swelling reduced cell-to-cell adhesion and caused cells to separate along their cell walls. When the surface of cracks was stained with monoclonal antibodies against specific polysaccharide epitopes, only LM19 that stains unesterified homogalacturonans strongly bound indicating exposure of pectins on the crack surface. Thus, failure of the pectin middle lamella caused the separation of adjacent cells. *In vivo* experiments on excised epidermal segments and *in vitro* studies using extracted cell walls revealed that swelling is a physical process that is completely reversible. The pressure exerted by the swelling cell wall was low and within the range of turgor values reported for sweet cherry. Swelling increased in the course of fruit development, particularly during early development (stage I and II). The cell wall fraction with the highest swelling ability were the pectins. Within the pectins, the hydrochloric acid-soluble fraction and the sodium hydroxide-soluble fraction were the most susceptible fractions for swelling. Ca^{2+}, like other multivalent cations, was effective in reducing cell wall swelling. It is capable of reversing swelling. The data demonstrated that cell wall swelling results from swelling of the pectin fraction which leads to separation of cells along cell walls in the strained fruit skin. Ca counteracts this process.

Keywords: Cracking, cell wall, pectin, fruit development, calcium, mAB

Zusammenfassung

Reife Süßkirschen (*Prunus avium* L.) sind anfällig für das Platzen während und nach Niederschlägen. Als Ursache des Platzens gilt nach dem „Reißverschlussmodell“ das lokale Versagen von Zellwänden als Auslöser einer Kettenreaktion. Lokales Platzen von Zellen führt zur Quellung von Zellwänden. Die Quellung reduziert die Adhäsion benachbarter Zellen und ermöglicht Rissbildung und -verlängerung in einer gedehnten Fruchthaut. Über das (Quellungs-)verhalten der Zellwand von Süßkirschen ist wenig bekannt. Ziel der Arbeit war es, (1) den Teil der Zellwand zu identifizieren, der ursächlich für das Platzen verantwortlich ist, (2) Methoden zur Quantifizierung der Zellwandquellung zu etablieren, (3) Zellwandquellung im Laufe der Fruchtentwicklung zu bestimmen und die verantwortlichen Zellwandbestandteile zu identifizieren und (4) zu prüfen, ob mit Ca Salzen Zellwandquellung manipuliert werden kann. Lichtmikroskopische Untersuchungen an Makrorissoberflächen zeigten, dass Zellwandquellung die Zelladhäsion verringerte und Zellen entlang der Zellwände versagten. Beim Anfärben der Bruchkanten mit monoklonalen Antikörpern gegen spezifische Polysaccharidepitope zeigte nur LM19 gegen unverestertes Homogalacturonan der Mittellamelle eine starke Bindung. Diese Pektine befanden sich auf der Rissoberfläche und wurden somit als Schwachstellen der gequollenen Zellwand identifiziert. *In vivo* Experimente an Epidermissegmenten und *in vitro* Untersuchungen an extrahierten Zellwänden ergaben, dass es sich bei der Quellung um einen physikalischen, vollständig reversiblen Prozess handelt. Der Quellungsdruck lag im Bereich des Turgors der Zellen. Über die Fruchtentwicklung nahm die Quellungsfähigkeit der Zellwände in Phase I und II zu und blieb danach nahezu konstant. Die hauptsächlich quellende Fraktion waren Pektine, vor allem Salzsäure- und natriumhydroxidlösliche Pektine. Ca^{2+} sowie andere mehrwertige Kationen reduzierten Zellwandquellung. Ca^{2+} konnte die Quellung rückgängig machen. Die Untersuchungen belegen, dass Pektine für die Zellwandquellung und die Trennung benachbarter Zellen in der gedehnten Fruchthaut verantwortlich sind. Ca wirkt diesem Prozess entgegen.

Schlüsselwörter: Platzen, Zellwand, Pektine, Entwicklung, Calcium, mABs

Abkürzungen

2F4	Monoclonal antibody anti-homogalacturonan	Monoklonaler Antikörper gegen Homogalacturonan
Abb	Figure	Abbildung
AIR	Alcohol insoluble residue	Alkoholunlöslicher Rückstand
Al^{3+}	Aluminium ion	Aluminium-Ion
$AlCl_3$	Aluminium chloride	Aluminium III chlorid
AOV	Analysis of variance	Varianzanalyse
$BaCl_2$	Barium chloride	Bariumchlorid
BF	Bright field illumination	Hellfeld-Beleuchtung
Ca	Calcium	Calcium
Ca^{2+}	Calcium ion	Calcium-Ion
$CaCl_2$	Calcium chloride	Calciumchlorid
$Ca(NO_3)_2$	Calcium nitrate	Calciumnitrat
$CaSO_4$	Calcium sulfate	Calciumsulfat
CFW	Calcofluor white	Calcofluorweiß
CL	Cellulose	Zellulose
D	Diameter	Durchmesser
DAFB	Days after full bloom	Tage nach Vollblüte
ΔV	Change of volume	Volumenänderung
ΔV_{5N}	Change of volume at 5 N	Volumenänderung bei 5 N
ΔV_{max}	Maximum swelling	Maximale Volumenzunahme
EGTA	Ethylene glycol-bis(β-aminoethyl ether)-N,N,N′,N′-tetraacetic acid	Ethylenglycol-bis(aminoethylether)-N,N,N',N'-tetraessigsäure
ES	Epidermal skin sections	Epidermissegment / Fruchthautsegment
Fe^{3+}	Ferric ion	Eisen III-Ion
$FeCl_3$	Ferric chlorid	Eisen III chlorid
Fig	Figure	Abbildung
FW_{tissue}	Fresh weight tissue	Frischmasse Gewebe
H^+	Hydrogen ion	Wasserstoff-Ion
h_1	Height 1	Höhe 1
h_2	Height 2	Höhe 2
H_2O	Water	Wasser
HC	Hemicellulose	Hemicellulose
HCl	Hydrogen chloride	Chlorwasserstoff

HEPES	2-[4-(2-Hydroxyethyl)piperazin-1-yl]ethane-1-sulfonic acid	2-(4-(2-Hydroxyethyl)-1-piperazinyl)-ethansulfonsäure
HG	Homogalacturonan	Homogalacturonan
HSP	Hydrogen chloride-soluble pectins	Salzsäurelösliche Pektine
KCl	Potassium chloride	Kaliumchlorid
KOH	Potassium hydroxide	Kaliumhydroxid
LiCl	Lithium chloride	Lithiumchlorid
LM5	Monoclonal antibody anti-galactan	Monoklonaler Antikörper gegen Galactan
LM6	Monoclonal antibody anti-arabinan	Monoklonaler Antikörper gegen Arabinan
LM7	Monoclonal antibody anti-homogalacturonan	Monoklonaler Antikörper gegen Homogalacturonan
LM8	Monoclonal antibody anti-xylogalacturonan	Monoklonaler Antikörper gegen Xylogalacturonan
LM11	Monoclonal antibody anti-xylan/arabinoxylan	Monoklonaler Antikörper gegen Xylan / Arabinoxylan
LM19	Monoclonal antibody anti-homogalacturonan (unesterified)	Monoklonaler Antikörper gegen gering verestertes Homogalacturonan
LM20	Monoclonal antibody anti-homogalacturonan (esterified)	Monoklonaler Antikörper gegen hoch verestertes Homogalacturonan
LM21	Monoclonal antibody anti-mannan	Monoklonaler Antikörper gegen Mannan
LM25	Monoclonal antibody anti-xyloglucan	Monoklonaler Antikörper gegen Xyloglucan
Ln P	Natural logarithm of the applied pressure	Natürlicher Logarithmus des angelegten Drucks
mAB	Monoclonal antibody	Monoklonaler Antikörper
MES	2-(N-morpholino)ethanesulfonic acid	2-(N-Morpholino)ethansulfonsäure
$MgCl_2$	Magnesium chloride	Magnesiumchlorid
n	Number of replicates	Anzahl der Wiederholungen
NaCl	Sodium chloride	Natriumchlorid
Na_2CO_3	Sodium carbonate	Natriumcarbonat
NaOH	Sodium hydroxide	Natriumhydroxid
NH_4	Ammonium	Ammonium
NH_4Cl	Ammonium chloride	Ammoniumchlorid
OHP	Sodium hydroxide-soluble pectins	Natriumhydroxidlösliche Pektine
OXP	Oxalate-soluble pectins	Oxalatlösliche Pektine
P	Pressure	Druck
P_0	Swelling pressure	Quellungsdruck
PBS	phosphate-buffered saline	Phosphatgepufferte Salzlösung

PE	Polyethylene	Polyethylen
PEG	Polyethylene glycol	Polyethylenglykol
pKa	Negative decadic logarithm of the acid constant	Negativer dekadischer Logarithmus der Säurekonstante
PME	Pectin methylesterase	Pektinmethylesterase
$\psi_{\pi 50}$	Osmotic potential at half maximum swelling	Osmotisches Potential bei 50 % Zellwandquellung
r	Coefficient of correlation	Korrelationskoeffizient
r^2	Coefficient of determination	Bestimmtheitsmaß
RGI	Rhamnogalacturonan I	Rhamnogalacturonan I
RGII	Rhamnogalacturonan I	Rhamnogalacturonan II
RH	Relative humidity	Relative Luftfeuchte
SC	Swelling capacity	Quellungsvermögen
SDS	Sodium dodecyl sulfate	Natriumdodecylsulfat
SE	Standard error	Standardfehler
$SrCl_2$	Strontium chloride	Strontiumchlorid
t	Time	Zeit
TP	Total pectin	Gesamtpektin
TRIS-HCl	Tris(hydroxymethyl)methylamin buffer	Tris(hydroxymethyl)aminomethan Puffer
V	Volume	Volumen
v/v	Volume by volume	Volumenanteil
V_{min}	Minimum volume	Minimales Volumen
WHC	Water holding capacity	Wasserhaltevermögen
WRC	Water retention capacity	Wasserrückhaltevermögen
WSP	Water-soluble pectins	Wasserlösliche Pektine

Inhaltsverzeichnis

1 Einleitung

Süßkirschen (*Prunus avium* L.) und andere weiche, fleischige Früchte, wie Weinbeeren (Becker et al., 2012), Tomaten (Matas et al., 2004), Pflaumen (Milad und Shakel, 1992) oder *Ribes*-Beeren (Khanal et al., 2011) sind zum Zeitpunkt der Reife anfällig für das Platzen infolge von Niederschlägen (Christensen, 1996). Auch Tauwasser kann zum Platzen von Früchten führen (Cline et al., 1995). Das Platzen führt weltweit zu großen ökonomischen Verlusten (Christensen, 1996). Auf nassen Fruchtoberflächen entstehen zunächst kleine, mit bloßem Auge nicht sichtbare, mikroskopisch kleine Risse (sog. Mikrorisse) (Knoche und Peschel, 2006). Diese können sich im weiteren Verlauf zu dramatischen, tiefen und makroskopisch sichtbaren Rissen über die gesamte Frucht ausweiten (sog. Makrorisse). Aufgrund langer Fruchtnässedauern ist das Wasser, das in der Stielgrube steht oder als Tropfen am Griffelansatz hängt, besonders problematisch. Geplatzte Früchte sind nicht zu vermarkten. Auch die Qualität makroskopisch nicht geplatzter Früchte ist durch die Bildung von Mikrorissen reduziert. Mikrorisse unterbrechen die Verdunstungsbarriere der Frucht. Die Folge ist übermäßiger Wasserverlust (Beyer et al., 2005; Knoche et al., 2002) bis hin zum Schrumpeln der Früchte (Knoche und Winkler, 2017). Zudem treten durch die Risse vermehrt Infektionen mit Fruchtfäuleerregern auf (Børve et al., 2000). Da bereits durch geringe Anteile geplatzter Früchte eine Ernte unökonomisch wird, verbleiben geplatzte Früchte oft am Baum (Looney, 1985). Die auf dem Baum verbleibenden Fruchtmumien erlauben die Überwinterung der Pathogene und bilden so das Inokulum für die folgende Saison. Bislang mangelt es an Verfahren und Mitteln, das Platzen zu verhindern. Alle derzeit bekannten Süßkirschensorten sind mehr oder weniger platzempfindlich.

Die derzeit sicherste Kulturmaßnahme ist die Überdachung von Obstanlagen, die entweder ab der Blüte (ab Phase I) oder ab der Steinhärtung (ab Phase II) während der frühen Fruchtentwicklung geschlossen wird (Børve und Stensvand, 2003; Cline et al, 1995; Thomidis und Exadaktylou, 2013). Überdachungen sind jedoch teuer. Als weitere Kulturmaßnahme

gegen das Platzen sollen Spritzungen mit Ca-Salzen die Platzfestigkeit der Früchte verbessern. Allerdings sind die Berichte zur Wirkung von Ca-Salzen widersprüchlich und die Wirkung von Spritzapplikationen von Ca-Salzen oft unzureichend (Winkler und Knoche, 2019).

Voraussetzung zur Züchtung neuer platzresistenter Genotypen sowie zur Entwicklung geeigneter Kulturmaßnahmen ist ein besseres Verständnis der Prozesse, die zum Platzen von Kirschen führen. Nach neueren Erkenntnissen spielt die Zellwandquellung dabei eine entscheidende Rolle. Gequollene Zellwände setzen die Zelladhäsion benachbarter Zellen herab und führen zur Rissbildung und Rissverlängerung in der gedehnten Fruchthaut (Brüggenwirth und Knoche, 2016).

Ziel der vorliegenden Arbeit war es, die Rolle der Zellwandquellung und die für die Quellung verantwortlichen Zellwandbestandteile genauer zu untersuchen. Hierfür sollten geeignete Methoden etabliert werden.

2 Hintergrundinformationen

In den letzten Jahrzehnten wurden zahlreiche Reviews zum Platzen von Früchten (u.a. Balbontín et al., 2013; Christensen, 1996; Khadivi-Khub, 2015; Knoche und Winkler, 2017; Sekse, 1995, 1998, 2008; Sekse et al., 2005; Simon, 2006) sowie zum Aufbau von Zellwänden (u.a. Bidhendi und Geitmann, 2016; Brummell, 2006; Caffall und Mohnen, 2009; Cosgrove, 2005; Jarvis, 2011; Jarvis et al., 2003; Mohnen, 2008; Zamil und Geitmann, 2017) veröffentlicht. Die nachfolgende Literaturübersicht erhebt keinen Anspruch auf Vollständigkeit. Sie dient vor allem dem Zweck, Hintergrundinformationen für ein besseres Verständnis der Arbeit zu liefern. Jedes Kapitel der vorliegenden kumulativen Dissertation verfügt über eine eigene Einleitung, in der der aktuelle Stand der Forschung zum jeweiligen Thema dargestellt ist.

2.1 Morphologie und Wachstum von Süßkirschen

Die Frucht der Süßkirsche entwickelt sich nach der Bestäubung zu einer Steinfrucht aus einem einzigen Fruchtblatt, das mit sich selbst verwächst. Die Verwachsungsnaht (engl. suture) ist mit bloßem Auge über die gesamte Fruchtentwicklung von der Stielgrube bis zur Narbe (Griffelansatz) erkennbar (Abb. 1). Die Seite, die der Verwachsungsnaht gegenüberliegt, wird als Backe (engl. cheek) bezeichnet. An beiden Seiten dazwischen befinden sich die Schultern (engl. shoulder). Die äquatoriale Ebene befindet sich horizontal mittig um die Frucht herum. Am oberen Ende haftet der Stiel in der Stielgrube (engl. stem cavity). Am gegenüberliegenden unteren Ende befindet sich die sogenannte Narbe, die dem Griffelansatz entspricht (engl. stylar end mit stylar scar).

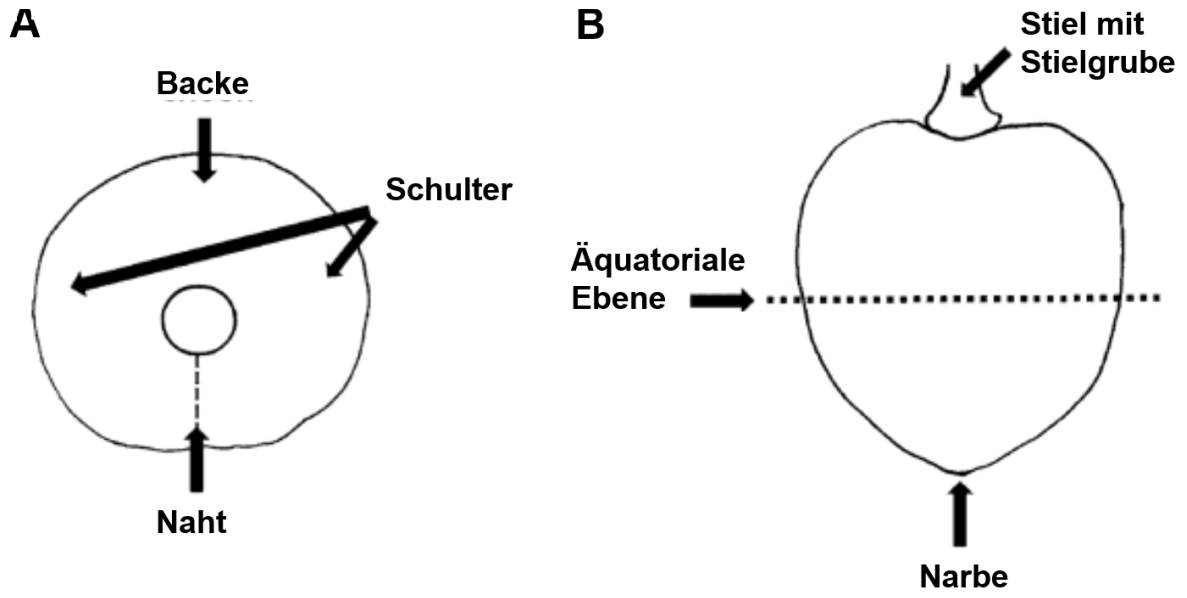

Abb. 1 Schematische Darstellung des Aufbaus einer Kirschfrucht zur Verdeutlichung der Bennenung verschiedener Bereiche der Frucht. A) Aufsicht; B) Vorderansicht Verändert nach Grimm et al. (2017)

Die Süßkirsche gehört zu den Steinfrüchten. Allen Steinfrüchten gemeinsam ist, dass der Samen von einem verholzten Gehäuse (Endokarp), dem Steinkern, umschlossen ist. Dieser wiederum wird von einem fleischigen Mesokarp und einem häutigen Exokarp umgeben. Die beiden letztgenannten Gewebe bestehen aus lebenden Zellen. Das Exokarp (Fruchthaut) besteht von innen nach außen aus den Zellschichten der Hypodermis und der Epidermis, auf welcher ein Polymerfilm, die Kutikula, aufliegt. Bei der Kutikula handelt es sich um einen aus Wachsen und Kutin bestehenden Polymerfilm, der während des Fruchtwachstums der Kirsche stark gedehnt wird (Grimm et al., 2012). Auf reifen Kirschen beträgt die Dicke der Kutikula lediglich 1.1 µm (Peschel und Knoche, 2012). Aufgrund ihrer hydrophoben Eigenschaften und der Ladung ist die Kutikula die entscheidende Barriere im Transport von Wasser und Ionen durch Frucht- und Blattoberflächen. Die Epidermis besteht aus einer einzigen Zellschicht. Diese Zellschicht ist etwa 25 µm dick und wird aus kleinen, kollenchymatischen Zellen mit verdickten Zellwänden gebildet. Darunter schließen sich 2 bis 7 Zellschichten weiterer kollenchymatischer Zellen an, welche die Hypodermis bilden (Glenn und Poovaiah, 1989). Die Zellen der Hypodermis sind deutlich größer als die der Epidermis. Die Zellgröße nimmt mit

zunehmender radialer Entfernung zur Epidermis zu (Brüggenwirth und Knoche, 2016). Die Dicke der Hypodermis beträgt zwischen 50 und 100 µm. Weiter im Inneren schließt sich direkt an die Hypodermis das parenchymatische Mesokarp mit großlumigen, isodiametrischen, dünnwandigen Zellen an (Yamaguchi et al., 2004). Durch das Mesokarp zieht sich das Leitbündelsystem der Frucht. Im Inneren verlaufen die einzelnen Adern vor allem radial. Im äußeren Bereich des Mesokarps hingegen bildet sich ein Netz aus sowohl radial als auch tangential zur Fruchthaut verlaufenden Adern, welche sich allerdings nicht bis in die Fruchthaut hinein erstrecken (Grimm et al., 2017). Die Fruchthaut der reifen Kirsche ist frei von Trichomen oder Haaren und besitzt eine im Vergleich zu den Blattunterseiten nur geringe Anzahl funktionsloser Stomata. Studien mit biaxialen Zugversuchen an epidermalen Segmenten (ES) haben gezeigt, dass die Fruchthaut in der tangentialen Ebene isotrop ist (Brüggenwirth et al., 2014). Die Zellschichten der Fruchthaut bilden das mechanische Rückgrat der Frucht, nicht aber die aufliegende Kutikula oder die darunterliegenden Mesokarpzellen (Brüggenwirth et al., 2014).

Wie für Steinfrüchte typisch, ist das Fruchtwachstum der Süßkirsche durch einen doppeltsigmoiden Verlauf gekennzeichnet. Es wird in drei Phasen unterteilt (Lilleland und Newsome, 1934; Tukey, 1934). In Phase I kommt es zu einer schnellen Zunahme an Frischmasse und Fruchtgröße. Diese wird hauptsächlich durch Zellteilung aller Zellschichten hervorgerufen (Olmstead et al., 2007; Tukey und Young, 1939). In der sich anschließenden Phase II ruht die Zunahme der Fruchtgröße nahezu. Diese Phase wird hauptsächlich durch die Entwicklung des Steins und des Embryos bestimmt. Der Übergang zwischen Phase II und Phase III ist gekennzeichnet durch die Steinhärtung und den Farbumschlag der Frucht von grün über gelb zu rot. In der sich anschließenden Phase III kommt es zu einer rasanten Zunahme der Frischmasse und der Fruchtoberfläche. In dieser Phase geschieht die Zunahme fast ausschließlich durch Zellstreckung. Lediglich in der Fruchthaut kommt es neben der Zellstreckung noch zur Zellteilung (Knoche et al., 2004). Daher unterliegt die Fruchthaut einer immer stärker zunehmenden Dehnung, da die Geschwindigkeit der Zellteilung nicht mit der Zunahme an Fruchtoberfläche mithalten kann (Grimm et al., 2012).

Platzempfindlich werden Kirschen ab Ende Phase III ihrer Entwicklung. Daher konzentrieren sich die Versuche dieser Arbeit auf diese Phase der Fruchtentwicklung.

2.2 Ursachen des Platzens

Lange wurde davon ausgegangen, dass die exzessive Wasseraufnahme entlang eines Wasserpotentialgradienten zwischen Niederschlagswasser und Zellsaft zum Anstieg des Turgors und zur Volumenzunahme der Frucht führt. Überschreitet der Turgor eine kritische Grenze, reißt die Fruchthaut (Ballon-Modell oder critical turgor hypothesis) (Considine und Kriedemann, 1972; Measham et al., 2009). Neuere Erkenntnisse zeigen, dass reife Früchte nur einen sehr geringen Turgor haben und dieser unabhängig von der Wasseraufnahme ist (Knoche et al., 2014; Schumann et al., 2014). Auch platzen lokal benetzte Früchte, obwohl sie Wasser verlieren (Knoche und Peschel, 2006; Winkler et al., 2016). Diese und andere Ergebnisse lassen das Ballon-Modell unrealistisch erscheinen. Stattdessen liefert das sog. Reißverschlussmodell (engl. zipper model) eine plausible Erklärung für das Platzen von Früchten, die im Einklang mit allen bislang veröffentlichten experimentellen Befunden steht (Brüggenwirth und Knoche, 2017; Winkler et al., 2016). Nach dem Reißverschlussmodell ist das Platzen das Ergebnis einer ganzen Abfolge an Ereignissen, bei der lokale Hautphänomene ursächlich sind. Ausgangspunkt ist die Dehnung der Kutikula infolge des rasanten Fruchtwachstums bei gleichzeitig fehlender Synthese von Kutin und Wachs (Knoche et al., 2004; Peschel et al., 2007). Die entstehende Spannung in der gedehnten Kutikula führt zur Bildung von Mikrorissen (Peschel und Knoche, 2005), die durch Nässe verstärkt wird (Knoche und Peschel, 2006). Die so entstandenen Mikrorisse legen Epidermiszellen frei und heben die Barrierefunktion der Kutikula auf. Freies Wasser kann nun ungehindert, örtlich begrenzt auf die Mikrorisse, entlang des osmotischen Potentialgradienten in den Symplasten der Epidermiszellen aufgenommen werden. Mesokarpzellen weisen in der Regel ein signifikant niedrigeres osmotisches Potential auf als Epidermis- und Hypodermiszellen (Grimm und Knoche, 2015). Wasser dringt folglich in den Symplasten der Mesokarpzellen ein. Infolge

der Wasseraufnahme platzen einzelne Mesokarpzellen (Brinkmann et al., 2022; Winkler et al., 2015). Der Zellsaft wird in den Apoplasten entlassen. Das osmotische Potential des Apoplasten sinkt und es kommt zu Plasmolysen in den angrenzenden Epidermiszellen. Im Zellsaft sind nicht nur Kohlenhydrate, sondern auch erhebliche Mengen an organischen Säuren (u.a. 70 mM Äpfelsäure; Herrmann, 2001) gelöst. Kommt diese Äpfelsäure in Kontakt mit den Zellwänden und Membranen, so führt dies zu einer Schwächung der Zellwände, einer erhöhten Membranpermeabilität und damit zu einem weiteren Austritt von Zellinhalt in den Zellwandraum (Winkler et al., 2015). Aufgrund des fehlenden Turgors und der beginnenden Plasmolyse der Hypodermis- und Epidermiszellen beginnen die Zellwände zu quellen (Grimm und Knoche, 2015). Da gequollene Zellwände deutlich schlechtere mechanische Eigenschaften aufweisen (Brüggenwirth und Knoche, 2017), können diese der Dehnung der Fruchthaut nicht mehr standhalten und reißen auf. Es kommt zur Öffnung weiterer Eintrittspforten für Wasser, dem Platzen weiterer Zellen und folglich zur Entstehung des Makrorisses.

2.3 Zellwände von Süßkirschen

Sowohl zur chemischen Zusammensetzung (u.a. Basanta et al., 2013; Basanta et al., 2014; Batisse et al., 1994; Batisse et al., 1996; Fils-Lycaon und Buret, 1990; Kondo und Danjo, 2001; Lahaye et al., 2021) als auch der Morphologie (u.a. Cosgrove, 2022; Zhang et al., 2021) und Rheologie (u.a. Basanta et al., 2013; Cantu et al., 2008; Raghavendra et al., 2004; Redgwell et al., 1997; Shomer et al., 1991; Vetter und Kunzek, 2003) von Zellwänden in Früchten sind in der Vergangenheit bereits einige Studien durchgeführt worden. Vergleichsweise wenig Beachtung fanden hingegen die mechanischen Eigenschaften von Zellwänden der Süßkirsche. Es ist nicht bekannt, ob eine Beziehung besteht zwischen den mechanischen Eigenschaften der Zellwände und dem Platzen der Früchte.

2.3.1 Chemische Zusammensetzung:

Bei der Zellwand handelt es sich um eine extrazelluläre Matrix, welche in wachsenden Zellen hauptsächlich aus den Polysacchariden Zellulose, Hemicellulose und Pektinen sowie Strukturproteinen besteht (Cosgrove, 2005; Cosgrove und Jarvis, 2012; Jarvis, 2011). Die die Zellen umgebende Primärwand besteht dabei aus linearen, kristallinen, 3-5 nm dicken Zellulosefibrillen. Die einzelnen Zelluloseketten einer Fibrille werden aus tausenden ß-(1,4)-verbundenen D-Glukose Einheiten gebildet und sind durch Wasserstoffbrückenbindungen miteinander vernetzt. Die Fibrillen bilden ein Netzwerk mit weiteren komplexen, verzweigten Polysacchariden, die in Hemicellulosen und Pektine unterteilt werden können (Carpita und Gibeaut, 1993; Cosgrove, 1999; Cosgrove, 2000, Cosgrove, 2022). Im Gegensatz zur unverzweigten Zellulose, bestehen Hemicellulosen zwar aus dem gleichen Rückgrat aus Glukosemolekülen, sind jedoch verzweigt durch die Einbindung weiterer Einfachzucker (Cosgrove, 2005). Die weitverbreitetsten Hemicellulosen sind die Xyloglucane sowie Arabinoxylane. Hemicellulosen können durch die Verzweigungen selbst keine Fibrillen ausbilden, jedoch verbinden sie die Zellulosefibrillen miteinander und bilden gemeinsam mit ihnen das lasttragende Gerüst (Cosgrove und Jarvis, 2012). Die Gruppe der Pektine ist eine heterogene Gruppe an sehr komplexen Makromolekülen. Allen Pektinen gemeinsam ist ein großer Anteil an negativ geladenen Galacturonsäureeinheiten, welche dazu führen, dass sie leicht hydratisiert werden können und eine hohe Affinität zu Kationen aufweisen (Cosgrove, 2005). Sie bilden eine füllende Matrix, welche die Zellulosefibrillen voneinander trennt (Cosgrove und Jarvis, 2012). Nach ihrem Aufbau können die Pektine in folgende Gruppen unterteilt werden: Homogalacturonan (HG), Rhamnogalacturonan I (RGI) und Rhamnogalacturonan II (RGII) (Mohnen, 1999). HG besteht ausschließlich aus α-(1,4)-verbundenen Galacturonsäureeinheiten. Die HG Ketten werden im Zuge der Zellentwicklung in einer hochmethylierten Form sekretiert. Erst im Laufe der Zeit werden sie anschließend enzymatisch durch das Enzym Pektinmethylesterase (PME) demethyliert. Es entstehen somit negative Ladungen (Wang et al., 2020). Die tatsächliche Anzahl der freien negativen Ladungen ist pH abhängig. Der pKa-Wert der Galacturonsäureeinheiten liegt bei 3,5 (Kohn

und Kovac, 1978). Bei diesem pH-Wert liegen etwa 50 % der unveresterten Säuregruppen der Galacturonsäureeinheiten dissoziiert vor. Die einzelnen Ketten können in Grad und in Muster der Veresterung variieren (Cosgrove, 2005; Mohnen, 1999). Nichtveresterte Galacturonsäureeinheiten dienen entweder der intramolekularen Vernetzung oder der Bindung mit anderen Zellwandpolymeren. Zusätzlich können unveresterte HG-Polymerketten Vernetzungen mit mehrwertigen Kationen eingehen, vor allem mit Ca^{2+}. Dies geschieht nach dem „egg-box Modell“ (Morris et al., 1982; Powell et al., 1982). Im Gegensatz zum HG hat RGI eine deutlich komplexere Struktur und bildet eine Gruppe heterogener Moleküle (Willats et al., 2001a). Das Rückgrat besteht hier aus sich abwechselnden Rhamnose- und Galacturonsäureeinheiten (McNeil et al., 1984). Im Gegensatz zu HG ist RGI abschnittsweise vor allem an der Rhamnose stark verzweigt („hairy-regions“). In anderen Abschnitten liegen die Galacturonsäureeinheiten unsubstituiert vor („smooth-regions“) (Schols und Voragen, 1996). Die Seitenketten bestehen zu einem Großteil aus den neutralen Zuckern Galactose und Arabinose (McNeil et al., 1984). RGII ist ein vergleichsweise kleines, verzweigtes Molekül mit einer hoch konservierten Struktur. Es besteht auch aus einem HG Rückgrat ist strukturell aber nicht mit den RGI Molekülen vergleichbar. In der Zellwand liegt es oft kovalent mit dem HG verbunden vor (Caffall und Mohnen, 2009; Willats et al., 2001a). Obwohl es nur einen kleinen Anteil der Pektine ausmacht, ist es für die Zellwandfunktion durch seine Fähigkeit mit Bor Dimere zu bilden wichtig (Ishii et al., 1999; Kobayashi et al., 1996; O´Neill et al., 2004). Es wird davon ausgegangen, dass die drei Stoffgruppen der Pektine kovalent miteinander verbunden sein können und ein Netzwerk über die gesamte primäre Zellwand sowie die Mittellamelle bilden (Willats et al., 2001a).

Die Zellwand der Süßkirsche entspricht in ihrer chemischen Zusammensetzung den oben beschriebenen Molekülgruppen. Einzelne Stoffklassen kommen je nach Sorte in höheren oder niedrigeren Anteilen vor (Basanta et al., 2014; Choi et al., 2002). Jedoch sind die Aussagen hinsichtlich einer möglichen Korrelation zur Fruchtfleischfestigkeit widersprüchlich. Auch eine Beziehung der Zusammensetzung der Zellwand zur Platzfestigkeit verschiedener Sorten konnte bisher nicht identifiziert werden.

2.3.2 Morphologie der Zellwand

Strukturell sind die einzelnen Bestandteile der Zellwand sehr gut charakterisiert. Der genaue Aufbau mit seinen intra- und intermolekularen Beziehungen zwischen Zellulosefibrillen und den Matrixpolysacchariden Hemicellulose und Pektin in der dreidimensionalen Matrix, ist nicht abschließend geklärt. Epidermale Zellwände von Zwiebelschuppen dienten in den letzten 20 Jahren als Modellobjekt für Untersuchungen, um ein neues Modell für den Zellwandaufbau zu entwickeln (Zhang et al., 2021). Da es sich bei den Zellwänden in Süßkirschen ebenso um Primärwände von wachsenden Zellen handelt, ist davon auszugehen, dass der Aufbau der Zellwand von Süßkirschen grundsätzlich identisch ist.

Die Primärwand dient der Pflanzenzelle als eine feste, und dennoch dynamische Hülle (Zamil und Geitmann, 2017). Für den prinzipiellen Aufbau der Primärwand ist nach Zhang et al. (2021) davon auszugehen, dass die langen Zellulosefibrillen schichtweise um die Zelle liegen. Dabei weisen die einzelnen Fibrillen eine gemeinsame Richtung mit geringer Streuung auf. Jede folgende Schicht ist im Gegensatz zu der vorherigen Schicht in der Ausrichtung der Fibrillen verschoben. Die Matrixpolysaccharide verbinden sowohl die Fibrillen innerhalb einer Schicht, als auch die Schichten untereinander, wobei die einzelnen Schichten deutlich voneinander abgegrenzt bleiben. Die Eigenschaften der Zellwand ergeben sich aus den physikalischen Wechselwirkungen der drei Wandpolymere.

Zwischen den Primärwänden benachbarter Zellen liegt die Mittellamelle. Sie hat die wichtige Aufgabe, die Integrität des Gewebes durch Verhinderung der Zellseparation oder des Auseinandergleitens der Zellen zu bewahren (Zamil und Geitmann, 2017). Dabei unterscheidet sich die Mittellamelle in ihrer Zusammensetzung und ihrem Aufbau zwischen zwei benachbarten Zellen von solchen Regionen, in denen drei und mehr Zellen aufeinandertreffen. Prinzipiell besteht die Mittellamelle aus HG, RGI und einem geringen Anteil an Proteinen. Das HG ist gering methyliert, was zu einer hohen Ladungsdichte und somit einer

hohen Kationenaffinität führt. Damit unterscheidet sich das HG der Mittellamelle von dem HG der Primärwand, in der es hauptsächlich blockweise demethyliert vorliegt (Willats et al., 2001b).

2.3.3 Mechanische Eigenschaften von Zellwänden

Zellwände geben den Zellen Halt gegen die auf sie einwirkenden Druck- und Zugkräfte. Solche Zugkräfte können unter anderem durch das Wachstum des Gewebes auftreten. Wie unter 2.1. bereits beschrieben, kommt es während des Wachstums der Süßkirsche in Phase III zu einer massiven Dehnung der Fruchthaut (Grimm et al., 2012; Grimm et al., 2013). Diese Dehnung hat sowohl elastische als auch plastische Anteile. Die Dehnung der Kutikula ist noch größer als die der darunterliegenden Zellschichten der Epidermis und der Hypodermis. Für die mechanischen Eigenschaften der Fruchthaut hat die Dehnung der Kutikula jedoch keine Bedeutung (Brüggenwirth et al., 2014; Grimm et al., 2012).

Wie in Kapitel 2.2 beschrieben, setzt durch Mikrorisse ins Gewebe eindringendes Wasser eine Kaskade an Ereignissen in Gang, an dessen Ende die mechanische Destabilisierung gequollener Zellwände steht. Reißen die Zellen folglich auseinander, sind grundsätzlich zwei verschiedene Versagensmuster der Zellwände zu unterscheiden (Knoche und Lang, 2017; Niklas, 1992; Zdunek et al., 2008). 1. Schizogen: Einzelne Zellen lösen sich voneinander ab, so dass jede Zelle intakt bleibt und an der Oberfläche der Bruchkannte Teile der Zellwand exponiert liegen. Sie reißen entlang der Zellwand. In diesem Fall übersteigt die Belastung die Zelladhäsion. 2. Lysigen: Ist die Zelladhäsion dagegen stark, reißen die Zellen durch die Zellwand. Es liegen auf beiden Seiten des Risses Zellfragmente an der Oberfläche. Die Zellen halten so stark aneinander, dass es zum lysigenen Aufbrechen der Zellwand selbst kommt.

In den Materialwissenschaften ist die Untersuchung des Versagensmusters einer Risskante eine gängige Praxis. Jedoch gibt es bisher kaum Untersuchungen an den Rissoberflächen geplatzter Kirschen oder zum Übergang vom Mikroriss zum Makroriss. Brüggenwirth und

Knoche (2017) identifizierten erstmals einen Zusammenhang zwischen Bruchdruck, Versagensmodus und Zellwandquellung in Süßkirschen. Mit biaxialen Zugtests wurde nachgewiesen, dass mit zunehmender Zellwandquellung der Bruchdruck sinkt. Gleichzeitig nimmt der Anteil schizogener Zellwandrisse entlang der Zellwand mit zunehmender Quellung zu, der Anteil lysigener Zellwanddurchrisse dagegen ab.

2.3.4 Quellung von Zellwänden

Im Reißverschlussmodell sind gequollene Zellwände die strukturelle Schwachstelle, die die Bruchkraft zum Aufreißen der Frucht herabsetzen. Bekannt ist, dass an Rissen, die entlang der Zellwand reißen, die Zellwände dicker sind als an Zellen mit Durchrissen (Brüggenwirth und Knoche, 2017). Dabei sind die Zellwände selbst als dynamisches System zu verstehen, welche Wasser aufnehmen und abgeben können und dadurch quellen oder entquellen. Frei vorliegendes Wasser wird dafür in Hohlräume zwischen den Polymerketten absorbiert und es kommt zur Volumenzunahme. Diese Hohlräume entstehen unter anderem durch das Herauslösen von Pektinen aus der Pektinmatrix (Redgwell et al., 1997). Die Fähigkeit zur Wasserabsorption ist ein Zusammenspiel der chemischen, physikalischen und mikrostrukturellen Eigenschaften des gesamten Zellwandnetzwerks (Raghavendra et al., 2004). Zellwandquellung ist ein charakteristisches Phänomen bei der Reifung von weichen Früchten (Redgwell et al., 1997). Das geschieht nicht nur, wie oben beschrieben, durch das Herauslösen der Pektine (Barbier und Thibault, 1982; Batisse et al., 1996), sondern auch durch die Veränderung des Veresterungsgrades der Pektine (Cosgrove, 2022). Dafür werden vor allem die HG-Ketten während der Zellwandsynthese zunächst stark verestert in die Zellwand inkorporiert (Pelloux et al., 2008). Die negativen Ladungen der Galacturonsäureeinheiten liegen zunächst meist methyliert vor. Im Laufe der Entwicklung wird der Veresterungsgrad durch die zellwandgebundene PME reduziert und die negativen Ladungen wieder frei (Mohnen, 2008). Die Ladungsdichte wird größer und somit die Fähigkeit zur Hydratation und die Kationenbindungskapazität erhöht. Zellwandquellung im Allgemeinen wird zwar an

diversen Stellen in der Literatur beschrieben, jedoch ist wenig bekannt über die Quellung der Zellwände in Kirschfrüchten. Auch die entwicklungsabhängigen Veränderungen der Zusammensetzung der Zellwand hinsichtlich ihrer Quellfähigkeit ist in Kirschen nicht untersucht.

2.3.5 Methoden zur Untersuchung der Zellwandquellung

Mikroskopische Untersuchung von Gewebeschnitten

Lichtmikroskopische Aufnahmen von Epidermis Segmenten können Aufschluss über die Dicke der Zellwände zwischen zwei Zellen geben. Mit Hilfe eines Durchlichtmikroskops und einer angeschlossenen Kamera wird dafür der Verbund aus den beiden Primärwänden und der dazwischenliegenden Mittellamelle zweier benachbarter Epidermiszellen fotografiert und anschließend vermessen (Grimm und Knoche, 2015; Schlegel et al., 2018). Auf diese Weise kann der Quellungszustand in Abhängigkeit von verschiedenen Faktoren *in vivo* bestimmt werden. Die Mikroskopie der Bruchkanten von Makrorissen kann der Auswertung des Versagensmusters dienen und es können Rückschlüsse auf die Zelladhäsion in Abhängigkeit von der Zellwandquellung gezogen werden (Brüggenwirth und Knoche, 2017). Zusätzlich zu quantitativen Aussagen über die Zellwandquellung lassen sich mit Hilfe von monoklonalen Antikörpern (mABs) spezifische Zellwandepitope anfärben (Pattathil et al., 2010). Bisher wurden die mABs lediglich an Ultradünnschnitten an fixiertem Gewebe eingesetzt. Untersuchungen an frischen Schnitten und Präparaten sind nicht bekannt, eine angepasste Methode existiert nicht. Auch gibt es keine Aussagen in der Literatur über Zellwandepitope, die an Rissoberflächen von Süßkirschen vorkommen.

Untersuchung extrahierter Zellwände

Andererseits können Zellwände chemisch unter anderem als alkoholunlöslicher Rückstand (alcohol insoluble residue (AIR)) isoliert werden (Sozzi et al., 2002). Das so gewonnene Zellwandmaterial kann seinerseits wiederum in einzelne Polymerfraktionen unterteilt werden. Dafür wird die unterschiedliche Bindungsstärke zwischen den Makromolekülen und die

differentielle Löslichkeit der Fraktionen genutzt. Die Fraktionen werden durch Auswaschen mit verschiedenen Lösungsmitteln gewonnen (Fügel et al., 2004, Fügel et al., 2006). Aus den Mengenverhältnissen der Fraktionen lassen sich Aussagen über die Zusammensetzung der Zellwand ableiten. Sowohl AIR als auch die einzelnen Fraktionen können anschließend *in vitro* Quellungsversuchen unterzogen werden (Basanta et al., 2013). Dafür werden die Kennwerte des Quellungsvermögens (engl. swelling capacity (SC)), Wasserhaltevermögens (engl. water holding capacity (WHC)) und Wasserrückhaltevermögens (engl. water retention capacity (WRC)) ermittelt (Raghavendra et al., 2004). Die Bestimmung dieser Kennwerte ist vor allem in den Lebensmittelwissenschaften ein gängiges und gut beschriebenes Verfahren, um die Hydratationseigenschaften von Polysacchariden zu untersuchen (Larrauri, 1999). Aussagen über die Hydratationseigenschaften von Kirschzellwänden und deren Fraktionen sind bisher rar (Basanta et al., 2013) und nicht in Bezug zur Platzfestigkeit der Früchte gesetzt.

2.4 Schlussfolgerungen

Aus den beschriebenen Sachverhalten können folgende Schlussfolgerungen abgeleitet werden:

(1) Das Reißverschlussmodell liefert eine plausible Erklärung für das Platzen von Früchten, die mit allen bislang veröffentlichten experimentellen Daten im Einklang steht.

(2) Die zellulären Schichten Epidermis und Hypodermis stellen das mechanische Rückgrat der Fruchthaut der Kirsche dar, die mechanischen Eigenschaften der Kutikula spielen keine Rolle.

(3) Gequollene Zellwände sind eng korreliert mit reduzierten Bruchdrücken von Fruchthautsegmenten. Die Häufigkeit schizogener Rissbildung steigt mit zunehmender Zellwandquellung.

(4) Indirekte Befunde sprechen für Pektine als Verursacher gequollener Zellwände.

(5) Detaillierte Arbeiten zur Rolle der Zellwandquellung beim Platzen von Kirschen liegen bislang nicht vor.

2.5 Ziele

Ziele der Untersuchung waren daher:

(1) den Teil der Zellwand, der für das Platzen ursächlich verantwortlich ist, zu identifizieren (Kapitel 3.1),
(2) eine Methode zur Quantifizierung der Zellwandquellung und zur Identifikation von Einflussfaktoren zu entwickeln (Kapitel 3.2),
(3) die Zellwandquellung im Laufe der Fruchtentwicklung zu bestimmen und die für die Quellung verantwortlichen Zellwandbestandteile zu identifizieren (Kapitel 3.3) und
(4) zu bestimmen, ob mithilfe von Ca-Salzen die Zellwandquellung manipuliert werden kann (Kapitel 3.4).

3 Ergebnisse

3.1 Crack initiation and propagation in sweet cherry skin: A simple chain reaction causes the crack to run

Das Original dieses Artikels wurde 2019 in der Zeitschrift „PLoS ONE“ veröffentlicht.

Schumann, C., Winkler, A., Brüggenwirth, M., Köpcke, K. and Knoche, M. (2019): Crack initiation and propagation in sweet cherry skin: A simple chain reaction causes the crack to run. *PLoS ONE*. 14(7): e0219794

DOI: https://doi.org/10.1371/journal.pone.0219794

Beteiligung der Autoren

M. Knoche warb die Drittmittel für das Vorhaben ein. M. Knoche, M. Brüggenwirth, A. Winkler und C. Schumann planten die Experimente. C. Schumann etablierte in Vorversuchen die Methode zur Anfärbung der Makrorisse an ganzen Kirschen mit monoklonalen Antikörpern. M. Brüggenwirth, A. Winkler, K. Köpke und C. Schumann führten die Experimente aus und analysierten die Daten. M. Knoche, A. Winkler, M. Brüggenwirth und C.Schumann schrieben und editierten das Manuskript. M. Knoche, A. Winkler, M. Brüggenwirth und C. Schumann revidierten das Manuskript.

PLOS ONE

RESEARCH ARTICLE

Crack initiation and propagation in sweet cherry skin: A simple chain reaction causes the crack to 'run'

Christine Schumann[☯], Andreas Winkler[☯], Martin Brüggenwirth[☯], Kevin Köpcke[☯], Moritz Knoche[*☯]

Institute for Horticultural Production Systems, Leibniz-University Hannover, Hannover, Germany

☯ These authors contributed equally to this work.
* moritz.knoche@obst.uni-hannover.de

OPEN ACCESS

Citation: Schumann C, Winkler A, Brüggenwirth M, Köpcke K, Knoche M (2019) Crack initiation and propagation in sweet cherry skin: A simple chain reaction causes the crack to 'run'. PLoS ONE 14(7): e0219794. https://doi.org/10.1371/journal.pone.0219794

Editor: Hernâni Gerós, Universidade do Minho, PORTUGAL

Received: February 28, 2019

Accepted: July 1, 2019

Published: July 31, 2019

Data Availability Statement: All relevant data are within the manuscript and its Supporting Information files.

Funding: This study was funded in part by a grant from the DFG (KN 402) to M.K. and from the Gisela Foundation to A.W. The publication of this article was funded by the Open Access fund of Leibniz Universität Hannover. The funders had no role in study design, data collection and analysis, decision to publish, or preparation of the manuscript.

Abstract

Rain cracking severely affects the commercial production of many fleshy-fruit species, including of sweet cherries. The objectives were to investigate how the gaping macroscopic cracks (macrocracks) of a rain-cracked fruit can develop from microscopic cracks in the cuticle (microcracks). Incubating fruit in deionized water is well known to cause significant macrocracking. We found that after a lag phase of 2 h, the numbers and lengths of macrocracks increased. Macrocrack number approached an asymptote at 12 h, whereas macrocrack length continued to increase. The rate of macrocrack propagation (extension at the crack tip) was initially 10.8 mm h^{-1} but then decreased to a near-constant 0.5 mm h^{-1}. Light microscopy revealed three characteristic zones along a developing macrocrack. In zone I (ahead of the crack), the cuticle was intact, the epidermal cells were unbroken and their cell walls were thin. In zone II, the cuticle was fractured, the first epidermal cells died and their cell walls began to thicken (swell). In zone III, most epidermal cells had died, their cell walls were swollen and cell:cell separation began along the middle lamellae. The thickness of the anticlinal epidermal cell walls and the percentage of intact living cells along a crack were closely and negatively related. Cracks were stained by calcofluor white, but there was no binding of monoclonal antibodies (mAbs) specific for hemicelluloses (LM11, LM21, LM25). Strong binding was obtained with the anti-homogalacturonan mAb (LM19), indicating the presence of unesterified homogalacturonans on the crack surface. We conclude that macrocrack propagation is related to cell death and to cell wall swelling. Cell wall swelling weakens the cell:cell adhesion between neighbouring epidermal cells, which separate along their middle lamellae. The skin macrocrack propagates like a 'run' in a fine, knitted fabric.

Introduction

When it rains near harvest, rain cracking can reduce both the yield and the quality of many species of fleshy fruit. Sweet cherry, grape and tomato are the most significant commercial crops thus affected–significant both because of the large scale of these industries and also because of the extreme susceptibility of these species to damage [1–4].

Competing interests: The authors have declared that no competing interests exist.

In recent years, and working mainly with sweet cherry, significant progress has been made in understanding the mechanistic basis of rain cracking–deep macrocracks that breach the skin and run deep into the flesh. Such macrocracks expose the interior of the fruit to rapid and catastrophic degradation through the combined ravages of drying, microbial invasion and sugar-seeking insects.

Till now, studies on rain cracking have focused on cuticle deposition [5], microcracking of the cuticle [6], the analysis of stress and strain in the skin [7, 8], the mechanical properties of the skin [9, 10] and the mechanisms/pathways of water movement through the skin [11, 12] and through the vascular system from the parent tree/vine [13].

Although it is thought that macrocracks develop from microcracks [6, 14]. Surprisingly little information is available on the final step of the macrocracking process–the initiation and propagation of these visible skin cracks. Considering the importance of fruit macrocracking, the lack of information on this putative link with microcracking is surprising.

In engineering, the analysis of fracture surfaces provides important clues as to the reason for the mechanical failure. Indeed, fractography has become a forensic discipline within materials science, where fracture surfaces are studied to identify the causes of failure in engineering structures, e.g. in failed buildings, bridges, airframes, etc. [15–17]. Fractography has also found a place in the study of animal structures, where, for example, it is used to develop and evaluate theoretical models of crack propagation in bones [18]. Here, we apply some of these engineering principles to plant structures and, in particular, to the skin of sweet cherry.

Fruit skins suffer of two different failure modes [19]. A fruit skin can fracture due to failure of the skin cell wall–here the failure line runs **across** the cell wall (lysigeny) and the cell contents are lost. Alternatively, a fruit skin can fracture due to the failure of cell:cell adhesion–here the failure line runs **along** the cell wall (schizogeny) and adjacent cells separate from one another along their middle lamellae and each cell remains intact [20].

Schizogenous skin failure is characteristic of sweet cherry fruit skins in the field and this failure is usually associated with rainfall. Schizogenous skin failure also occurs in the laboratory when a sweet cherry fruit is incubated in deionized water [21]. The fraction of cells failing along cell walls (schizogenously) was closely and positively related to the extent of cell wall swelling [22]. Although the detailed mechanism of schizogeny in this context has yet to be determined, the pectins of the middle lamellae are thought likely candidates for the associated cell wall swelling [23, 24]. We would thus expect pectins to be exposed on the broken surfaces of a developing macrocrack.

Immunolabeling of cell wall epitopes has proved a useful technique for obtaining detailed information on the spatial distribution of cell wall carbohydrates in a plant tissue [25, 26]. With immunolabeling, a primary monoclonal antibody from the LM series (generated in rat) that is specific for a particular cell wall epitope, is bound to the tissue. Next, a secondary antibody (anti rat) carrying a fluorescent tracer is applied that binds to the primary cell wall specific antibody. This antibody can then be detected by fluorescence light microscopy. Immunolabeling has been used to identify constituents of cell walls that are involved in cell to cell adhesion [27]. Usually, the tissue is fixed to prepare thin-sections for light microscopy. However, in principle, the technique should also be able to be used with a fresh tissue, for example to identify cell wall constituents exposed on the facture surface of macrocracked cherry fruit. Nevertheless, its use with a fresh tissue poses some challenges. First, tissue sectioning must be avoided because it is inevitably accompanied with stress and strain relaxation [7]. Second, the use of antibodies requires very small volumes of reaction solution and, hence, excludes the incubation and submersion of a whole cherry fruit. Third, artifacts resulting from uptake of water by the fruit, from the reaction solution, must be excluded as a factor. These difficulties may be avoided. The first by using intact fruit (no cutting), the second by restricting

the reaction solution to a tiny portion of the fruit surface and the third by using an osmotically-buffered isotonic reaction solution.

The purpose of our study was: 1) to characterize the initiation of macrocracks (macroscopic cracks) in intact cherry fruit, 2) to determine the relationship between macrocrack initiation and cell wall swelling and 3) to identify the cell wall constituents exposed on the surface of a propagating macrocrack. We used sweet cherry fruit as a model system because there is a large body of published information on this economically important fruit crop.

Materials and methods

Plant material

Mature fruit of sweet cherry (*Prunus avium* L.) were sampled from trees of the cultivars Adriana, Burlat, Early Korvic, Gill Peck, Hedelfinger, Kordia, Regina, Sam, Samba and Sweetheart. All cultivars were grafted on 'Gisela 5' rootstocks (*P. cerasus* L. x *P. canescens* Bois). The trees were cultivated in a greenhouse or under a rain shelter at the horticultural research station in Ruthe (52.2N, 9.8E) or in the open field at an experimental orchard in Hannover (52.4N, 9.7E) according to current regulations for integrated fruit production. Fruit were picked at commercial maturity based on color, selected for freedom from defects and for uniformity based on color and size. They were used for the experiments on the same day.

Macrocracking assays

The position of macrocracks on the fruit surface and their propagation were recorded by incubating cultivars Adriana, Early Korvic, Gill Peck and Hedelfinger fruit in deionized water in polyethylene (PE) boxes placed on a light box in a temperature controlled room at 22˚C. The pedicel was cut to a length of about 5 mm. Fruit were held in position in the PE box using silicone rubber (RTV 3140; Dow Corning, Midland, MI). After allowing the silicone rubber to cure for 30 min, the PE boxes were positioned under a custom multiple camera stand, equipped with six digital cameras (WG-20; Ricoh, Tokyo, Japan). Each camera viewed six fruit simultaneously. Cameras were set in time-lapse mode and images were recorded every 2 h. Before initiation of the cracking assay, the camera setup was calibrated. This setup allowed monitoring of the time course of macrocrack propagation in the regions of the pedicel cavity, the cheek, the suture, the left and right shoulders and the stylar scar.The number of fruit replicates was six. A detailed short term time course was established by analyzing thirteen macrocracks at 10 min intervals. The macrocracks selected for this analysis fulfilled the following requirements: They progressed without branching and stayed within a particular region. The region monitored remained free of other macrocracks.

So that no crack was counted twice and errors due to surface curvature remained below 10%, the fruit surface was partitioned into six orthogonal windows (1. . .6) for data analysis. To delineate the pedicel cavity 1) and stylar-scar 2) regions, a circle of 0.55 times the diameter d was drawn about the fruit long axis (Fig 1A). To delineate the cheek 3) and the suture 4) and the two shoulders 5–6), four trapezoids were used. The top half of a torus of height h_1 was positioned in the pedicel cavity region and used to define the upper margins of the four trapezoids (Fig 1B) while their lower margins were defined by the cap of a sphere. The height h_2 of the cap was calculated from the maximum diameter d of the fruit:

$$h_2 = \frac{d}{2} - \sqrt{(\frac{d}{2})^2 - 0.55 * d^2}.$$

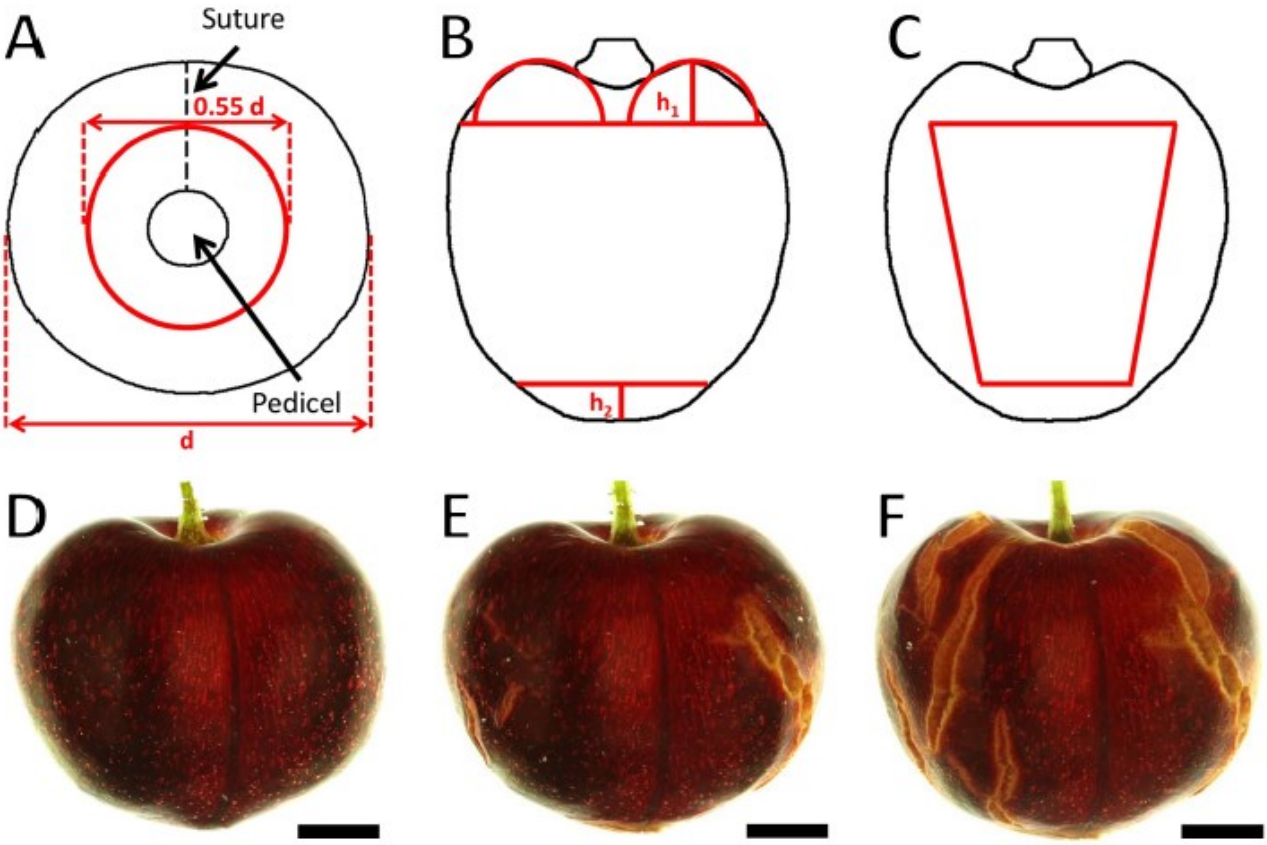

Fig 1. Schematic illustrating the procedure used to quantify crack number and crack length on the six orthogonal regions of the fruit surface. A) Top view of a fruit with receptacle and pedicel in the center of a circle. B) Front view of a fruit illustrating the pedicel cavity and stylar scar regions. The pedicel cavity region was approximated by a circle with 0.55 times the diameter of the fruit and a (half) torus having a radius defined as height h_1. The stylar scar region was approximated by the cap of a sphere of height h_2. C) Side view of a fruit with four trapezoids (only one is visible) representing the cheek, the suture and the two shoulders of a fruit. The trapezoids were drawn such that their heights were delineated by the base of the torus marking the pedicel cavity region, and their bases by the cap delineating the stylar scar region. The vertical margins of each trapezoid were delineated by the respective width of the fruit from which a 10% boundary was subtracted to minimize errors due to curvature of the surface. D-F) Representative images taken from a video clip at 0 h (D), 13 h (E) and 24 h (F) of the suture region of a 'Regina' sweet cherry when incubated in deionized water. Scale bar = 5 mm.

https://doi.org/10.1371/journal.pone.0219794.g001

A 10% safety distance was subtracted from each of the four sides and the points were connected to form four trapezoids (Fig 1C).

The numbers and lengths of macrocracks and the cumulative crack lengths within each of the six windows were measured using image analysis (cellSens Dimension 1.7.1; Olympus, Hamburg, Germany).

Light microscopy

Mature fruit, free from visible defects, were incubated in deionized water at 22˚C for 8 to 22 h to induce macrocracking. Epidermal segments were excised by tangential cuts using a razor blade. Segments were promptly mounted on a glass slide, transferred to the stage of a light microscope (BX-60; Olympus, Hamburg, Germany; Axioplan; Carl Zeiss Microscopy, Jena, Germany) and covered with silicone oil to prevent water uptake/loss. Subsequently, segments were inspected for microcracks at ×40 in transmitted white light. Calibrated light micrographs

of tips of cracks were taken using a digital camera (DP71 and DP73; Olympus, Hamburg, Germany). Thicknesses of anticlinal epidermal cell walls were measured along a developing crack in zones I, II and III using image analysis (CellSens; Olympus, Hamburg, Germany). The three crack zones are defined as proposed by [22]. Briefly, zone I represents the healthy epidermal tissue ahead of a crack, characterized by an intact cuticle. In zone II a microcrack has developed in the cuticle. In zone III the microcrack has extended through the cuticle deep into the underlying epidermis, hypodermis and outer cortex. The cracking in zone II is microcracking, these fine cracks do not extend any deeper than the base of the cuticle and are barely visible to the naked eye [6]. Zone III cracks are clearly visible to the naked eye, macrocracks, and extend deep into epidermis and hypodermis and later into the flesh, sometimes right down to the pit.

The time course of swelling of anticlinal epidermal cell walls and the percentages of intact vital and dead epidermal cells along a developing macrocrack were determined on the cheek of 'Regina'. Dead cells were identified by their brownish coagulated cytoplasm and the loss of anthocyanin from the vacuole.

Swelling of epidermal cell walls was also compared across cultivars. Fruit of cultivars Adriana, Kordia, Regina, Sam and Sweetheart were incubated in deionized water for 18–23 h at room temperature (22˚C) before cell wall swelling was assessed.

Subsequently, cell wall swelling in the cheek, the pedicel cavity and the stylar scar regions of 'Regina' fruit was recorded and analyzed.

Fruit of 'Regina' sweet cherry were incubated in 70 mM malic acid for 20 h at 22˚C and the effects on cell wall swelling and on the percentages of ruptured and intact epidermal cells were recorded. Malic acid at this concentration was used because 1) it corresponds to the typical concentration of this moiety in the expressed juice of mature sweet cherry fruit [28] and 2) because the release of juice (containing malic acid) from ruptured mesocarp cells is known to be a crucial factor in the propagation of macrocracks in mature sweet cherry fruit [29, 30]. Fruit incubated in deionized water served as controls.

Immunolabeling of cell walls

The cell wall constituents exposed on the broken surface of cracks in mature fruit of cultivars Burlat and Samba sweet cherry were identified by immunolabeling of the exposed epitopes. The pedicel was removed and pedicel cavity, including receptacle and pedicel end, sealed with silicone rubber (3140 RTV Coating; Dow Corning, Midland, MI, USA). This procedure restricted water uptake to the fruit surface [31]. Sections of silicone rubber tubing (inner diameter 14 mm) were mounted in the stylar scar region of sweet cherry fruit and allowed to cure for 2 h. The sections of the tubing served as wells for solutions used in the labeling process. Fruit with tube sections attached were incubated in deionized water overnight. In the mornings, fruit were selected for immunolabeling which had cracks of comparable dimensions in the attached tube sections. The entire labeling procedure was carried out using fresh (i.e. non-fixed) tissue. We followed the multi-step protocol described by [26] and [27] with minor modifications. (I) Non-specific protein binding sites in the crack were blocked using 200 μl of isotonic phosphate-buffered saline (PBS) containing 3% (w/v) nonfat dry milk powder and held in the well for 30 min. Tonicity of the buffer was adjusted using glucose. (II) After removal of the blocking solution, the surface was thoroughly washed for 3 x 5 min using three changes of isotonic PBS to remove any remaining milk protein from the surface. (III) The following primary monoclonal antibodies (mAbs; PlantProbes, Leeds, UK) were prepared in a ten-fold dilution in isotonic PBS buffer at pH 7.0. The mAbs reacting with hemicelluloses were: LM11 (anti-xylan/arabinoxylan [32]), LM21 (anti-mannan [33]) and LM25 (anti-xyloglucan [34]). Those against pectins were: LM5 (anti-galactan [35]), LM6 (anti-arabinan [36]), LM7 (anti-

homogalacturonan [37]), LM8 (anti-xylogalacturonan [38]), LM19 (anti-homogalacturonan [39]) and LM20 (anti-homogalacturonan [39]). The mAb 2F4 (anti-homogalacturonan [40]) was made up in 20 mM Tris(hydroxymethyl)methylamin buffer (TRIS-HCl) adjusted to pH 8.2. All primary mAbs from the LM series were anti rat. Only 2F4 was anti mouse. Solutions were applied to the wells on the fruit (200 μl each) and allowed to react for 1 h at room temperature (c. 22˚C). Buffer solution containing no primary mAbs was applied to the control. The mAb 2F4 that identifies Ca^{2+} crosslinks in homogalacturonans was also applied in the presence of 0.5 mM $CaCl_2$, as a second control. The second control was needed to demonstrate potential Ca^{2+} binding sites on the surface of a macrocrack. (IV) The solutions containing the primary antibodies were removed and the wells were carefully washed using isotonic PBS buffer. (V) The antibodies bound to the exposed cell wall epitopes were next labeled using a secondary antibody carrying a fluorescence marker (Alexa Fluor 488 anti rat for LM mAbs and Alexa Fluor 488 anti mouse for 2F4). The treatment solutions comprised a 200-fold dilution of the secondary antibody prepared in isotonic PBS buffer (200 μl per well). Fruit were incubated for 1.5 h at room temperature (22˚C) in darkness in PE boxes at high humidity (maintained using wet filter paper). (VI) Fruit surfaces were rinsed twice with isotonic PBS (5 min each) and subsequently treated with 0.1% (w/w) calcofluor white (fluorescent brightener 28; Sigma-Aldrich Chemie, Munich, Germany) solution for 5 min to identify cellulosic cell walls exposed in the cracks. (VII) The calcofluor white solution was removed, the surface washed once with deionized water before 200 μl of a PBS-based antifadent solution (Citifluor AF3; Science services, Munich, Germany) was applied. Preliminary experiments established that the antifadent solution prevented the decrease in signal intensity that occurred following the staining procedure. Finally, (VIII) the antifadent solution was removed and the surface in the well carefully blotted dry. The antibody-labeled fruit were viewed using a dissecting fluorescence microscope (MZ10F; filters GFP-plus 480–440 nm excitation, ≥510 nm emission; UV 360–440 mm excitation, ≥420 emission; Leica Microsystems, Wetzlar, Germany) at ×0.8, ×2, ×4 and ×8 equipped with epifluorescence. For comparing the bound antibodies, exposure times were held constant and set to 3, 8 and 15 s at ×0.8 and to 0.3 and 0.8 s at ×2, ×4 and ×8. For viewing calcofluor white stained specimens, exposure times were 1 and 3 s at ×0.8 and at 0.3 s at ×2, ×4 and ×8.

Data analysis and terminology

Data are presented in scatter plots and tables as means ± standard errors of the means. Where not shown, error bars were smaller than data symbols. Data were analyzed by analysis of variance using the statistical software package SAS (version 9.1.3; SAS Institute, NC, USA).

We refer to the thickness of anticlinal epidermal cell walls as 'cell wall thickness' and to the increase in their thickness as 'swelling'. Our thickness estimates comprise the sum of the thicknesses of the two cell walls of abutting epidermal cells, plus the pectin middle lamella between the two cells.

Results

Incubating mature fruit in deionized water caused significant macroscopic cracking (Fig 1D–1F). After a lag phase of about 2 h of incubation, crack number (Fig 2A and 2B), mean crack length (Fig 2C and 2D) and cumulative crack length per fruit all increased (Fig 2E and 2F). This pattern was consistent across all regions of the fruit surface and across all cultivars (Table 1).

Quantitatively, cracking was more severe in the stylar scar and the pedicel cavity regions compared in the cheek, suture or shoulder regions (Fig 2) and more severe in cv. 'Kordia' compared with all other cultivars (Fig 2, Table 1).

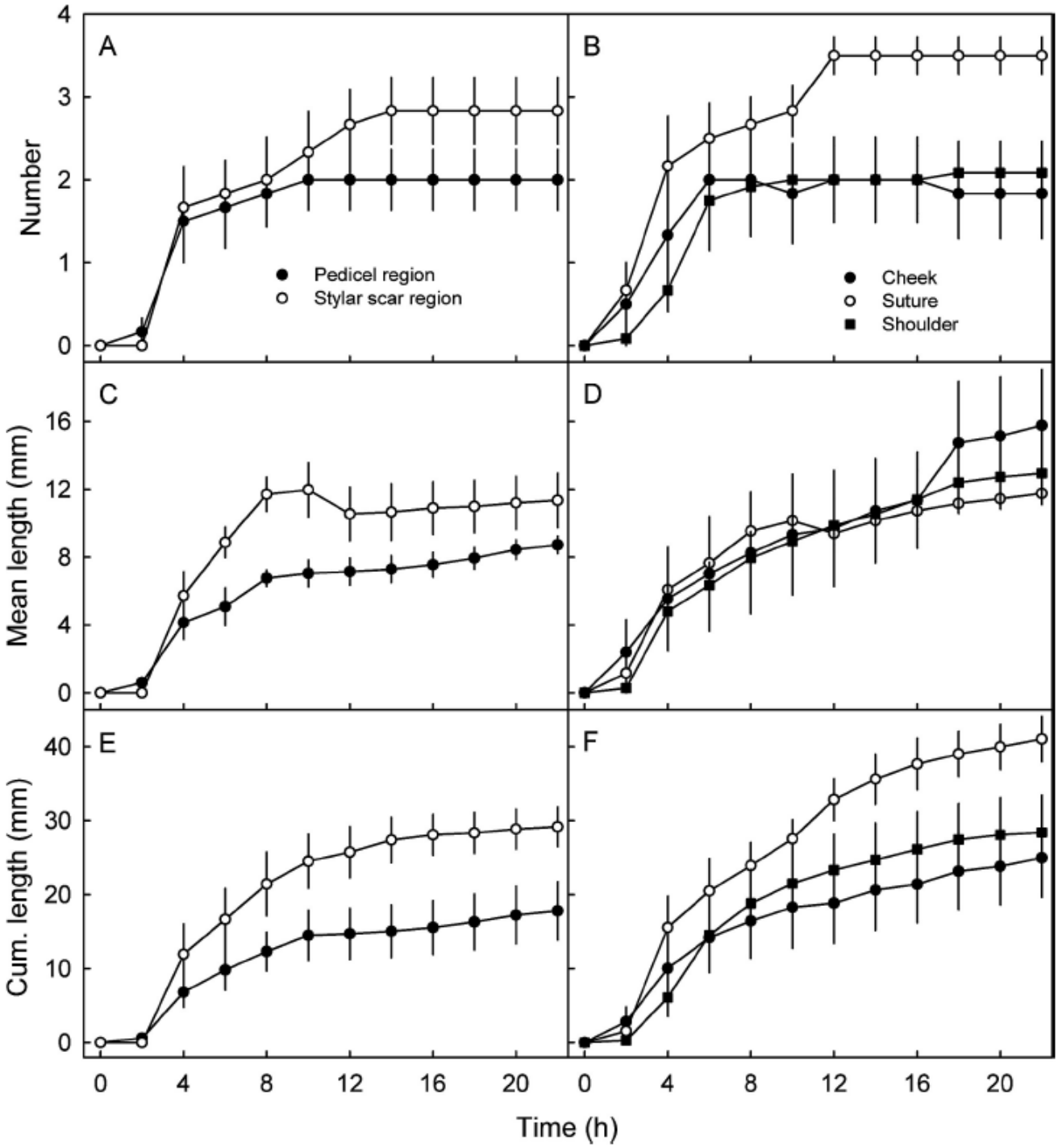

Fig 2. Time course of macroscopic cracking in different regions of the fruit surface of 'Kordia' sweet cherry. A,C,E. Numbers of macrocracks (A), average lengths of macrocracks (C), and cumulative length of macrocracks (E) in stylar scar and pedicel cavity regions. B,D,F. Number of macrocracks (B), average lengths of macrocracks (D) and cumulative lengths of macrocracks (F) in cheek, suture and shoulder regions. Fruit were incubated in deionized water to induce cracking.

https://doi.org/10.1371/journal.pone.0219794.g002

Table 1. Number of cracks and cumulative length of cracks per fruit in various sweet cherry cultivars.

Cultivar	8 h			22 h		
	Cracks (No. per fruit)	Mean length (mm)	Cum. length (mm per fruit)	Cracks (No. per fruit)	Mean length (mm)	Cum. length (mm per fruit)
Adriana	-[a]	-	-	4.7 ± 1.0 b	8.7 ± 1.7 c	40.6 ± 10.3 b
Early Korvic	3.3 ± 0.3 b[b]	6.4 ± 0.6 b	21.4 ± 2.3 b	4.3 ± 0.7 b	8.9 ± 1.0 bc	38.6 ± 5.4 b
Gill Peck	2.3 ± 0.4 b	8.6 ± 1.2 b	20.0 ± 4.3 b	3.3 ± 0.8 b	12.7 ± 1.6 bc	42.3 ± 5.4 b
Hedelfinger	1.2 ± 0.5 b	9.6 ± 1.2 ab	11.2 ± 5.8 b	2.0 ± 0.6 b	15.7 ± 1.7 ab	31.5 ± 7.0 b
Kordia	7.7 ± 1.4 a	14.6 ± 1.0 a	111.8 ± 10.9 a	8.7 ± 1.0 a	19.6 ± 1.0 a	169.8 ± 11.3 a

Fruit was incubated in deionized water for up to 22 h to induce cracking.

[a]No cracked fruit.

[b]Mean separation within columns by Tukey's Studentised range test (<5%).

https://doi.org/10.1371/journal.pone.0219794.t001

Averaged across regions, length of a macrocrack increased with time (Fig 3A, inset). The extension rate was most rapid immediately after crack initiation and then decreased (Fig 3A). A detailed short term time course revealed thatmaximum rates of on average 10.8 ± 1.3 mm h^{-1} (range 2.6 to 17.8 mm h^{-1}) were measured within the first 10 min of macrocrack formation (Fig 3B). Thereafter, the rates of extension of macrocracks slowed to about 0.5 mm h^{-1} (Fig 3A)

Light microscopy of the tips of developing macrocracks revealed the three characteristic zones along a crack (Fig 4A and 4B). In zone I, ahead of the crack, epidermal cells were closely adherent, their anticlinal walls were thin (non-swollen) and they were intact (Fig 4B, Fig 5A). In zone II, the cuticle had fractured, the epidermal cells just beneath the microcrack were still adherent and many had died as indexed by the presence of coagulated cytoplasm and loss of anthocyanin from their vacuoles. Finally, in zone III, the microcrack had widened and deepened into the epidermis and hypodermis of the skin and into flesh to form a gaping macrocrack. The epidermal cell walls were swollen and had separated from one another (predominately along their anticlinal walls) and nearly all were dead.

Monitoring cell wall swelling during crack development indicates that–once a microcrack has been initiated–the thickness of the anticlinal cell walls increases with time (Fig 5A). The increase in cell wall thickness in zone III exceeded that in zone II, which exceeded that in zone I. By 72 h, there was essentially no difference in cell wall thickness between the three former zones of a crack. As crack development proceeded, the percentage of living cells decreased. Again, the proportion of living cells was least in zone III, and greater in zone II, while all appeared to be alive in zone I (Fig 5B). Differences in cell wall swelling and cell death between the former zones diminished with time and as the microcrack deepened into a gaping macrocrack. There was a close negative relationship between the thickness of anticlinal cell walls and the percentage of still-living cells along a macrocrack (Fig 5C).

Swelling of anticlinal epidermal cell walls during macrocrack formation was observed in all cultivars investigated (Table 2). However, initial cell wall thickness (zone I, ahead of a macrocrack) and the extent of cell wall swelling during macrocracking, did depend on cultivar. 'Regina' and 'Sam' sweet cherry had the thickest cell walls, and 'Adriana', 'Kordia' and 'Sweetheart' had the thinnest. The increase in cell wall thickness upon macrocracking was largest in 'Regina' and Sweetheart, and least in 'Kordia', 'Sam' and 'Adriana'.

Swelling of cell walls did not differ significantly between regions of a fruit within a cultivar (Table 3).

Malic acid at a concentration typical for juice of sweet cherry dramatically increased swelling of cell walls (Table 4). In the presence of malic acid, epidermal cell walls were consistently

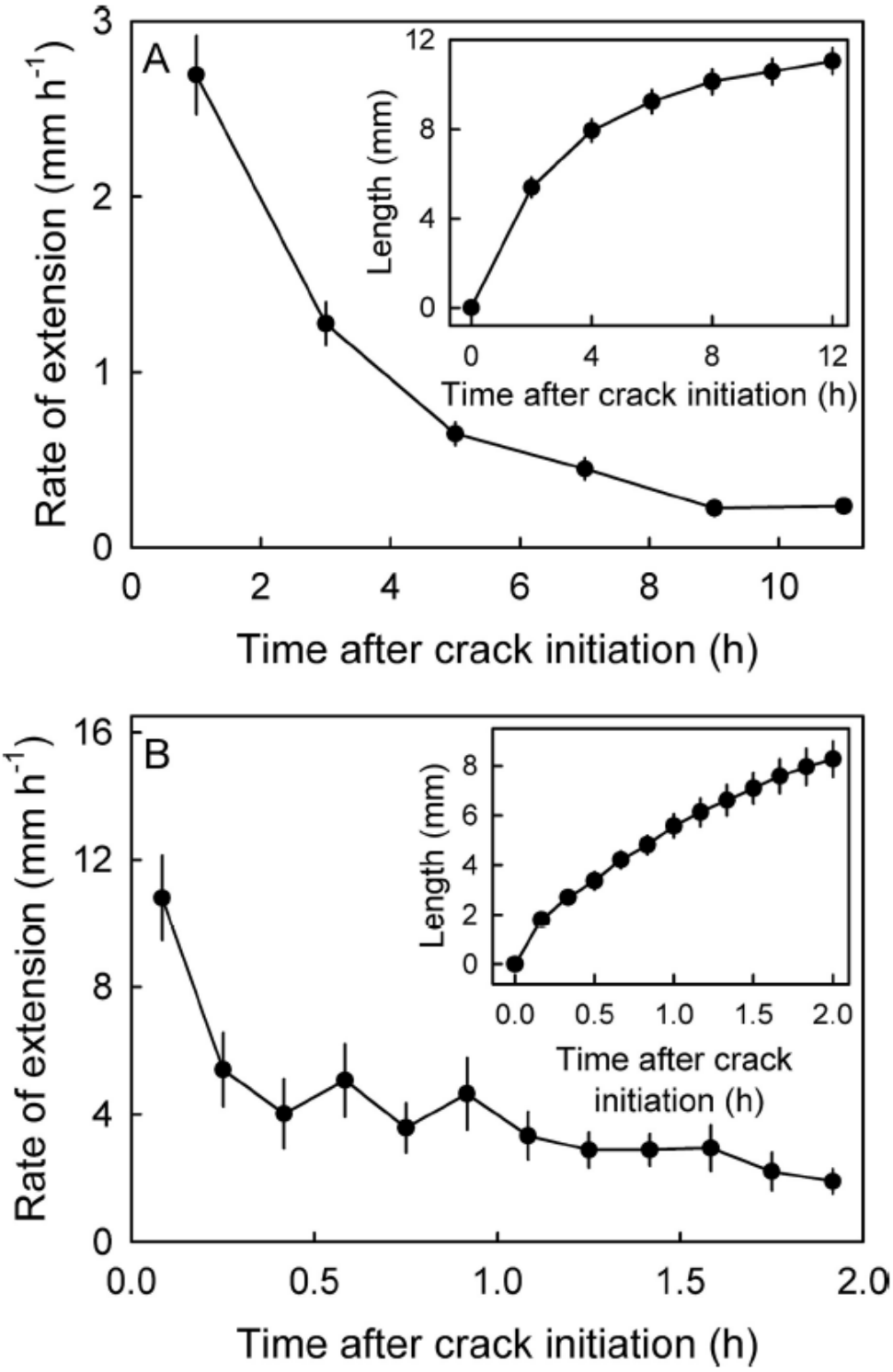

Fig 3. Long term (A) and short term time courses (B) of change in rate of extension of macrocracks (main graphs) and in length of individual macrocracks (insets) in 'Kordia' sweet cherry. Fruit were incubated in deionized water to induce cracking.

https://doi.org/10.1371/journal.pone.0219794.g003

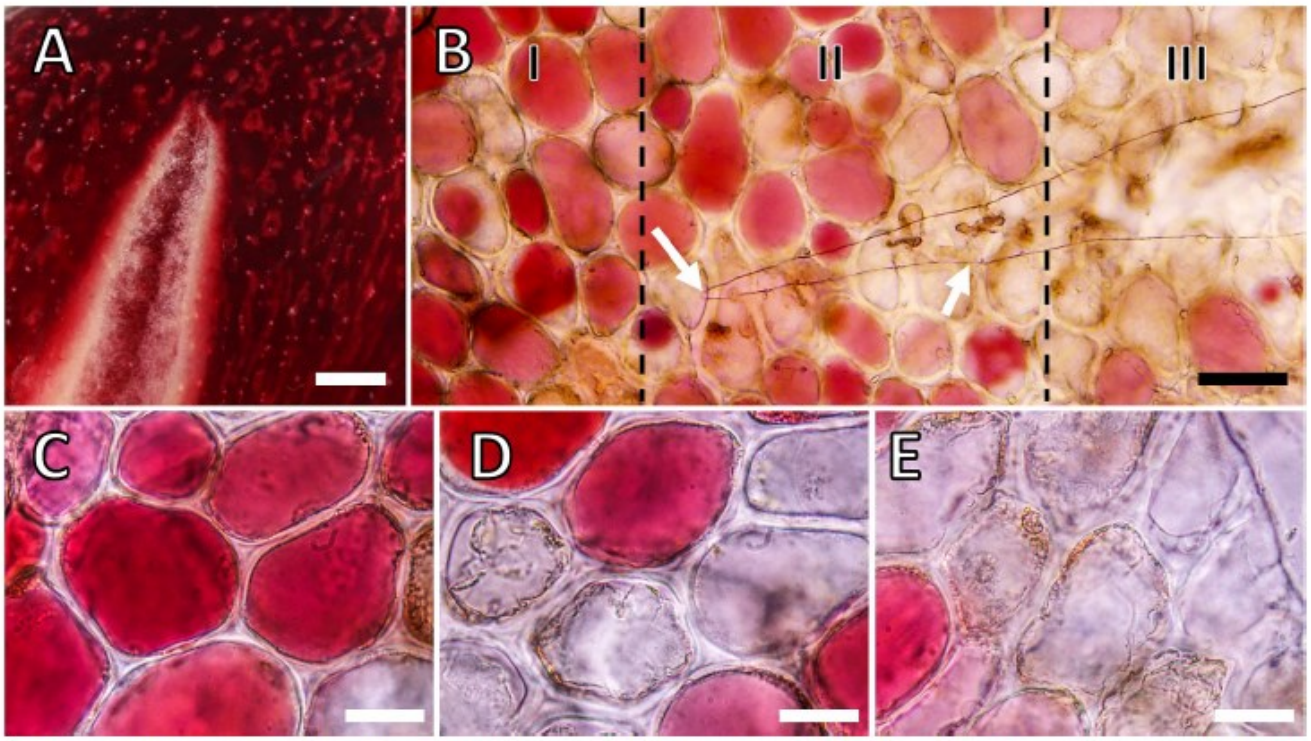

Fig 4. Micrographs of macroscopic cracks (macrocracks) and microscopic cracks (microcracks) in the skin of 'Regina' sweet cherry. A) Close up view of the tip of an extending macrocrack. B) Light micrograph of the tip of a macrocrack in the cuticle of the skin of a mature sweet cherry fruit depicting zones I, II and III of a developing macrocrack. C) Light micrograph of fruit skin in zone I. Zone I is the zone ahead of a developing crack with an intact cuticle and adherent, still-living, epidermal cells. D) Light micrograph of fruit skin in zone II. Zone II represents the tip of the microcrack (indicated by the white arrow) showing rupture of the cuticle. In zone II, the first separation of epidermal cells occurs, some of which are dead. E) Light micrograph of fruit skin in zone III. In zone III, the microcrack develops into a macrocack that extends deep into the epidermal and hypodermal cell layers and begins to gape. Essentially all the cells along a macrocrack are dead. Bars in A = 1 mm, B = 50 μm, C-E = 20 μm.

https://doi.org/10.1371/journal.pone.0219794.g004

thicker in all zones than in those of water treated controls. It is interesting that, compared to the water controls, in the malic acid treated skins, the cell walls were about twice as thick and a large proportion of the cells was dead, even in zone I, ahead of the macrocrack. In zone 1 of the control, cell walls remained thin and all cells appeared alive.

Micrographs reveal that sweet cherry suffered severe macrocracking in the stylar scar region and that both microcracks and macrocracks stained with calcofluor white. When treating macrocracks with mAbs, we observed no significant binding of the mAbs specific for hemicelluloses (LM11, LM21) but some weak binding with LM25 specific for xylo-glucans. Among the mAbs specific for pectins, the strongest binding was with LM19 specific for unesterified homogalacturonan. Other pectic epitopes were identified at markedly lower levels as indexed by very weak fluorescence. These included arabinans (LM6), xylo-galacturonans (LM8) and esterified homogalacturonans (LM20). Compared to unesterified homogalacturonan (LM19), esterified homogalacturonan was exposed on the macrocrack surface at low level (Fig 6).

Detailed investigations of macrocracks using the mAbs LM6, LM8, LM19 and LM20, all against pectins, in a different sweet cherry cultivar, revealed a similar pattern of binding to the surfaces of microcracks and macrocracks (Fig 7). At higher magnification, stretching of cells normal to a microcrack and the beginning of cell:cell separation along a developing macrocrack were detectable, following calcofluor white staining or following binding of LM19.

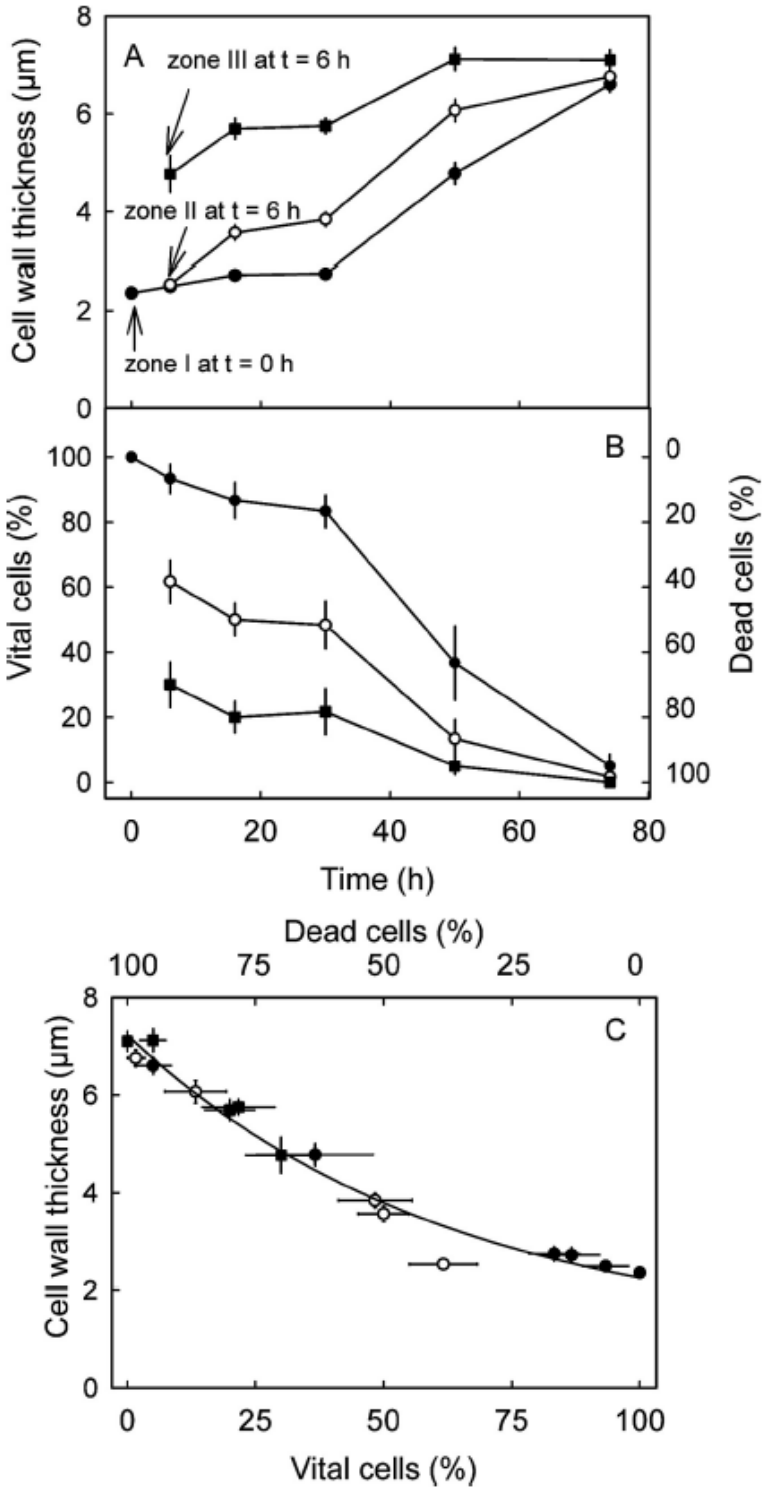

Fig 5. Time course of cell wall swelling (A) and the proportions of living vs. dead cells (B) along a developing macrocrack. C) Relationship between cell wall thickness and percentage of living cells. 'Regina' fruit were

incubated in deionized water and removed from solution at different times to investigate the development of a skin macrocrack. Zone I represents the intact, healthy skin ahead of a macrocrack at time zero (t = 0 h), zone II the tip of a macrocrack at t = 6 h and zone III a macrocrack where gaping has begun. The macrocrack is now bordered by dead cells.

https://doi.org/10.1371/journal.pone.0219794.g005

Table 2. Cell wall thickness in different zones of a developing macrocrack in the fruit skin.

Cultivar	Cell wall thickness (μm)			
	Zone I	Zone II	Zone III	Zone III–zone I[b]
Adriana	2.8 ± 0.1aA[a]	2.9 ± 0.1aA	3.7 ± 0.2bA	0.9 ± 0.2
Kordia	2.8 ± 0.2aA	4.8 ± 0.2bB	5.6 ± 0.3cB	2.7 ± 0.3
Regina	4.0 ± 0.2aB	5.8 ± 0.3bC	7.5 ± 0.4cC	3.5 ± 0.4
Sam	3.9 ± 0.2aB	4.6 ± 0.3abB	6.0 ± 0.3bB	2.1 ± 0.3
Sweetheart	2.7 ± 0.1aA	4.5 ± 0.2bB	5.9 ± 0.3cB	3.2 ± 0.3
Grand Mean	3.3 ± 0.1	4.5 ± 0.2	5.7 ± 0.3	

Fruit were incubated in deionized water to induce macrocracking. Zone I is just ahead of a developing macrocrack. Zone II is where the cuticle has cracked (microcracked) but not the underlying cellular layers. Zone III is where cell separation has begun and a macrocrack is clearly to be seen.

[a]Means within rows followed by the same lowercase letter and those within columns followed by the same uppercase letter are not significantly different (<5%).

[b]Cell wall thickness in zone I subtracted from cell wall thickness in zone III.

https://doi.org/10.1371/journal.pone.0219794.t002

Table 3. Cell wall thickness in different zones of a macrocrack in the cheek, pedicel cavity and stylar scar regions of 'Regina' sweet cherry.

Region	Cell wall thickness (μm)		
	Zone I	Zone II	Zone III
Pedicel cavity	4.2 ± 0.3	4.8 ± 0.3	6.4 ± 0.6
Cheek	3.3 ± 0.4	4.4 ± 0.6	6.4 ± 0.8
Stylar scar	4.2 ± 0.2	5.7 ± 0.3	6.4 ± 0.2
Grand Mean	4.0 ± 0.1 a[a]	5.1 ± 0.2 b	6.4 ± 0.2 c

Fruit were incubated in deionized water to induce cracking. Zone I is ahead of a macrocrack, zone II is where the cuticle has cracked (microcracked) and zone III is where cell separation has begun (a macrocrack is forming).

[a]Two-factorial analysis of variance revealed a significant main effect for 'zone', the main effect for 'region' and for the interaction 'region x zone' were not significant. Means followed by the same letter do not differ significantly (<5%).

https://doi.org/10.1371/journal.pone.0219794.t003

Table 4. Effect of malic acid on cell wall thickness in different zones of a developing skin macrocrack of 'Regina' sweet cherry.

Regions	Cell wall thickness (μm)		
	Zone I	Zone II	Zone III
Control	3.3 ± 0.2 a[a]	4.5 ± 0.2 a	6.0 ± 0.2 a
Malic acid	7.7 ± 0.3 b	8.0 ± 0.2 b	8.7 ± 0.3 b

To induce macrocracking, fruit were incubated for 20 h in deionized water (control) or in 70 mM malic acid (treatment). Zone I lies ahead of a macrocrack, zone II is where the cuticle has cracked (microcracked) and zone III is where cell separation has begun (a macrocrack is forming).

[a]Mean separation within columns by Tukey's Studentised range test (<5%).

https://doi.org/10.1371/journal.pone.0219794.t004

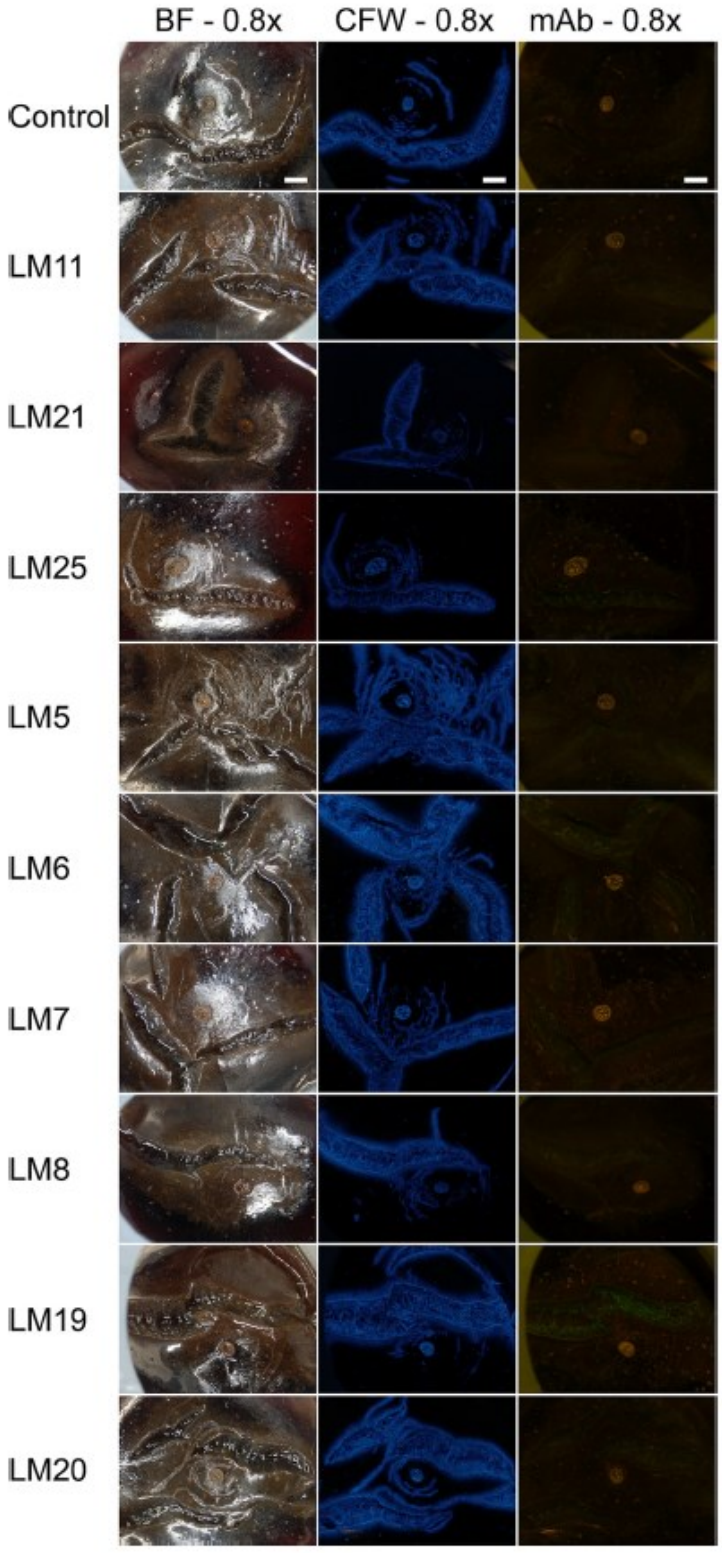
BF - 0.8x
CFW - 0.8x
mAb - 0.8x
Control
LM11
LM21
LM25
LM5
LM6
LM7
LM8
LM19
LM20

Fig 6. Composite of micrographs of 'Burlat' sweet cherry fruit that macrocracked in the stylar scar region during incubation in deionized water. Images were obtained following staining with calcofluor white or following binding of monoclonal antibodies (mAbs) against epitopes on cell walls exposed in the macrocrack surface. The mAbs reacting with epitopes of hemicelluloses were LM11 (anti-xylan/arabinoxylan), LM21(anti-mannan) and LM25 (anti-xyloglucan). The mAbs against pectin epitopes were LM5 (anti-galactan), LM6 (anti-arabinan), LM7 (anti-homogalacturonan), LM8 (anti-xylogalacturonan), LM19 (anti-homogalacturonan) and LM20 (anti-homogalacturonan). The first column of the composite was obtained under bright field illumination, the second column following calcofluor white staining (CFW) using UV light and the third column under fluorescent light following mAbs binding. All images 0.8x. Scale bar = 1 mm.

https://doi.org/10.1371/journal.pone.0219794.g006

At times, microcracks and macrocracks branched or merged, particularly when cracking density was high, as was often the case in the stylar scar region (Fig 8A–8C). Nevertheless, the characteristic zoning (I, II and III) of macrocracking was still clearly discernible. Fig 8D shows a microcrack (zone II) that branched into a macrocrack (zone III). In the microcrack, the cuticle has fractured but epidermal cells are largely intact. Here, the mAb LM19 labeled the periclinal epidermal cell walls just beneath the ruptured cuticle. In the macrocrack (zone III), cell:cell separation of anticlinal epidermal walls began close to the macrocrack tip. Cell:cell separation proceeded along the macrocrack, with gaping indicating the release of stress and strain. Here, the mAb LM19 labeled the anticlinal cell walls at an intensity similar to the periclinal walls in zone II.

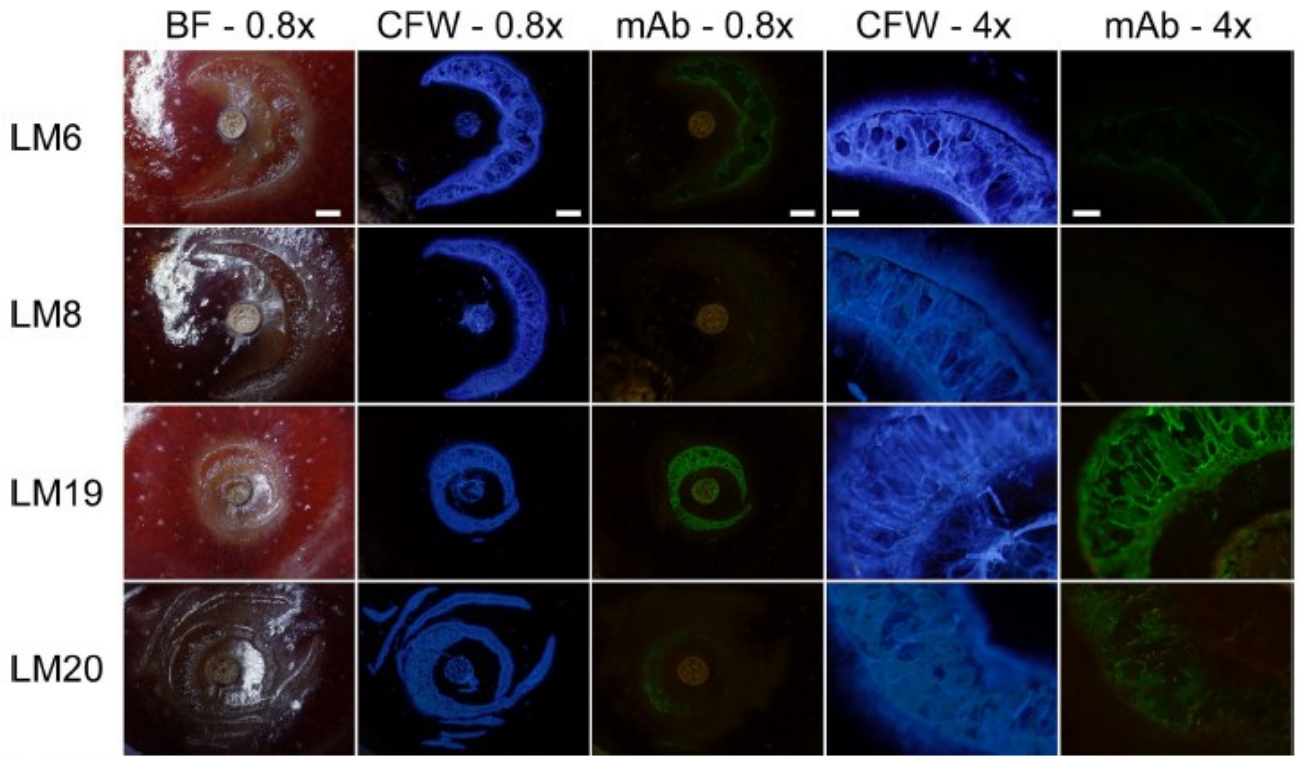

Fig 7. Composite of micrographs of 'Samba' sweet cherry fruit that had macrocracked in the stylar scar region during incubation in deionized water. Images were taken following staining with calcofluor white (CFW) or following binding of monoclonal antibodies (mAbs) against epitopes on cell wall surfaces exposed in macrocracks. The mAbs reacting with epitopes of hemicelluloses were LM6 (anti-xylan/arabinoxylan), LM8 (anti-xylogalacturonan), LM19 (anti-homogalacturonan), and LM20 (anti-homogalacturonan). Images were viewed under bright field illumination (BF), under UV (CFW) or under fluorescent light (mAb). Scale bars in the first, second and third columns = 1 mm, in the fourth and fifth columns = 0.2 mm.

https://doi.org/10.1371/journal.pone.0219794.g007

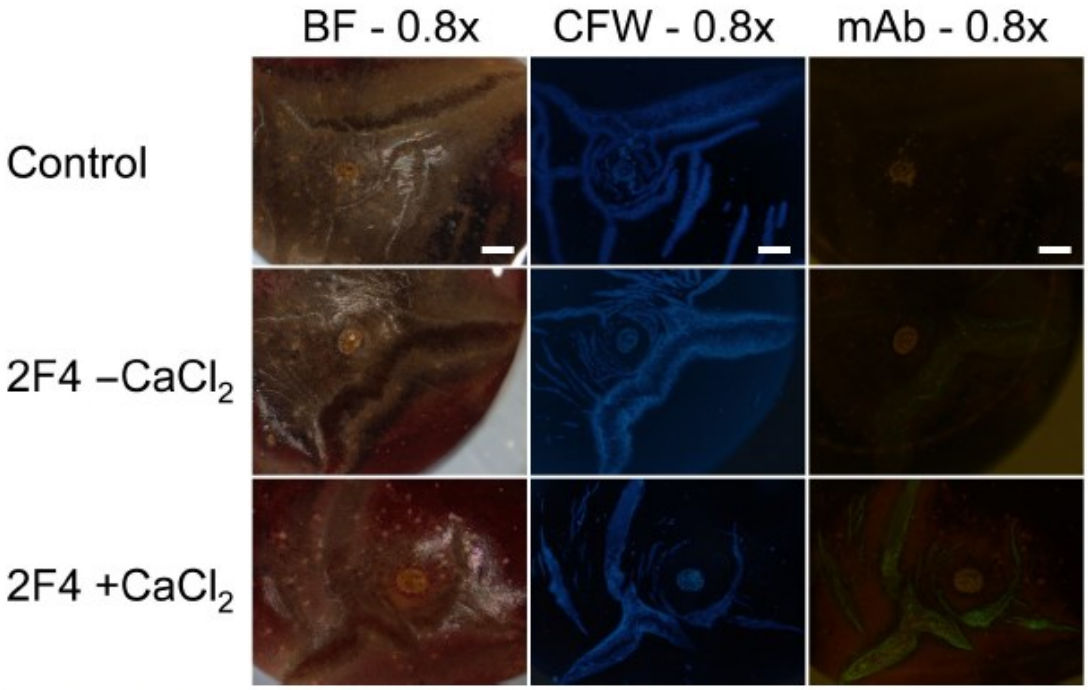

Fig 8. Composite of micrographs of 'Burlat' sweet cherry fruit that cracked in the stylar scar region during incubation in deionized water. A) Bright field image (BF). B) Same specimen as A, but macrocracks stained using calcofluor white (CFW) and viewed under UV light. Same specimen as A, but now treated with the monoclonal antibodies LM19 (anti-homogalacturonan) and viewed under fluorescent light. D) Detailed view of cracks labeled with LM19 showing crack network with a microcrack ('zone II') and a developing macrocrack ('zone III'). Scale bars = 1 mm (A-C) or 100 μm (D). In the microcrack (zone II), the cuticle has fractured, but epidermal cells are largely intact. The mAb LM19 labeled the periclinal cell walls. In the macrocrack in zone III separation of epidermal cells along their anticlinal cell walls began near the tip. Separation proceeded along the macrocrack and gaping began (indicating release of stress and strain).

https://doi.org/10.1371/journal.pone.0219794.g008

Applying the mAb 2F4 specific for dimeric associations of homogalacturonans through calcium (Ca), revealed little binding to macrocracks indicating a low degree of Ca^{2+} cross linking. That Ca^{2+} binding sites were present is demonstrated by the stronger binding obtained when 2F4 was applied together with $CaCl_2$ (Fig 9).

Discussion

Our results indicate 1) that macroscopic cracking (macrocracking) of sweet cherry fruit resulted from increases in both macrocrack number and length, 2) that microcracking of the cuticle, the swelling of epidermal cell walls, the death of epidermal cells along a microcrack and the anticlinal separation of epidermal cells are all closely related, 3) that epidermal cells separated predominately along their anticlinal cell walls, and 4) that failure of cross linking in the middle lamella was responsible for the extension of a cuticular microcrack to a dermal macrocrack that extends deep into the flesh.

Macrocracking, microcracking, swelling of epidermal cell wall, death of epidermal cells and separation of epidermal cells are all closely related

The time-lapse videos of fruit cracking reveal that macrocracking results from both the formation of new cracks and from crack extension–both measures increase during macrocracking. The macrocracks developed from microcracks by extension in the tangential direction (i.e. in

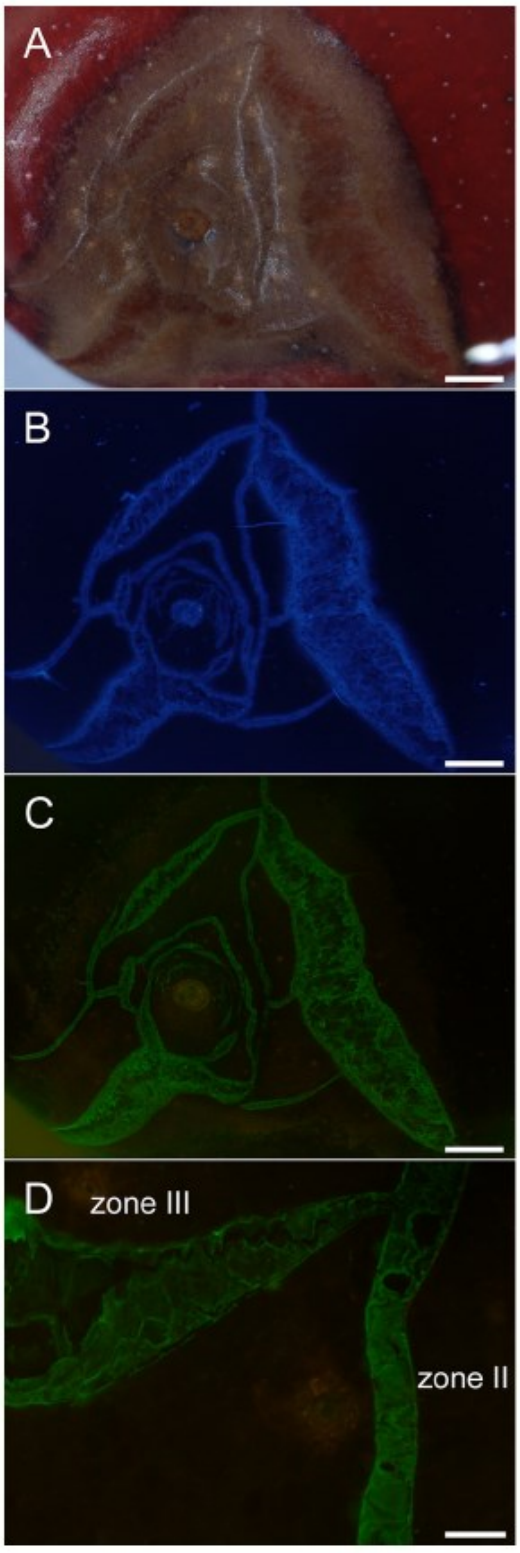
A
B
C
D
zone III
zone II

Fig 9. Composite of micrographs of 'Burlat' sweet cherry fruit that had cracked in the stylar scar region during incubation in deionized water. Images were taken following staining with calcofluor white (CFW) or following binding of the monoclonal antibody (mAb) 2F4 in the absence (2F4, -$CaCl_2$) or presence of Ca (2F4, +$CaCl_2$). The mAb 2F4 identifies dimeric associations of homogalacturonan chains with Ca^{2+}. Images were viewed under bright field (BF), in UV (CFW) or in fluorescent light (mAb). All images at 0.8x. Scale bars = 1 mm.

https://doi.org/10.1371/journal.pone.0219794.g009

the plane of the skin) and also in the radial direction (i.e. deep into the flesh) once the epidermal cells began to separate from one another. Cell separation was preceded by swelling of epidermal cell walls and by cell death. We obtained a close, positive, curvilinear relationship between the proportion of dead epidermal cells and the thickness of their anticlinal cell walls. As cell death progressed along a macrocrack, cell walls began to swell. That cell death occurred is concluded from the brownish coagulated cytoplasm and the loss of anthocyanin from the vacuole. Cell death is accompanied by a loss of turgor. Hence, the pressure on the cell wall decreases. This allows cell walls to swell. This conclusion is consistent with earlier findings where cell wall swelling was greatest for a cell wall between two non-living cells and least when both bordering cells were healthy and fully turgid [41]. The extent of cell wall swelling was intermediate for a cell bordering a healthy cell on one side and a non-living one on the other. Also, in mature fruit, cell wall swelling increased as the proportion of plasmolyzed cells increased, but not in immature fruit [41]. These observations indicate 1) that it is not cell death *per se* that is causal in the swelling of cell walls but the loss of turgor associated with cell death (or plasmolysis) [22] and 2) that chemical modifications of the cell walls, such as those during maturation [42], must precede cell wall swelling. In addition, cell death releases malic acid into the apoplast. Malic acid is a major osmolyte in sweet cherry that will tend to extract Ca^{2+} from the cell wall, thereby decreasing cross linking and exacerbating cell wall swelling [29]. From a physical point of view, cell turgor simply prevents water absorption and, hence, cell wall swelling as long as cell turgor exceeds the 'swelling pressure' of the cell wall matrix. Because turgor is very low in stage III sweet cherry [43, 44], the swelling pressure generated by the cell wall is expected to be even lower. Cell wall swelling is not unique to sweet cherry but occurs in fruit of many other species during normal ripening [24]. Cell wall swelling markedly decreases the fracture tension of the skin, hence, normal growth-induced skin tension [7] is enough to bring about its failure [22].

Epidermal cells separate along their anticlinal walls indicating failure of the middle lamella

Skin failure is predominately schizogenous–i.e. cell:cell separation due to failure of the middle lamellae between the anticlinal walls of adjacent epidermal cells. Few cells fail lysigenously–i.e. rupture across the cell walls. This observation is consistent with results obtained in biaxial tensile tests using excised skins [22]. In these tests, an excised skin segment is pressurized from its inner surface and the extent of bulging quantified. Skin segments of mature fruit with swollen cell walls mostly failed schizogenously. Schizogenous failure is indicative of failure of the pectins of the middle lamella. This conclusion is supported by the binding of mAbs specific for epitopes of pectins. The strongest binding was obtained with LM19 and markedly with weaker LM20, LM6, LM8 and 2F4. These mAbs identify homogalacturonan domains (LM19, LM20, 2F4), xylogalacturonan (LM8) and arabinan domains (LM6) of pectic polysaccharides. It is worth noting that LM19 and LM20 are specific for unesterified and esterified homogalacturonans, respectively. Hence, the homogalacturonans exposed on the surfaces of an extending skin macrocrack are largely de-methylated, as would be expected for a mature, ripe fruit. During maturation and ripening, we would expect the intensity of labeling of homogalacturonans with LM19 to increase

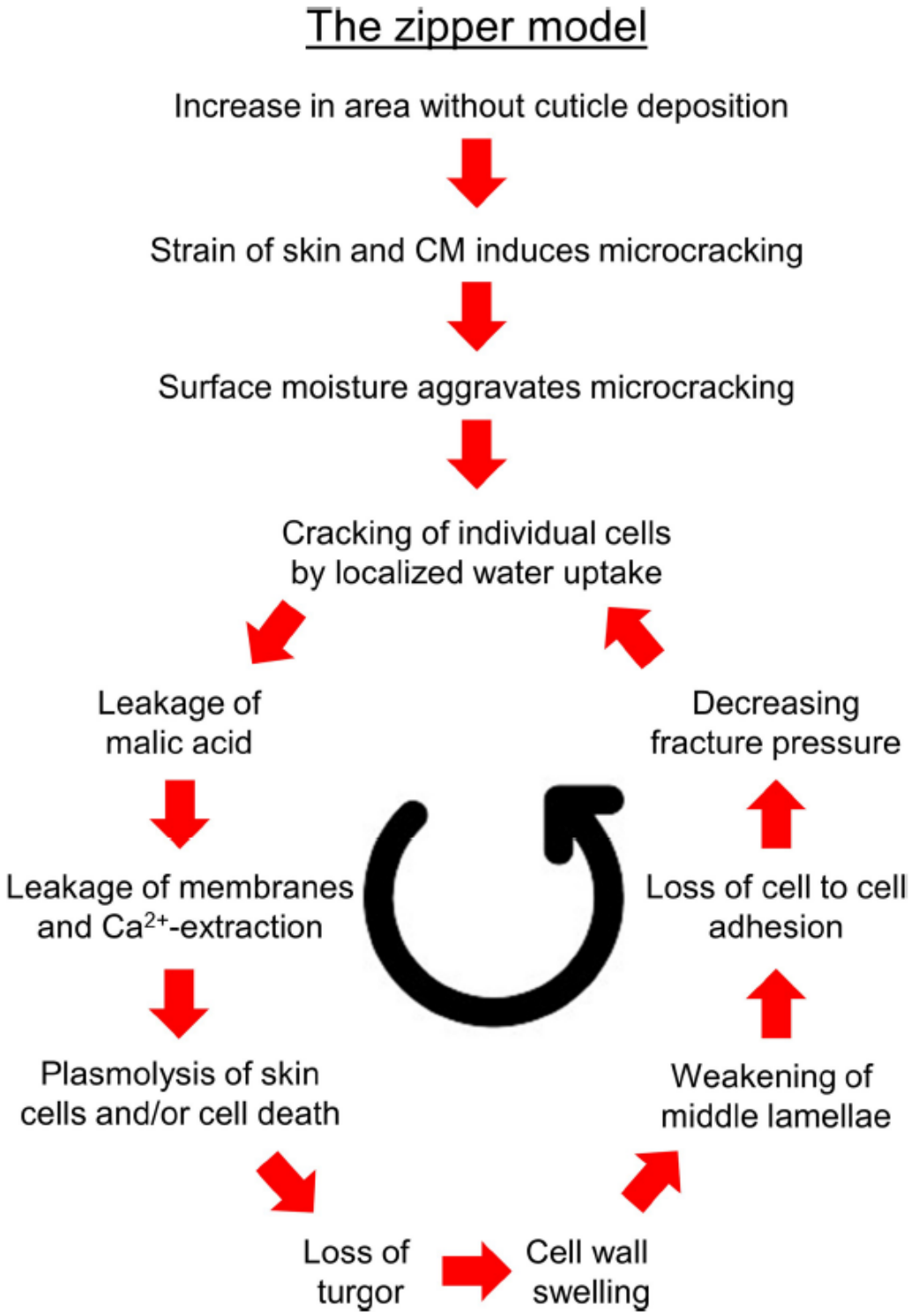

Fig 10. Sketch illustrating the sequence of events in macroscopic rain-cracking of sweet cherry. The increase in surface area in the absence of cuticle deposition [5] causes tension [7] and formation of microcracks [6]. Microcracking is aggravated by surface

moisture [50]. Microcracks impair the cuticle's barrier function [50] and focus water uptake in a particular region of the fruit surface [30]. Water penetration causes individual cells to burst, probably in the outer mesocarp where the osmotic potential is more negative than in the skin [41]. Malic acid leaks into the apoplast causing further leakage of membranes in surrounding cells and the extraction of Ca^{2+} from the cell wall [29]. Cells plasmolyse and collapse. Due to the loss of turgor, cell walls swell [22]. Swelling results in a weakening of the pectin middle lamella, the loss of cell to cell adhesion and decreased fracture pressure [22]. The cells separate along the middle lamella (this paper), the crack propagates as the skin "unzips" like a ladder in knitted fabric. This model is referred to as the zipper model [30].

https://doi.org/10.1371/journal.pone.0219794.g010

and that by LM20 to decrease. Furthermore, the weak binding of 2F4 (relative to the number of binding sites available) indicates a low level of crosslinking between pectins by Ca^{2+}.

Failure of the pectin middle lamella is also consistent with the observation that the rate of strain affected the mode of failure of excised fruit skins [21]. The percentage of cells where fracture occurred schizogenously was higher at low strain rates, compared with at high rates [21]. Pectins exhibit viscoelasticity and time-dependent deformation (as also does the fruit skin) which are typical for viscoelastic materials [45].

From a practical point of view, schizogenous separation of skin cells, i.e. along the middle lamellae, offers the chance that macrocracking can be reduced by applications of Ca-salts. As shown by binding of 2F4 with simultaneous applications of Ca-salts, Ca^{2+} ions increase homogalacturonan cross linking [42, 46]. Increased cross linking also accounts for reduced macrocracking when Ca solutions are applied in the field during rain by overhead sprinklers [47] (for review see [48]). Similarly, a decrease in the amount of water uptake at 50% fruit cracking when fruit were incubated in solutions of $CaCl_2$, $FeCl_3$ and $AlCl_3$ was reported [49]. Interestingly, the morphology of the cracks was also affected. Cracks were deep and gaping after incubation in water but less deep and less extensive when incubated in $FeCl_3$. Both observations are easily accounted for in terms of cross linking of homogalacturonans by di- and trivalent ions [49]. Cross linking delays or stops the development of a microcrack into a macrocrack.

Conclusion

Cuticular microcracks develop into skin macrocracks. This progression involves 1) cell death, 2) leakage of cell contents (esp. malate) and 3) cell wall swelling. These conclusions were obtained in experiments involving a range of different cultivars. There was no indication for cultivar specific interactions. Thus, the above conclusions are applicable to sweet cherry in general. The structural properties of sweet cherry skin are determined predominantly by the cellular layers (epidermis and hypodermis) while its barrier properties are determined predominantly by the cuticle. Microcracks impair the barrier properties. They result from strain of the cuticle due to a cessation of cuticle deposition during early fruit development and—possibly–from exposure of the strained cuticle to surface wetness (Fig 10). Microcracks focus water uptake in a particular region of the fruit surface. Due to the impaired barrier function of the cuticle, water penetrates–probably into the outer mesocarp where the osmotic potential is more negative than in the skin. Individual cells collapse. The liberation of malic acid following cell damage causes leakage of membranes of adjacent cells and extracts Ca^{2+} from the cell walls. Cell walls begin to swell. This weakens the skin locally, so it tends to unzip as the crack propagates–much like a ladder (run) in a knitted fabric. Cell wall swelling particularly weakens cell:cell adhesion causing dermal cells to separate schizogenously–i.e. neighbouring cells part from one another along their anticlinal middle lamellae. The schizogenous failure mode is indexed by the exposure of non-esterified homogalacturonans (LM19) on the fracture surfaces of a skin macrocrack. This sequence of events accounts for rain cracking in sweet cherry and will more than likely be found to occur also in other rain-susceptible fleshy fruit.

Supporting information

S1 Dataset. Raw data on crack formation and cell wall swelling that are displayed in figures and tables.
(XLSX)

Acknowledgments

We thank Dr. Paul Knox, University of Leeds, UK for useful comments on technical aspects of immunolabeling of cell walls in fleshy fruit and the generous gift of the antibodies LM7, LM11, LM15, LM21 and LM25 and Dr. Alexander Lang for helpful comments on an earlier version of this manuscript.

Author Contributions

Conceptualization: Christine Schumann, Andreas Winkler, Martin Brüggenwirth, Moritz Knoche.

Data curation: Christine Schumann, Andreas Winkler, Martin Brüggenwirth.

Funding acquisition: Moritz Knoche.

Investigation: Christine Schumann, Andreas Winkler, Martin Brüggenwirth, Kevin Köpcke.

Methodology: Christine Schumann, Andreas Winkler, Martin Brüggenwirth.

Supervision: Andreas Winkler, Moritz Knoche.

Validation: Andreas Winkler, Martin Brüggenwirth.

Visualization: Christine Schumann, Andreas Winkler, Martin Brüggenwirth.

Writing – original draft: Christine Schumann, Moritz Knoche.

Writing – review & editing: Christine Schumann, Andreas Winkler, Martin Brüggenwirth, Moritz Knoche.

References

1. von Wetzhausen C. Systematische Classification und Beschreibung der Kirschensorten. In: Heim FT, editor. Stuttgart: Cottaische Buchhandlung; 1819. p. 65.
2. Considine JA, Kriedemann PE. Fruit splitting in grapes: Determination of the critical turgor pressure. Aust J Agric Res. 1972; 23: 17–24.
3. Opara LU, Studman CJ, Banks NH. Fruit skin splitting and cracking. In: Janick J, editor. Hortic Rev. 19. New York: John Wiley & Sons, Inc.; 1997. p. 217–262.
4. Knoche M, Winkler A. Rain-induced cracking of sweet cherries. In: Quero-Garcia J, Iezzoni A, Puławska J, Lang G, editors. Cherries: Botany, production and uses. Wallingford, UK: CAB International; 2017. p. 140–165.
5. Alkio M, Jonas U, Sprink T, van Nocker S, Knoche M. Identification of putative candidate genes involved in cuticle formation in *Prunus avium* (sweet cherry) fruit. Ann Bot. 2012; 110: 101–112. https://doi.org/10.1093/aob/mcs087 PMID: 22610921
6. Peschel S, Knoche M. Characterization of microcracks in the cuticle of developing sweet cherry fruit. J Am Soc Hortic Sci. 2005; 130: 487–495.
7. Grimm E, Peschel S, Becker T, Knoche M. Stress and strain in the sweet cherry skin. J Am Soc Hortic Sci. 2012; 137: 383–390.
8. Lai X, Khanal BP, Knoche M. Mismatch between cuticle deposition and area expansion in fruit skins allows potentially catastrophic buildup of elastic strain. Planta. 2016; 244: 1145–1156. https://doi.org/10.1007/s00425-016-2572-9 PMID: 27469168

9. Brüggenwirth M, Fricke H, Knoche M. Biaxial tensile tests identify epidermis and hypodermis as the main structural elements of sweet cherry skin. AoB Plants. 2014; https://doi.org/10.1093/aobpla/plu019 PMID: 24876301
10. Brüggenwirth M, Knoche M. Mechanical properties of skins of sweet cherry fruit of differing susceptibilities to cracking. J Am Soc Hortic Sci. 2016; 141: 162–168.
11. Beyer M, Peschel S, Knoche M, Knörgen M. Studies on water transport through the sweet cherry fruit surface: IV. Regions of preferential uptake. HortScience. 2002; 37: 637–641.
12. Weichert H, Knoche M. Studies on water transport through the sweet cherry fruit surface. 10. Evidence for polar pathways across the exocarp. J Agric Food Chem. 2006; 54: 3951–3958. https://doi.org/10.1021/jf053220a PMID: 16719520
13. Brüggenwirth M, Winkler A, Knoche M. Xylem, phloem, and transpiration flows in developing sweet cherry fruit. Trees. 2016; 30: 1821–1830.
14. Glenn GM, Poovaiah BW. Cuticular properties and postharvest calcium applications influence cracking of sweet cherries. J Am Soc Hortic Sci. 1989; 114: 781–788.
15. Gong SY, Bandyopadhyay S. Fracture properties and fracture surface morphologies in rubber-PMMA composites. J Mater Eng Perform. 2007; 16: 607–613.
16. Mecholsky JJ. Fractography: Determining the sites of fracture initiation. Dent Mater. 1995; 11: 113–116. https://doi.org/10.1016/0109-5641(95)80045-X PMID: 8621031
17. Lin GM, Lai JKL. Fracture mechanism in short fiber reinforced thermoplastic resin composites. J Mater Sci. 1993; 28: 5240–5246.
18. Vashishth D, Tanner KE, Bonfield W. Contribution, development and morphology of microcracking in cortical bone during crack propagation. J Biomech. 2000; 33: 1169–1174. PMID: 10854892
19. Niklas KJ. Plant biomechanics: an engineering approach to plant form and function. Chigago, IL, USA: The University of Chicago Press; 1992.
20. Knoche M, Lang A. Ongoing growth challenges fruit skin integrity. CRC Crit Rev Plant Sci. 2017; 36: 190–215.
21. Brüggenwirth M, Knoche M. Time to fracture and fracture strain are negatively related in sweet cherry fruit skin. J Am Soc Hortic Sci. 2016; 141: 485–489.
22. Brüggenwirth M, Knoche M. Cell wall swelling, fracture mode, and the mechanical properties of cherry fruit skins are closely related. Planta. 2017; 245: 765–777. https://doi.org/10.1007/s00425-016-2639-7 PMID: 28012001
23. Jarvis MC. Control of thickness of collenchyma cell walls by pectins. Planta. 1992; 187: 218–220. https://doi.org/10.1007/BF00201941 PMID: 24178046
24. Redgwell RJ, MacRae E, Hallett I, Fischer M, Perry J, Harker R. In vivo and in vitro swelling of cell walls during fruit ripening. Planta. 1997; 203: 162–173.
25. Lee KJ, Marcus SE, Knox JP. Cell wall biology: perspectives from cell wall imaging. Mol Plant. 2011; 4: 212–219. https://doi.org/10.1093/mp/ssq075 PMID: 21199879
26. Avci U, Pattathil S, Hahn MG. Immunological approaches to plant cell wall and biomass characterization: Immunolocalization of glycan epitopes. In: Himmel ME, editor. Biomass conversion methods in molecular biology (methods and protocols), vol. 908: Humana Press, Totowa, NJ; 2012.
27. Ordaz-Ortiz JJ, Marcus SE, Knox JP. Cell wall microstructure analysis implicates hemicellulose polysaccharides in cell adhesion in tomato fruit pericarp parenchyma. Mol Plant. 2009; 2: 910–921. https://doi.org/10.1093/mp/ssp049 PMID: 19825668
28. Herrmann K. Inhaltsstoffe von Obst und Gemüse. Stuttgart: Ulmer; 2001.
29. Winkler A, Ossenbrink M, Knoche M. Malic acid promotes cracking of sweet cherry fruit. J Am Soc Hortic Sci. 2015; 140: 280–287.
30. Winkler A, Peschel S, Kohrs K, Knoche M. Rain cracking in sweet cherries is not due to excess water uptake but to localized skin phenomena. J Am Soc Hortic Sci. 2016; 141: 653–660.
31. Beyer M, Peschel S, Knoche M, Knörgen M. Studies on water transport through the sweet cherry fruit surface: IV. Regions of preferential uptake. HortScience 2002; 37: 637–641.
32. McCartney L, Marcus SE, Knox JP. Monoclonal antibodies to plant cell wall xylans and arabinoxylans. J Histochem Cytochem. 2005; 53: 543–546. https://doi.org/10.1369/jhc.4B6578.2005 PMID: 15805428
33. Marcus SE, Blake AW, Benians TAS, Lee KJD, Poyser C, Donaldson L, et al. Restricted access of proteins to mannan polysaccharides in intact plant cell walls. Plant J. 2010; 64: 191–203. https://doi.org/10.1111/j.1365-313X.2010.04319.x PMID: 20659281
34. Pedersen HL, Fangel JU, McCleary B, Ruzanski C, Rydahl MG, Ralet MC, et al. Versatile high resolution oligosaccharide microarrays for plant glycobiology and cell wall research. J Biol Chem. 2012; 287.

35. Jones L, Seymour GB, Knox JP. Localization of pectic galactan in tomato cell walls using a monoclonal antibody specific to (1->4)-beta-D-galactan. Plant Physiol. 1997; 113: 1405–1412. https://doi.org/10.1104/pp.113.4.1405 PMID: 12223681

36. Willats WGT, Marcus SE, Knox JP. Generation of a monoclonal antibody specific to (1->5)-α-L-arabinan. Carbohydr Res. 1998; 308: 149–152. PMID: 9675359

37. Willats WGT, Orfila C, Limberg G, Buchholt HC, van Alebeek GJWM, Voragen AGJ, et al. Modulation of the degree and pattern of methyl-esterification of pectic homogalacturonan in plant cell walls: Implications for pectin methyl esterase action, matrix properties, and cell adhesion. J Biol Chem. 2001; 276: 19404–19413. https://doi.org/10.1074/jbc.M011242200 PMID: 11278866

38. Willats WGT, McCartney L, Steele-King CG, Marcus SE, Mort A, Huisman M, et al. A xylogalacturonan epitope is specifically associated with plant cell detachment. Planta. 2004; 218: 673–681. https://doi.org/10.1007/s00425-003-1147-8 PMID: 14618325

39. Verhertbruggen Y, Marcus SE, Haeger A, Ordaz-Ortiz JJ, Knox JP. An extended set of monoclonal antibodies to pectic homogalacturonan. Carbohydr Res. 2009; 344: 1858–1862. https://doi.org/10.1016/j.carres.2008.11.010 PMID: 19144326

40. Liners F, Letesson JJ, Didembourg C, Vancutsem P. Monoclonal antibodies against pectin: Recognition of a conformation induced by calcium. Plant Physiol. 1989; 91: 1419–1424. https://doi.org/10.1104/pp.91.4.1419 PMID: 16667195

41. Grimm E, Knoche M. Sweet cherry skin has a less negative osmotic potential than the flesh. J Am Soc Hortic Sci. 2015; 140: 472–479.

42. Brummell DA. Cell wall disassembly in ripening fruit. Funct Plant Biol. 2006; 33: 103–119.

43. Knoche M, Grimm E, Schlegel HJ. Mature sweet cherries have low turgor. J Am Soc Hortic Sci. 2014; 139: 3–12.

44. Schumann C, Schlegel HJ, Grimm E, Knoche M, Lang A. Water potential and its components in developing sweet cherry. J Am Soc Hortic Sci. 2014; 139: 349–355.

45. Vincent JFV. Fracture properties of plant. Adv Bot Res. 1990; 17: 235–287.

46. Jarvis MC, Briggs SPH, Knox JP. Intercellular adhesion and cell separation in plants. Plant Cell Environ. 2003; 26: 977–989.

47. Lang G, Guimond C, Flore J, Southwick S, Facteau T, Kappel F, et al. Performance of calcium/sprinkler-based strategies to reduce sweet cherry rain-cracking. Acta Hortic. 1998; 468: 649–656.

48. Winkler A, Knoche M. Calcium and the physiology of sweet cherries: A review. Sci Hortic. 2019; 245: 107–115.

49. Weichert H, von Jagemann C, Peschel S, Knoche M, Neumann D, Erfurth W. Studies on water transport through the sweet cherry fruit surface: VIII. Effect of selected cations on water uptake and fruit cracking. J Am Soc Hortic Sci. 2004; 129: 781–788.

50. Knoche M, Peschel S. Water on the surface aggravates microscopic cracking of the sweet cherry fruit cuticle. J Am Soc Hortic Sci. 2006; 131: 192–200.

PLOS ONE

CORRECTION

Correction: Crack initiation and propagation in sweet cherry skin: A simple chain reaction causes the crack to 'run'

Christine Schumann, Andreas Winkler, Martin Brüggenwirth, Kevin Köpcke, Moritz Knoche

The images for Figs 8 and 9 are incorrectly switched. The image that appears as Fig 8 should be Fig 9, and the image that appears as Fig 9 should be Fig 8. The figure captions appear in the correct order.

Citation: Schumann C, Winkler A, Brüggenwirth M, Köpcke K, Knoche M (2021) Correction: Crack initiation and propagation in sweet cherry skin: A simple chain reaction causes the crack to 'run'. PLoS ONE 16(2): e0247692. https://doi.org/10.1371/journal.pone.0247692

Published: February 19, 2021

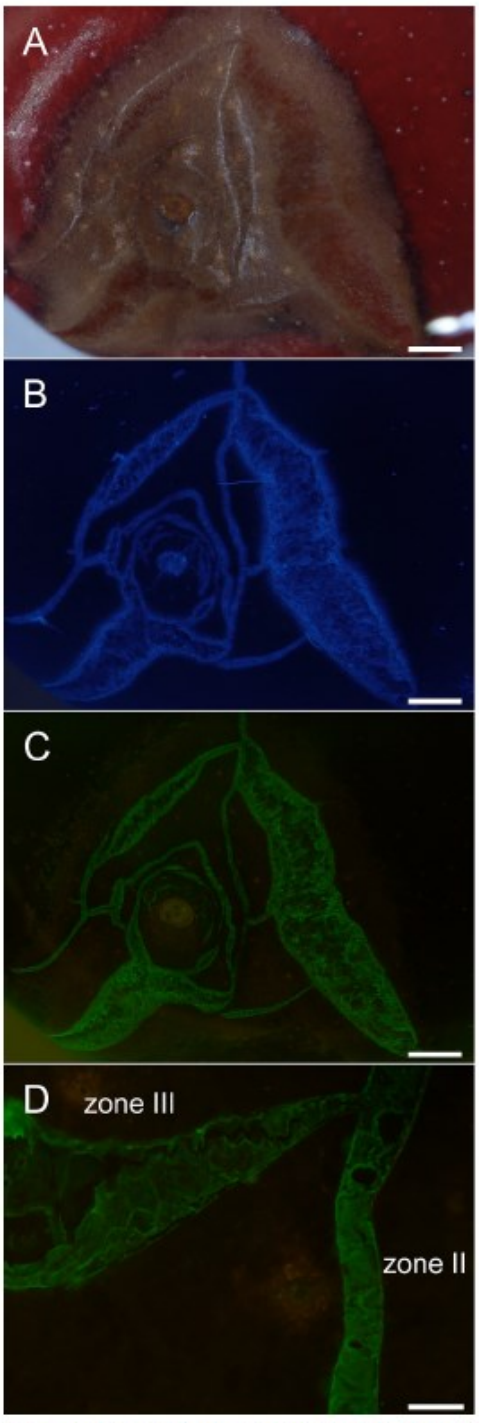

Fig 8. Composite of micrographs of 'Burlat' sweet cherry fruit that cracked in the stylar scar region during incubation in deionized water. A) Bright field image (BF). B) Same specimen as A, but macrocracks stained using calcofluor white (CFW) and viewed under UV light. Same specimen as A, but now treated with the monoclonal antibodies LM19 (anti-homogalacturonan) and viewed under fluorescent light. D) Detailed view of cracks labeled with LM19 showing crack network with a microcrack ('zone II') and a developing macrocrack ('zone III'). Scale bars = 1

mm (A-C) or 100 μm (D). In the microcrack (zone II), the cuticle has fractured, but epidermal cells are largely intact. The mAb LM19 labeled the periclinal cell walls. In the macrocrack in zone III separation of epidermal cells along their anticlinal cell walls began near the tip. Separation proceeded along the macrocrack and gaping began (indicating release of stress and strain).

https://doi.org/10.1371/journal.pone.0247692.g001

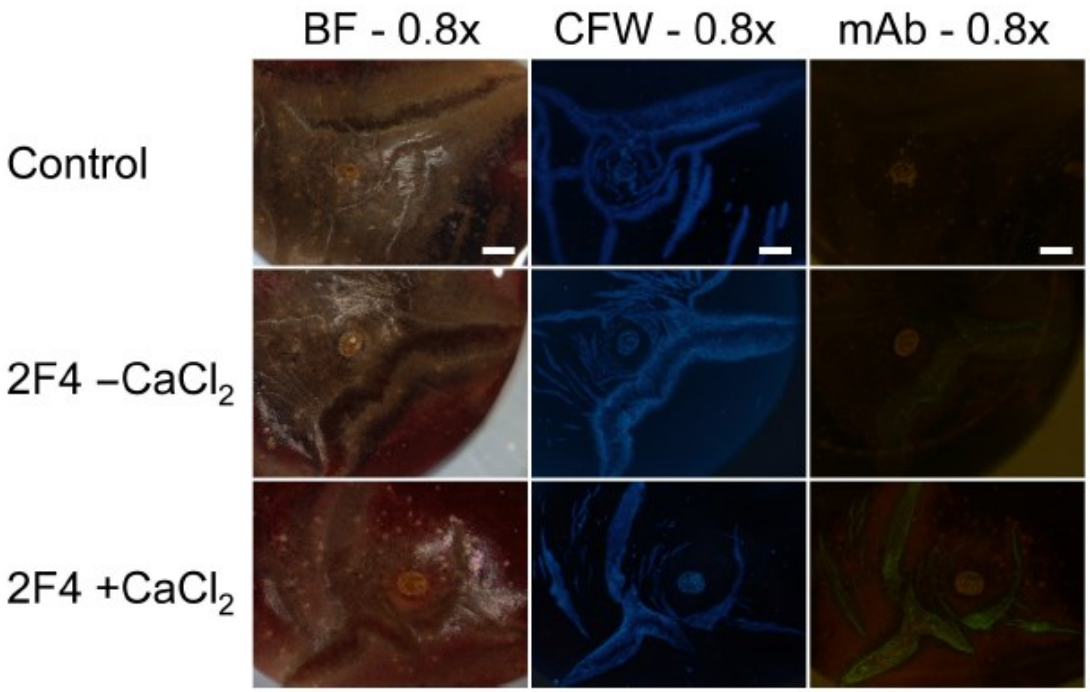

Fig 9. Composite of micrographs of 'Burlat' sweet cherry fruit that had cracked in the stylar scar region during incubation in deionized water. Images were taken following staining with calcofluor white (CFW) or following binding of the monoclonal antibody (mAb) 2F4 in the absence (2F4, -$CaCl_2$) or presence of Ca (2F4, +$CaCl_2$). The mAb 2F4 identifies dimeric associations of homogalacturonan chains with Ca^{2+}. Images were viewed under bright field (BF), in UV (CFW) or in fluorescent light (mAb). All images at 0.8x. Scale bars = 1 mm.

https://doi.org/10.1371/journal.pone.0247692.g002

Reference

1. Schumann C, Winkler A, Brüggenwirth M, Köpcke K, Knoche M (2019) Crack initiation and propagation in sweet cherry skin: A simple chain reaction causes the crack to 'run'. PLoS ONE 14(7): e0219794. https://doi.org/10.1371/journal.pone.0219794 PMID: 31365556

3.2 Swelling of cell walls in mature sweet cherry fruit: factors and mechanisms

Das Original dieses Artikels wurde 2020 in der Zeitschrift „Planta“ veröffentlicht.

Schumann, C. and Knoche M. (2020): Swelling of cell walls in mature sweet cherry fruit: factors and mechanisms. *Planta*. 251:65

DOI: https://doi.org/10.1007/s00425-020-03352-y

Beteiligung der Autoren

M. Knoche warb die Drittmittel für das Vorhaben ein. M. Knoche, und C. Schumann planten die Experimente. C. Schumann führten die Experimente durch. M. Knoche und C. Schumann analysierten die Daten. M. Knoche und C. Schumann schrieben und editierten das Manuskript. M. Knoche und C. Schumann revidierten das Manuskript.

Planta (2020) 251:65
https://doi.org/10.1007/s00425-020-03352-y

ORIGINAL ARTICLE

Swelling of cell walls in mature sweet cherry fruit: factors and mechanisms

Christine Schumann[1] · Moritz Knoche[1]

Received: 27 August 2019 / Accepted: 30 January 2020 / Published online: 14 February 2020

Abstract

Main conclusion **Swelling of sweet cherry cell walls is a physical process counterbalanced by turgor. Cell turgor prevents swelling in intact cells, whereas loss of turgor allows cell walls to swell.**

Abstract Swelling of epidermal cell walls precedes skin failure in sweet cherry (*Prunus avium*) cracking. Swollen cell walls lead to diminished cell:cell adhesions. We identify the mechanism of cell wall swelling. Swelling was quantified microscopically on epidermal sections following freeze/thaw treatment or by determining swelling pressure or swelling capacity of cell wall extracts. Releasing turgor by a freeze/thaw treatment increased cell wall thickness 1.6-fold within 2 h. Pressurizing cell wall extracts at > 12 kPa prevented swelling in water, while releasing the pressure increased swelling. The effect was fully reversible. Across cultivars, cell wall thickness before and after turgor release in two subsequent seasons was significantly correlated (before release of turgor: $r = 0.71^{**}$, $n = 14$; after release of turgor: $r = 0.73^{**}$, $n = 14$) as was the swelling of cell walls upon turgor release ($r = 0.71^{**}$, $n = 14$). Close relationships were also identified for cell wall thickness of fruit of the same cultivars grown in the greenhouse and the field (before release of turgor: $r = 0.60$, $n = 10$; after release of turgor: $r = 0.78^{**}$, $n = 10$). Release of turgor by heating, plasmolysis, incubation in solvents or surfactants resulted in similar swelling (range 2.0–3.1 µm). Cell wall swelling increased from 1.4 to 3.0 µm as pH increased from pH 2.0 to 5.0 but remained nearly constant between pH 5.0 and 8.0. Increasing ethanol concentration decreased swelling. Swelling of sweet cherry cell walls is a physical process counterbalanced by turgor.

Keywords Cell wall swelling · Cracking · Epidermis · Pectin · *Prunus avium* · Splitting

Abbreviations

AIR	Alcohol-insoluble residue
ES	Epidermal skin section(s)
PEG	Polyethylene glycol
SC	Swelling capacity

Introduction

Rain cracking severely limits the production of many soft, fleshy, fruit species in all regions of the world where rain occurs during the harvest period. Sweet cherries (*Prunus avium*) and grapes (*Vitis vinifera*) are prominent examples of high-value crops in which rain cracking can be commercially devastating—but there are many others, including tomatoes (*Solanum lycopersicum*), blueberries (*Vaccinium corymbosum*) and plums (*Prunus* × *domestica*).

The primary cause of rain cracking in a fleshy fruit has for many years been thought to be an excessive internal (tissue) pressure (Considine and Kriedemann 1972; Sekse et al. 2005; Measham et al. 2009), where this excessive pressure is a direct result of osmotic water uptake through the fruit's rain-wetted skin. Thus, the fruit has been assumed to resemble a thin-walled pressure vessel containing a solution rich in osmotically active carbohydrates. The very negative osmotic potential of this solution is the driving force for the osmotic uptake of surface water. The increase in fruit volume and surface area occasioned by water uptake increases the tissue pressure ('turgor') inside the fruit. The fruit is believed to crack when certain critical thresholds of turgor and/or of skin strain are exceeded (Considine and Kriedemann 1972; Andersen and

✉ Moritz Knoche
moritz.knoche@obst.uni-hannover.de

[1] Institute for Horticultural Production Systems, Leibniz-University Hannover, Herrenhäuser Straße 2, 30419 Hannover, Germany

Richardson 1982; Measham et al. 2009). Thus, what we shall refer to as the 'critical turgor/strain' hypothesis offers an intuitively plausible explanation of fruit cracking and, moreover, it is consistent with the observation that rain cracking usually follows extended periods of surface wetness after rainfall and/or dew. However, in recent years, an increasing body of experimental evidence has started to bring this old hypothesis into question. More recently, still it has led to its rejection among many researchers. For a review, see Knoche and Winkler (2017).

The 'zipper' hypothesis offers an alternative understanding that remains consistent with the general phenomenological observations—cracking is associated with rain/dew-wetted fruit skin—but is also consistent with a new body of careful experimental data which does not align well with the 'critical turgor/strain' hypothesis (Knoche and Winkler 2017). Cracking is now considered to be a multistep process comprising: (i) the formation of microcracks due to cuticular strain caused by downregulation of cutin and wax synthesis and deposition during early growth (Knoche et al. 2004; Peschel and Knoche 2005; Alkio et al. 2012) and the later exposure of the strained cuticle to wetness (Knoche and Peschel 2006), (ii) localized water penetration through microcracks (Winkler et al. 2016), (iii) the bursting of individual mesocarp cells and the consequent leakage of malic acid into the cell-wall-free space that further damages adjacent cells including those of the epidermis (Winkler et al. 2015; Grimm et al. 2019), and (iv) the complete loss of the (already low) turgor that results in cell wall swelling (Grimm and Knoche 2015). Lastly, cell wall swelling decreases cell wall stiffness, fracture tension and cell:cell adhesion resulting in the separation of neighboring cells (Brüggenwirth and Knoche 2017). The tension generated by the skin strain is sufficient to cause cells to separate along their swollen walls and to rupture the skin. Thus, the skin 'unzips'—that is, starting from a single-point failure, a skin crack propagates linearly in a manner similar to the opening up of a garment with a 'zipper' and somewhat analogous to the propagation of a 'ladder' in a piece of knitted fabric (Grimm et al. 2019). Based on the 'zipper' hypothesis, the swelling of cell walls is an essential part of the decrease in the fracture stress and in cell:cell adhesion. The swelling of cell walls is also a key textural characteristic of fleshy fruit that develops a desirable 'melting' texture during ripening (Redgwell et al. 1997). Little is known about cell wall swelling in sweet cherry.

The objectives of our study were (i) to characterize swelling of epidermal cell walls in sweet and sour cherries and (ii) to identify the underlying mechanism(s). These steps are a prerequisite for identifying the cell wall fraction responsible for cell wall swelling. A better understanding of cell wall swelling may be helpful in developing strategies to counter the cracking of fleshy fruit by a combination of breeding and cultural means.

Materials and methods

Plant material

Sweet cherry fruit (*Prunus avium* L.) of 14 cultivars ('Adriana', 'Burlat', 'Dönissens Gelbe', 'Earlise', 'Fabiola', 'Hedelfinger', 'Kordia', 'Merchant', 'Regina', 'Sam', 'Samba', 'Schneiders Späte', 'Staccato' and 'Sweetheart') and sour cherry fruit (*Prunus cerasus*) of 2 cultivars ('Achat' and 'Morellenfeuer') were harvested at commercial maturity. The stage of maturity was judged based on fruit size and color by our experienced workers at the Horticultural Research Station of the Leibniz University in Ruthe (lat. 52°14′ N, long. 9°49′ E) over two growing seasons. The growing conditions differed between the two season. In 2015, average temperatures in the field in May and June were lower by 3.3 and 1.7 °C than in 2016, respectively, the July temperatures were about similar. Average temperatures in August 2015 were warmer by 1.5 °C than in 2016. The sweet cherries were grafted on 'Gisela 5' rootstocks (*Prunus cerasus*×*P. canescens*) and the sour cherries on 'Maxma Delbard' rootstocks (*P. avium*×*P. mahaleb*). The trees were cultivated either under a rain cover in the field or in a greenhouse. Mean temperatures in the greenhouse were higher by 1.6 °C and 1.1 °C in the 2015 and 2016 growing season as compared to the field. There was no application of foliage applied Ca fertilizers in either season at either site. Unless otherwise stated, fruit were processed fresh on the day of sampling or stored at − 20 °C until cell-wall extraction. In addition, off-season 'Lapins' sweet cherries from New Zealand (2016) and 'Santina' sweet cherry from Chile (2019) were purchased locally. All fruits were selected for uniformity of development based on size and color and for freedom from visual defects.

Microscopy

To determine cell wall swelling, epidermal skin sections (ES) were prepared, usually from the equatorial plane of the cheek. Narrow strips of skin were excised using parallel razor blades (3 mm between blades). The ES were then pared down from the inner surface, to remove much of the cortical tissue. The ES were carefully blotted using soft tissue paper, transferred immediately to the stage of a microscope (BX-60; Olympus, Hamburg, Germany), placed in a droplet of test solution (usually a 10 mM MES solution at pH 5.8) and viewed at a magnification of 40×. Calibrated digital photographs (camera: DP73; Olympus) were taken and the thickness of the anticlinal cell walls quantified by image analysis (cellSens; Olympus Soft Imaging Solutions, Münster, Germany). This measurement reflects the initial cell wall thickness between two living turgid cells,

and before the imposition of any treatment ('+turgor'). This measurement—protoplast to protoplast—included the cell walls of two abutting cells, plus the intervening middle lamella. Cell wall thickness was later re-measured following treatment to minimize turgor ('− turgor') and to maximize cell wall swelling (a freeze/thaw treatment for a minimum of 12 h at − 20 °C followed by (usually) 48 h equilibration at room temperature). The only exceptions were experiments on the effects of plasmolysis (Fig. 6, Table 4), ethanol concentration (Fig. 9), temperature and turgor removal (Table 3) which were carried out without the freeze/thaw treatment. A total of 10 ES were prepared per treatment (1 ES from each of 10 fruit), 2 micrographs were taken per ES, and 2 cell walls were measured per micrograph, such that the total number of cell wall thickness measurements was 40 per treatment. Cell wall swelling (Δthickness) was calculated by subtracting cell wall thickness immediately after excision ('+turgor') from that 48 h after the freeze/thaw treatment ('− turgor'). Thus, cell wall swelling represented the increase in thickness of two abutting cell walls plus that of the intervening middle lamella.

Experiments

The time course of cell wall swelling was measured on microscopic images of ES prepared from 'Burlat' and 'Lapins' fruit directly after excision (0 h). Thereafter, half of the ES were subjected to a freeze/thaw treatment at − 20 °C overnight to eliminate turgor. Following thawing at ambient temperature (23 °C), cell wall thickness was determined at 0.5, 2, 4, 8, 24, 48, 78 and 144 h. The other half of the sample remained without a freeze/thaw treatment. Here, the ES were incubated in deionized water and cell wall thickness was determined after 2, 4, 8, 24, 56, 96, 120 and 144 h of incubation ('control'). Because the loss of turgor is a prerequisite for cell wall swelling, only cell walls between two non-turgid cells were measured in the control. The only exceptions were those ES that were inspected immediately after excision (0 h).

Swelling of cell walls in different regions of the fruit surface was studied by preparing ES from the shoulder, cheek, suture or the stylar scar region of 'Lapins' fruit.

The effect of turgor on cell wall swelling was established in 'Sam' by eliminating cell turgor. Turgor was eliminated by one of four methods: (i) destroying membrane integrity by a freeze/thaw treatment (16 h at − 20 °C followed by incubation at room temperature for 48 h); (ii) plasmolyzing cells in 2.5 M glucose for 24 h or (iii) solubilizing plasma membranes in either acetone or 20 mM sodium dodecyl sulfate (SDS) for 48 h. In addition, a role of enzymatic activity in cell wall swelling was investigated by denaturation of proteins by heating the ES for 1 h to 60 °C followed by 48 h incubation at room temperature. This treatment also destroyed cell turgor. Another set of ES were incubated for 48 h at room temperature without any pretreatment; these served as controls.

The effects of fruit mass loss during storage (2 °C, 95% RH, 35 d) on cell wall swelling were established in 'Merchant'.

The relationship between turgor and cell wall swelling was studied in ES excised from 'Staccato'. Turgor was varied by incubating ES in 0, 0.25, 0.5, 0.75, 1.0 or 1.5 M sucrose solutions for 48 h. The percentage of plasmolyzed cells and cell wall thickness were determined by microscopy for each sucrose concentration. A cell was counted as plasmolyzed when the symplast began to detach from the cell wall. The osmotic potential at 50% plasmolysis and that at 50% cell wall swelling were calculated using a sigmoidal regression model.

The reversibility of cell wall swelling was studied in a two-phase experiment using 'Santina' sweet cherry. Following measurement of initial cell wall thickness, phase I of the experiment was initiated by incubating ES in hypotonic (0.25 M, − 0.6 MPa) or hypertonic sucrose solutions for 22 h (1.25 M, − 4.8 MPa). Incubation in hypertonic solutions induced plasmolysis in all cells. Cells of ES incubated in hypotonic solutions remained largely turgescent. For phase II of the experiment, half of the ES from the hypertonic sucrose solution (phase I) were transferred to a hypotonic solution and vice versa. Incubation was continued for a further 22 h. For the remaining half of the ES incubation continued in the same solution as during phase I. Incubation in deionized water served as control. Cell wall thickness was quantified after 22 h (end of phase I) and after 44 h (end of phase II).

Whether cell wall thickness is affected by exposure to juice from the same fruit was assessed in ES excised from 'Adriana'. Cell wall thickness was quantified after excision and after incubation in juice extracted from the same batch of fruit using a spaghetti press. In addition, ES were incubated in an 'artificial juice' comprising the major osmolytes of sweet cherry juice (Herrmann 2001). These osmolytes were glucose (277 mM), fructose (253 mM), sorbitol (49 mM), potassium malate (36 mM) and malic acid (9 mM). Together, these account for about 98% of the osmolarity of the juice. Osmolarities were measured by vapor pressure osmometry (VAPRO® 5520 and 5560; Wescor, Logan, UT, USA). To separate the effect of juice from a potential pH effect, artificial juice was prepared without malic acid. Furthermore, the pH of the natural juice was adjusted to pH 6.4 using KOH. Cell wall thickness was quantified after excision ('+turgor') and after a freeze/thaw treatment followed by 48 h incubation in the respective juices ('− turgor'). Deionized water served as control.

The effect of organic acids on cell wall swelling was investigated in 'Adriana'. Cell wall thickness was quantified

after excision of the ES. The ES were then incubated in oxalic, tartaric, malic, citric and ascorbic acid (all at 20 mM, all solutions prepared in 10 mM MES at pH 5.8). An MES buffer treatment without addition of acid served as control. Thereafter, the ES were subjected to a freeze/thaw cycle. Following a 48 h equilibration period, cell wall thickness was quantified again. The effect of pH on cell wall swelling was investigated in 'Adriana' fruit. The ES were incubated in 10 mM MES buffer with pH adjusted to pH 2, 3, 4, 5, 6, 7 and 9 using HCl (all pH ≤ 4) or KOH (all pH > 4). Thereafter, the effect of different buffers on cell wall swelling was studied at constant pH. The ES were incubated in citrate, phosphate, HEPES, MES and TRIS buffer (all at 10 mM) at pH 6.7. The pH was adjusted using HCl or KOH. Separate ES incubated in deionized water served as controls. Cell wall thicknesses after excision ('+turgor') and after a freeze/thaw treatment followed by 48 h of incubation ('− turgor') were quantified and cell wall swelling calculated as described earlier.

The effect of ethanol concentration on cell wall thickness was determined using ES and extracted cell walls prepared from 'Sweetheart'. In phase I of the experiment, 20 skin sections were prepared from 10 fruits. Cell wall thickness was determined after excision and after incubation in 0, 25, 50, 75, 87.5 and 99.8% aqueous ethanol for 48 h. For the subsequent phase II, half the sections were transferred from the initial incubation solution to 99.8% ethanol. The other half were transferred into 100% deionized water. All were again incubated for 48 h and cell wall thickness re-determined.

The effect of temperature on cell wall swelling was studied in 'Merchant' ES incubated in 10 mM MES at 4 °C or at 23 °C for 48 h.

The effect of the molar mass (g mol^{-1}) and concentration (g kg^{-1}) of polyethylene glycols (PEGs) on the thickness of cell walls was estimated in ES from 'Staccato'. Initial cell wall thickness was measured ($n = 50$ fruit with four cell walls measured per image). The cell wall thickness so obtained, represented the native thickness of fully turgid cells. Thereafter, fruit were incubated in solutions of PEGs of mean molar mass: 300, 600, 1000, 1500, 3350 and 6000 g mol^{-1} of 0, 100, 200, 300, 350, 400, 450 or 500 g kg^{-1}. Sucrose solutions at comparable osmolarities served as controls. The osmolarities of all solutions were measured by vapor pressure osmometry. Following a freeze/thaw treatment to destroy turgor, and after 48 h of incubation, cell wall thickness was re-determined according to the procedure described above. The osmotic potential at half maximum swelling was calculated for the different PEG molecules from a non-linear regression line fitted through a plot of cell wall swelling vs. osmotic potential. In addition, swelling was expressed as a function of the concentration of ethylene glycol units for all PEG molecules, at all PEG concentrations.

Preparation of extracted cell walls

Extracted cell walls were prepared using the protocol by Sozzi et al. (2002) with minor modifications. Pedicel and pit were removed from ten frozen fruit and the remaining tissue homogenized in 4 ml per g tissue of 80% (v/v) ice cold ethanol for 2 min. The homogenate was boiled for 30 min, cooled and then filtered through glass filter paper (Whatman GF/C; Sigma-Aldrich, St. Louis, MO, USA). The insoluble material was washed with 95% (v/v) ethanol and filtered again, then extracted with 3 ml per g tissue of chloroform:methanol (1:1, v/v) for 15 min, filtered and washed again with the same solvent mixture followed by a final washing step with acetone. The resulting alcohol insoluble residue (AIR) was dried overnight, weighed and stored over dry silica gel until further usage.

Determination of swelling pressure

To quantify the pressure generated by swelling cell walls the following procedure was developed. A 25 mg sample of AIR was transferred to a custom-built pressure chamber. This chamber had an inner diameter of 25.5 mm and a port in the base for drainage covered by a stainless steel frit. Wetting of the AIR in the pressure chamber was achieved using 70% (v/v) aqueous ethanol and a mild vacuum of 20 kPa for 10 min. Earlier experiments established that there is no cell wall swelling when incubating ES in 70% aqueous ethanol. The pressure chamber was positioned under a universal material testing machine (BXC-FR2.5TN; ZwickRoell GmbH & Co. KG, Ulm, Germany) equipped with a 50 N force transducer (KAP-Z; ZwickRoell). A second stainless steel frit (25.4 mm diameter) was fitted to the force transducer. This frit served as a plunger to pressurize the cell wall in the pressure chamber. To reproducibly determine the minimum volume (V_{min}) of the hydrated and non-swollen cell wall, the AIR was pressurized with 10.3 kPa for 12 h at the onset of each experiment and the V_{min} was read. After 10 min, the supernatant containing 70% aqueous ethanol was replaced by the same volume of deionized water. Swelling was quantified by reducing the pressure stepwise: 9.9, 4.9, 2.0, 1.0, 0.5–0.2 kPa. The pressure was held constant at each step for 12 h. Preliminary experiments established this time was required to approach an equilibrium volume of swollen cell walls at each pressure. During the experiment, the position of the plunger was recorded by the distance transducer of the universal testing machine. From the position of the plunger, the volume change (ΔV) due to cell

wall swelling was calculated as the difference between the volume at a particular pressure minus the minimum volume (V_{min}). The swelling pressure (P_0) of the AIR was calculated as the x-intercept of a plot of the change in volume (ΔV) at equilibrium at each pressure vs. the natural logarithm of the applied pressure. The determination of swelling pressure was carried out with three replications.

In a second run of the experiment, the 70% aqueous ethanol was not removed from the supernatant. The volumes resulting from stepwise releases of pressure were recorded as described before. Here, the equilibration time was set at 6 h. The experiment was conducted in triplicate.

Whether swelling of AIR is reversible was investigated by subjecting extracted cell walls to ascending and descending pressures. During phase I, pressure was decreased stepwise as described above. In phase II, pressure was increased again using the same pressure steps as in phase I. The treatments were repeated during the subsequent phases III and IV. The volumes of the cell wall extracts at anyone pressure were recorded with an equilibration time of 6 h and the (ΔV) and the swelling pressures for phases I–IV calculated as described above. The experiment was conducted in triplicate.

Determination of swelling capacity (SC)

The swelling capacity (SC) of the AIR is an established characteristic to quantify cell wall swelling (Raghavendra et al. 2004; Basanta et al. 2014). Here, we followed the procedure described by Raghavendra et al. (2004) and Basanta et al. (2014) with minor modifications. The AIR was ground thoroughly using a pestle and mortar. A sample of 50 mg (±0.1 mg) of AIR was weighed into a graduated conical tube and 7.5 ml of degassed 10 mM MES (pH 5.8) was added. To ensure thorough wetting and remove all air, the AIR was vacuum infiltrated three times for 10 min each at 3 kPa. Following an 18 h incubation at 22 °C to reach equilibrium swelling, the final volume of the swollen cell wall was read and the SC was calculated as follows:

$$\mathrm{SC}\left(\mathrm{ml\,g^{-1}}\right) = \frac{\text{Volume of swollen AIR (ml)}}{\text{Original sample dry weight (g)}}.$$

The SC determinations were always carried out with three replications.

The effect of different ethanol concentrations on swelling of the AIR was studied. The AIR was prepared from the same batch of 'Sweetheart' fruit as that investigated in the microscopy assay. The AIR was incubated in 0, 25, 50, 75 and 100% of aqueous ethanol for 18 h. The swelling capacity was calculated as described below.

Data analyses

The data presented in the tables and figures represent the arithmetic means and standard errors. Where error bars are not visible in figures, they are smaller than the data symbols. Data were examined by analysis of variance (AOV) followed by mean comparisons using Tukey's Studentized range test at $p < 0.05$ with R (packet multcomp 1.4–0, procedure glht, R 3.0.2; R Foundation for Statistical Computing, Vienna, Austria). Linear and non-linear regression analysis was conducted using R (packet multcomp 1.4–0, procedure lm and nls). Significance of coefficients of correlation (r) and determination (R^2) at $p < 0.05$, 0.01 or 0.001 is indicated by *, ** or ***, respectively.

Results

Increasing percentages of epidermal cells collapsed when skin segments were incubated in deionized water. This was indexed by loss of anthocyanins from the vacuoles (Fig. 1). The cell walls between pairs of collapsed (non-turgid) cells began to swell. Thickness of cell walls between collapsed cells did not differ from those in tissue that had lost turgor following membrane damage caused by a freeze/thaw treatment (data not shown).

A time course study of cell wall swelling following loss of turgor caused by a freeze/thaw treatment established that swelling was rapid. Within 24 h, cell wall swelling had approached an asymptote averaging 5.4 µm (Fig. 2). This represents a 61% increase in cell wall thickness compared with that for turgid cells before the freeze/thaw treatment. To ensure equilibrium swelling in all subsequent comparisons, we chose a standard equilibration time of 48 h after turgor removal.

When extracted cell walls were pressurized to 10.3 kPa, their change in volume was as depicted in Fig. 3a. This pressure was selected, because it corresponds to the mean turgor reported for mature sweet cherry fruit (Schumann et al. 2014). When holding this pressure for 12 h, there was no further detectable increase in volume, indicating that swelling had reached equilibrium (Fig. 3a). When cell walls were incubated in water (but not when incubated in 70% aqueous ethanol, Fig. 3c), stepwise releases of pressure resulted in corresponding stepwise increases in cell wall volume (Fig. 3b). The relationship between the change in cell wall volume (ΔV) and the natural logarithm of the applied pressure was linear (Fig. 3d). From this relationship, the pressure required to prevent swelling (P_0) was estimated at ≈ 12 kPa ($R^2 = 0.99$; Fig. 3d).

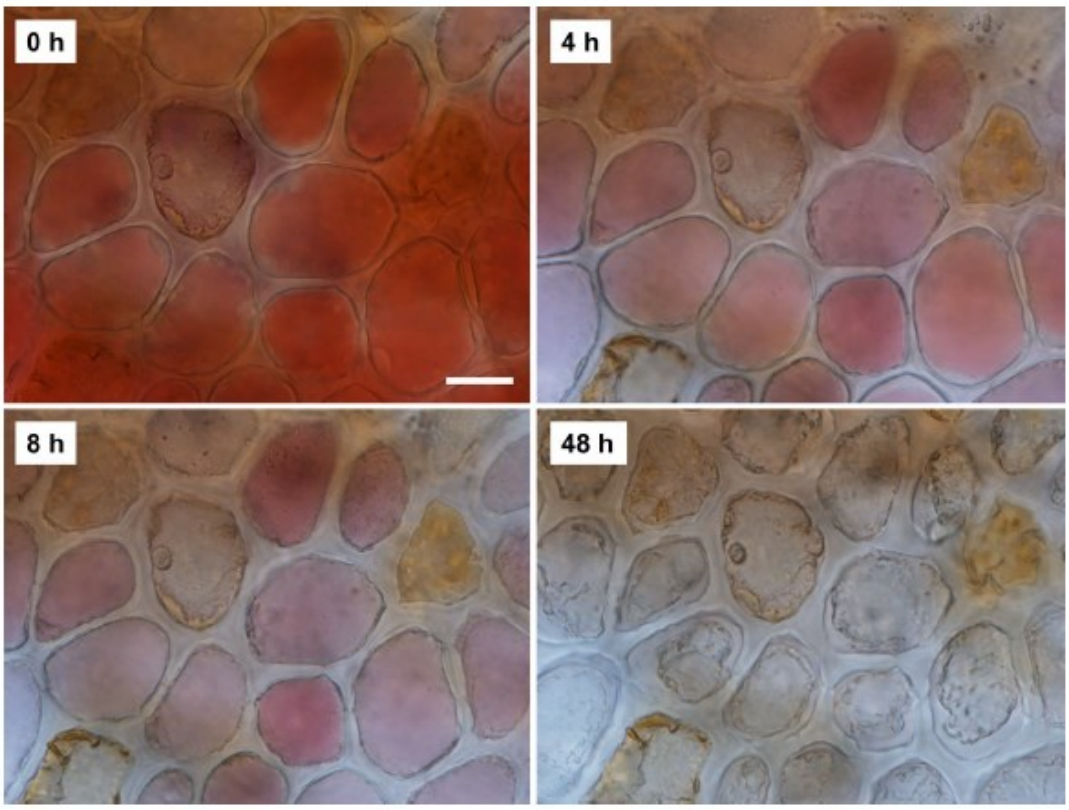

Fig. 1 Micrographs of a time course of change in cell wall thickness of anticlinal walls of epidermal cells of mature 'Lapins' sweet cherry after incubation in deionized water for 0, 4, 8 or 48 h. Bar = 20 µm

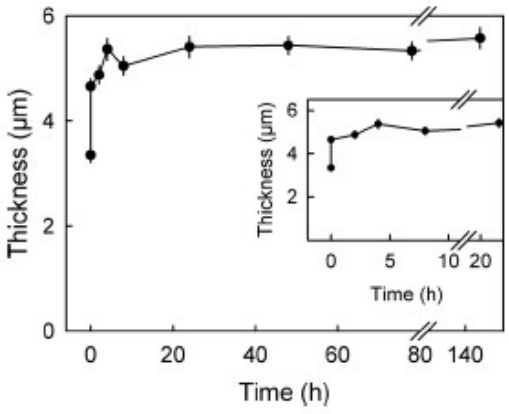

Fig. 2 Time course of change in thickness of anticlinal epidermal cell walls of mature 'Burlat' sweet cherry skin sections. Main graph: long-term time course. Inset: short-term time course. Data are redrawn from main graph but on a different scale. The increase in thickness was monitored after releasing turgor by a freeze/thaw treatment ($n = 40$)

Ascending and descending pressure had the same effect on cell wall swelling regardless of whether these were applied during the first cycle (phases I and II) or the second cycle (phases III and IV) (Fig. 4). There was no significant difference in swelling pressure between ascending and descending pressures during the first or second cycle (Fig. 4c).

Significant differences in cell wall thickness and swelling were detected between different sweet cherry cultivars. Swelling was largest in 'Staccato' and lowest in 'Dönissens Gelbe' (Table 1). There were no consistent differences between the sweet and the sour cherries in the extent of cell wall swelling with turgor release.

Across cultivars, cell wall thickness and cell wall swelling following turgor release were significantly correlated between different seasons (Fig. 5a, b). Also, cell wall thickness did not differ significantly between greenhouse-grown fruit and rain-shelter-grown fruit, i.e. cell wall thickness data from the two sites were closely related (Fig. 5c). The

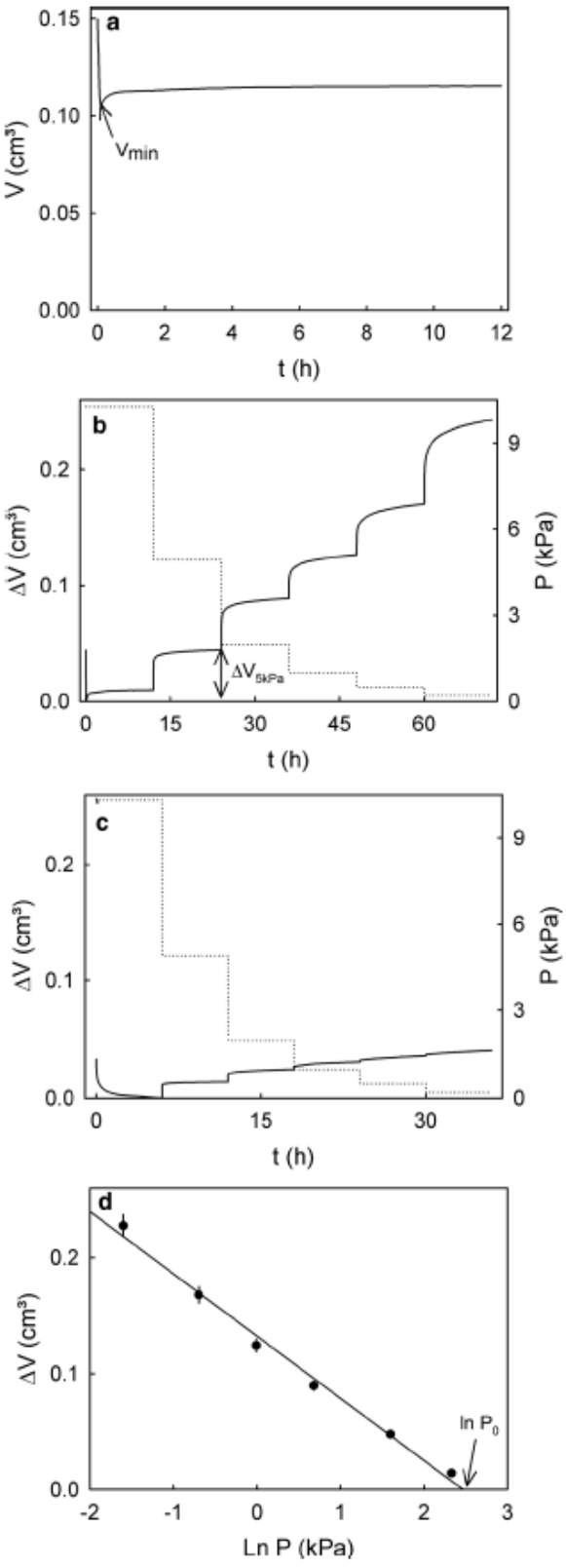

Fig. 3 Swelling of extracted cell walls of mature 'Staccato' sweet cherry when incubated in deionized water (**a, b, d**) or in ethanol (**c**). Swelling was quantified as the change in volume (ΔV) at different pressures (P) using a custom-built pressure chamber. Extracted cell wall was incubated in water to induce swelling. The volume of swollen cell walls after loading the cell wall with different pressures was quantified. **a** Time course of water-induced swelling of cell walls at a pressure of 10.3 kPa. **b, c** Representative test program to monitor the increase in volume of extracted cell walls when decreasing the applied pressure stepwise from 10.3 to 0.1 kPa. At any one pressure step, pressure was held constant for 12 h (**a**) or 6 h (**c**) to allow for equilibration of cell wall swelling. **d** Relationship between the swelling of cell walls (ΔV) at equilibrium and the applied pressure. The swelling pressure P_0 corresponds to the pressure at which no swelling occurs. The value P_0 was estimated as the x-intercept of a regression line fitted through a plot of ΔV vs. ln P. The regression equation was $\Delta V = -0.054\ (\pm 0.002) * \ln P\ (\text{kPa}) + 0.132\ (\pm 0.003)$, $R^2 = 0.99^{***}$. Data in **a, b** and **c** represent a single replicate, those in **d** means ± SE, $n = 3$

increase in cell wall thickness was independent of the initial cell wall thickness (Fig. 5d).

Cell wall swelling was greater in the stylar scar region than in the cheek, suture or shoulder regions (Table 2).

There was little difference in the extent of cell wall swelling among the various methods used to release turgor (Table 3). Thus, significant swelling occurred following release of turgor by: freeze/thaw, heating to 60 °C, plasmolysis, or incubation in acetone or in SDS surfactant.

Incubation of ES in sucrose solutions of decreasing (increasingly negative) osmotic potential caused progressive increases in plasmolysis (Fig. 6a). ES incubated in deionized water but not those in sucrose solutions lost vitality as indexed by a coagulated cytoplasm and the absence of an intact vacuole. Incubation in sucrose solutions increased cell wall swelling markedly when osmotic potential was more negative than about − 2 MPa (Fig. 6b; Table 4). There was no difference in cell wall swelling between ES incubated in deionized water and those incubated in solutions having an osmotic potential below − 2 MPa Fig. 6b; Table 4). The fraction of cells plasmolyzed increased as the osmotic potential of the incubation solution decreased (Fig. 6c). The values of osmotic potential corresponding to 50% cell wall swelling and to 50% plasmolysis were estimated at − 2.0 and − 1.3 MPa, respectively. Deplasmolysing cells by transferring ES from a hypertonic into a hypotonic sucrose solution decreased cell wall thickness to the level not significantly different from the thickness immediately after excision of the ES (Table 4). Thus, the increase in cell wall thickness upon plasmolysis was completely reversible (Table 4).

Fruit weight loss during a 35 day storage period had no significant effect on cell wall thickness or on cell wall swelling (following turgor release) (Fig. 7).

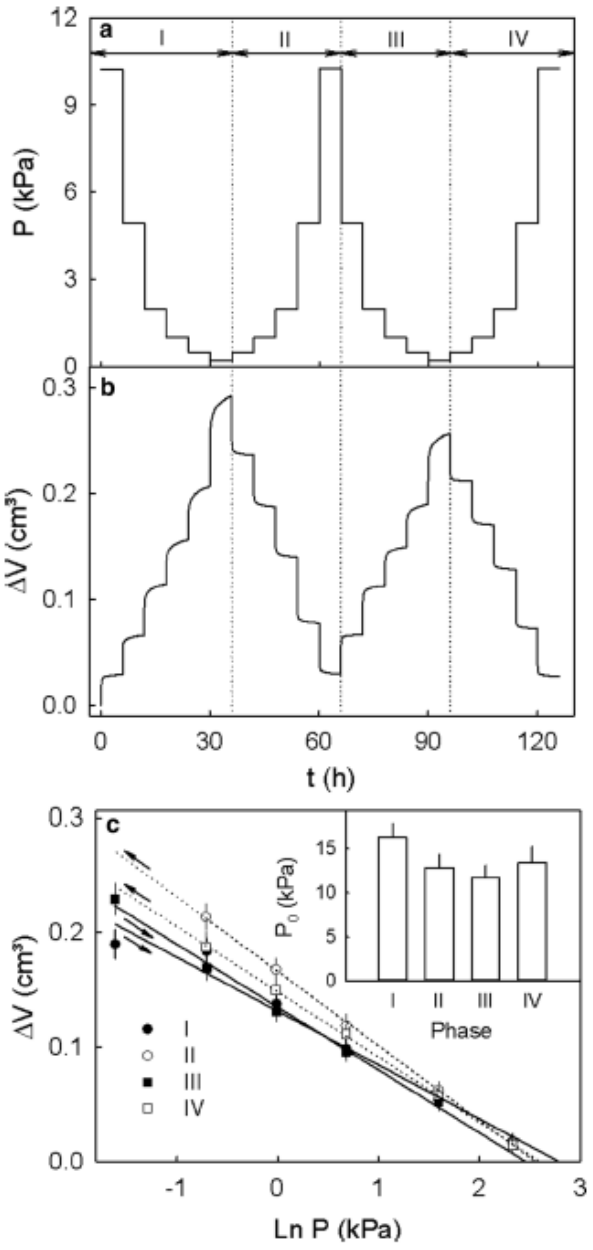

Fig. 4 Effect of ascending and descending pressures on the swelling of extracted cell walls of mature 'Staccato' sweet cherry when incubated in deionized water. Swelling was quantified as the change in volume (ΔV) at different pressures (P) using a custom-built pressure chamber. **a**, **b** Time course of (**a**) descending (phases I, III) and ascending pressures (phases II and IV) and (**b**) corresponding changes in volume of extracted cell walls (ΔV). Horizontal arrows in **a** indicate the four consecutive phases I to IV of the experiment. During phases I and III pressure was decreased stepwise, during phases II and IV pressure was increased. **c** Relationship between the swelling of cell walls at equilibrium and the natural logarithm of the applied pressure in phases I to IV. Inset: swelling pressures (P_0) during phases I, II, III and IV. The P_0 corresponds to the pressure at which no swelling occurs. Data in **b** represent a single replicate, those in **c** means ± SE, $n = 3$

Interestingly, when ES were incubated in sweet cherry juice extracted from the same batch of fruit, marked swelling of cell walls occurred after turgor release by a freeze/thaw treatment (Table 5). The increase in cell wall thickness following turgor release was large when ES were incubated in juice extracted from the same batch of fruit at the natural pH 3.9. Adjusting the pH of the juice to a value comparable to that of the MES control, markedly reduced cell wall swelling to values even lower than in the MES control. Compared to natural juice at natural pH, artificial juice prepared using the five major osmolytes present in sweet cherries had a low pH and an even larger effect on cell wall swelling following freeze/thaw turgor release. As in the natural juice, the effect on swelling decreased markedly to below the control values following the pH adjustment.

There was little difference in cell wall thickness of ES incubated in a range of organic acids, compared to the swelling of cell walls incubated in an MES-buffered control (Table 6). The only exception was in oxalic acid that caused significantly more swelling than in the control.

The pH of the incubation solution had a marked effect on cell wall thickness and swelling in the absence of turgor (Fig. 8). Relationships were biphasic. Cell wall thickness and swelling were essentially independent of pH between pH 8.0 and pH 5.0. Then, as pH decreased from pH 5.0 to pH 2.0, swelling increased markedly (Fig. 8a, b). The breakpoint of the biphasic relationship was calculated to be pH 5.2. The buffer used to adjust pH also had a significant effect on cell wall swelling (Fig. 8c). Swelling was greatest in citric acid buffer, intermediate in phosphate, MES or TRIS buffer and the water control, and it was least in HEPES.

There was no cell wall swelling when ES were then incubated in 99.8, 87.5 or 75% ethanol (Fig. 9a). As the ethanol concentration decreased below 75%, cell wall swelling increased and reached a maximum when the ES was incubated in deionized water (no ethanol). When an ES was transferred from aqueous ethanol to water or to 99.8% ethanol, the ES now incubated in water had fully swollen cell walls regardless of the ethanol concentration during the phase I of the experiment. Meanwhile, those now incubated in 99.8% ethanol were all non-swollen regardless of the initial ethanol concentration during the first phase of the experiment (Fig. 9b). When determining the effect of the ethanol concentration on the swelling capacity of the AIR prepared from the same batch of fruit, the swelling capacity decreased linearly as ethanol concentrations increased (Fig. 9c). There was a close and linear relationship between the swelling capacity of extracted cell walls and the swelling quantified microscopically using ES (Fig. 9c, inset). The regression equation was: SC (ml g^{-1}) = 82.65 (± 1.79) − 0.63 (± 0.03) × Thickness (µm); $R^2 = 0.99$***.

Table 1 Thickness and swelling (Δthickness) of anticlinal epidermal cell walls of the epidermis of mature sweet and sour cherry fruit of various cultivars before ('+turgor') and after incubation for 48 h in deionized water ('− turgor')

Fruit cultivar	Mass (g)	Osmolarity (mmol kg^{-1})	Thickness (µm)		ΔThickness	
			+turgor	− turgor	µm	% increase
Achat	6.2±0.2	1252±15	3.5±0.2 a[a]	5.3±0.2 a	1.8±0.2	50
Burlat	10.8±0.5	1230±59	2.2±0.1 bd	5.4±0.2 ab	3.2±0.2	144
Dönissens Gelbe	5.7±0.2	1232±46	3.2±0.1 ac	5.8±0.1 ab	2.6±0.2	83
Fabiola	13.0±0.2	1227±28	2.4±0.1 bd	5.4±0.1 ab	3.0±0.2	126
Hedelfinger	9.2±0.1	1284±40	3.1±0.1 c	6.0±0.2 b	3.0±0.2	97
Kordia	8.4±0.4	991±36	2.6±0.1 bc	5.9±0.1 ab	3.3±0.1	126
Morellenfeuer	5.7±0.2	1006±42	2.3±0.1 bd	5.0±0.2 ac	2.8±0.2	125
Regina	9.8±0.6	1271±82	2.6±0.1 b	5.6±0.2 ab	3.1±0.2	121
Sam	10.1±0.5	1456±85	2.5±0.1 bd	5.5±0.2 ab	3.0±0.2	124
Samba	8.8±0.1	1089±35	2.1±0.1 bd	4.5±0.1 c	2.4±0.1	114
Staccato	8.10±0.2	1117±79	2.8±0.1 c	6.9±0.2 d	4.2±0.2	150
Grand mean	8.7±0.7	1196±41	2.7±0.1	5.6±0.2	2.9±0.2	114

Swelling was calculated as the cell wall thickness after incubation, minus that before incubation. All fruit were grown in the field in the 2015 growing season. 'Achat' and 'Morellenfeuer' are sour cherries, all the others are sweet cherries. Data are means ± SE, $n = 10$ for mass and osmolarity, $n = 40$ for cell wall thickness

[a]Mean separation within columns by Tukey's Studentized range test, $p < 0.05$

Increasing the temperature from 4 to 23 °C slightly increased cell wall swelling by 3.6 ± 0.2 µm at 4 °C and by 4.3 ± 0.2 µm at 23 °C.

Following a freeze/thaw treatment, incubation of ES in PEG solutions induced cell wall swelling. For a particular size of PEG molecule, decreasing (more negative) the osmotic potential, caused a decrease in cell wall swelling, compared to the fully swollen control (Fig. 10a). The osmotic potential at half maximum swelling ($\psi_{\pi 50}$) was calculated from the relationship between cell wall thickness and PEG solution osmotic potential. The value for $\psi_{\pi 50}$ decreased exponentially as the molar mass of the PEG molecules increased (Fig. 10b). Interestingly, a common relationship for the different PEG molecules at the different osmotic potentials was obtained when cell wall thickness was expressed as a function of the number of ethylene glycol units in solution across all PEGs and across all osmotic potentials (Fig. 10c). Cell wall swelling increased markedly at low ethylene glycol concentrations (i.e. below 50 units ethylene glycol kg^{-1}). In concentrations above 50 units of ethylene glycol kg^{-1}, there were no changes in cell wall swelling.

Discussion

Our experiments establish several important findings.

1. Significant cell wall swelling occurs in mature sweet cherry fruit as indexed by microscopy of skin sections, by determinations of the swelling capacity or by the swelling pressure of extracted cell walls;
2. Cell wall swelling is a physical process resulting from the release of cell turgor.

Characterizing swelling using microscopy of skin sections, determinations of the swelling capacity or using a pressure chamber

Microscopy of skin sections, assessment of their swelling capacity and swelling pressure, established that there is significant swelling of cell walls in mature sweet cherry fruit. Furthermore, correlation analysis demonstrated that in vivo swelling (as quantified by microscopy on ES) and in vitro swelling (as indexed by determinations of the swelling capacity in AIR) were significantly and positively related across a range of ethanol concentrations. Sweet cherry belongs to that group of fruit species characterized by their possession of a 'soft and melting' texture for which cell wall swelling during ripening is typical (Redgwell et al. 1997).

In our research, we used different cultivars and production sites to extend the experimental season. Because sweet cherry is a highly perishable crop, fruit of anyone cultivar is available at the optimal stage of commercial maturity only for a few days. The change of cultivars is, therefore, mandatory, if compromises in fruit quality (for example due to the

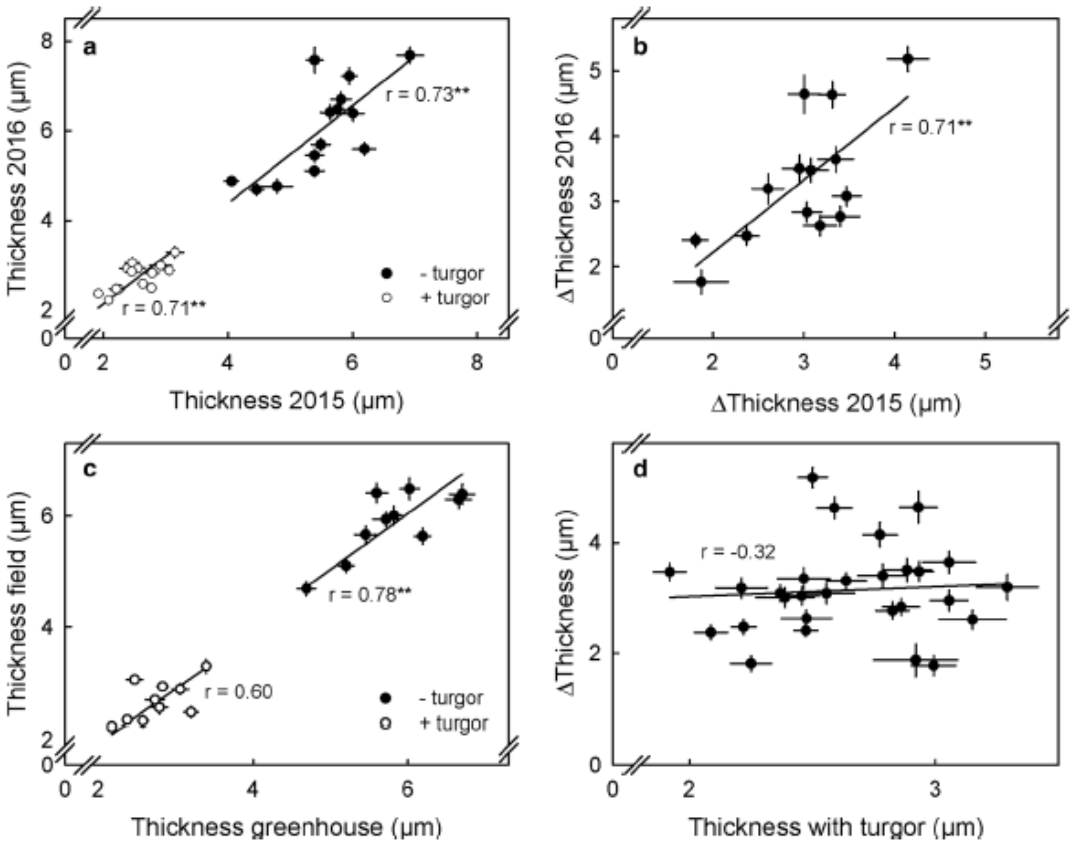

Fig. 5 **a**, **b** Relationship between thickness (**a**) or Δthickness (swelling, **b**) of anticlinal epidermal cell walls of skin sections of 14 sweet cherry cultivars over two consecutive growing seasons. Data points represent means ± SE ($n = 40$). **c**, **d** Relationship between thickness (**c**) or Δthickness (**d**) of anticlinal epidermal cell walls of skin sections of ten sweet cherry cultivars grown in a greenhouse or in the field under a rain-shelter. The change in cell wall thickness (Δthickness) was 48 h after the release of turgor by a freeze/thaw treatment. Skin sections were incubated in 10 mM MES buffered deionized water at pH 5.8. The Δthickness was calculated as the thickness of swollen cell walls (without turgor, '− turgor') minus that of cells with turgor ('+ turgor'). Data points represent means ± SE ($n = 40$)

Table 2 Thickness and swelling (Δthickness) of anticlinal epidermal cell walls of skin sections excised from different positions on the surface of 'Lapins' sweet cherry fruit following incubation in deionized water

Position	Thickness (µm)		ΔThickness (µm)
	+ turgor	− turgor	
Cheek	2.6 ± 0.1 a[a]	4.3 ± 0.1 a	1.7 ± 0.1
Suture	2.6 ± 0.1 a	4.5 ± 0.1 a	1.9 ± 0.2
Stylar scar	2.7 ± 0.1 a	5.7 ± 0.1 b	3.0 ± 0.2
Shoulder	2.8 ± 0.1 a	4.5 ± 0.1 a	1.7 ± 0.1

Swelling was calculated as the difference in cell wall thickness after release of turgor ('− turgor'), minus that before release of turgor ('+ turgor'). Data present means ± SE, $n = 40$

[a]Mean separation within columns by Tukey's Studentized range test, $p < 0.05$

use of immature or overmature fruit) were to be avoided. The change of cultivars ensures that our findings are not limited to a specific cultivar, but are applicable to all cherries investigated. The data obtained indicate that swelling was reproducible among genotypes, seasons and environments (i.e. green house or rain shelter in the field) suggesting a high level of genetic control. Considerable differences exist in cell wall thickness and in the amount of swelling between cultivars. The reasons for these differences are unknown but may be related to one or both of the following: (i) Swelling differs between cell wall constituents and cell wall constituents differ between cultivars. In particular, pectins and/or xyloglucans may be involved (Brummell 2006). (ii) In an earlier study, we observed marked decreases in cell wall swelling in the presence of free Ca ions (Brüggenwirth and Knoche 2017). In contrast, swelling increased in the

Table 3 Effect of turgor release on the thickness and swelling (Δthickness) of anticlinal cell walls of epidermal cells of skin sections (ES) of 'Sam' sweet cherry fruits following incubation in deionized water

Treatment	Thickness (µm)		ΔThickness (µm)
	+ turgor	− turgor	
Frost	2.8 ± 0.1 a[a]	5.6 ± 0.2 ab	2.9 ± 0.2
Heat	2.7 ± 0.1 a	5.8 ± 0.2 a	3.1 ± 0.2
Plasmolysis	2.8 ± 0.1 a	5.1 ± 0.2 ab	2.3 ± 0.2
Solvent	2.7 ± 0.1 a	5.6 ± 0.2 ab	2.8 ± 0.2
SDS	2.9 ± 0.1 a	4.9 ± 0.3 b	2.0 ± 0.3
Control	2.7 ± 0.1 a	5.2 ± 0.1 ab	2.5 ± 0.1

Turgor was released by a freeze/thaw treatment, or by heating fruit to 60 °C for 1 h, or plasmolyzing by incubation in 2.5 M glucose for 24 h, or by destroying membranes by incubation in acetone or in 20 mM sodium dodecyl sulfate (SDS) for 48 h. Incubation of ES for 48 h in 10 mM MES buffer served as control. Swelling was calculated as the cell wall thickness after release of turgor ('− turgor') minus that before release of turgor ('+ turgor'). Data presented are means ± SE, $n = 40$

[a]Mean separation within columns by Tukey's Studentized range test, $p < 0.05$

presence of malic acid, probably due to extraction of Ca from the cell wall. Hence, differences may exist between cultivars in the uptake of Ca and in its adsorption to the cell wall constituents.

From a practical point of view the question arises as to whether cell wall swelling and cracking susceptibility are closely correlated. Unfortunately, there is no comprehensive study on cracking susceptibility published that assessed more than four of the cultivars investigated in our study. However, for a larger set of unpublished data from our group, there was no significant correlation between cell wall swelling and cracking susceptibility as indexed by the time to 50% cracking ($n = 11$, $r = -0.04$) or the water uptake required for 50% cracking ($n = 11$, $r = -0.13$; Winkler, unpublished data). It is important to note, however, that the lack of such a relationship must not be interpreted as negative evidence. Swelling is only the final step in a series of events that ultimately leads to cracking.

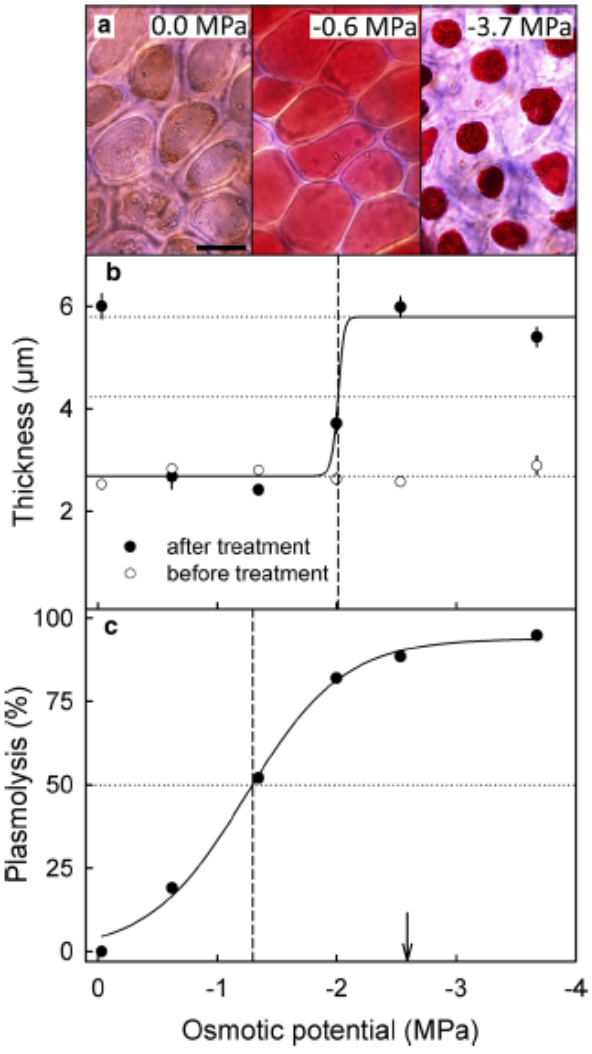

Fig. 6 **a** Micrographs of the effect of the osmotic potential of sucrose solutions on cell wall thickness and plasmolysis of excised 'Staccato' epidermal skin sections. Deionized water (osmotic potential 0 MPa) served as control. Bar = 20 µm. **b**, **c** The effect of the osmotic potential of sucrose solutions on the thickness of epidermal cell walls of skin sections (**b**) and the percentage of plasmolyzed cells (**c**). Dotted horizontal lines indicate cell wall thickness at 100, 50 and 0% cell wall swelling (**b**) and at 50% plasmolysis (**c**), the dashed vertical lines indicate the osmotic potentials at 50% cell wall swelling (**b**) and at 50% plasmolysis (**c**). The arrow indicates the osmotic potential of the fruit (− 2.6 ± 0.1 MPa). The equation for the sigmoid regression model describing the relationship between cell wall thickness and osmotic potential was:

$$\text{Thickness}(\mu\text{m}) = \text{Thickness with turgor } (\mu\text{m}) + \frac{a}{\left(1+e^{-\left(\frac{\text{osmotic potential (MPa)} - x_0}{b}\right)}\right)}$$

The maximum thickness (upper asymptote) was calculated as the average cell wall thickness of all treatments with fully swollen cell walls (without turgor, 5.8 ± 0.2 µm), the minimum thickness (lower asymptote) as the average thickness of all treatments with non-swollen cell walls (with turgor, 2.7 ± 0.1 µm). The regression equation for the relationship between the percentage of plasmolyzed cells and the osmotic potential was:

$$\text{Plasmolysis}(\%) = \frac{a}{1+e^{-\left(\frac{\text{osmotic potential (MPa)} - x_0}{b}\right)}}$$

. The osmotic potentials of the sucrose solutions at half maximum thickness of the epidermal cell walls (− 2.0 MPa) and at 50% plasmolysis of epidermal cells (− 1.3 MPa) were calculated from the respective regression equations. Data in **b** and **c** represent means ± SE, $n = 40$ for **b**, $n = 20$ for **c**

Table 4 Thickness of anticlinal epidermal cell walls of excised skin segments (ES) of 'Santina' sweet cherry fruit following incubation in hypotonic or hypertonic sucrose solutions. Incubation in water served as control

Treatment sequence	Thickness (µm)		
Phase I/Phase II	Initial	Phase I	Phase II
Control/control	2.5 ± 0.2 a[a]	3.9 ± 0.2 b*	4.0 ± 0.2 b*
Hypotonic/hypotonic	2.7 ± 0.1 a	2.8 ± 0.1 a	2.9 ± 0.1 a
Hypotonic/hypertonic	2.5 ± 0.1 a	2.7 ± 0.1 a	3.7 ± 0.1 b**
Hypertonic/hypotonic	2.7 ± 0.1 a	4.8 ± 0.2 b**	2.8 ± 0.1 a
Hypertonic/hypertonic	2.5 ± 0.1 a	4.3 ± 0.2 b**	4.3 ± 0.2 b**

Treatments were applied sequentially. Following establishment of thickness immediately after excision (Initial), phase I and phase II treatments were applied for 22 h each and thicknesses quantified. Data present mean ± SE, $n = 40$

[a]Mean separation within rows by Tukey's Studentized range test, $p < 0.05$. The symbol *indicates that cells collapsed as indexed by the loss of anthocyanins and the presence of a coagulated cytoplasm, **indicates plasmolyzed vital cells. In all other treatments cells were vital without plasmolysis

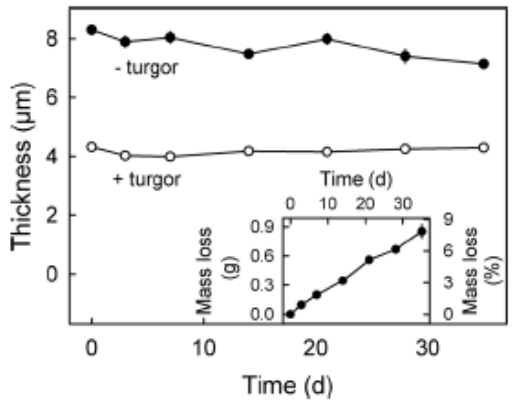

Fig. 7 Effect of storage duration of mature 'Merchant' sweet cherry fruit on swelling of anticlinal epidermal cell walls of skin sections following the release of turgor by a freeze/thaw treatment and a 48 h incubation period in 10 mM MES buffered deionized water at pH 5.8 ('− turgor'). Cell wall thickness before the freeze/thaw treatment served as control ('+turgor'). Inset: mass loss of whole fruit during storage. Whole fruit were held for up to 35 days at 2 °C and 95% relative humidity before skin sections were excised and incubated to quantify cell wall swelling. Data represent means ± SE, $n = 40$ for main graph, $n = 10$ for inset

Swelling is a physical process resulting from loss of cell turgor

Cell wall swelling is a physical process resulting from the release of pressure on the cell wall due to loss of cell turgor (in most cases associated with cell death). This hypothesis is supported by the following arguments:

First, the magnitude of the pressure generated by extracted cell wall material and the turgor pressure in mature sweet cherry parenchyma cells are of the same order of magnitude (Knoche et al. 2014; Schumann et al. 2014; Grimm et al. 2019). Hence, it is plausible that cell turgor balances and (and thus prevents) cell wall swelling in turgid cells. We recognize that the cell wall swelling pressure and cell turgor are both negligibly low relative to the very negative osmotic potential of juice extracted from sweet cherry fruit. Hence, cell wall swelling does not contribute significantly to fruit water potential (which is the sum of a number of water potential components—including osmotic, pressure, matric, etc.).

Second, pressurizing and depressurizing cell walls resulted in corresponding changes in volume of the swollen cell wall and in nearly identical swelling pressures indicating that cell wall swelling was completely reversible.

Third, the release of cell turgor (realized in this study through a number of quite different and unrelated treatments) always resulted in a similar level of cell wall swelling. We did, however, note some significant (but minor) differences in wall swelling depending on the chemical nature of the organic acid or buffer used. For example, more wall swelling was observed with citric or oxalic acid. This was probably due to complexing with Ca ions, which altered the amount of bound Ca in the cell wall matrix. Removal of Ca from the cell wall will result in reduced cross-linking, thus a loosening of cell wall constituents, and thus an increase in swelling (Brüggenwirth and Knoche 2017).

Fourth, in vital cells, incubation in hypertonic solutions caused plasmolysis and cell wall swelling. There was no swelling in hypotonic solutions provided that cells remained vital and turgescent. Furthermore, upon transferring cells from a hypertonic to hypotonic solution cells deplasmolysed and cell wall swelling was completely reversed. In the water, control cells lost vitality and turgor and hence, cell walls swelled. These observations support the idea of a role for turgor in cell wall swelling. However, while over a small range of osmotic potential (between − 0.6 and − 1.3 MPa) cells began to plasmolyze, we could detect no corresponding increase cell wall swelling. The reason for this discrepancy is unknown but it may be related to a non-uniform distribution of osmotic potential within the tissue (Grimm and Knoche 2015) and/or to different kinetics of plasmolysis and cell wall swelling.

Fifth, incubation of ES in a concentration series of aqueous ethanol resulted in less or even no swelling at high ethanol concentrations. This effect is familiar to light microscopists, being associated with tissue dehydration during fixation. As expected for a physical process, the effects of ethanol on cell wall swelling were simply reversible.

Table 5 Effect of expressed juice and artificial juice, without and with pH adjustment on the thickness and swelling (Δthickness) of anticlinal epidermal cell walls of 'Adriana' sweet cherry fruit

Treatment	Concentration (mmol kg^{-1})	pH	Thickness (µm)		ΔThickness (µm)
			+turgor	− turgor	
Control	10	5.8	2.6±0.1 a[a]	5.5±0.1 a	2.9±0.2
Juice	663	3.9	2.6±0.1 a	6.5±0.2 b	4.0±0.3
Juice pH adjusted	675	6.3	2.5±0.1 a	4.7±0.1 c	2.2±0.2
Artificial juice	665	3.9	2.7±0.1 a	7.8±0.2 d	5.0±0.3
Artificial juice pH adjusted	671	6.4	2.7±0.1 a	4.9±0.1 c	2.2±0.2

Swelling was calculated as the cell wall thickness after release of turgor ('− turgor') minus that before release of turgor ('+turgor'). Deionized water served as control. Data presented are means±SE, $n=40$. Artificial juice (containing glucose, fructose, sorbitol and potassium malate) was prepared at the same osmolarity as the juice expressed from the fruit. NB These five osmolytes represent the major components of sweet cherry fruit, accounting for around 98% of juice osmolarity (Herrmann 2001)

[a]Mean separation within columns by Tukey's Studentized range test, $p<0.05$

Table 6 Thickness and swelling (Δthickness) of anticlinal epidermal cell walls of excised skin segments (ES) of 'Adriana' sweet cherry fruit before and after incubation in solutions of citric, tartaric, malic or oxalic acid (all at 20 mM)

Treatment	pH	Thickness (µm)		ΔThickness (µm)
		+turgor	− turgor	
Control	5.9	2.5±0.1 ab[a]	5.2±0.1 a	2.7±0.1
Citric acid	4.8	2.4±0.1 ab	5.7±0.2 ab	3.2±0.2
Tartaric acid	4.5	2.4±0.1 ab	5.6±0.2 a	3.3±0.2
Malic acid	4.9	2.3±0.1 a	5.7±0.2 ab	3.4±0.2
Oxalic acid	4.4	2.4±0.1 ab	6.2±0.2 b	3.8±0.2
Ascorbic acid	5.5	2.6±0.1 b	5.4±0.1 a	2.8±0.1

MES buffer at 10 mM served as control. Swelling was calculated as the cell wall thickness after release of turgor ('− turgor') minus that before release of turgor ('+turgor'). Data present mean±SE, $n=40$

[a]Mean separation within columns by Tukey's Studentized range test, $p<0.05$

Lastly, for the PEG series investigated, there was no simple relationship between the solution osmotic potential and the extent of swelling. Interestingly, a close relationship across all PEG molecules and all osmotic potentials was obtained when swelling was expressed as a function of the number of ethylene glycol units. This observation was unexpected and may find its explanation in terms of the physicochemical interactions between PEG and water.

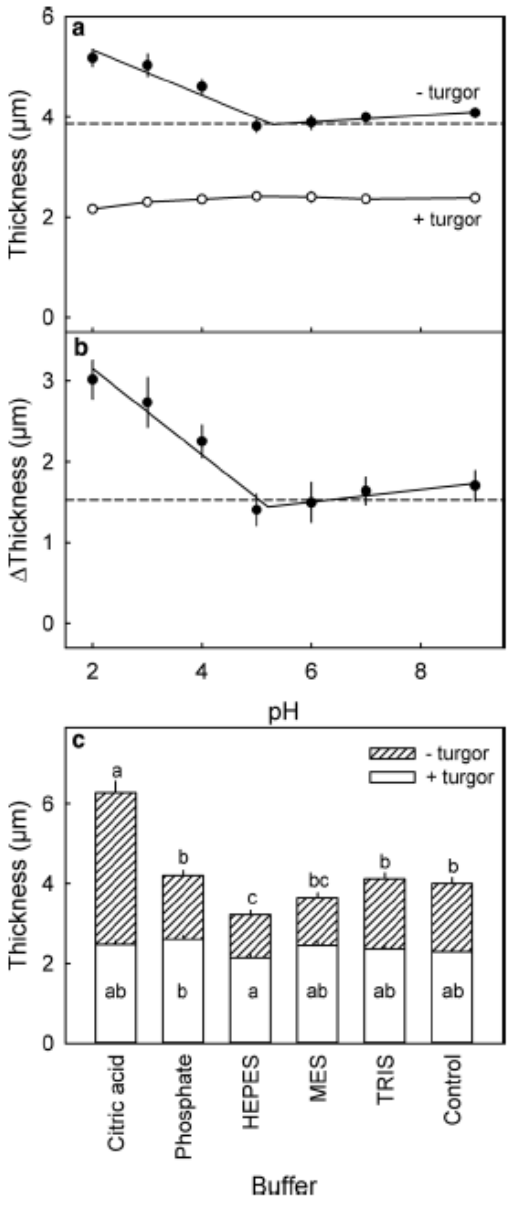

Fig. 8 **a**, **b** Effect of pH on thickness (**a**) and swelling (Δthickness, **b**) of anticlinal epidermal cell walls of skin sections of 'Adriana' sweet cherry fruit. The dashed horizontal line indicates the cell wall thickness (**a**) and swelling of the cell wall (**b**) after a freeze/thaw treatment and subsequent incubation in 10 mM MES buffered deionized water at pH 5.8. Swelling was calculated as the cell wall thickness after releasing turgor by a freeze/thaw treatment and subsequent incubation in solutions of different pH ('− turgor') minus that before ('+turgor'). **c** Effect of different buffer systems at pH 6.7 on thickness of anticlinal epidermal cell walls before and after releasing turgor by a freeze/thaw treatment and subsequent incubation in the buffer solutions. The effect of the buffer was established on the same batch of fruit as that used in **a**, **b**. Skin sections incubated in deionized water served as control. Mean separation in **c** by Tukey's Studentized range test, $p<0.05$. Data represent means±SE, $n=40$

PEG is an amphiphilic molecule that binds to the cell wall, thereby physically blocking the surface and preventing swelling. Binding, and hence blockage, will increase with the molecular weight of the PEG molecule and with PEG concentration. In addition, the direct binding of water by the PEG molecules will reduce swelling. The molar ratio of water molecules bound to ethylene glycol units is up to 2:1 (Makogon and Bondarenko 1985; Lüsse and Arnold 1996). Water bound to ethylene glycol units (in contrast to free water) does not participate in the swelling process. Both effects explain why swelling should be related to the number of ethylene glycol units, and not related to the osmotic potential of the PEG solution.

The effect of pH on swelling is consistent with literature data on tomato cell walls (MacDougall et al. 2001; MacDougall and Ring 2003). It is also supported by the hypothesis of turgor control of swelling. Pectins are a potential candidate for cell wall swelling. They represent weak polyelectrolytes cross-linked by divalent Ca ions. The pKa of the uronic acid moiety of galacturonic acid is pH 3.5 (Kohn and Kovac 1978). As pH decreases, dissociation decreases and so will the Ca-content of the cell wall (and hence cell wall cross-linking) (MacDougall et al. 2001). This is expected to result in greater cell wall swelling. Extraction and complexing of Ca would also account for differential swelling among buffers of different chemistry but of the same pH. Additional indirect evidence for the involvement of pectins in swelling comes from (i) the exposure of pectins on the fracture surface of the sweet cherry fruit skin (Schumann et al. 2019), (ii) the mode of fracture of the skin along and not across cell walls (Brüggenwirth and Knoche 2017) and (iii) data on other fruit crops demonstrating that swelling is associated with the pectin fraction (Redgwell et al. 1997; Basanta et al. 2013).

Interestingly, expansins show a similar response of cell wall loosening to variation of pH as the cell wall swelling in our study (Cosgrove 1998). Whether they contributed to cell wall swelling in sweet cherry at low pH, is unknown. In the normal pH range, a role of expansins in swelling is unlikely. Because expansins are proteins, they should have been inactivated by heat, surfactant or solvent treatments summarized in Table 3. These, however, did not differ in swelling from the control.

Conclusion

Our results demonstrate that cell wall swelling in mature sweet cherry fruit is substantially a physical process. In a healthy cell, the wall swelling is countered by cell turgor. The pressure generated by cell wall swelling is very low relative to the very negative osmotic potential of the juice.

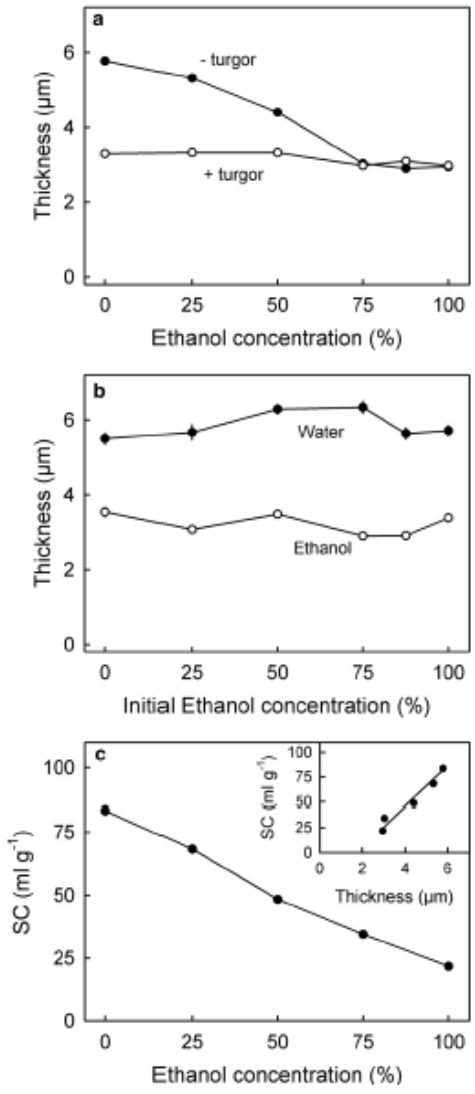

Fig. 9 Effect of the concentration of ethanol on the thickness of anticlinal epidermal cell walls of skin sections of mature 'Sweetheart' sweet cherry. **a** Effect of incubating skin sections in aqueous ethanol. Cell wall thickness was quantified before ('+turgor') and after release of turgor by the ethanol treatment ('– turgor'). **b** Reversibility of the effect of ethanol on swelling of cell walls. The reversibility was studied by replacing the aqueous ethanol solution from (**a**) by deionized water ('Water') or by 100% ethanol ('Ethanol'), as the incubation solution. **c** Effect of ethanol concentration on the swelling capacity (SC) of an extracted cell wall preparation from fruit of the same batch. Inset: relationship between the swelling capacity of extracted cell walls and the cell wall thickness of swollen cell walls (without turgor) as determined by microscopy (see data in **a**). The coefficient of correlation was $r = 0.98^{***}$. Data represent means ± SE, $n = 40$ for **a** and **b**, $n = 3$ for **c**

We do not yet know which fraction(s) of the cell wall are responsible for swelling. Nevertheless, we suggest that pectins and, possibly, xyloglucans are likely candidates.

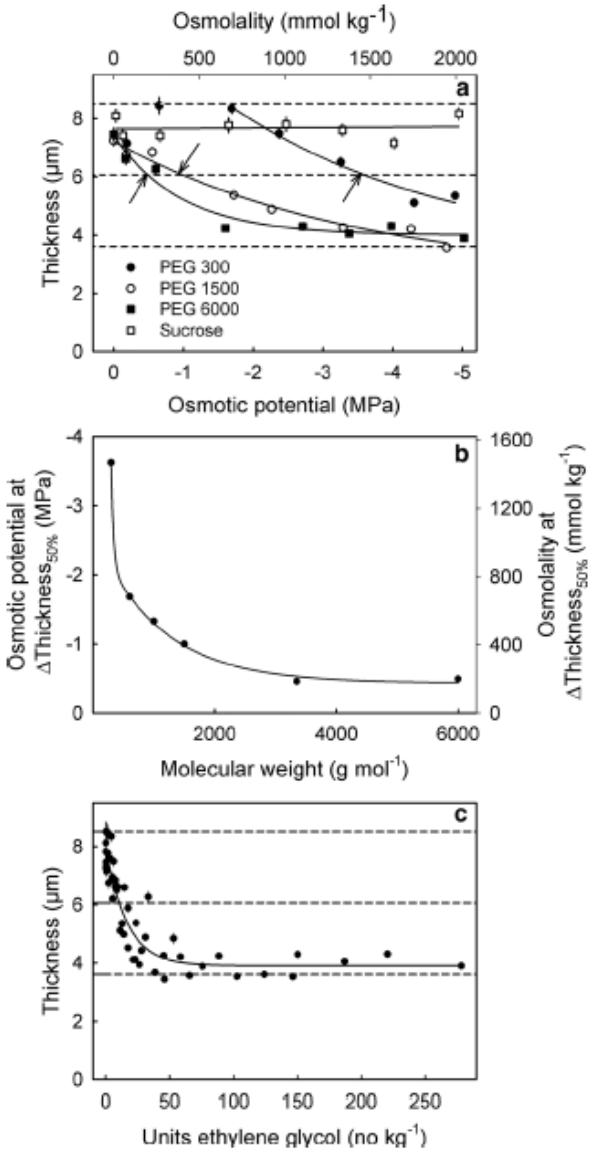

Fig. 10 Effect of osmotic potential of polyethylene glycol (PEG) solutions of different molar masses on the thickness of anticlinal epidermal cell walls of 'Staccato' sweet cherry. Mean molar mass of PEGs were 300 (PEG 300), 1500 (PEG 1500) and 6000 g mol^{-1} (PEG 6000). The lower dashed horizontal line indicates the mean cell wall thickness of skin sections before treatment, the upper dashed line the maximum swelling after releasing turgor by a freeze/thaw treatment (averaged across all treatments). Half maximum swelling is indicated by the dashed horizontal line in the middle. Sucrose solutions of the respective osmotic potentials served as control. **b** Relationship between the osmotic potential at 50% cell wall swelling and the molar mass of the PEGs. The osmotic potential at 50% swelling was calculated as the intercept of the regression line with the line for half maximum swelling (middle horizontal dashed line in **a**, intercept indicated by arrows). **c** The regression model was $\text{Thickness}(\mu\text{m}) = y_0 + ae^{b*}$ osmotic potential (MPa) for the relationship of thickness of cell walls and osmotic potential and $\text{Thickness}(\mu m) = y_0 + ae^{-b} * \text{units ethylene glycol} * \text{kg}^{-1}$ for that between thickness of cell walls and the number of units ethylene glycol. Data represent means ± SE, $n = 40$ for **a** and **c**

We expect that further study will reveal which cell wall fractions are responsible for swelling. The effects of Ca ions on cell wall swelling also warrant further study. Field applications of Ca may prove a useful tool for decreasing susceptibility of soft fruit species to rain cracking.

Author contribution statement

CS and MK conceived and designed the experiments. CS conducted the measurements and analysed the data. CS and MK wrote the manuscript. All authors read and approved the manuscript.

Acknowledgements Open Access funding provided by Projekt DEAL. We thank Andreas Meyer for constructing the pressure chamber, Simon Sitzenstock for technical help, Drs. Chong Cheng and Eli Ruckenstein for useful discussion of the PEG effect and Dr. Alexander Lang for useful comments on an earlier version of this manuscript. This study was funded in part by a grant from the German Science Foundation (DFG).

Compliance with ethical standards

Conflicts of interest The authors declare that they have no conflict of interest.

References

Alkio M, Jonas U, Sprink T, van Nocker D, Knoche M (2012) Identification of putative candidate genes involved in cuticle formation in *Prunus avium* (sweet cherry) fruit. Ann Bot 110:101–112

Andersen PC, Richardson DG (1982) A rapid method to estimate fruit water status with special reference to rain cracking of sweet cherries. J Am Soc Hort Sci 107:441–444

Basanta MF, de Escalada Pla MF, Stortz CA, Rojas AM (2013) Chemical and functional properties of cell wall polymers from two cherry varieties at two developmental stages. Carbohydr Polym 92:830–841

Basanta MF, Nora MA, Ponce ML, Salum MD, Raffo AR, Vicente REB, Stortz CA (2014) Compositional changes in cell wall polysaccharides from five sweet cherry (*Prunus avium* L.) cultivars during on-tree ripening. J Agr Food Chem 62:12418–12427

Brüggenwirth M, Knoche M (2017) Cell wall swelling, fracture mode, and the mechanical properties of cherry fruit skins are closely related. Planta 245:765–777

Brummell DA (2006) Cell wall disassembly in ripening fruit. Funct Plant Biol 33:103–119
Considine JA, Kriedemann PE (1972) Fruit splitting in grapes. Determination of the critical turgor pressure. Austr J Agr Res 23:17–24
Cosgrove DJ (1998) Cell wall loosening by expansins. Plant Physiol 118:333–339
Grimm E, Knoche M (2015) Sweet cherry skin has a less negative osmotic potential than the flesh. J Am Soc Hort Sci 140:472–479
Grimm E, Hahn J, Pflugfelder D, Schmidt M, van Dusschoten D, Knoche M (2019) Localized bursting of mesocarp cells triggers catastrophic fruit cracking. Hort Res 6:79
Herrmann K (2001) Inhaltsstoffe von Obst und Gemüse. Ulmer, Stuttgart
Knoche M, Peschel S (2006) Water on the surface aggravates microscopic cracking of the sweet cherry fruit cuticle. J Am Soc Hort Sci 131:192–200
Knoche M, Winkler A (2017) Rain-induced cracking of sweet cherries. In: Quero-García J, Iezzoni A, Puławska J, Lang G (eds) Cherries: botany, production and uses. CAB International, Wallingford, pp 140–165
Knoche M, Beyer M, Peschel S, Oparlakov B, Bukovac MJ (2004) Changes in strain and deposition of cuticle in developing sweet cherry fruit. Physiol Plant 120:667–677
Knoche M, Grimm E, Schlegel HJ (2014) Mature sweet cherries have low turgor. J Am Soc Hort Sci 139:3–12
Kohn R, Kovac P (1978) Dissocation constants of D-galacturonic and D-glucuronic acid and their O-methyl derivatives. Chemické Zvesti 32:478–485
Lüsse S, Arnold K (1996) The interaction of poly(ethylene glycol) with water studied by 1H and 2H NMR relaxation time measurements. Macromolecules 29:4251–4257
MacDougall AJ, Ring SG (2003) The hydration behaviour of pectin networks and plant cell walls. In: Voragen F, Schols H, Visser R (eds) Advances in pectin and pectinase research. Springer, Dordrecht, pp 123–135
MacDougall AJ, Rigby NM, Ryden P, Tibbits CW, Ring SG (2001) Swelling behavior of the tomato cell wall network. Biomacromol 2:450–455
Makogon BP, Bondarenko TA (1985) The hydration of polyethylene oxide and polyacrylamide in solution. Polym Sci USSR 27:630–634
Measham PF, Bound SA, Gracie AJ, Wilson SJ (2009) Incidence and type of cracking in sweet cherry (*Prunus avium* L.) are affected by genotype and season. Crop Pasture Sci 60:1002–1008
Peschel S, Knoche M (2005) Characterization of microcracks in the cuticle of developing sweet cherry fruit. J Am Soc Hort Sci 130:487–495
Raghavendra SN, Rastogi NK, Raghavarao KSMS, Tharanathan RN (2004) Dietary fiber from coconut residue: effects of different treatments and particle size on the hydration properties. Eur Food Res Technol 218:563–567
Redgwell RJ, MaxRae E, Hallett I, Fischer M, Perry J, Harker R (1997) In vivo and in vitro swelling of cell walls during fruit ripening. Planta 203:162–173
Schumann C, Schlegel HJ, Grimm E, Knoche M, Lang A (2014) Water potential and its components in developing sweet cherry. J Am Soc Hort Sci 139:349–355
Schumann C, Winkler A, Brüggenwirth M, Köpcke K, Knoche M (2019) Crack initiation and propagation in sweet cherry skin: a simple chain reaction causes the crack to 'run'. PLoS ONE 14(7):e0219794. https://doi.org/10.1371/journal.pone.0219794
Sekse L, Bjerke KL, Vangdal E (2005) Fruit cracking in sweet cherries—An integrated approach. Acta Hort 667:471–474
Sozzi GO, Greve LC, Prody GA, Labavitch JM (2002) Gibberellic acid, synthetic auxins, and ethylene differentially modulate alpha-L-arabinofuranosidase activities in antisense 1-aminocyclopropane-1-carboxylic acid synthase tomato pericarp discs. Plant Physiol 129:1330–1340
Winkler A, Ossenbrink M, Knoche M (2015) Malic acid promotes cracking of sweet cherry fruit. J Am Soc Hort Sci 140:280–287
Winkler A, Peschel S, Kohrs K, Knoche M (2016) Rain cracking in sweet cherries is not due to excess water uptake but to localized skin phenomena. J Am Soc Hort Sci 141:653–660

3.3 Decreased deposition and increased swelling of cell walls contribute to increased cracking susceptibility of developing sweet cherry fruit

Das Original dieses Artikels wurde 2020 in der Zeitschrift „Planta“ veröffentlicht.

Schumann, C., Sitzenstock, S., Erz, L. and Knoche, M. (2020): Decreased deposition and increased swelling of cell walls contribute to increased cracking susceptibility of developing sweet cherry fruit. *Planta*. 252:96

DOI: https://doi.org/10.1007/s00425-020-03494-z

Beteiligung der Autoren

M. Knoche warb die Drittmittel für das Vorhaben ein. M. Knoche, S. Sitzenstock und C. Schumann planten die Experimente. C. Schumann etablierte in Vorversuchen das Testsystem zur Messung des Quellungsdrucks extrahierter Zellwände. L. Erz, S. Sitzenstock und C. Schumann führten die Experimente durch. M. Knoche und C. Schumann analysierten die Daten. M. Knoche und C. Schumann schrieben und editierten das Manuskript. M. Knoche und C. Schumann revidierten das Manuskript.

Planta (2020) 252:96
https://doi.org/10.1007/s00425-020-03494-z

ORIGINAL ARTICLE

Decreased deposition and increased swelling of cell walls contribute to increased cracking susceptibility of developing sweet cherry fruit

Christine Schumann[1] · Simon Sitzenstock[1] · Lisa Erz[1] · Moritz Knoche[1]

Received: 3 July 2020 / Accepted: 6 October 2020 / Published online: 3 November 2020

Abstract

Main conclusion **During fruit development, cell wall deposition rate decreases and cell wall swelling increases. The cell wall swelling pressure is very low relative to the fruit's highly negative osmotic potential.**

Abstract Rain cracking of sweet cherry fruit is preceded by the swelling of the cell walls. Cell wall swelling decreases both the cell: cell adhesion and the cell wall fracture force. Rain cracking susceptibility increases during fruit development. The objectives were to relate developmental changes in cell wall swelling to compositional changes taking place in the cell wall. During fruit development, total mass of cell wall, of pectins and of hemicelluloses increases, but total mass of cellulose remains constant. The mass of these cell wall fractions increases at a lower rate than the fruit fresh mass—particularly during stage II and early stage III. During stage III, on a whole-fruit basis, the HCl-soluble pectin fraction, followed by the water-soluble pectin fraction, the NaOH-soluble pectin fraction and the oxalate-soluble pectin fraction all increase. At maturity, just the HCl-soluble pectin decreases. Cell wall swelling increases during stages I and II of fruit development, with little change thereafter. This was indexed by light microscopy of skin sections following turgor release, and by determinations of the swelling capacity, water holding capacity and water retention capacity. The increase in cell wall swelling during development was due primarily to increases in NaOH-soluble pectins. The in vitro swelling of cell wall extracts depends on the applied pressure. The swelling pressure of the alcohol-insoluble residue is low throughout development and surprisingly similar across different cell wall fractions. Thus, swelling pressure does not contribute significantly to fruit water potential.

Keywords Cell wall swelling · Cellulose · Cracking · Epidermis · Hemicellulose · Pectin · *Prunus avium*

Abbreviations

AIR	Alcohol-insoluble residue
ES	Epidermal skin section(s)
WSP	Water-soluble pectins
OXP	Oxalate-soluble pectins
HSP	HCl-soluble pectins
OHP	NaOH-soluble pectins
CL	Cellulose fraction
HC	Hemicellulose fraction
TP	Total pectins

Communicated by Dorothea Bartels.

✉ Moritz Knoche
moritz.knoche@obst.uni-hannover.de

[1] Institute for Horticultural Production Systems, Leibniz-University Hannover, Herrenhäuser Straße 2, 30419 Hannover, Germany

Introduction

Rain cracking is a critical production problem for many fleshy fruitcrops, especially when rainfall occurs during the later stages of fruit maturation. Sweet cherry and grape are prominent examples of rain-susceptible fruitcrops but many others are also rain-susceptible including: tomatoes, plums, blueberries, currants and gooseberries (Mrozek and Burkhardt 1973; Lichter et al. 2002; Khanal et al. 2011). The economic losses associated with rain cracking in this diversity of fruitcrop species range from a minor impairment of fruit quality due to shallow cracks within the cuticle (microcracks) that can trigger russeting (Knoche et al. 2011) and increase the incidence of fruit rots (Borve et al. 2000) and increase the rate of postharvest water loss (Maguire et al. 1999), to deep cracks (macrocracks) that propagate down through the cell layers of the skin into the flesh opening the way for massive invasion by insects and rots. In this way,

macrocracks can destroy an entire crop (Opara et al. 1997; Knoche and Lang 2017).

In sweet cherry, macrocracked fruit are not worth harvesting and so are usually left on the tree where they do not always abscise. These overwintering fruit mummify, and so serve as sources of inoculum for fruit-rot pathogens for the following season's crop. Rain covers are probably the most effective way to mitigate rain damage in sweet cherries but they do not totally eliminate it and they do involve high levels of capital expenditure.

The appearance of a macrocrack in a sweet cherry is only the final step in a series of events that have already predisposed it to damage from prolonged surface wetness (usually, but not always, associated with rainfall). According to the recent 'Zipper' hypothesis (Winkler et al. 2016), these steps include the early cessation of cuticle deposition and the subsequent rapid increase in fruit surface area during final expansion growth (Knoche et al. 2004). The resulting strain in the cuticle can lead to the formation of microscopic cracks (Peschel and Knoche 2005). Exposure to surface wetness and high humidity further exacerbates microcracking (Knoche and Peschel 2006). The microcracks so formed, impair the barrier properties of the cuticle (Borve et al. 2000), allowing highly localized water uptake (Winkler et al. 2016). As a consequence, the cells of the skin and outer flesh that lie immediately beneath a cuticular microcrack, expand rapidly and burst. The giant flesh cells have more negative osmotic potentials and thinner cell walls than the much-smaller, thicker-walled cells of the skin's epidermis and hypodermis (Grimm and Knoche 2015). Not all cells of the flesh are of the same osmotic potential (Grimm et al. 2020). Hence, those having the most negative osmotic potentials will likely burst first (Grimm et al. 2019). When a cell bursts, it liberates malic acid into the apoplast (Herrmann 2001; Winkler et al. 2015). Here, the malic acid serves to increase the permeability of the membranes of the adjacent cells, and it also weakens their cell walls. This triggers a cascade of cell collapse with further leakage and further damage to adjacent cell walls. This chain reaction we refer to as the Zipper effect.

Malic acid is a common osmolyte in sweet cherries that occurs at a concentration of about 70 mM (Herrmann 2001). Loss of cell turgor causes swelling of both epidermal and hypodermal cell walls (Schumann and Knoche 2020). Together, these cell layers form the structural backbone of the sweet cherry fruit (Brüggenwirth et al. 2014). Cell wall swelling also decreases cell:cell adhesion and so lowers the fracture force of the skin (Brüggenwirth and Knoche 2017). Cuticular microcracks now extend deeper into the skin forming schizogenous macrocracks as epidermal, hypodermal and cortical cells separate one from another along their middle lamellae (Schumann et al. 2019). It would seem that pectins also play a role in these processes as both cell wall swelling and macrocracking are exacerbated by the removal of Ca (e.g. by applications of EGTA; Glenn and Poovaiah 1989) and are inhibited by the application of Ca (e.g. Glenn and Poovaiah 1989).

Occasionally, fruit macrocracking occurs as early as color change (stage II/III) but most macrocracking occurs nearer maturity (late stage III). Increased macrocracking at maturity may result from any of the above processes. The activities of cell wall degrading enzymes also increase at this time (Kondo and Danjo 2001). Little is known about how cell wall swelling changes during fruit development. A better understanding of cell wall swelling requires to quantify swelling in developing fruit and relate changes in swelling to changes in the major cell wall fractions and to the intrinsic swelling behavior of these fractions. Different methods have been used in the past to quantify major cell wall constituents. A well-established procedure is the sequential fractionation of the alcohol-insoluble residue (AIR) of the tissue of interest (Sozzi et al. 2002). The AIR is extracted using a range of solvents (Saulnier and Thibault 1987; Barbier and Thibault 1982; Batisse et al. 1996; Fügel et al. 2004, 2006; Yapo et al. 2007; Yapo and Koffi 2008). The fractions are selectively extracted based on differential solubility of the fraction in the respective solvent. This procedure not only allows to separate pectins, hemicelluloses and cellulose, but also to fractionate pectins into water-soluble pectins (WSP), oxalate-soluble pectins (OXP), HCl-soluble pectins (HSP) and an NaOH-soluble pectins (OHP). Chemical analyses of the extracted fractions confirmed the identity of the fractions in a range of plant species including grapes (Saulnier and Thibault 1987), sour cherries, strawberries and apples (Fügel et al. 2004), sweet cherry (Batisse et al. 1996), sugar beet (Rombouts and Thibault 1986), passion fruit (Yapo and Koffi 2008) and citrus (Yapo et al. 2007). The objectives of this study are: (1) to identify any changes in the major cell wall fractions in developing sweet cherry fruit, (2) to quantify cell wall swelling during fruit development and (3) to identify which cell wall fractions account for cell wall swelling during fruit development. We focus on sweet cherry as a model for fleshy fruit because of the large body published information already available on this species.

Materials and methods

Plant material

Developing sweet cherry fruit (*Prunus avium* L.) of the cultivar 'Regina' were sampled weekly from 33 to 96 days after full bloom (DAFB). The cultivars 'Adriana', 'Burlat', 'Dönissens Gelbe', 'Earlise', 'Fabiola', 'Hedelfinger', 'Kordia', 'Merchant', 'Regina', 'Sam', 'Samba', 'Schneiders Späte', 'Staccato', and 'Sweetheart' were sampled

at the beginning of pit hardening (stage II) and at maturity (stage III). The timings for each cultivar were judged based on fruit size and color. All trees were cultivated under a rain shelter at the Horticultural Research Station of the Leibniz University in Ruthe (lat. 52°14′ N, long. 9°49′ E). Trees were grafted on 'Gisela 5' rootstocks (*Prunus cerasus* × *P. canescens*). Unless otherwise stated, fruit were processed fresh on the day of sampling or stored at − 20 °C pending extraction of cell walls. Fruits used in the experiments were selected for uniformity of development based on size and color and freedom from visual defects.

Fruit and pit fresh and dry weights were recorded. For dry weight, fruit and pits were dried at 103 °C to constant weight and the dry weight taken. Further, the osmolarity of juice extracted using a garlic press was quantified by water vapor pressure osmometry (VAPRO® 5600, Wescor, Logan, UT). All determinations were carried out with ten replicates except for the fruit fresh weight, where 50 replicates were used.

Light microscopy

Cell wall swelling was determined using the procedure described in detail by Schumann and Knoche (2020). Briefly, epidermal skin sections (ES) were prepared from a fruit's equator in the cheek region. Skin strips were excised (3 mm wide) using parallel-mounted razor blades and the ES cut as thin sections parallel to the surface. The ES were blotted using soft tissue paper, positioned on a microscope slide in a drop of deionized water, transferred to the stage of a microscope (BX-60, Olympus, Hamburg, Germany) and inspected at 40×. Calibrated digital photographs (camera: DP73; Olympus) were taken and the thicknesses of anticlinal cell walls quantified by image analysis (cellSens; Olympus Soft Imaging Solutions; Münster; Germany). The measurement was of the cell wall thickness between two turgid living cells. It thus comprised the sum of the walls of two neighboring cells plus the intervening pectin middle lamella. Earlier studies (Schumann and Knoche 2020) had established that cell wall swelling does not occur in turgid cells—it would seem cell turgor somehow prevents wall swelling. Therefore, to quantify swelling in vivo, cell turgor in the ES was released by exposing it to a freeze/thaw cycle. Following equilibration at room temperature, cell wall thickness was again measured between two now-flaccid cells. Swelling was quantified as the difference between the thickness measured before turgor release from that measured just after turgor release. One ES was cut from each of ten replicate fruit per treatment, two micrographs were taken per ES and two cell walls were measured per micrograph. The number of observations was thus 40 per treatment (10 × 2 × 2).

Cell wall extraction and fractionation

Cell walls were extracted as the AIR using the protocol of Sozzi et al. (2002) with minor modifications. Briefly, ten replicate fruit were pitted and the remaining skins and flesh were homogenized for 2 min in 4 ml of ice-cold ethanol (80%, v:v) per g of tissue. The homogenate was then boiled for 30 min, cooled and filtered through glass filter paper (Whatman GF/C). The insoluble residue was then washed with 95% (v:v) ethanol and re-filtered. Next, the residue was extracted for 15 min with 3 ml of chloroform:methanol (1:1, v:v) per g tissue, filtered and re-washed with the same solvent mixture, followed by a final wash with acetone. The resulting AIR was dried overnight, weighed and stored over dry silica gel. The developmental time course was established with six biological replicates for 'Regina'. All other comparisons were carried out with three replications.

The AIR of developing 'Regina' fruit was fractionated using a standard protocol (e.g. Rombouts and Thibault 1986; Saulnier and Thibault 1987; Barbier and Thibault 1982; Batisse et al. 1996; Fügel et al. 2004, 2006; Yapo et al. 2007; Yapo and Koffi 2008). The total AIR of ten fruit was suspended and stirred for 30 min at 40 °C in 50 ml deionized water per 0.8 g of AIR. The slurry was centrifuged (Sorvall RC-5B Plus; Thermo Scientific, Waltham, Massachusetts, USA) at 14,000 g for 25 min at 20 °C. The supernatant was removed and kept separate. The procedure was repeated, except that the pellet was now re-suspended and stirred in deionized water for 1 h at 40 °C. The aqueous supernatants were then combined, dialyzed (Carl Roth, Karlsruhe, Germany, MWCO: 14,000) for 2 d against deionized water at room temperature and lyophilized for 6 d. The fraction obtained represents the water-soluble pectins (WSP). Next, a series of four extractions was carried out to create a series of differentially soluble cell wall fractions. After each extraction, the slurry was centrifuged, the supernatant retained and the pellet re-suspended in the next solvent. The sequence of the extraction series was (1) in 50 ml 0.5% (w:v) NH_4-oxalate solution per 0.8 g AIR for 90 min at 40 °C (the oxalate-soluble pectins, OXP), next (2) in 0.05 M HCl for 90 min at 60 °C (the HCl-soluble pectins, HSP), next (3) in 0.05 M NaOH for 90 min at 30 °C (the NaOH-soluble pectins, OHP) and last (4) in 16% (w:w) aqueous NaOH for 90 min at 30 °C (the hemicelluloses, HC). The pellet remaining after the final extraction represents the cellulose fraction (CL) plus some minor amounts of lignin originating from the fruit's xylem.

The pellets were then washed twice with 100 ml deionized water, resuspended and re-centrifuged, the appropriate supernatants were combined and lyophilized as described above. The supernatants of both NaOH extraction steps were adjusted to pH 6.5 with HCl prior to dialysis. The pellet of the remaining CL fraction was suspended in 50 ml distilled

water, dialyzed and lyophilized. The dry weight of each fraction was recorded after lyophilization and the fractions stored above dry silica gel. The whole procedure was done in triplicate.

On a single occasion a cell wall extraction was carried out of an exocarp-enriched tissue sample vs. a mesocarp tissue sample. The purpose of this separation was to identify potential spatial heterogeneity in the swelling of cell walls extracted from the skin (exocarp) and from the flesh (mesocarp). For this, the fruit was taken from the same lot of mature 'Regina' fruit. These were peeled and pitted while still frozen. Because it is technically impossible to separate exocarp and mesocarp in sweet cherry, the peel represents the exocarp-enriched tissue sample (with some adhering mesocarp), the remaining flesh the pure mesocarp tissue sample (no adhering skin) (Alkio et al. 2012). For comparison 3 × 20 fruit were pitted and the exocarps and mesocarps processed together. The frozen tissue samples were lyophilized and ground with pestle and mortar. The extractions were carried out as described above with three replications of 20 fruit each.

Hydration properties

The hydration properties as indexed by the swelling capacity, the water holding capacity and the water retention capacity (Raghavendra et al. 2004; Basanta et al. 2013) were estimated for the AIR of developing 'Regina' fruit. Values for the swelling capacity and the water retention capacity were also determined for the five cell wall fractions OXP, HSP, OHP, HC and CL, each at six stages of fruit development. The hydration properties were estimated according to procedures described previously, with minor adjustments (Raghavendra et al. 2004; Basanta et al. 2013). All determinations were carried out using three replicates. Briefly, for the determination of the swelling capacity, 50 mg (±0.1 mg) of the AIR or 25 mg of the respective cell wall fraction were weighed in a graduated conical glass tube and 12.5 ml of deionized water was added. To remove any entrapped air and to ensure thorough wetting of the samples, the tubes were vacuum infiltrated (3 kPa) three times, for 10 min each. To improve reproducibility of the determinations, each tube was stirred once, 6 h after the start of incubation. After a total equilibration time of 20 h at room temperature, the final swollen volume of the AIR and of the respective fractions was recorded. The swelling capacity (SC) was calculated as:

$$\mathrm{SC}\ \left(\mathrm{ml}\times\mathrm{g}^{-1}\right)=\frac{\text{Volume of swollen AIR(ml)}}{\text{Original sample dry weight(g)}}.$$

For the determination of the water holding capacity, 50 mg (±0.1 mg) of the AIR was weighed into a glass tube and 12.5 ml of deionized water added as described above. Following vacuum infiltration and equilibration for 20 h, the supernatant was removed and the weight of the wet pellet recorded. The wet pellet was dried to constant weight at 70 °C and the dry weight recorded. The water holding capacity (WHC) was calculated as:

$$\mathrm{WHC}\left(\mathrm{g}\times\mathrm{g}^{-1}\right)=\frac{\text{Weight of wet pellet(g)}-\text{Weight of dry pellet(g)}}{\text{Weight of dry pellet(g)}}.$$

For the determination of the water retention capacity, we used the same procedure as for the water holding capacity, except for an additional centrifugation (30 min at 2000*g*) before removal of the supernatant. Thus, the water holding capacity also includes loosely associated water, whereas the water retention capacity is an index for more strongly bound water (Basanta et al. 2013).

For the water retention capacity, the mass of the cell wall fraction was reduced to 25 mg instead of 50 mg for the AIR sample. The cell wall fractions were also lyophilized for 3 d instead of oven drying. The water retention capacity (WRC) was calculated as:

$$\mathrm{WRC}\left(\mathrm{g}\times\mathrm{g}^{-1}\right)=\frac{\text{Weight of wet centrifuged pellet(g)}-\text{weight of dry pellet(g)}}{\text{Weight of dry pellet(g)}}.$$

Swelling pressure

The swelling pressure was determined for the AIR samples for the developing sweet cherry fruit and also for the OXP, HSP, OHP, HC and CL fractions of mature fruit. The procedure described previously was used (Schumann and Knoche 2020). Briefly, AIR (25 mg per replicate for the developmental time course and the exocarp/mesocarp comparison, 20 mg per replicate for comparing fractions at maturity) was placed on a stainless steel frit in a custom-built pressure chamber (inner diameter 25.5 mm). The cell wall was wetted using 70% (v/v) aqueous ethanol supported by vacuum infiltration (20 kPa for 10 min). Initial experiments had established that a concentration of 70% ethanol substantially prevented swelling. Using a universal material testing machine (BXC-FR2.5TN; Zwick GmbH & Co. KG, Ulm, Germany; 50 N force transducer, KAP-Z; Zwick/Roell), a plunger was placed on the hydrated cell wall in the pressure chamber. The plunger was fitted with a 25 mm diameter stainless steel frit. Using this setup, the cell wall sample was pressurized at 5.2 N. When this pressure was reached, the 70% ethanol was replaced by deionized water to initiate swelling. At this point, the minimum height of the cell wall sample was recorded to calculate its minimum volume (V_{min}). The pressure was held at 5.2 N for 12 h. Subsequently, the pressure was reduced stepwise to 2.5, 1.0, 0.5, 0.25, to 0.1 N, each pressure step followed by a 12 h holding period. As pressure was decreased, cell wall volume increased (swelled). The

extent of cell wall swelling was recorded by the material testing machine's displacement transducer and the applied pressure was recorded by its force transducer. From the position change of the plunger, the volume change (ΔV) due to swelling was calculated. The swelling pressure (P_0) of the cell wall sample was calculated as the intercept of a plot of the maximum change in volume (ΔV) at any one pressure vs. the natural logarithm of the applied pressure. Swelling pressures were determined using three replicate machine runs, where each run involved an independent extraction or fractionation sample.

Data analyses and statistics

Data are presented as means ± standard errors. Where not shown, error bars are smaller than the data symbols. Data were analyzed statistically by analysis of variance (Proc GLM) or by regression analysis (Proc REG) using the statistical software package SAS (version 9.1.4; SAS Institute, Cary, NC). Mean comparisons were made using the Tukey Studentized Range Test at $P < 0.05$ using R (packet multcomp 1.4–0, procedure glht, R3.0.2; R Foundation for Statistical Computing, Vienna, Austria). Pearson correlation coefficients were calculated using R.

Results

Fruit growth and the deposition of cell wall

Fruit fresh and dry masses typically increased in a double-sigmoidal pattern with time characterized by stages I, II and III of fruit development (Fig. 1a, b). Pit masses increased until about mid stage II and then remained constant. The dry mass content of the flesh was also constant throughout development, whereas the dry mass of the pit increased. The osmotic potential decreased (became more negative), particularly during stage III (Fig. 1a (inset)). During fruit development, and on a whole-fruit basis, the total mass of cell wall material increased (Fig. 1c). The increase in cell wall mass failed to keep pace with the increase in fresh mass as indexed by a marked decrease, particularly during stage II and early stage III (Fig. 1d). Inspection of the light microscope images revealed that the thickness of cell walls of epidermal cells increased during stages I and II but then remained constant until maturity (Figs. 1e and 2).

The exocarp accounted for 27% of the total cell wall mass of a fruit, and the mesocarp for the remaining 73% (Table 1). The cell wall mass, on a per-fresh-weight basis, was 2.7-fold higher in the exocarp than in the mesocarp. Despite the large differences in cell wall mass, exocarp and mesocarp had very similar swelling properties (swelling capacity, water holding capacity, water retention capacity and swelling pressure).

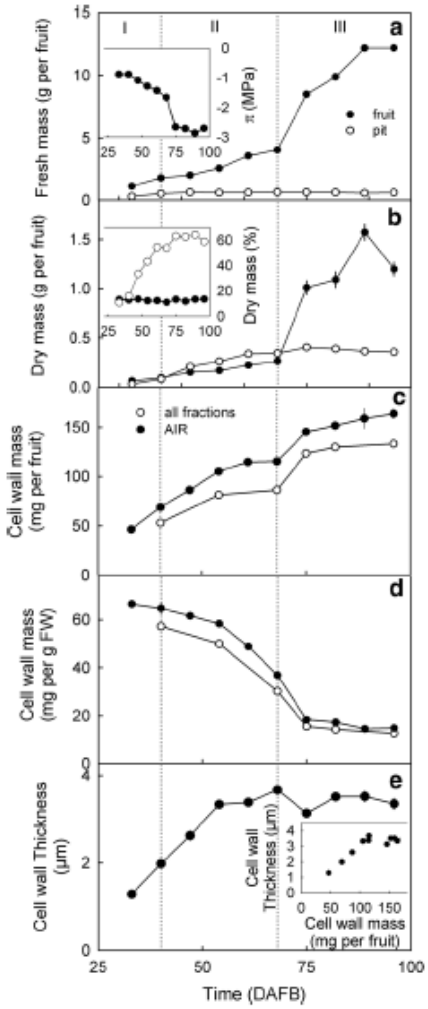

Fig. 1 Developmental time course of fruit growth (**a**, **b**), osmotic potential (Inset in **a**), dry matter content (Inset in **b**) deposition of cell wall material determined as the alcohol-insoluble residue ('AIR') and the total cell wall mass calculated as the sum of the extracted cellulose, hemicellulose and all pectin fractions on a per fruit basis (**c**) and on a unit fresh mass basis (**d**). **e** Developmental time course of cell wall thickness of epidermal cell walls as determined by light microscopy. Inset in **e**: Relationship between the mass of AIR on a per fruit basis and the cell wall thickness. Fruit growth was indexed as the increase in fresh mass (**a**) and dry mass (**b**) of fruit and pit. Time scale in days after full bloom (DAFB)

These did not differ significantly from those of the mean AIR sample obtained for whole (pitted) fruits.

The cell wall masses of immature vs. mature fruit were significantly related across the 12 different sweet cherry cultivars (Fig. 3). The slope of the regression line was 1.31 indicating that (averaged across cultivars) the cell wall mass had increased by 31% (1.31-fold) from stage II to mature stage III. In the same interval fruit fresh mass had increased

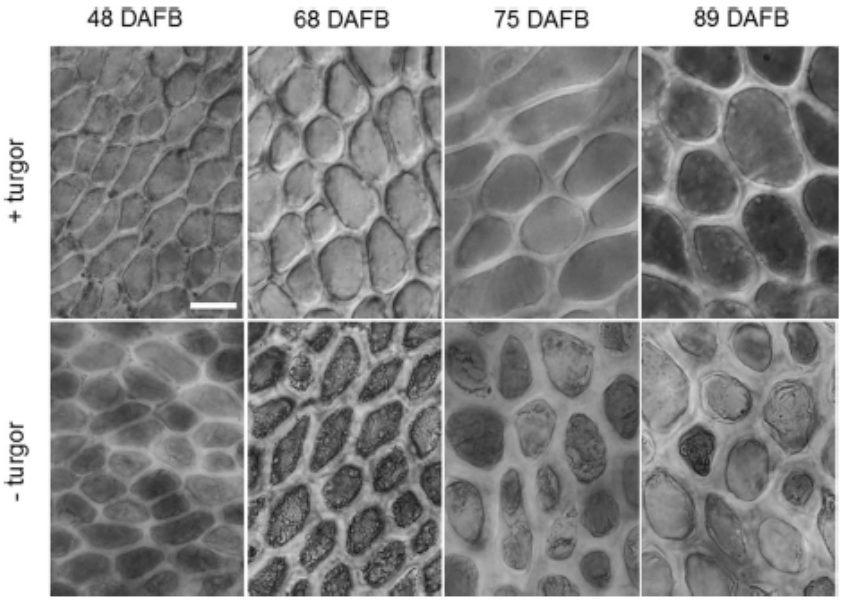

Fig. 2 Micrographs of the time course of change in thickness of anticlinal cell walls of excised epidermal skin sections before (top row) and after release of turgor (bottom row) 48, 68, 75 and 89 days after full bloom (DAFB). Bar 20 µm

Table 1 Tissue fresh mass and cell wall mass after extraction of alcohol-insoluble solids (AIR) of different tissues at 96 days after full bloom and the hydration properties water holding capacity (WHC), swelling capacity (SC), water retention capacity (WRC) and swelling pressure

Tissue	FW_{tissue} (g per fruit)	Cell wall mass		WHC (g g^{-1})	SC (ml g^{-1})	WRC (g g^{-1})	Swelling pressure (kPa)
		(mg per fruit)	(mg per g FW_{tissue})				
Exocarp	1.0 ± 0 a[a]	39.0 ± 1 a	38.6 ± 1 a	37 ± 1 a	33 ± 2 a	24 ± 2 a	12 ± 1 a
Mesocarp	7.6 ± 0 b	107.3 ± 4 b	14.2 ± 1 b	41 ± 5 a	38 ± 2 a	21 ± 1 a	10 ± 0 a
Whole fruit[b]	10.6 ± 0 c	164.2 ± 2 c	15.4 ± 0 b	39 ± 2 a	33 ± 1 a	19 ± 0 a	11 ± 2 a

Data present means ± SE. Swelling properties were determined on 25 mg of the AIR of the respective tissue

[a]Mean separation within columns by Tukey's Studentized range test, $P < 0.05$

[b]Pitted fruit. Different fruit from same batch

about 300% (about threefold) from 3.4 ± 0.3 g to 10.0 ± 0.5 g per fruit).

Developmental time course of major cell wall constituents

Marked changes occurred in the cell wall fractions of developing fruit (Fig. 4). Here, the WSP, OXP, OHP, and HC all increased during stages II and III (Fig. 4a, b, d, e, f). The HSP increased only until about 82 DAFB and then decreased, the CL remained about constant (Fig. 4c, f). Pectins represented the largest fraction within the AIR. Their contribution to the AIR increased, whereas that of the HC remained constant and that of the CL decreased (Fig. 5a). At maturity the individual fractions averaged 11.6% (WSP), 9.4% (OXP), 16.9% (HSP), 15.4% (OHP), 21.1% (HC) and 9.7% (CL) of the total AIR (Fig. 5). Expressed as fractions of the total pectins, these values were 21.7% (WSP), 17.6% (OXP), 31.7% (HSP) and 29.0% (OHP).

On a per-gram-fresh-mass basis, all pectin fractions (except for WSP) and the HC and CL decreased during fruit development, indicating that the increasing fruit fresh mass 'diluted' the pectin fractions (Fig. 4, insets).

It is worth noting that averaged across development, the sum of all fractions amounted to about 85% of the AIR, indicating that only minor losses occurred during fractionation (Fig. 1c).

Swelling of cell walls and its major constituents

Following the release of turgor by a freeze/thaw cycle, cell wall thickness increased 1.3–1.9-fold depending on stage of fruit development (Fig. 6a). Calculating the extent of cell wall swelling revealed a near-linear increase in thickness during fruit development (Fig. 6b). Similarly, the swelling

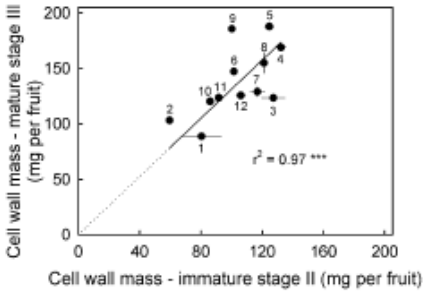

Fig. 3 Relationship between the amount of cell wall mass per fruit at the fully mature (stage III) and the immature stage II. Data symbols represent means of different sweet cherry cultivars. The cultivars were Adriana (1), Dönissens Gelbe (2), Early Korvic (3), Fabiola (4), Gill Peck (5), Hedelfinger (6), Kordia (7), Rainier (8), Regina (9), Sam (10), Schneiders (11) and Sweetheart (12). The y-axis intercept of the regression line was not significantly different from zero. Hence, the regression line was forced through the origin. The equation was: Cell wall mass ripe (mg per fruit) = 1.31 ± 0.07 × Cell wall mass unripe (mg per fruit), $r^2 = 0.97$***

capacity, the water holding capacity and the water retention capacity of cell wall extracts increased up to the stage II/III transition, and then remained constant (swelling capacity and water holding capacity, Fig. 6c, d) or decreased (water retention capacity, Fig. 6e). Values of the swelling capacity and of the water holding capacity were significantly correlated to cell wall swelling (Fig. 6c, d, insets). Only the relationship between the water retention capacity and cell wall swelling was not significant (Fig. 6e, inset). Furthermore, the water holding capacity ($r = 0.91$***) and the water retention capacity ($r = 0.76$*) were significantly correlated with the swelling capacity.

On a whole-fruit basis the swelling capacity of the AIR increased during each developmental stage. Calculated as the sum of the intrinsic swelling capacity of each single fraction (except for WSP), the swelling capacity increased until about 75 DAFB and then decreased slightly (Fig. 7a). In the in vitro assays, the WSP will be in solution in the supernatant and, therefore, its swelling capacity (and the water retention capacity) cannot be determined in vitro. The sum of the swelling capacities of the remaining fractions was on average 3.0-times higher than the swelling capacity of the AIR.

The fraction that had the highest intrinsic swelling capacity was the HSP followed by the OHP and then the OXP (Fig. 7b, c, d). Two factors account for this: (1) the large swelling of the HSP and OHP fractions (Fig. 7c, d; insets) and (2) their large mass fraction on a per-fruit basis, in case of the HSP. The intrinsic swelling capacities of the HC

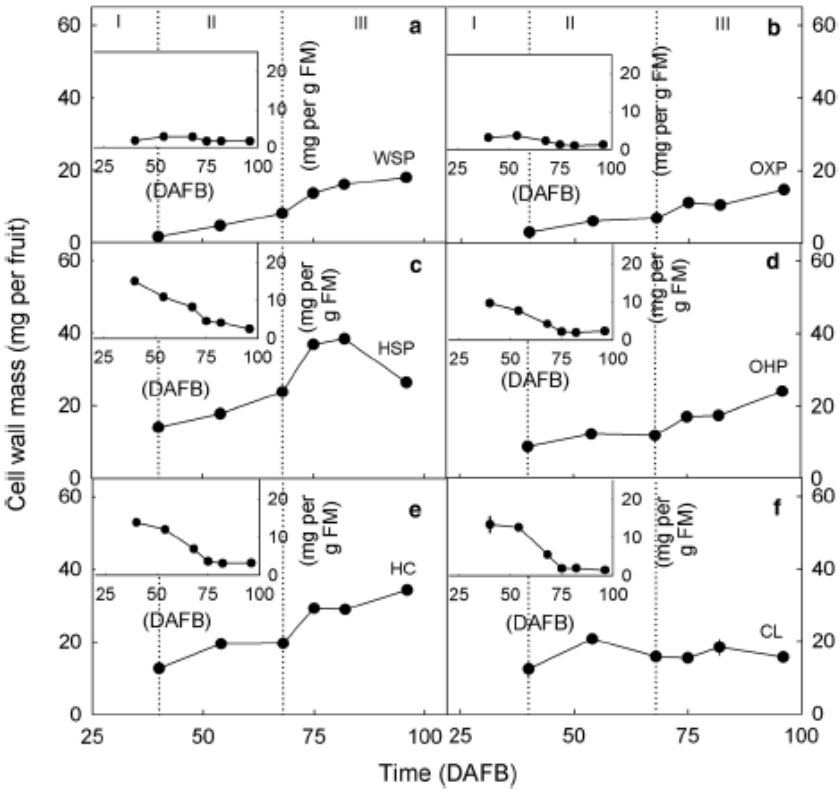

Fig. 4 Developmental time course of the deposition of various pectin fractions on a per fruit basis (main graphs) and on a unit fresh mass basis (insets). **a** Water-soluble pectins (WSP). **b** Oxalate-soluble pectins (OXP). **c** HCl-soluble pectins (HSP). **d** NaOH-soluble pectins (OHP). **e** Hemicelluloses (HC). **f** Cellulose (CL). Time scale in days after full bloom (DAFB)

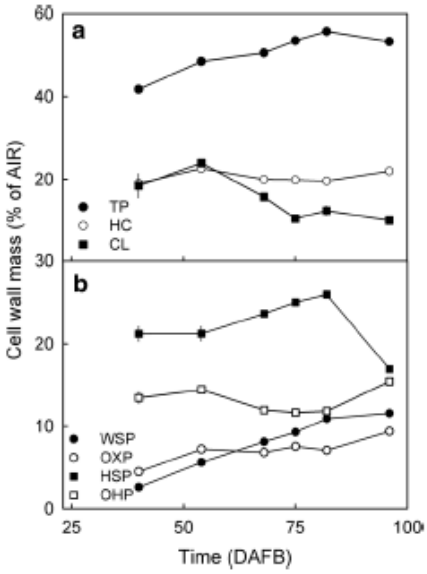

Fig. 5 Developmental time course of the change in composition of the cell wall material determined as the alcohol-insoluble residue ('AIR'). **a** Total pectins ('TP'), hemicelluloses ('HC') and cellulose ('CL'). **b** Water-soluble pectins ('WSP'), oxalate-soluble pectins ('OXP'), HCl-soluble pectins ('HSP') and NaOH-soluble pectins ('OHP'). The TP was calculated as the sum of the WSP, OXP, HSP and OHP

(Fig. 7e) and the CL (Fig. 7f) were low, both when expressed on a unit-mass basis and on a per-fruit basis.

On a whole-fruit basis, the water retention capacity of the AIR and, even more so, the sum of the intrinsic water retention capacities of the OXP, HSP, OHP and CL fractions all increased during fruit development (Fig. 8a). In this summation, the WSP and the HC were both excluded. The WSP is solubilized in the supernatant. The HC fraction does not swell which makes it impossible to quantify its water retention capacity reliably. On average, the sum of the water retention capacities of the individual fractions was about 2.0-fold greater than that of the AIR. The increase in the water retention capacity was primarily due to an increase in the HSP, followed by an increase in the OHP and the OXP fractions (Fig. 8b, c, d). The water retention capacity of the CL fraction remained about constant and at a low level (Fig. 8e).

Swelling pressure

The swelling of the cell wall extracts depended on the applied pressure. Stepwise decreases in the applied pressure allowed the cell wall extracts to swell (Fig. 9a). Swelling was similar for extracts prepared from fruit at

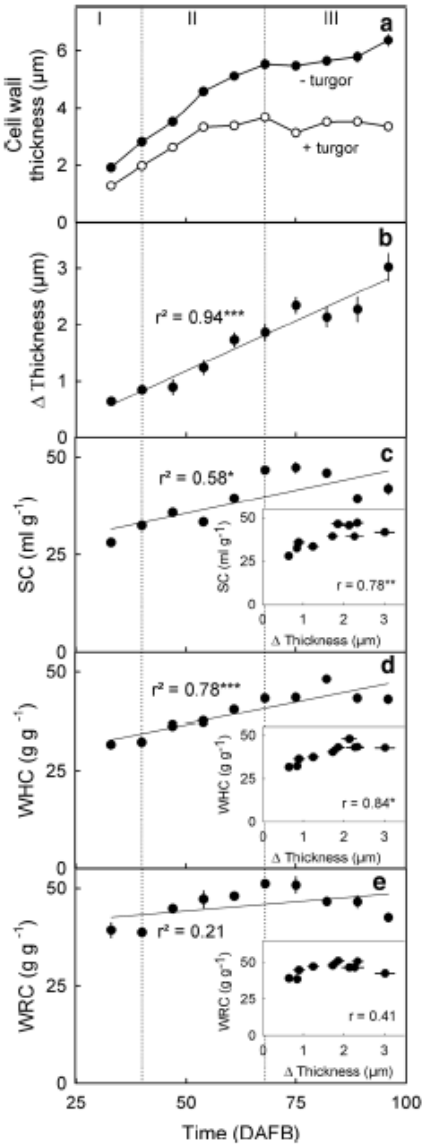

Fig. 6 **a** Developmental time course of the change in thickness of epidermal cell walls before ('+ turgor') and after removal of turgor ('− turgor'). Swelling was induced by releasing turgor using a freeze/thaw cycle. Inset: Cell wall swelling ('Δ Thickness') calculated as the difference between the cell wall thickness before and after release of turgor. **b**, **c**, **d** Developmental time courses of change of hydration properties of cell wall extracts as indexed by the swelling capacity (SC) (**b**), the water holding capacity (WHC) (**c**), and the water retention capacity (WRC). Cell wall extracts were prepared by extraction with ethanol (alcohol-insoluble residue, AIR). Insets in **b**, **c**, **d**: relationship between the SC, WHC and WRC, respectively, and cell wall swelling. Hydration properties and cell wall swelling were determined on fruit from the same batch. Time scale in days after full bloom (DAFB). For calculation of SC, WHC and WRC see Materials and Methods

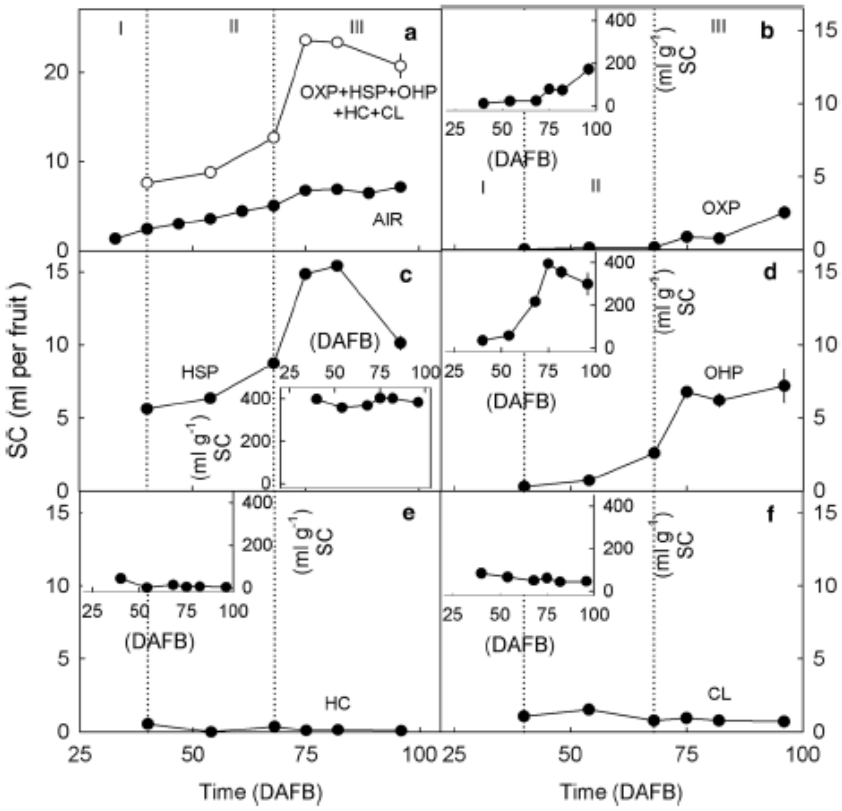

Fig. 7 Developmental time course of change in the swelling capacity (SC) of different cell wall fractions extracted from developing sweet cherry fruit. The SC was calculated on a whole fruit basis (Main graphs **a**–**f**) and on a unit dry mass basis of the respective cell wall fraction (Insets **b**–**f**). **a** Alcohol-insoluble cell wall residue (AIR) and the sum of oxalate-soluble pectins (OXP), HCl-soluble pectins (HSP), NaOH-soluble pectins (OHP), hemicelluloses (HC) and cellulose (CL). **b** OXP. **c** HSP. **d** OHP. **e** HC. **f** CL

54 and at 96 DAFB. The changes in volume were linearly related to the natural logarithm of the applied pressures (Fig. 9b). The extrapolated X-axis intercepts define the pressures required to prevent any swelling of the cell wall, i.e., the swelling pressure. Swelling pressure was low throughout development and increased towards maturity (Fig. 9c). Furthermore, only small differences were obtained between the swelling pressures of the different cell wall fractions (Table 2). The OHP had the highest swelling pressure, the other fractions did not differ significantly.

Discussion

Important findings are:

1. Cell wall deposition does not keep pace with fruit growth.
2. The swelling potential of cell walls increases during development.
3. Across all developmental stages and across all cell wall fractions, the swelling pressures were low, relative to the very negative osmotic potentials of the fruit.

Cell wall deposition does not keep pace with fruit growth

Cell wall deposition lags behind the increase in fruit fresh mass. This observation was consistent among all cultivars investigated. It is also consistent with earlier reports for 'Biggarreau Burlat' (Batisse et al. 1994) and 'Sweetheart' and 'New Star' sweet cherry (Salato et al. 2013). Apparently, the increase in fruit fresh mass distributed ('diluted') the cell wall mass throughout a steadily increasing fruit volume. This result is expected, because the stage III volume growth of the mesocarp is driven primarily by cell expansion (bigger cells) rather than by cell division (more cells) (Tukey and Young 1939; Olmstead et al. 2007). It is interesting that the 'dilution' of cell wall material by fruit volume growth did not affect all the cell wall fractions to the same extent. In particular, the HC and CL fractions and within the pectins the HSP, followed by the OHP were more strongly 'diluted'. There was no 'dilution' of the WSP or the OXP.

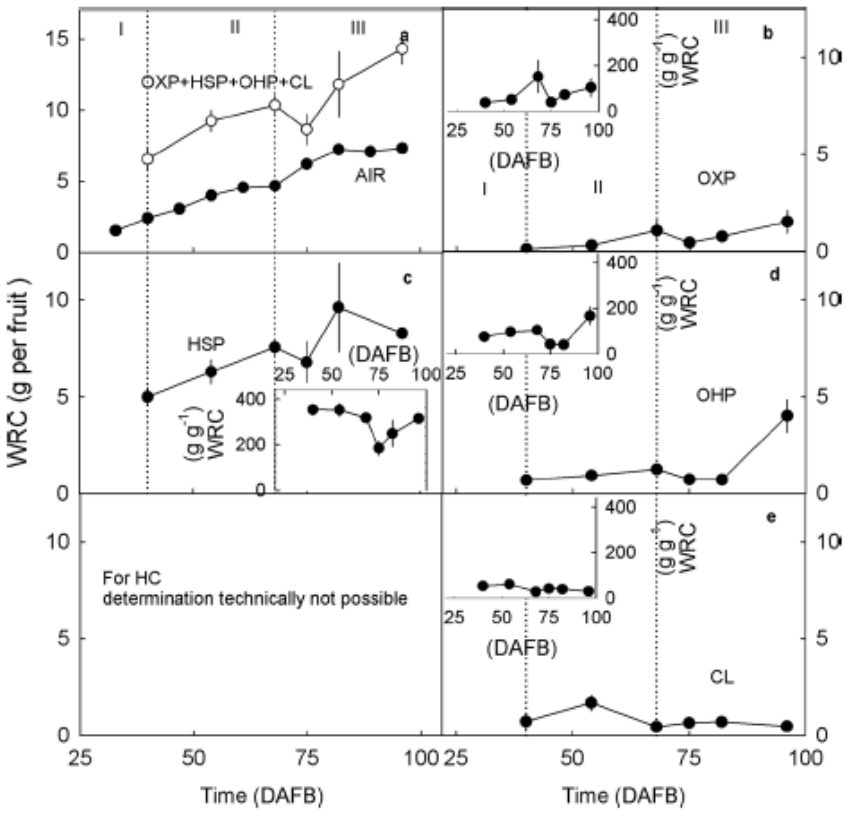

Fig. 8 Change in the water retention capacity (WRC) of different cell wall fractions extracted from developing sweet cherry fruit. The WRC was calculated on a whole fruit basis (Main graphs **a**–**f**) and a unit dry mass basis of the respective cell wall fraction (Insets **b**–**f**). **a** Alcohol-insoluble cell wall residue (AIR) and sum of oxalate-soluble pectins (OXP), HCl-soluble pectins (HSP), NaOH-soluble pectins (OHP), and cellulose (CL). **b** OXP. **c** HSP. **d** OHP. **e** HC. **f** CL. Due to the absence of significant swelling, the WRC of the HC cannot be determined reliably. Therefore, the HC data are omitted from this comparison

The composition of the major pectin fraction of the 'Regina' fruit used in our study was similar to that in earlier reports. In 'Regina', the HSP was the largest contributor (31%) to total pectins whereas the OXP fraction was the smallest (18% of total pectins). Barbier and Thibault (1982) reported 38% HSP and 19% OHP for 'Bigarreaux Napoléon' using the same extraction method. The percentages of WSP and OXP were about the same in 'Bigarreaux Napoléon' as in 'Regina' in this study.

On a fresh weight basis, the decrease in HSP and, to a lesser extent, in OHP accounted for the decrease of the AIR. This is consistent with studies by Basanta et al. (2013, 2014) who reported the largest decrease to occur in tightly-bound pectins which are represented by the Na_2CO_3-soluble fraction. Similar results were reported by Choi et al. (2002) and Salato et al. (2013). Also, the low percentage of the WSP and its increase towards maturity is consistent with earlier reports (Choi et al. 2002; Basanta et al. 2014). According to Ponce et al. (2010), the increase in the WSP may have been due to a weakening of the crosslinking of pectins by Ca leading to a solubilization of pectins.

Our findings have two important consequences. First, the cell walls are increasingly strained due to the increase in fruit mass particularly during stage III development. During stage III, fruit mass increases primarily due to increase in cell size and, to a lesser extent, in cell number. In contrast, growth in stages I and II is primarily accounted for by increases in cell number. Indeed, cell wall and tissue strain, and hence stress, in the fruit increased markedly during stage III development. The increasing stress is indexed by the gaping of a 'slit' wound in a fruit, made with a razor blade (Grimm et al. 2012). The strain and resulting stress in the cell walls are important in the cracking of fleshy fruit. Strain generates the stress, which is the driving force for the propagation of microcracks to form macrocracks (Schumann et al. 2019). However, the cell wall strain did not result in a decrease in cell wall thickness as one might expect. Indeed, cell wall thickness (between healthy, living, turgid cells) increased to 54 DAFB and then remained constant to 96 DAFB. This, despite of a 4.8-fold increase in fruit fresh mass (see Fig. 1a, d). At the same time, the mass of AIR per g fresh mass decreased indicating that the increase in fresh mass resulted in a 'dilution' of the cell wall material. The discrepancy between these results may be related to the observation that cell wall thickness represents the thickness of the epidermal (anticlinal) cell walls in the skin (Fig. 1d), whereas the cell wall mass is primarily determined by the cells of the flesh (Fig. 1b, c; Table 1). However, in the flesh, stage III growth (after 68 DAFB) is primarily due to cell expansion. Only during stage I, does cell division take place in the mesocarp

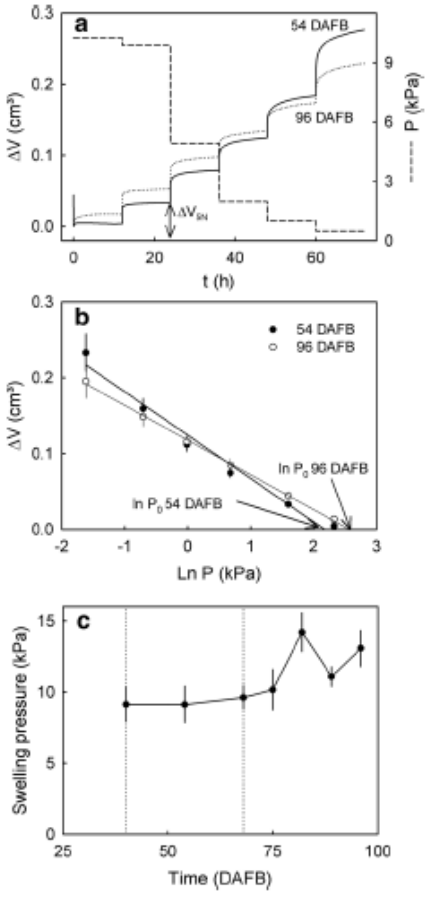

Fig. 9 Swelling of cell wall materials extracted from 'Regina' sweet cherry 54 and 96 days after full bloom (DAFB) when incubated in deionized water. Swelling was quantified in vitro as the change in volume (ΔV) at different pressures (P) using a custom-built pressure chamber. Extracted cell wall material was incubated in water to induce swelling. The ΔV of the swollen cell walls after loading the cell wall with different pressures was quantified. **a** Time course of water-induced swelling of cell walls when the applied pressure was decreased stepwise from 10.3 to 0.1 kPa. At each pressure step, the pressure was held constant for 12 h to allow equilibration of cell wall swelling. **b** Relationship between the swelling of cell walls (ΔV) at equilibrium and the applied pressure. The swelling pressure P_0 corresponds to the pressure at which no swelling occurs. The value P_0 was estimated as the *x*-axis intercept of a regression line fitted through a plot of ΔV vs. ln P. The regression equation was $\Delta V = -0.37\,(\pm 0.02) \times \ln P\,(kPa) + 1.42\,(\pm 0.04)$, $r^2 = 0.97^{***}$ **c** Developmental time course of the change in swelling pressure P_0. Time scale in days after full bloom (DAFB)

(Tukey and Young 1939; Olmstead et al. 2007). In contrast, the fruit skin undergoes continuing cell division into stage III growth (Knoche et al. 2004).

Second, the 'dilution' of the cellulose fraction of the cell wall material indicates a likely weakening of the cell wall. The cellulose fraction confers the structural strength and rigidity to the cell wall composite. In contrast, the pectins and hemicelluloses contribute to the cell wall's plasticity and viscoelasticity (Chanliaud et al. 2002).

Table 2 The in vitro swelling pressure of different fractions of extracted cell walls at 96 days after full bloom

Fraction	Swelling pressure (kPa)
OXP	10.5 ± 0.3 a[a]
HSP	7.7 ± 1.2 a
OHP	14.0 ± 0.2 b
HC	10.0 ± 0.8 a
CL	9.41 ± 0.6 a

The sum of the oxalate-soluble pectin (OXP), HCl-soluble pectin (HSP), NaOH-soluble pectin (OHP), hemicellulose (HC) and cellulose (CL) fractions comprised 80% of the alcohol-insoluble residue (AIR) of mature sweet cherry fruit. Data represent means ± SE. The swelling pressure was determined on 20 mg samples of each fraction

[a]Mean separation within columns by Tukey's Studentized range test, $P < 0.05$

Swelling of cell walls increases during development

The extent of cell wall swelling in sweet cherries was similar to that in other fruitcrop species (Redgwell et al. 1997). For example, for the AIR of pumpkin, De Escalada Plá et al. (2007) reported a swelling capacity of 42 ml g^{-1}, a water holding capacity of 43 g g^{-1} and a water retention capacity of 44 g g^{-1}. Similarly, for apple the water retention capacity was between 25 and 48 g g^{-1} depending on the extraction procedure (Vetter and Kunzek 2003). Furthermore, marked swelling of extracted cell walls was also reported for plum, persimmon, strawberry (Redgwell et al. 1997), kiwi (Redgwell et al. 1997; Fullerton 2015) and tomato (Shomer et al. 1991; Redgwell et al. 1997; Cantu et al. 2008). Significantly lower swelling capacities and water retention capacities were measured by Figuerola et al. (2005) for concentrates of apple and citrus fiber (no AIR) but their extraction procedures were different. Thus, it is fair to conclude the swelling of sweet cherry cell walls is within the range observed for other fruitcrop species.

That cell wall swelling increases during maturation is typical of fruit that, when ripe, have soft/melting textures. This observation holds for sweet cherry and also for persimmon, avocado, blackberry, strawberry and European plum (Redgwell et al. 1997). Cell wall swelling is the result of the absorption of water into voids within the cell wall. These voids are left behind after solubilization of pectins from the cellulose/hemicellulose network

(Redgwell et al. 1997). According to Raghavendra et al. (2004), the water absorption depends on the chemical, physical and microstructural properties of the entire cell wall network. Large values of water holding capacity and water retention capacity are expected for pectins that are readily solubilized in water (Basanta et al. 2013). In particular, hydrophilic polysaccharides such as rhamnogalacturonan I, increase water absorption and swelling (de Escalada Plá 2007). For example, in our study, the swelling capacity and the water retention capacity of the HC and CL were lower than of the pectins. An occlusion of pectins by HC or CL would decrease swelling. This is not unlikely. Recent evidence suggests that the CL and HC fractions may contain some pectins (Broxterman and Schols 2018). For fruit, the pectin content in the CL ranges from 5% of the total content of galacturonic acid of the cell wall in strawberry, to 10% in tomato (Broxterman and Schols 2018). If this was also the case in sweet cherry in our study, these hypothetical pectins in the HC and CL fractions did not contribute to swelling as indexed by the low intrinsic swelling capacity and water retention capacity of the HC and CL. Thus, our conclusion that the swelling was mostly due to the HSP and OHP (and possibly to the WSP) remains unaffected.

Although the in vitro swelling capacity and water retention capacity of the AIR were significantly correlated with the in vivo cell wall swelling, we observed a discrepancy between in vivo and in vitro assessments of swelling of the AIR, particularly during stage III. The microscopic in vivo assessments indicated continuing swelling, whereas the in vitro assays revealed little further change. This discrepancy may be accounted for by the sharp increase in the WSP fraction. This more than doubled from the stage II/III transition to late stage III. This fraction will be in solution and, hence, in the supernatant in the in vitro assays. Therefore, it will not contribute to the in vitro swelling as assessed by determination of the swelling capacity, the water holding capacity and the water retention capacity.

That the sum of the swelling capacities and the water retention capacities of the individual cell wall fractions exceeded that of the AIR is not surprising. The swelling capacities and the water retention capacities of the individual cell wall fractions characterize the 'intrinsic' swelling behavior in vitro of the extracted fraction in the absence of interactions with other cell wall constituents that occur in the cell wall composite in vivo. Consequently, the absence of swelling in vitro indicates that there will also be no swelling of the respective fraction in vivo, i.e., when still part of the cell wall composite. However, significant swelling of the extracted fraction in vitro indicates that the respective fraction may contribute to swelling in vivo, i.e., the swelling observed by microscopy of the epidermal cell walls. Whether it indeed contributes to swelling in vivo, will depend on its interaction with other cell wall constituents. For the swelling in vivo, the spatial arrangement of cell wall constituents within the cell wall composite and the interaction with cross-linking ions such as calcium is a critical factor (Basanta et al. 2013).

Cell wall swelling pressure is very low

The swelling pressure determined in vitro using extracted cell wall material was very low across all developmental stage and also across the different cell wall fractions. This finding is consistent with earlier ones indicating that the swelling of cell walls is a physical process, normally counterbalanced by cell turgor (Grimm and Knoche 2015; Schumann and Knoche 2020). Swelling occurs when turgor is lost, regardless of whether this is the result of turgor release following imposition of a freeze/thaw cycle or by plasmolyzing epidermal cells by exposure to a hypertonic osmoticum (Schumann and Knoche 2020). Because swelling pressures are very low, even the low cell turgors in stage III sweet cherry fruit are quite sufficient to prevent the swelling of cell walls in vivo (Schumann et al. 2014). Hence, cell wall swelling pressure is not a significant component of the water potential of sweet cherry fruit. That the sum of the swelling pressures of the individual extracted cell wall fractions exceeded that of the AIR is accounted for by the lack of interaction of the extracted fraction with other cell wall constituents as explained above for the swelling capacity and the water retention capacity.

Conclusion

Three explanations can be offered that contribute to the increase in cracking susceptibility of developing sweet cherry fruit reported in the literature (Christensen 1973). First, the low rate of cell wall deposition during growth results in a 'dilution' of cell walls as ongoing expansion growth increases cell wall strain. This results in a buildup of cell wall stress, which represents the driving force for cracking of sweet cherry and other fleshy fruitcrops. Second, the compositional changes that occur during cell wall development render the fruit flesh and skin less rigid and structurally weaker due to a relative decrease in the cellulose fraction. In addition, a general increase in the pectins fraction renders the cell walls more plastic and viscoelastic. Third, cell wall swelling increases due, in particular, to relative increases in the pectin fraction. As a result, cell:cell adhesion decreases making cells more susceptible to schizogony the separation of adjacent cells along the line of the middle lamella (Brüggenwirth and Knoche 2017; Schumann et al. 2019). This is the dominant fracture mode for rain cracking in sweet cherry.

Author contribution statement CS and MK conceived and designed the experiments. CS, SS and LE conducted the measurements. CS analyzed the data. CS and MK wrote the manuscript. All authors read and approved the manuscript.

Acknowledgements This research was funded in part by grants from the Deutsche Forschungsgesellschaft. We thank Andreas Meyer for constructing the pressure chamber, Chyntia Rosmaniar for help in extracting cell walls, Dr. Andreas Winkler for processing the microscopic images, Dr. Alexander Lang for useful comments on an earlier version of this manuscript and Prof. Andreas Schieber for helpful comments during the revision of this manuscript. This study was funded in part by a grant from the German Science Foundation (DFG).

Funding Open Access funding enabled and organized by Projekt DEAL.

Compliance with ethical standards

Conflict of interest The authors declare that they have no conflict of interest.

References

Alkio M, Jonas U, Sprink T, van Nocker S, Knoche M (2012) Identification of putative candidate genes involved in cuticle formation in *Prunus avium* (sweet cherry) fruit. Ann Bot 110:101–112

Barbier M, Thibault JF (1982) Pectic substances of cherry fruits. Phytochemistry 21:111–115

Basanta MF, de Escalada PM, Stortz CA, Rojas AM (2013) Chemical and functional properties of cell wall polymers from two cherry varieties at two developmental stages. Carbohydr Polym 92:830–841

Basanta MF, Ponce NMA, Salum ML, Raffo MD, Vicente AR, Erra-Balsells R, Stortz CA (2014) Compositional changes in cell wall polysaccharides from five sweet cherry (*Prunus avium* L.) cultivars during on-tree ripening. J Agric Food Chem 62:12418–12427

Batisse C, Fils-Lycaon B, Buret M (1994) Pectin changes in ripening cherry fruit. J Food Sci 59:389–393

Batisse C, Buret M, Coulomb PJ (1996) Biochemical Differences in cell wall of cherry fruit between soft and crisp fruit. J Agric Food Chem 44:453–457

Borve J, Sekse L, Stensvand A (2000) Cuticular fractures promote postharvest fruit rot in sweet cherries. Plant Dis 84:1180–1184

Broxterman SE, Schols HA (2018) Interactions between pectin and cellulose in primary plant cell walls. Carbohydr Polym 192:263–272

Brüggenwirth M, Knoche M (2017) Cell wall swelling, fracture mode, and the mechanical properties of cherry fruit skins are closely related. Planta 245:765–777

Brüggenwirth M, Fricke H, Knoche M (2014) Biaxial tensile tests identify epidermis and hypodermis as the main structural elements of sweet cherry skin. Ann Bot Plants. https://doi.org/10.1093/aobpla/plu019

Cantu D, Vicente AR, Greve LC, Dewey FM, Bennett AB, Labawitch JM, Powell ALT (2008) The intersection between cell wall disassembly, ripening, and fruit susceptibility to *Botrytis cinerea*. Proc Natl Acad Sci USA 105:859–864

Chanliaud E, Burrows KM, Jeronomidis G, Gidley MJ (2002) Mechanical properties of primary plant cell wall analogues. Planta 215:989–996

Choi C, Toivonen P, Wiersma PA, Kappel F (2002) Differences in levels of pectic substances and firmness in fruit from six sweet cherry genotypes. J Am Pomol Soc 56:197–201

Christensen JV (1973) Cracking in cherries. VI. Cracking susceptibility in relation to the growth rhythm of the fruit. Acta Agric Scand 23:52–54

de Escalada Pla MF, Ponce NMA, Stortz CA, Rojas AM, Gerschenson LN (2007) Composition and functional properties of enriched fibre products obtained from pumpkin (*Cucurbita moschata*, Duchesne ex Poiret). LWT-Food Sci Technol 40:1176–1185

Figuerola F, Hurtado ML, Estévez AM, Chiffelle I, Asenjo F (2005) Fibre concentrates from apple pomace and citrus peel as potential fibre sources for food enrichment. Food Chem 91:395–401

Fügel R, Carle R, Schieber A (2004) A novel approach to quality and authenticity control of fruit products using fractionation and characterisation of cell wall polysaccharides. Food Chem 87:141–150

Fügel R, Schieber A, Carle R (2006) Determination of the fruit content of cherry fruit preparations by gravimetric quantification of hemicellulose. Food Chem 95:163–168

Fullerton CG (2015) Kiwifruit softening: a cell wall study. Dissertation, University of Auckland.

Glenn GM, Poovaiah BW (1989) Cuticular properties and postharvest calcium applications influence cracking of sweet cherries. J Am Soc Hortic Sci 114:781–788

Grimm E, Knoche M (2015) Sweet cherry skin has a less negative osmotic potential than the flesh. J Am Soc Hortic Sci 140:472–479

Grimm E, Peschel S, Becker T, Knoche M (2012) Stress and strain in the sweet cherry fruit skin. J Am Soc Hortic Sci 137:383–390

Grimm E, Hahn J, Pflugfelder D, Schmidt M, van Dusschoten D, Knoche M (2019) Localized bursting of mesocarp cells triggers catastrophic fruit cracking. Hortic Res 6:79. https://doi.org/10.1038/s41438-019-0161-3

Grimm E, Pflugfelder D, Hahn J, Schmidt MJ, Dieckmann H, Knoche M (2020) Spatial heterogeneity of flesh-cell osmotic potential in sweet cherry affects partitioning of absorbed water. Hortic Res 7:51. https://doi.org/10.1038/s41438-020-0274-8

Herrmann K (2001) Inhaltsstoffe von Obst und Gemüse. Ulmer, Stuttgart

Khanal BP, Grimm E, Knoche M (2011) Fruit growth, cuticle deposition, water uptake, and fruit cracking in jostaberry, gooseberry, and black currant. Sci Hortic 128:289–296

Knoche M, Lang A (2017) Ongoing growth challenges fruit-skin integrity. Crit Rev Plant Sci 36:190–215. https://doi.org/10.1080/07352689.2017.1369333

Knoche M, Peschel S (2006) Water on the surface aggravates microscopic cracking of the sweet cherry fruit cuticle. J Am Soc Hortic Sci 131:192–200

Knoche M, Beyer M, Peschel S, Oparlakov B, Bukovac MJ (2004) Changes in strain and deposition of cuticle in developing sweet cherry fruit. Physiol Plant 120:667–677

Knoche M, Khanal BP, Stopar M (2011) Russeting and microcracking of "Golden Delicious" apple fruit concomitantly decline due to Gibberellin A4+7 application. J Am Soc Hortic Sci 136:159–164

Kondo S, Danjo C (2001) Cell wall polysaccharide metabolism during fruit development in sweet cherry "Satohnishiki" as affected by gibberellic acid. J Japan Soc Hortic Sci 70:178–184

Lichter A, Dvir O, Fallik E, Cohen S, Golan R, Shemer Z, Sagi M (2002) Cracking of cherry tomatoes in solution. Postharvest Biol Technol 26:305–312

Maguire K, Lang A, Banks NH, Hall A, Hopcroft D, Bennett R (1999) Relationship between water vapour permeance of apples and micro-cracking of the cuticle. Postharvest Biol Technol 17:89–96

Mrozek RF, Burkhardt TH (1973) Factors causing prune side cracking. Trans Am Soc Agric Eng 16:686–695

Olmstead JW, Iezzoni AF, Whiting MD (2007) Genotypic differences in sweet cherry fruit size are primarily a function of cell number. J Am Soc Hortic Sci 132:697–703

Opara LU, Studman CJ, Banks NH (1997) Fruit skin splitting and cracking. Hortic Rev 19:217–262

Peschel S, Knoche M (2005) Characterization of microcracks in the cuticle of developing sweet cherry fruit. J Am Soc Hortic Sci 130:487–495

Ponce NMA, Ziegler VH, Stortz CA, Sozzi GO (2010) Compositional changes in cell wall polysaccharides from Japanese plum (*Prunus salicina* Lindl.) during growth and on-tree ripening. J Agric Food Chem 58:2562–2570

Raghavendra SN, Rastogi NK, Raghavarao KSMS, Tharanathan RN (2004) Dietary fiber from coconut residue: effects of different treatments and particle size on the hydration properties. Eur Food Res Technol 218:563–567

Redgwell RJ, MacRae E, Hallett I, Fischer M, Perry J, Harker R (1997) In vivo and in vitro swelling of cell walls during fruit ripening. Planta 203:162–173

Rombouts FM, Thibault JF (1986) Feruloylated pectic substances from sugar-beet pulp. Carbohydr Res 154:177–187

Salato GS, Ponce NMA, Raffo MD, Vicente AR, Stortz CA (2013) Developmental changes in cell wall polysaccharides from sweet cherry (*Prunus avium* L.) cultivars with contrasting firmness. Postharvest Biol Technol 84:66–73

Saulnier L, Thibault JF (1987) Extraction and characterization of pectic substances from pulp of grape berries. Carbohydr Polym 7:329–343

Schumann C, Knoche M (2020) Swelling of cell walls in mature sweet cherry fruit: Factors and mechanisms. Planta 251:65. https://doi.org/10.1007/s00425-020-03352-y

Schumann C, Schlegel HJ, Grimm E, Knoche M, Lang A (2014) Water potential and its components in developing sweet cherry. J Am Soc Hort Sci 139:349–355

Schumann C, Winkler A, Brüggenwirth M, Köpcke K, Knoche M (2019) Crack initiation and propagation in sweet cherry skin: a simple chain reaction causes the crack to 'run.' PLoS ONE 14(7):e0219794. https://doi.org/10.1371/journal.pone.0219794

Shomer I, Frenkel H, Polinger C (1991) The existence of a diffuse electric double layer at cellulose fibril surfaces and its role in the swelling mechanism of parenchyma plant cell walls. Carbohydr Polym 16:199–210

Sozzi GO, Greve LC, Prody GA, Labavitch JM (2002) Gibberellic acid, synthetic auxins, and ethylene differentially modulate α-L-arabinofuranosidase activities in antisense 1-aminocyclopropane-1-carboxylic acid synthase tomato pericarp discs. Plant Physiol 129:1330–1340

Tukey HB, Young JO (1939) Histological study of the developing fruit of the sour cherry. Bot Gaz 100:723–749

Vetter S, Kunzek H (2003) The influence of suspension solution conditions on the rehydration of apple cell wall material. Eur Food Res Technol 216:39–45

Winkler A, Ossenbrink M, Knoche M (2015) Malic acid promotes cracking of sweet cherry fruit. J Am Soc Hortic Sci 140:280–287

Winkler A, Peschel S, Kohrs K, Knoche M (2016) Rain cracking in sweet cherries is not due to excess water uptake but to localized skin phenomena. J Am Soc Hortic Sci 141:653–660

Yapo BM, Koffi KL (2008) The polysaccharide composition of yellow passion fruit rind cell wall: chemical and macromolecular features of extracted pectins and hemicellulosic polysaccharides. J Sci Food Agric 88:2125–2133

Yapo BM, Lerouge P, Thibault JF, Ralet MC (2007) Pectins from citrus peel cell walls contain homogalacturonans homogenous with respect to molar mass, rhamnogalacturonan I and rhamnogalacturonan II. Carbohydr Polym 69:426–435

3.4 Calcium decreases cell wall swelling in sweet cherry fruit

Das Original dieses Artikels wurde 2022 in der Zeitschrift „Scientific reports“ veröffentlicht.

Schumann, C., Winkler, A. and Knoche, M. (2022): 3.4 Calcium decreases cell wall swelling in sweet cherry fruit. *Scientific reports* 12, 16496

DOI: https://doi.org/10.1038/s41598-022-20266-9

Beteiligung der Autoren

M. Knoche warb die Drittmittel für das Vorhaben ein. M. Knoche und C. Schumann planten die Experimente. A. Winkler und C. Schumann führten die Experimente durch. M. Knoche und C. Schumann analysierten die Daten. M. Knoche, A. Winkler und C. Schumann schrieben und editierten das Manuskript. M. Knoche, A. Winkler und C. Schumann revidierten das Manuskript.

www.nature.com/scientificreports

scientific reports

Check for updates

OPEN

Calcium decreases cell wall swelling in sweet cherry fruit

Christine Schumann, Andreas Winkler & Moritz Knoche✉

Swelling of epidermal cell walls decreases cell-to-cell adhesion and increases cracking susceptibility in sweet cherry. Ca is suggested to decrease cracking susceptibility by crosslinking of cell wall components and, possibly, by decreasing swelling. The objective is to test this hypothesis. The effect of Ca on swelling of anticlinal epidermal cell walls was quantified microscopically in vivo using excised skin sections and in vitro using extracted cell walls. After removal of turgor, cell wall thickness increased. Incubation in $CaCl_2$ decreased cell wall thickness up to 3 mM $CaCl_2$. At higher concentrations thickness remained constant. Decreased cell wall swelling in vivo also occurred with other salts of divalent and trivalent cations, but not with those of monovalent cations. Decreased swelling was due to the Ca cation, the anions had no effect. Ca also decreased swelling of cell walls that were already swollen. $CaCl_2$ also decreased swelling of extracted cell walls in vitro. There was no effect on swelling pressure. The effect on swelling increased as the $CaCl_2$ concentration increased. Chlorides of divalent and trivalent cations, but not those of monovalent cations decreased swelling in vitro. The decrease in swelling among the divalent cations was linearly related to the radius of the cation. The results indicate that Ca decreases cracking susceptibility by decreasing swelling.

Rain-induced fruit cracking is a serious problem for producers of sweet cherry fruit in all areas worldwide where rainfall occurs before and during the harvest season[1]. Even low percentages of cracked fruit render a harvest uneconomic. Meanwhile, the quality of the remaining macroscopically un-cracked fruit is seriously compromised due to microcracking of the cuticle as a result of exposure of the fruit skin to surface moisture[2]. As a consequence of this microcracking, postharvest fruit transpiration is increased, fruit firmness is decreased, shrivel is more likely and the incidence of fruit rots is markedly increased[3]. Moreover, fruit skins with cuticular microcracks allow unrestricted water uptake[3,4].

Reliable remedies against rain cracking are limited. They include the cultivation of trees under rain covers or in tunnels[5,6]. Except for extreme cases, cracking is markedly reduced, but the capital costs of production are markedly increased. Foliar applications of Ca-salts are reported to reduce rain cracking at times[7]. However, this effect is not reliably reproducible. In many cases, foliar Ca applications have no effect at all. A variety of mechanisms for the putative role of Ca in reducing rain cracking have been proposed.

First, the effects of Ca have been attributed to decreased water uptake as a result of a decrease in the driving force for osmotic water uptake. However, based on the concentrations of the Ca salts used, the osmotic potential of sweet cherry juice and the lack of a significant fruit turgor, the decrease in osmotic driving force is negligibly low and unlikely to be detectable in the field[3]. For example, for a spray concentration of 34 mM $CaCl_2$ (equiv. to 0.5% $CaCl_2 \cdot 2H_20$), the osmotic potential of the solution would be −0.25 MPa. At a fruit water potential of 3 MPa, this would correspond only to a 8.3% decrease in driving force[7]. Hence, decreased water uptake due to this osmotic effect can be excluded as a factor.

Second, Ca is known to increase crosslinking of cell wall constituents[8–10]. This also occurs in the load-bearing fruit skin of sweet cherry fruit[11,12]. Consistent with this observation is a shift in the fracture mode from (a) fracture by separation of adjacent cells along their middle lamella to (b) fracture across the cellulosic cell wall. The most likely explanation for these observations is a decrease in cell-wall swelling that results in increased cell-to-cell adhesion[12].

The interactions between Ca ions and cell wall components have been studied in great detail (for a review see[13]). Basic studies employed well-defined linear pectins in standardized systems (pH, concentration of Ca and other cations). These studies led to the 'egg box model' that is widely used to describe the interactions of the Ca ion and homogalacturonans in cross linking[14,15]. The effects of Ca on isolated cell walls were investigated before[16–19]. In these studies, the focus was on the role of Ca in cell-to-cell adhesion during the preharvest[20] and postharvest periods, and with respect to fruit quality traits such as firmness[21–23]. We are aware of no reports on the effects of Ca on cell walls at the tissue level or at the organ level.

Institute of Horticultural Production Systems, Leibniz University Hanover, Herrenhäuser Straße 2, 30419 Hannover, Germany. ✉email: moritz.knoche@obst.uni-hannover.de

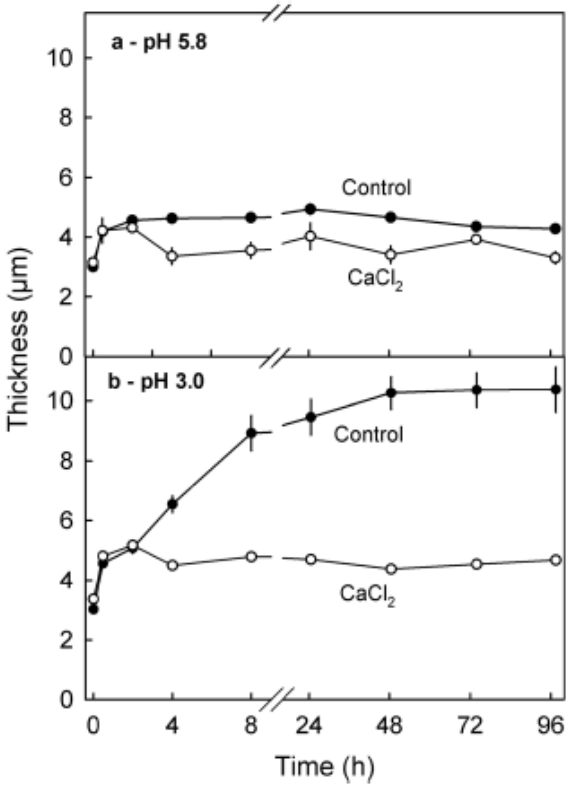

Figure 1. Time course of change in thickness of anticlinal cell walls of excised epidermal segments (ES) of mature 'Santina' sweet cherry fruit after a freeze/thaw cycle. The ES were incubated in buffered 10 mM $CaCl_2$ or in buffer only. The concentration of the MES buffer was 10 mM MES and the pH was adjusted to pH 5.8 (**a**) or pH 3.0 (**b**).

The objective of our study was to establish the effects of Ca salts on cell wall swelling in mature sweet cherry fruit. Since the bursting of cells is associated with rain cracking and also that sweet cherry juice is acidic (pH 3.6), we were particularly interested in potential interactions between the effects of Ca and of pH on cell wall swelling.

Results

Following release of turgor by a freeze/thaw cycle, cell wall thickness increased rapidly and reached an asymptote within 24 h when the pH was 5.8. The increase in cell wall thickness was larger at pH 3.0 than at pH 5.8. Incubation in $CaCl_2$ resulted in less swelling. Decreasing the pH from pH 5.8 to pH 3.0 had little effect on swelling in the presence of $CaCl_2$ as compared to the control without $CaCl_2$ (Fig. 1).

At all pHs, $CaCl_2$ decreased cell wall swelling after turgor release with the decrease depending on Ca concentration. There was little difference in response between concentrations of 3 mM and 100 mM (Fig. 2a). The decrease in thickness was largest at pH 3.0 and decreased as pH increased (Fig. 2b). The effect of $CaCl_2$ on cell wall swelling was larger than that of increasing pH.

The trivalent cations $AlCl_3$ and $FeCl_3$ also decreased cell wall swelling in a concentration-dependent manner. These solutions, however, precipitated when buffered at higher pH. They were only stable at higher concentrations when the pH remained low. The decrease in cell wall thickness was largest for $AlCl_3$ at 10 mM and for $FeCl_3$ at 3 mM (Fig. 3a,b). It is interesting that 30 mM $FeCl_3$ (pH 2.0) or 100 mM $FeCl_3$ (pH 1.5) had no additional effect on cell wall swelling despite their very acid pHs. The decrease in swelling was not confined to $CaCl_2$, $AlCl_3$ and $FeCl_3$ but also occurred with the other chloride salts of divalent cations. Only the chlorides of monovalent cations had no effect on cell wall swelling (Table 1).

The decrease in cell wall swelling by $CaCl_2$ was due to the Ca cation. There was no difference in cell wall swelling between various Ca salts, indicating the anion had essentially no effect on the response (Table 2).

Consistent with the effect of $CaCl_2$ on cell wall swelling was the effect of EGTA. Incubating ES after turgor release in EGTA markedly increased cell wall swelling (+84%). The increase in swelling was slightly reduced when EGTA was applied together with $CaCl_2$ (Table 3).

The decrease in cell wall swelling following incubation in $CaCl_2$ was slightly reduced but remained significant, even after the $CaCl_2$ solution was replaced by buffer only. Surprisingly, $CaCl_2$ decreased swelling even of swollen cell walls (Table 4).

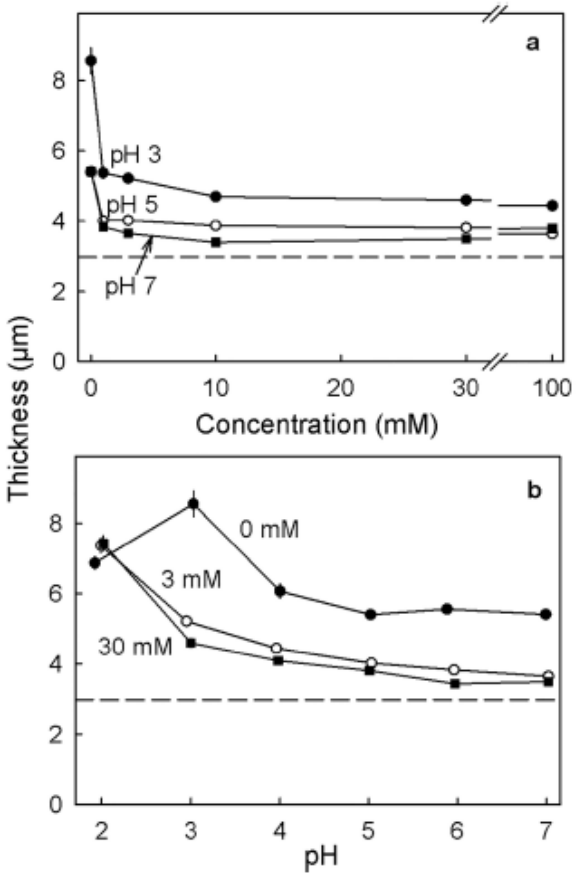

Figure 2. (**a**) Effect of the concentration of $CaCl_2$ at pH 3.0, pH 5.0 or pH 7.0 on the thickness of the anticlinal cell walls of excised epidermal segments (ES) of mature 'Burlat' sweet cherry fruit. (**b**) Effect of pH at $CaCl_2$ concentrations of 0, 3 and 30 mM. All ES were treated with a freeze/thaw cycle to release turgor followed by an incubation in the respective solution for 48 h. All solutions were buffered with 10 mM MES. The dashed horizontal line indicates the cell wall thickness in the native state, i.e., before the release of turgor.

Incubating ES in hypotonic solutions (phase I) without $CaCl_2$ had little effect on cell wall swelling. Under these conditions, cells remained turgid. However, when $CaCl_2$, was added, cell wall thickness decreased also of turgid cells. This decrease was essentially independent of whether $CaCl_2$ was added during phase I or phase II of the experiment. The decrease in cell wall thickness remained, even after $CaCl_2$ was removed from the solution. Repeating the same experiment but incubating ES in hypertonic solutions during phase I, induced plasmolysis. The effect of $CaCl_2$ was qualitatively the same as when incubating fruit first in hypotonic solutions. The only difference was that $CaCl_2$ had a markedly larger effect on cell wall thickness in the absence of turgor. $CaCl_2$ consistently reduced cell wall thickness even when cell walls were previously swollen (Table 5).

Incubating ES in hypertonic solutions (phase I) resulted in plasmolysis and swelling of cell walls at pH 3.0, and less so at pH 5.8 (Table 6). When incubation continued and pH was increased from pH 3.0 (phase I) to pH 5.8 (phase II), cell wall swelling increased even more. There was no decrease in cell wall swelling, indicating the effect of pH on swelling was not reversible. Quantitatively similar data, albeit at a lower level, were obtained in plasmolyzed cells during incubation in a hypertonic solution at pH 5.8.

When intact fruit were pretreated by incubation in isotonic $CaCl_2$, sucrose, EGTA or MES, cell wall thickness of $CaCl_2$-treated skins remained low and not significantly different from the un-incubated controls whereas cell wall thickness increased in isotonic sucrose, EGTA and MES (Table 7). When turgor was released by a freeze/thaw cycle, cell wall thickness of $CaCl_2$-treated fruit increased slightly but remained significantly lower than that of control fruit or of fruit pretreated with isotonic sucrose, EGTA and MES.

The time course of change in volume of extracted cell walls during incubation in buffer revealed a transient decrease in volume that was followed by an increase in volume. The increase in volume reached an equilibrium within about 24 h (Fig. 4). When the MES buffer was replaced by buffered EGTA, cell wall volume increased slightly indicating increased swelling compared to the MES control. However, when the MES was replaced by buffered $CaCl_2$, cell wall volume decreased markedly.

Stepwise decreases in the pressure applied to the extracted cell wall material resulted in stepwise increases in volume. These increases were lowest in the presence of $CaCl_2$ and highest in presence of EGTA (Fig. 5a). The

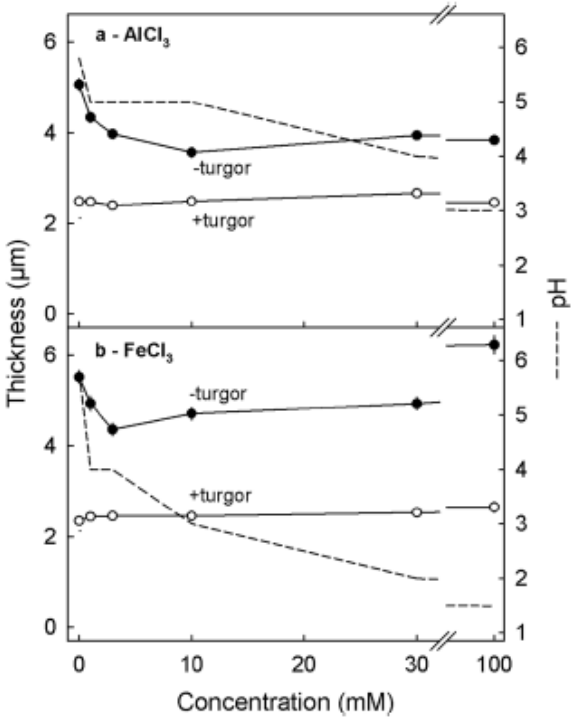

Figure 3. Effect of the concentration of $AlCl_3$ (**a**) or $FeCl_3$ (**b**) on the thickness of the anticlinal cell walls of excised epidermal segments (ES) of mature 'Sam' sweet cherry fruit. All ES were treated with a freeze/thaw cycle to release turgor followed by an incubation in one of a range of concentrations for 48 h. The dashed lines indicate the solution pH after incubation.

Treatment	Thickness (µm)		ΔThickness (µm)
	+ turgor	−turgor	
Control (MES)	2.9 ± 0.1	5.6 ± 0.1	2.7 ± 0.1
Control (water)	2.9 ± 0.1	5.6 ± 0.1	2.8 ± 0.1
KCl	2.8 ± 0.1	5.6 ± 0.1	2.8 ± 0.2
LiCl	2.9 ± 0.1	5.6 ± 0.1	2.7 ± 0.1
NaCl	2.9 ± 0.1	5.6 ± 0.1	2.7 ± 0.2
NH_4Cl	2.9 ± 0.1	5.8 ± 0.1	2.9 ± 0.2
$CaCl_2$	2.9 ± 0.1	3.7 ± 0.1*	0.9 ± 0.1
$BaCl_2$	2.8 ± 0.1	3.6 ± 0.1*	0.8 ± 0.1
$MgCl_2$	2.9 ± 0.0	4.6 ± 0.0*	1.7 ± 0.1
$SrCl_2$	2.9 ± 0.1	3.9 ± 0.1*	1.0 ± 0.1

Table 1. Effects of selected chloride salts on the thickness and swelling (Δthickness) of anticlinal epidermal cell walls of excised skin segments (ES) of 'Sam' sweet cherry fruit before (+turgor) and after turgor release (−turgor) by a freeze/thaw cycle. The ES were incubated in salt solutions at concentrations of 10 mM buffered with 10 mM MES. The pH was adjusted to pH 5.8 using KOH or HCl. Buffer only (10 mM MES, pH 5.8) and deionized water served as the controls. ΔThickness was calculated as the difference between cell wall thickness measured after turgor release, minus that measured before turgor release. Data are means ± SE. *Mean separation within columns against the MES control indicated by *, Dunnett test at $p < 0.05$.

relationship between the change in volume and the logarithm of the pressure applied was linear and highly significant (Fig. 5b). There were no significant effects of $CaCl_2$ or EGTA on the swelling pressure. The slope of the relationship, however, was significantly decreased by $CaCl_2$ (Table 8).

When the pressure applied to extracted cell walls was decreased stepwise in the presence of $CaCl_2$, the corresponding increases in cell wall volume depended on both $CaCl_2$ concentration and on the applied pressure (Fig. 6a). There was no consistent effect of $CaCl_2$ concentration on swelling pressure (Fig. 6a). However, the slope

Treatment	Thickness (µm)		ΔThickness (µm)
	+turgor	−turgor	
Control (MES)	2.8 ± 0.1	5.3 ± 0.1	2.5 ± 0.1
Control (water)	2.8 ± 0.1	5.2 ± 0.1	2.4 ± 0.1
$CaCl_2$	2.8 ± 0.1	3.5 ± 0.1*	0.6 ± 0.1
$Ca(NO_3)_2$	2.8 ± 0.1	3.5 ± 0.1*	0.7 ± 0.1
$CaSO_4$	2.8 ± 0.1	3.6 ± 0.1*	0.8 ± 0.1
Ca-acetate	2.9 ± 0.1	3.6 ± 0.1*	0.7 ± 0.1
Ca-propionate	2.8 ± 0.1	3.6 ± 0.1*	0.8 ± 0.1
Ca-formate	2.8 ± 0.1	3.6 ± 0.1*	0.8 ± 0.1
Ca-lactate	2.8 ± 0.1	3.6 ± 0.1*	0.8 ± 0.1
Ca-heptagluconate	2.8 ± 0.1	3.6 ± 0.1*	0.8 ± 0.1

Table 2. Effects of selected anions of Ca salts on thickness and swelling (Δthickness) of anticlinal epidermal cell walls of excised skin segments (ES) of 'Sam' sweet cherry fruit before (+turgor) and after turgor release (−turgor) by a freeze/thaw cycle. The ES were incubated in salt solutions at concentrations of 10 mM and buffered with 10 mM MES. The pH was adjusted to pH 5.8 using KOH or HCl. Buffer only (10 mM MES, pH 5.8) and deionized water served as controls. ΔThickness was calculated as the difference between the thickness measured after turgor release minus that measured before turgor release. Data are means ± SE. *Mean separation within columns against the MES control indicated by *, Dunnett test at $p < 0.05$.

Treatment	pH	Thickness (µm)		ΔThickness (µm)
		+turgor	−turgor	
Control	5.8	2.3 ± 0.1 a[a]	4.9 ± 0.1 a	2.7 ± 0.2
Control	8.0	2.4 ± 0.1 a	4.8 ± 0.1 a	2.4 ± 0.2
$CaCl_2$	8.0	2.1 ± 0.1 a	3.3 ± 0.1 b	1.2 ± 0.2
EGTA	8.1	2.2 ± 0.1 a	8.8 ± 0.3 c	6.6 ± 0.4
EGTA + $CaCl_2$	8.0	2.3 ± 0.1 a	6.7 ± 0.3 d	4.5 ± 0.4

Table 3. Effects of $CaCl_2$ (5 mM), EGTA (5 mM) or $CaCl_2$ (2.5 mM) plus EGTA (2.5 mM) on thickness and swelling (Δthickness) of anticlinal epidermal cell walls of excised skin segments (ES) of 'Burlat' sweet cherry fruit before (+turgor) and after turgor release (−turgor) by a freeze/thaw cycle. All solutions were buffered with 10 mM MES and pH adjusted with KOH to 8.0. MES at pH 5.8 and pH 8.0 served as controls. ΔThickness was calculated as the difference between the thickness measured after turgor release minus that measured before turgor release. Data are means ± SE. [a]Mean separation within columns, Tukey's Studentized range test at $p < 0.05$.

Treatment sequence	Thickness (µm)		
Phase I / phase II	Initial	Phase I	Phase II
$-CaCl_2/-CaCl_2$	3.2 ± 0.1 a[a]	6.5 ± 0.2 a	6.8 ± 0.2 a
$-CaCl_2/+CaCl_2$	3.1 ± 0.1 a	6.3 ± 0.2 a	4.3 ± 0.1 b
$+CaCl_2/-CaCl_2$	3.5 ± 0.1 b	3.9 ± 0.1 b	4.3 ± 0.1 b
$+CaCl_2/+CaCl_2$	3.2 ± 0.1 ab	3.9 ± 0.1 b	3.7 ± 0.1 c

Table 4. Effects of $CaCl_2$ on thickness of anticlinal epidermal cell walls of excised skin segments (ES) of 'Burlat' sweet cherry fruit. The experiment was conducted by imposing sequential treatments on the same specimen. First, initial thickness of the cell walls was measured and then the turgor was released by a freeze/thaw cycle. The experiment then continued with two phases. The sequences of treatments (phase I / phase II) were $-CaCl_2/-CaCl_2$, $-CaCl_2/+CaCl_2$, $+CaCl_2/-CaCl_2$, $+CaCl_2/+CaCl_2$. The durations of phase I and phase II were both 48 h. At the ends of both phases, cell wall thickness was again measured. The concentrations of $CaCl_2$ were all 10 mM. All solutions were buffered with 10 mM MES and pH adjusted with KOH to pH 5.8. Data are means ± SE. [a]Mean separation within columns, Tukey's Studentized range test at $p < 0.05$.

Treatment sequence	Thickness (µm)		
Phase I / Phase II	Initial	Phase I	Phase II
hypotonic – $CaCl_2$ / hypertonic – $CaCl_2$	2.8 ± 0.1 a[a]	3.1 ± 0.2 a	4.1 ± 0.1 a
hypotonic – $CaCl_2$ / hypertonic + $CaCl_2$	2.8 ± 0.1 a	3.2 ± 0.1 a	2.8 ± 0.1 bc
hypotonic + $CaCl_2$ / hypertonic – $CaCl_2$	2.7 ± 0.1 a	2.3 ± 0.0 b	2.8 ± 0.1 bc
hypotonic + $CaCl_2$ / hypertonic + $CaCl_2$	3.0 ± 0.1 a	2.3 ± 0.1 b	2.6 ± 0.1 c
hypertonic – $CaCl_2$ / hypertonic – $CaCl_2$	2.7 ± 0.1 a	4.8 ± 0.1 c	4.5 ± 0.1 d
hypertonic – $CaCl_2$ / hypertonic + $CaCl_2$	2.9 ± 0.1 a	4.6 ± 0.1 c	2.9 ± 0.1 bc
hypertonic + $CaCl_2$ / hypertonic – $CaCl_2$	2.9 ± 0.1 a	2.9 ± 0.1 a	3.3 ± 0.1 e
hypertonic + $CaCl_2$ / hypertonic + $CaCl_2$	2.9 ± 0.1 a	3.0 ± 0.1 a	3.2 ± 0.1 be

Table 5. Effects of $CaCl_2$ and cell turgor on thickness of anticlinal epidermal cell walls of excised skin segments (ES) of 'Burlat' sweet cherry fruit. Cell turgor was manipulated by incubating ES in 0.25 M sucrose (hypotonic) or 1.5 M sucrose (hypertonic) in the presence of 10 mM $CaCl_2$ ('+$CaCl_2$') or its absence ('–$CaCl_2$'). The experiment was conducted by imposing sequential treatments on the same specimens. First, initial thickness of cell walls was measured ('initial'). The experiment then continued with two phases lasting 24 h each. All solutions were buffered using 10 mM MES at pH 5.8. At the end of each phase, cell wall thickness was measured. Data are means ± SE. [a]Mean separation within columns, Tukey's Studentized range test at $p < 0.05$.

Treatment sequence	Thickness (µm)		
Phase I / phase II	Initial	Phase I	Phase II
hypotonic pH 3.0 / hypertonic pH 3.0	2.9 ± 0.1 ab[a]	9.5 ± 0.3 a	8.2 ± 0.3 a
hypotonic pH 3.0 / hypertonic pH 5.8	3.0 ± 0.1 ab	10.6 ± 0.4 b	11.9 ± 1.1 b
hypotonic pH 5.8 / hypertonic pH 3.0	2.8 ± 0.1 ab	3.2 ± 0.1 c	4.7 ± 0.1 c
hypotonic pH 5.8 / hypertonic pH 5.8	2.8 ± 0.1 ab	3.2 ± 0.1 c	4.0 ± 0.1 c
hypertonic pH 3.0 / hypertonic pH 3.0	2.7 ± 0.1 a	5.3 ± 0.1 d	5.7 ± 0.2 c
hypertonic pH 3.0 / hypertonic pH 5.8	2.8 ± 0.0 ab	5.6 ± 0.1 d	9.3 ± 0.3 a
hypertonic pH 5.8 / hypertonic pH 3.0	2.6 ± 0.1 a	4.0 ± 0.1 ce	4.8 ± 0.1 c
hypertonic pH 5.8 / hypertonic pH 5.8	2.7 ± 0.1 a	4.1 ± 0.1 e	4.0 ± 0.1 c

Table 6. Effects of pH and turgor on the thickness of anticlinal epidermal cell walls of excised skin segments (ES) of 'Adriana' sweet cherry fruit. [a] Mean separation within columns, Tukey's Studentized range test at $p < 0.05$. Turgor was manipulated by incubating ES in 0.25 M sucrose ('hypotonic') or 1.5 M sucrose ('hypertonic') at pH 3.0 or pH 5.8. The experiment was conducted by imposing sequential treatments on the same specimens. First, initial thickness of cell walls was measured ('initial'). The experiment then continued with two phases (phase I / phase II) lasting 24 h each. All solutions were buffered using 10 mM MES. At the end of each phase, cell wall thickness was again measured. Data are means ± SE.

Treatment	pH	Thickness (µm)		ΔThickness (µm)
		+ turgor	– turgor	
$CaCl_2$	8.2	2.6 ± 0.1 a[a]	3.8 ± 0.1 a	1.3 ± 0.1
Sucrose	8.2	3.6 ± 0.1 bc	4.6 ± 0.1 b	1.0 ± 0.2
EGTA	8.2	3.8 ± 0.2 b	5.1 ± 0.1 c	1.3 ± 0.2
MES	8.2	3.4 ± 0.1 c	5.0 ± 0.1 bc	1.6 ± 0.2
Control	n.d	2.8 ± 0.1 a	4.9 ± 0.1 bc	2.1 ± 0.2

Table 7. Thickness of anticlinal cell walls of excised skin segments (ES) of 'Burlat' sweet cherry fruit after pretreating whole fruits by incubation for 24 h in isotonic $CaCl_2$ solution containing 10 mM MES, isotonic sucrose solutions without $CaCl_2$ or in hypotonic 5 mM EGTA containing 10 mM MES or 10 mM MES buffer only. Thickness of cell walls was determined on ES after excision and pretreating intact fruit for 24 h (+turgor). The turgor was then released by a freeze/thaw cycle (–turgor). After 48 h, the cell wall thickness was again measured. Fruits for control were held for 24 h at room temperature. Swelling (Δthickness) was calculated as the difference in cell wall thickness without turgor, minus that with turgor. Data are means ± SE. n.d. not determined. [a]Mean separation within columns, Tukey's Studentized range test at $p < 0.05$.

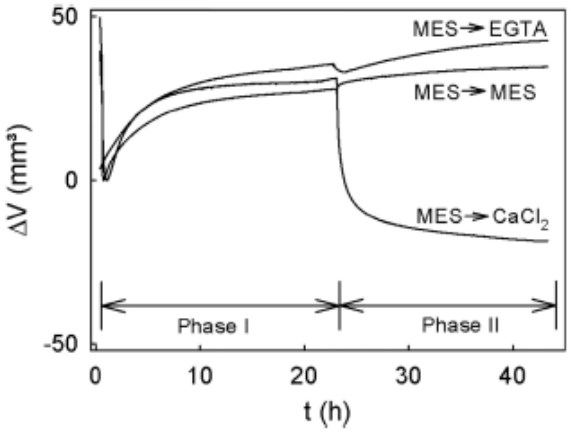

Figure 4. Time course of swelling of cell walls extracted from mature 'Burlat' sweet cherry. The experiment was conducted as a two-phase experiment by performing sequential treatments. During phase I, the cell walls were swelling in MES buffer. During the subsequent phase II, the buffer was replaced and swelling was monitored in buffered 10 mM $CaCl_2$ or buffered 5 mM EGTA (phase II) or MES buffer only (10 mM). The pH of all solutions was adjusted to pH of 5.8. Swelling was quantified as the change in volume (ΔV) of the cell wall at a constant pressure of 3.9 kPa.

of the regression lines did decrease significantly as $CaCl_2$ concentration increased (Fig. 6b). This relationship was log linear and highly significant.

The effect of the Ca concentration on the swelling of extracted cell wall material mirrored that on cell walls as assessed by microscopy. Both, the slope ($\Delta V * \ln P^{-1}$) and the ΔV_{max} were significantly related to the microscopically determined swelling (Fig. 6c).

Cations that decreased the swelling of intact cell walls in vivo also decreased the swelling of extracted cell walls in vitro. Generally, there was no effect on P_0. However, the slopes of plots of the relationship change of cell wall volume vs. the natural logarithm of the applied pressure increased markedly (less negative) in the presence of divalent and trivalent cations. Monovalent cations had no effect on P_0, the slope term or the maximum volume (ΔV_{max}) as compared to MES only. The effect of the divalent cations would seem to depend on the radius of the cation. The slope term ($\Delta V * \ln P^{-1}$) and ΔV_{max} were both linearly related to ionic radius. The two trivalent cations must be excluded from this comparison. Their effects were confounded by the effects of pH. Here, solutions were un-buffered and highly acidic because neither solution was stable at a higher pH (Fig. 7 and Table 9).

There was no significant relationship between the swelling of the cell wall in vivo and the swelling pressure P_0 of extracted cell walls in vitro (Fig. 8a). However, the slope term ($\Delta V * \ln P^{-1}$) as well as the ΔV_{max} of extracted cell walls were both significantly related to the swelling of cell walls in vivo (Fig. 8b,c). Furthermore, these relationships did not differ from those established using a range of $CaCl_2$ concentrations (Fig. 6).

Discussion

Our discussion focuses on the following aspects: (1) The effects of calcium and other di- and trivalent cations on swelling of cell walls and (2) the effects of pH on the swelling of cell walls.

Our results indicate that divalent and trivalent cations decrease swelling of cell walls in vivo as determined by microscopy and also in vitro as determined by quantifying swelling pressure in extracted cell wall material. We infer that the decrease in swelling must have been due to a cross linking of negative charges in the cell wall. First, only cations carrying two or more charges were effective. There was no effect of monovalent cations. Second, the anion that would bind to any positive charge had no effect. Third, the crosslinking effects of Ca^{2+} on pectins are well documented and usually described using the analogy of the egg box model[14]. In this model, Ca represents the egg that "cross links" to adjacent chains of homogalacturonans. Fourth, pectins contain galacturonic acid as the dominating monomers. The acid function carries a negative charge at physiological pHs and, hence, will bind cations. Lastly, the middle lamella is comprised of pectin[8]. The crosslinking by di- or trivalent cations decreases cell wall swelling. Decreased swelling, in turn, increases cell to cell adhesion, thereby strengthening the cell wall. This behaviour is consistent with the observation that cell separation during cracking occurs by separation of adjacent cells and exposure of the middle lamellae at the crack surface—as opposed to the fracture of cellulosic cell walls[12,24]. Our results in sweet cherry are also consistent with observations in other crops[25]. It has been reported that cell to cell adhesion depended on the presence of Ca^{2+} cations and the degree of esterification[25].

Among the divalent cations, the effects on cell wall swelling increase in order of the increasing radius of the cation. This effect is consistent with both the in vivo assay, using microscopy and thin sections of fresh fruit and with the in vitro assay, using extracted cell wall material and the determination of swelling pressure.

Among the divalent cations, the maximum volume of the swollen cell wall material (ΔV_{max}) and the amount of swelling per unit pressure ($\Delta V * \ln P^{-1}$) both correlated with the increase in swelling of intact cell walls observed by microscopy. In contrast, the swelling pressure P_0 was unaffected by any of the cations. This is not surprising,

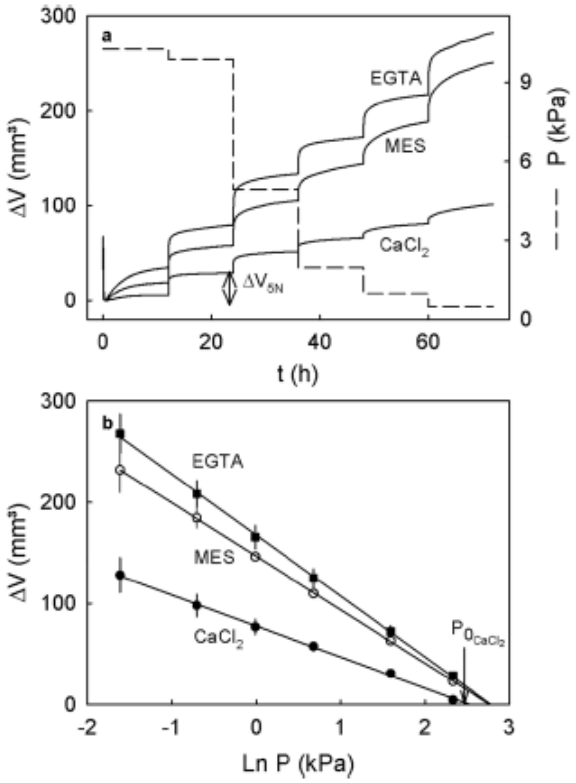

Figure 5. Effect of a stepwise decrease in pressure on swelling of extracted cell walls of mature 'Burlat' sweet cherry fruit. Cell walls were allowed to swell in the presence of buffered 10 mM $CaCl_2$, buffered 5 mM EGTA or buffer only. The buffer was 10 mM MES at a pH of 5.8. Swelling was quantified in vitro as the change in volume (ΔV) of the extracted cell walls as the pressure applied to the cell walls was decreased. (**a**) Time course of change in pressure and change on volume of cell walls as the pressure was decreased stepwise from 10.3 to 0.1 kPa. At each pressure step, the pressure was held constant for 12 h to allow equilibration of cell wall swelling. (**b**) Relationship between the swelling of cell walls (ΔV) at equilibrium and the natural logarithm of the applied pressure. The swelling pressure P_0 corresponds to the pressure at which no swelling occurs. The value P_0 was estimated as the x-axis intercept of a regression fitted through a plot of ΔV vs. ln P. The change in cell wall volume per unit pressure represents the slope of this regression and may be interpreted as a volumetric modulus of elasticity of the cell wall.

Treatment	P_0 (kPa)	$\Delta V * \ln P^{-1}$ ($mm^3 * kPa^{-1}$)	ΔV_{max} (mm^3)
Control (MES)	16 ± 3 a[a]	− 53 ± 6 b	232 ± 22
$CaCl_2$	12 ± 1 a	− 30 ± 5 a	124 ± 18
EGTA	16 ± 1 a	− 60 ± 4 b	268 ± 19

Table 8. Effects of $CaCl_2$ (10 mM) and EGTA (5 mM) on in vitro swelling pressure (P_0), the change in cell wall volume per unit pressure ($\Delta V * \ln P^{-1}$) and the maximum volume after swelling at 0.2 kPa (ΔV_{max}) of cell walls of mature 'Burlat' sweet cherry fruit. Cell walls were extracted as the alcohol insoluble residue (AIR). All solutions were buffered using 10 mM MES. Buffer only served as control. The swelling pressure was calculated as the extrapolated x-axis intercept of a linear regression fitted through a plot of the change in AIR volume vs. the natural logarithm of the applied pressure (ln P). The change in AIR volume per unit pressure represents the slope of this regression and may be interpreted as the volumetric modulus of elasticity of the AIR. The pH of each solution was adjusted to pH 5.8 using KOH or HCl. Data are means ± SE. [a]Mean separation within columns, Tukey's Studentized range test at $p < 0.05$.

considering that P_0 represents the pressure that must be overcome by the cell walls before swelling begins. Earlier studies established that the value of P_0 is the same order of magnitude as cell turgor (21 kPa[26,27]) indicating that in turgid cells it is the turgor that prevents cell wall swelling (Grimm and Knoche[28] and Table 5).

Among the cations investigated, Ca was found effective in decreasing swelling. Also, the Ca cation has been found beneficial for fruit quality[7]. The effect of Ca on cell wall swelling was rapid and reversible, as inferred from

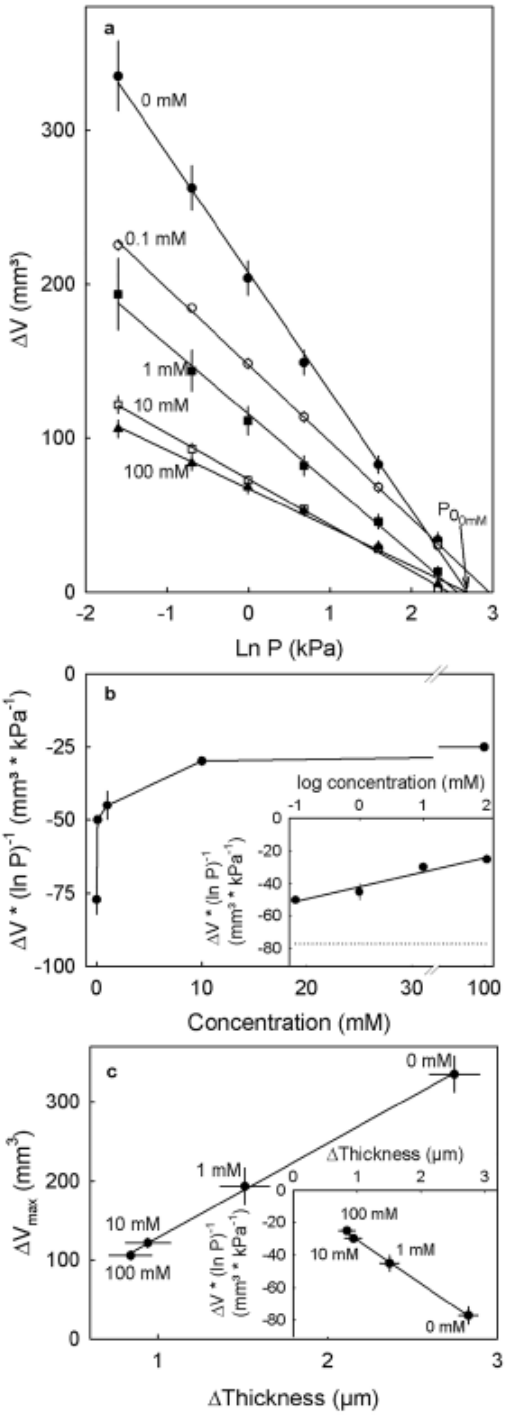

Figure 6. (**a**) Swelling of cell wall material extracted as the alcohol insoluble residue from 'Burlat' sweet cherry fruit when incubated in different concentration of $CaCl_2$. All solutions were buffered with 10 mM MES and pH adjusted with KOH to 5.8. Swelling was quantified in vitro as the change in volume (ΔV) at different pressures (P) using a custom-built pressure chamber. The ΔV of the swollen cell walls after loading the cell wall with different pressures was quantified. (**a**) Relationship between the swelling of cell walls (ΔV) at equilibrium and the natural logarithm of the applied pressure. The swelling pressure P_0 corresponds to the pressure at which no swelling occurs. The value P_0 was estimated as the x-axis intercept of a regression fitted through a plot of ΔV vs. ln P. Each curve represents the mean of three repetitions. (**b**) Slope of the regression of ΔV vs. ln P depending on the $CaCl_2$ concentration of the incubation solution. Inset: Slope ΔV vs. ln P depending on the logarithm of the applied concentration of $CaCl_2$. The dotted horizontal line represents the control of 0 mM $CaCl_2$. (**c**) Relationship between maximum swelling of the extracted cell walls incubated with different $CaCl_2$ concentrations and the cell wall swelling examined on anticlinal cell walls of excised epidermal segments of 'Burlat' sweet cherry fruit incubated in the same incubation solutions. The ES were treated with a freeze/thaw cycle to release turgor followed by an incubation of 48 h. The cell wall swelling was calculated by the difference in the cell wall thickness after release of turgor minus that before release of turgor. Inset: Relationship of the slope ΔV vs. ln P and the microscopically determined cell wall swelling.

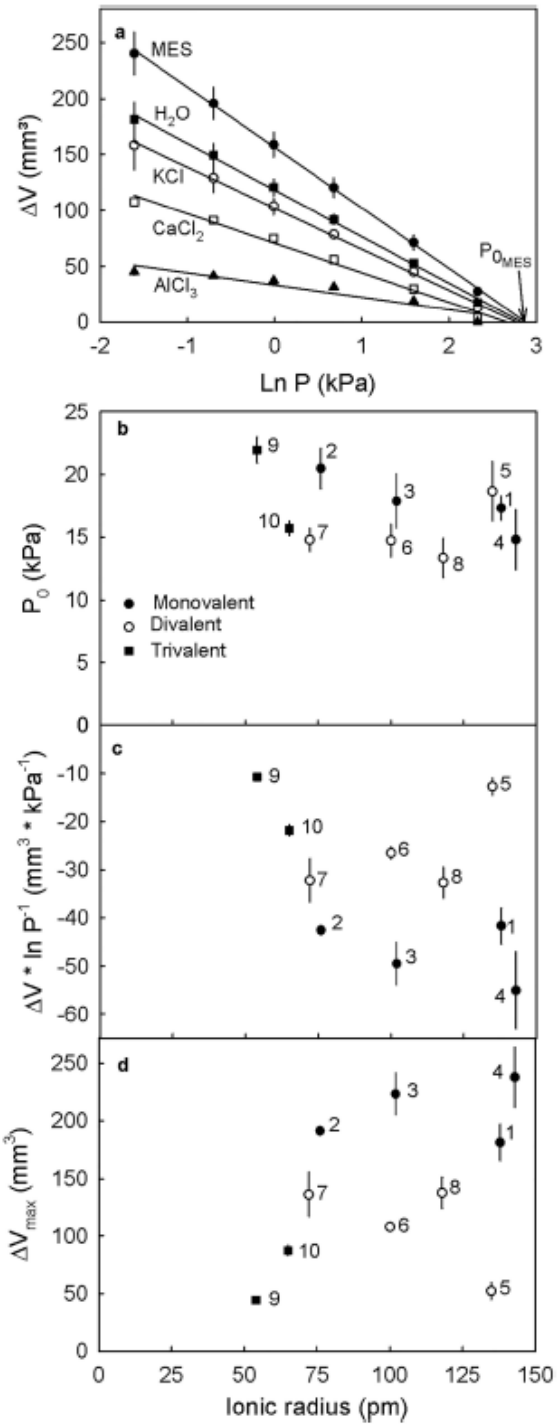

Figure 7. Swelling of cell wall material extracted from ripe 'Burlat' sweet cherry fruit when incubated in representative solutions of mono-, di- and trivalent cations. Solutions with monovalent and divalent cations were buffered with 10 mM MES and pH adjusted with KOH or HCl to pH 5.8. Solutions with trivalent cations were unbuffered and pH was measured (Table 9). 10 mM MES and deionized water served as control. Swelling was quantified in vitro as the change in volume (ΔV) at different pressures (P) using a custom-built pressure chamber. The ΔV of the swollen cell walls after loading the cell wall with different pressures was quantified. (**a**) Relationship between the swelling of cell walls (ΔV) at equilibrium and the natural logarithm of the applied pressure. The swelling pressure P_0 corresponds to the pressure at which no swelling occurs. The value P_0 was estimated as the x-axis intercept of a regression fitted through a plot of ΔV vs. ln P. Each curve represents the mean of three repetitions. (**b**) Swelling pressure P_0 of solutions with different cations depending on the ionic radius of the cation. (**c**) Slope ΔV vs. ln P and maximum swelling of extracted cell walls (**d**) depending on the ionic radius of the cation in the incubation solution. (**b**–**d**) The numbers next to the data symbols refer to the following cations: KCl (1), LiCl (2), NaCl (3), NH_4Cl (4), $BaCl_2$ (5), $CaCl_2$ (6), $MgCl_2$ (7), $SrCl_2$ (8), $AlCl_3$ (9) and $FeCl_3$ (10).

Treatment	pH	P_0 (kPa)	$\Delta V * \ln P^{-1}$ ($mm^3 * kPa^{-1}$)	ΔV_{max} (mm^3)
Control (MES)	5.7	18 ± 1	−54 ± 4	240 ± 19
KCl	5.8	17 ± 1	−42 ± 4	181 ± 16*
LiCl	5.8	21 ± 2	−43 ± 1	191 ± 2
NaCl	5.8	18 ± 2	−49 ± 4	224 ± 18
NH_4Cl	5.8	15 ± 2	−55 ± 8	238 ± 26
$BaCl_2$	5.8	19 ± 2	−13 ± 2*	53 ± 7*
$CaCl_2$	5.8	15 ± 1	−27 ± 1*	108 ± 4*
$MgCl_2$	5.8	15 ± 1	−32 ± 4*	136 ± 19*
$SrCl_2$	5.8	13 ± 2	−33 ± 3*	138 ± 13*
Control (water)	5.5	19 ± 3	−34 ± 5	150 ± 17
$AlCl_3$	3.8	22 ± 1	−11 ± 1*	45 ± 2*
$FeCl_3$	2.4	16 ± 1	−22 ± 1*	88 ± 4*

Table 9. Effect of various chloride salts on the in vitro swelling pressure (P_0), the change in cell wall volume per unit pressure ($\Delta V * \ln P^{-1}$) and the maximum volume after swelling at 0.2 kPa (ΔV_{max}) of cell walls of mature `Burlat` sweet cherry fruit. Cell walls were extracted as the alcohol insoluble residue (AIR). All solutions were buffered using 10 mM MES and the pH adjusted to pH 5.8 using KOH or HCl. The only exceptions were $AlCl_3$ and $FeCl_3$ that were used without buffer. Buffer only served as control. The swelling pressure was calculated as the extrapolated x-axis intercept of a linear regression fitted through a plot of the change in AIR volume vs. the natural logarithm of the applied pressure (ln P). The change in AIR volume per unit pressure represents the slope of this regression and may be interpreted as a volumetric modulus of elasticity of the AIR. Data are means ± SE. *Mean comparisons within columns against the MES control by Dunnett test, $p < 0.05$. Only $AlCl_3$ and $FeCl_3$ were used un-buffered and hence, are compared with the water control by Dunnett test, $p < 0.05$.

the response of swelling to treatment with EGTA. EGTA has a high affinity for Ca and, hence, it extracts Ca from the cell wall thereby increasing swelling. It is worth noting that Ca also decreased the swelling of cell walls that were already swollen. These properties make Ca an ideal candidate for manipulating cell wall swelling at the whole-fruit level in the orchard. However, for Ca to be effective requires that Ca can reach the appropriate site of action in the cell wall, at a sufficiently high concentration. Due to the progressive loss of xylem functionality in the developing sweet cherry fruit[29], vascular delivery from tree to fruit is very low, so instead Ca must be applied to the fruit directly as a spray[30].

Swelling of cell walls depended not only on the presence of Ca ions but also on the pH of the incubation solution. At low pH, carboxyl groups of sugar acids of pectins are non-dissociated. As a result, the binding capacity for cations decreases[18]. In addition, more and more Ca^{2+} is replaced by H^+ due to competition for the same binding sites. The decreasing binding capacity and the replacement of Ca by H both decrease crosslinking of cell walls, increase cell wall swelling and thereby weaken cell-to-cell adhesion. The effect of low pH is thus somewhat comparable to that of EGTA. However, in addition to the effect of EGTA, the number of sorption sites also decreases at low pH due to decreased dissociation. To study the interaction of Ca and pH we used living ES in which enzymes are still active. It has been shown, that the degree and the pattern of esterification also depended on pH[20]. At low pH, the activity of pectinmethylesterases increases leading to a lower degree of esterification. This, in turn, would thus oppose the effect of pH on dissociation. It is therefore conceivable, that the number of binding sites for cations increased at low pH. This could increase the effect of Ca at low pH despite a decrease in binding sites due to the dissociation of the carboxylgroups. In contrast to the effect of pH on dissociation, the effect of deesterification would be irreversible. This effect will also occur in vivo for an intact fruit on the tree, when water uptake through microcracks causes localized bursting of cells of the outer flesh[31]. The cells of the outer flesh are the most susceptible because they are large, thin-walled and have a more negative osmotic potential than the epi- and hypodermal cells of the skin[28,31]. Sweet cherry juice is rich in malic acid[32]. Upon cell bursting, malic acid enters the apoplast and the apoplast pH decreases. Malic acid extracts and complexes with cell wall-bound Ca, thereby weakening the cell wall. Local swelling is induced. Ca rapidly binds to the binding sites before the pH of the apoplast decreases thereby decreasing cell wall swelling (Fig. 1). These considerations demonstrate that Ca and pH interact in their effects on cell wall swelling. The lower the pH of the incubation solution, the larger is the effect of Ca in decreasing cell wall swelling. However, if pH drops below the pKa of galacturonic acids (pKa 2.8–4.1)[33], any non-methylesterified carboxyl groups exist in the undissociated form[34]. Then, due to the too low density of negative charges, binding sites are absent and crosslinking is prevented (Fig. 2b at pH 2.0).

In contrast to the effects of Ca, the effect of pH on swelling is irreversible. Cell walls that had swollen when exposed to low pH, remain swollen when transferred to a solution of high pH. Apparently, the increasing number of binding sites at the higher pH remain free without the binding by divalent or trivalent cations. This would be the case if Ca was extracted at low pH and removed from the cell wall.

It is important to note that the effects of the trivalent $AlCl_3$ and $FeCl_3$ on swelling are confounded by a simultaneous effect of pH. Both salts produce highly acidic solutions that have pH values around pH 2.0. At this pH, cell adhesion is essentially eliminated. At the same time, swelling is greatly reduced due to the crosslinking of cell wall constituents by Fe^{3+} or Al^{3+}. This interpretation is consistent with earlier findings demonstrating decreased cracking as a result of decreased cell wall swelling[35].

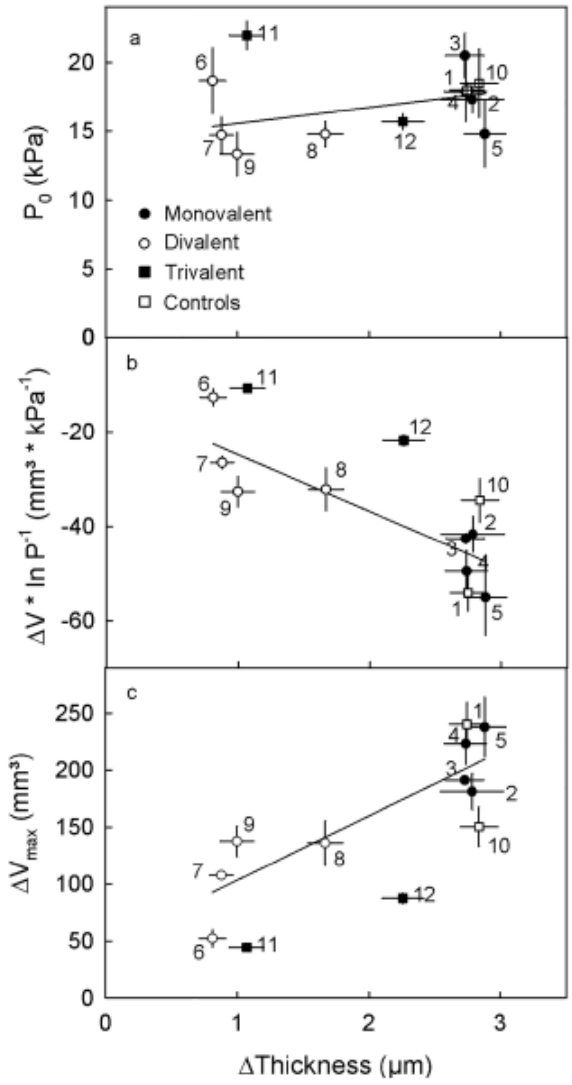

Figure 8. Relationship between the swelling pressure (P_0) (**a**), the change in volume per unit pressure ($\Delta V * \ln P^{-1}$) (**b**) and the maximum swelling volume (ΔV_{max}) (**c**) of extracted cell walls in vitro and the swelling of cell walls in vivo as affected by mono-, di- and trivalent chlorides of the following salts: KCl (2), LiCl (3), NaCl (4), NH_4Cl (5), $BaCl_2$ (6), $CaCl_2$ (7), $MgCl_2$ (8), $SrCl_2$ (9), $AlCl_3$ (11) and $FeCl_3$ (12). MES buffer (1) and water (10) served as controls. The mono- and divalent salts were buffered in 10 mM MES. Only the trivalent salts were not buffered. Swelling of extracted cell walls in vitro was determined using a custom-built pressure chamber, the swelling in vivo was determined by microscopy on skin sections.

Practical implications. The results obtained in this study demonstrate that salts of divalent and trivalent cations markedly reduce cell wall swelling, most likely by crosslinking the pectin middle lamellae. Decreased swelling maintains and improves cell-to-cell adhesion which is an important factor in the cracking process of sweet cherry. Among the salts tested, Ca salts are effective and have an acceptable ecotoxicological profile. However, their limitation is their consistently low ability to penetrate an intact cuticle[7,36,37]. To take advantage of their potential to decrease cracking susceptibility, the Ca must come into contact with the emerging cracks. This may possibly be achieved by application of Ca sprays during or immediately after rainfall[38].

Material and methods

Plant material. Mature sweet cherry fruit (*Prunus avium* L.) of the cultivars Burlat, Sam and Regina were harvested at commercial maturity based on color and size from the Horticultural Research Station of the Leibniz University in Ruthe (lat. 52°14'N, long. 9°49'E). All trees were grafted on 'Gisela 5' rootstocks (*Prunus cerasus* x *P. canescens*) and cultivated in a greenhouse or under a rain shelter. Fresh fruits were used on the day of harvest or

frozen and stored at − 20 °C until cell wall extraction. Additionally, off-season 'Santina' sweet cherries from Chile were purchased locally. All fruits selected for experiments were uniform in size and free from visual defects.

Microscopy. Cell wall swelling was quantified microscopically using the procedure described earlier[26]. Briefly, thin rectangular epidermal skin sections (ES) were excised using a razor blade from the equatorial region of the cheek parallel to the fruit surface. An ES was excised, carefully blotted with soft tissue paper and transferred to a droplet of test solution on a microscope slide. The ES was then inspected by light microscopy (BX-60; Olympus, Hamburg, Germany). Calibrated digital images (camera: DP73; Olympus) were taken at × 40 magnification and the wall thickness of the anticlinal cell walls between pairs of turgid epidermal cells was measured by image analysis (cellSens 1.7.1; Olympus Soft Imaging Solutions, Muenster, Germany). This wall thickness measure actually represents the sum of two abutting cell walls, belonging to the two adjacent cells, plus the thickness of the interfacing middle lamella. This measure also represents the cell wall thickness of turgid cells—we will call this specimen '+turgor'. Removal of turgor is a prerequisite for cell wall swelling[26]. To enable cell wall swelling, the same ESs were then subjected to a single freeze/thaw cycle. They were frozen in 3 ml of test solution at -20 °C for at least 12 h, then returned to room temperature and held for 24 h. This freeze thaw cycle eliminated cell turgor—we now call this specimen '−turgor'. Cell wall-thickness was re-quantified as described above—this time between two non-turgid cells. Cell wall swelling was then calculated as the difference in thickness, after (−turgor) minus before (+turgor) the freeze–thaw treatment. Unless otherwise specified, one ES was cut per fruit from 10 fruit per treatment. Two micrographs were taken per ES and two cell walls were measured per micrograph. The total number of observations per treatment was thus 40.

Experiments. The time course of cell wall swelling of anticlinal cell walls was studied in ES from 'Santina' fruit. The ES were incubated in 10 mM $CaCl_2$ buffered (10 mM MES) either at pH 5.8 or pH 3.0. There were two controls with buffer only (no $CaCl_2$) one at each of the pHs. The pH was adjusted using HCl (pH 3.0) or KOH (pH 5.8). The cell wall thickness was measured as described above immediately after excision (0 h). The ES were then frozen for at least 12 h, after which cell wall thickness was again quantified at 0.5, 2, 4, 8, 24, 48, 72 and 97 h after thawing.

Potential interactions between $CaCl_2$ and pH on cell wall swelling were determined using ES of 'Burlat'. The $CaCl_2$ concentrations were 0, 1, 3, 10, 30 and 100 mM. All solutions were prepared in 10 mM MES buffer and the pH adjusted to pH 2, pH 3, pH 4, pH 5, pH 6 and pH 7, using HCl for the pHs < pH 4.2 and KOH for the others. The initial cell wall thickness was determined immediately after excision of ES from 20 fruit. A separate set of ES (n = 10) were excised, frozen, thawed and incubated for 48 h in the respective salt solutions to determine cell wall thickness in the absence of turgor. Cell wall thickness was determined as described above.

The effect of concentration of $AlCl_3$ and $FeCl_3$ on cell wall swelling was studied on ES excised from 'Sam'. The concentrations were 0, 1, 3, 10, 30 and 100 mM. Due to the solubility characteristics of $AlCl_3$ and $FeCl_3$, the pHs of these solutions were not buffered but their pHs were determined after termination of incubation. For each solution, at each concentration, cell wall thickness was determined immediately after excision of the ES and again following a freeze/thaw cycle and a subsequent 48 h incubation period in the respective test solution.

The effects on cell wall swelling of the chlorides of a range of mono- and divalent cations were determined using ES excised from 'Sam'. The chlorides were selected because of their high water-solubility. The following salts were compared at a concentration of 10 mM KCl, LiCl, NaCl, NH_4Cl, $CaCl_2$, $BaCl_2$, $MgCl_2$ and $SrCl_2$. Solutions were buffered with 10 mM MES and pH adjusted with either KOH or HCl to pH 5.8. Deionized water and 10 mM MES served as control. Cell wall thickness before and after the removal of turgor was determined.

The effects of the anion accompanying the Ca cation was investigated using $CaCl_2$, $Ca(NO_3)_2$, $CaSO_4$, Ca-acetate, Ca-propionate, Ca-formate, Ca-lactate and Ca-heptagluconate, all at 10 mM. All solutions were buffered with 10 mM MES and the pH adjusted using either KOH or HCl to pH 5.8. Buffer solution (10 mM MES) served as control. Cell wall thickness was determined immediately after ES excision and after a freeze/thaw cycle followed by a 48 h incubation period in the respective salt solution.

The effect of extracting Ca^{2+} from the ES was investigated using a chelating agent. The ES were incubated in 5 mM EGTA, 5 mM $CaCl_2$ or in 2.5 mM $CaCl_2$ plus 2.5 mM EGTA. All solutions were buffered using 10 mM MES and pH was adjusted to pH 8.0 using KOH. Buffer only (10 mM MES), pH 8.0 or buffer only at pH 5.8 served as controls. Cell wall thickness was determined before and after removal of turgor as described above.

Whether the effect of calcium on cell wall swelling was reversible or not was investigated in a two-phase experiment. Initial cell wall thickness was determined in ES of 'Burlat'. The turgor was then removed by a freeze/thaw cycle. In phase I of the subsequent experiment, the non-turgid ES were incubated for 48 h either in 10 mM $CaCl_2$ buffered with 10 mM MES or in 10 mM MES only. Thereafter, cell wall thickness was re-measured. For the following phase II, the ES were split randomly into two groups. One group was again incubated for 48 h in 10 mM MES and the second group was incubated for 48 h in 10 mM $CaCl_2$ prepared in 10 mM MES. After this, cell wall thickness was re-measured. A sequence of treatments in 10 mM MES (phase I) / 10 mM MES (phase II) served as controls.

Potential interactions between the effects of calcium and of turgor were studied in another 2-phase experiment using ES from 'Burlat'. Initial cell wall thickness was determined immediately after excision as described above. Thereafter, the ES were incubated for 48 h in either a hypotonic (0.25 M sucrose) or a hypertonic (1.5 M sucrose) solution with and without 10 mM $CaCl_2$ (phase I). After re-measuring cell wall thickness, each group was then divided randomly into two subgroups that were incubated in a hypertonic solution (1.5 M sucrose) with (subgroup 1) or without (subgroup 2) 10 mM $CaCl_2$ (phase II). After 48 h, cell wall thickness was re-measured. All solutions were buffered in 10 mM MES (pH 5.8). A buffered (10 mM) hypotonic sucrose solution served as control.

Potential interactions between low and high pH and turgor on cell wall swelling were studied in another two-phase experiment. Initial cell wall thickness was determined. Thereafter, (phase I) the ES were incubated for 48 h in hypotonic (0.25 M sucrose) or hypertonic sucrose (1.5 M sucrose) at pH 3.0 or at pH 5.8. The pH was then (phase II) adjusted to pH 3.0 using HCl or to pH 5.8 using KOH. After re-measuring cell wall thickness, each group was divided into two subgroups. These were incubated in a hypertonic solution (1.5 M sucrose) at pH 3.0 (subgroup 1) or at pH 5.8 (subgroup 2). After 48 h, cell wall thickness was re-measured. All solutions were buffered in 10 mM MES (pH 5.8). A buffered (10 mM) hypotonic sucrose solution (pH 5.8) served as control.

The effect on cell wall swelling of pre-treating whole fruit by incubation in $CaCl_2$ was studied in 'Burlat'. Fruit (n = 25) were sealed at the stylar scar and at the pedicel/fruit junction using a fast-curing silicone rubber (SE 9186 Clear; Dow Corning Corp., Midland, USA). Sealed fruit were then incubated for 24 h in deionized water, isotonic $CaCl_2$, isotonic sucrose or in 5 mM EGTA. All solutions were prepared in 10 mM MES. In this experiment, the pH was adjusted to pH 8.2 using KOH to maintain the EGTA in solution. For the controls, untreated fruit were placed under a wet paper towel for 24 h. The ES were then excised and cell wall thickness measured as above. Subsequently, turgor was released by a freeze/thaw cycle followed by 48 h incubation in 10 mM MES. Cell wall thickness was then remeasured.

Preparation of cell wall material. Cell walls were extracted as the alcohol-insoluble residue (AIR) from 'Burlat' sweet cherry fruit[26,39]. A sample of ten fruit was pitted after thawing, transferred into 4 ml per g tissue of 80% (v/v) ice-cold ethanol and homogenized for 2 min using a kitchen blender (Zauberstab M 160 WH; ESGE, Mettlen, Switzerland). The slurry was boiled for 30 min, cooled to ambient temperature and then filtered through glass fiber filter paper (Whatman GF/C; Sigma-Aldrich, St. Louis, MO, USA). After washing with 95% (v/v) ethanol, the insoluble residue was extracted with 3 ml per g tissue of chloroform:methanol (1:1, v/v) for 15 min, filtered, washed again with chloroform:methanol (1:1, v/v) and filtered again. Finally, the residue was washed with acetone and dried overnight. The AIR was then weighed and ground with pestle and mortar.

Swelling pressure of extracted cell walls. The swelling pressure of the AIR was quantified using the method described before[26]. Briefly, 25 mg of AIR was weighed into a custom pressure chamber (25.5 mm diam.). The AIR was wetted using 20 ml of 70% (v/v) ethanol and a negative pressure of 20 kPa for 10 min, followed by 30 min at atmospheric pressure to allow the suspension to settle. The chamber was then positioned under a universal testing machine (BXC-FR2.5TN; ZwickRoell GmbH & Co. KG, Ulm, Germany). A stainless-steel frit (diam. 25.4 mm, 1.57 mm thick, pore diam. 10 µm) attached to a 50 N force transducer (KAP-Z; ZwickRoell) was used to pressurize the wetted AIR at 3.9 kPa and the system allowed to equilibrate for 30 min. The experiment was conducted in two-phases, using repeated observations on the same specimen. During phase I, the supernatant was replaced by 15 ml of 10 mM MES. The pressure was held constant at 3.9 kPa for 22.5 h and the change in volume of the cell wall was monitored. The effects of $CaCl_2$ and of EGTA on swelling were established in phase II by replacing the MES buffer by either 10 mM $CaCl_2$ in 10 mM MES or by 5 mM EGTA in 10 mM MES solution. Buffer only (10 mM MES) served as control. The pressure was held constant for another 22.5 h. Swelling was recorded as an increase in height of the frit and, hence, an increase in volume of the cell wall material using the distance transducer of the universal testing machine. By multiplying the measured change in height of the frit by the known cross-sectional area of the chamber, the change in volume of the cell wall due to swelling was calculated. The pH of all solutions was adjusted to pH 5.8. The experiment was carried out in triplicate where one replicate corresponded to a separate extraction of AIR from ten fruit.

The effect of $CaCl_2$ and EGTA on swelling pressure was studied using the same experimental setup as above in a repeated measures design. The AIR (25 mg) was wetted in 70% (v/v) ethanol supported by a negative pressure of 20 kPa for 10 min, followed by 30 min at atmospheric pressure to allow the suspension to settle. The cell walls were then pressurized at 10.3 kPa. After a 30 min equilibration period, the aqueous ethanol was replaced by 15 ml of 10 mM MES buffer as control, by 10 mM $CaCl_2$ in 10 mM MES or by 5 mM EGTA in 10 mM MES. All solutions were at pH 5.8. First, the pressure was held constant at 10.3 kPa for 12 h. At this pressure, cell wall volume was minimum. Next, the pressure was reduced stepwise to 9.9, 4.9, 2.0, 1.0, 0.5 and 0.2 kPa. After each pressure step, the new (lower) pressure was held constant for 12 h, and the new increased volume due to cell wall swelling was recorded as described above. The amount of swelling (ΔV) at anyone pressure step was calculated by subtracting the minimum volume of the cell wall material (Vmin) at 10.3 kPa from the final cell wall volume at the end of each step. The 10.3 kPa pressure approximated the turgor of a sweet cherry fruit, and thus the pressure experienced by the cell wall *in vivo*[27]. The swelling pressure (P_0) was estimated as the x-axis intercept of a linear regression through a plot of ΔV at equilibrium, at each pressure, vs. the natural logarithm of the applied pressure (ln P). The value of P_0 represents the pressure required to suppress cell wall swelling. The slope of the regression ($\Delta V * \ln P^{-1}$) represents the volume change of the extracted cell wall material per unit pressure change. We interpret this slope as the volumetric modulus of elasticity of the compressed cell wall material and will subsequently refer to it as such. The swelling pressures were determined with three replicates, where one replicate corresponds to an individual extraction of AIR from ten fruit.

The effect of the concentration of $CaCl_2$ on the swelling pressure was investigated using the protocol described above. Following an initial wetting, supported by a negative pressure of 20 kPa for 10 min and a 30 min equilibration period in 70% (v/v) ethanol, the supernatant was replaced by 0, 0.1, 1, 10 or 100 mM $CaCl_2$. All solutions were buffered using 10 mM MES and pH adjusted to pH 5.8. The pressure was decreased stepwise as described above and the P_0 and the slope term ($\Delta V * \ln P^{-1}$) determined as described above.

The effects of mono-, di- and trivalent cations on swelling pressure were determined using the protocol described above. Here, following wetting of the AIR by 70% v/v ethanol, supported by a negative pressure of 20 kPa for 10 min and a 30 min equilibration period, the supernatant was replaced by KCl, LiCl, NaCl, NH_4Cl

$BaCl_2$, $CaCl_2$, $MgCl_2$, $SrCl_2$, $AlCl_3$ or $FeCl_3$ all at a concentration of 10 mM. Solutions with mono- and divalent cations were buffered with 10 mM MES and the pH adjusted to pH 5.8. Due to the limited solubility of $AlCl_3$ and $FeCl_3$ at pH 5.8, these solutions remained unbuffered. Deionized water and 10 mM MES buffer served as control. The pressure was decreased stepwise as described above and the P_0 and the slope term ($\Delta V * \ln P^{-1}$) determined as described above.

Statistics and data presentation. All experiments were performed in accordance with relevant institutional, national, and international guidelines and legislation. Data in the Tables and Figures represent arithmetic means and standard errors. Where not visible, error bars were smaller than data symbols. Only in Figs. 4 and 5a are individual replicates shown. Data were analyzed by regression analysis and analysis of variance. Mean separation was carried out using Tukey´s Studentized range test or Dunnett´s test ($P<0.05$, package multcomp 1.3–1, procedure glht, R version 3.3.2; R Foundation for Statistical Computing, Vienna, Austria). Significance of coefficients of determination (r^2) at $p<0.05$ is indicated by *.

Data availability

The datasets generated during the current study are available from the corresponding author on reasonable request.

Received: 17 June 2022; Accepted: 12 September 2022
Published online: 03 October 2022

References

1. Christensen, J. V. In *Cherries: Crop physiology, production and uses* (eds Webster, A. D. & Looney, N. E.) 297–327 (CAB International, 1996).
2. Knoche, M. & Peschel, S. Water on the surface aggravates microscopic cracking of the sweet cherry fruit cuticle. *J. Am. Soc. Hortic. Sci.* **131**, 192–200. https://doi.org/10.21273/JASHS.131.2.192 (2006).
3. Knoche, M. & Winkler, A. In *Cherries: Botany, production and uses* (eds Quero-García, J. *et al.*) 140–165 (CAB International, 2017).
4. Knoche, M. & Lang, A. Ongoing growth challenges fruit skin integrity. *Crit. Rev. Plant Sci.* **36**, 190–215. https://doi.org/10.1080/07352689.2017.1369333 (2017).
5. Cline, J., Meland, M., Sekse, L. & Webster, A. D. Rain cracking of sweet cherries: II. Influence of rain covers and rootstocks on cracking and fruit quality. *Acta Agric. Scand. B-S P* **45**, 224–230. https://doi.org/10.1080/09064719509413108 (1995).
6. Lang, G. A., Sage, L. & Wilkinson, T. T. years of studies on systems to modify sweet cherry production environments: Retractable roofs, high tunnels, and rain-shelters. *Acta Hortic.* **1130**, 83–89. https://doi.org/10.17660/ActaHortic.2016.1130.12 (2016).
7. Winkler, A. & Knoche, M. Calcium and the physiology of sweet cherries: A review. *Sci. Hortic.* **245**, 107–115. https://doi.org/10.1016/j.scienta.2018.10.012 (2019).
8. Demarty, M., Morvan, C. & Thellier, M. Calcium and the cell wall. *Plant Cell Environ.* **7**, 441–448. https://doi.org/10.1111/j.1365-3040.1984.tb01434.x (1984).
9. Hocking, B., Tyerman, S. D., Burton, R. A. & Gilliham, M. Fruit calcium: Transport and physiology. *Front. Plant Sci.* **7**, 569. https://doi.org/10.3389/fpls.2016.00569 (2016).
10. Thor, K. Calcium - nutrient and messenger. *Front. Plant Sci.* https://doi.org/10.3389/fpls.2019.00440 (2019).
11. Brüggenwirth, M., Fricke, H. & Knoche, M. Biaxial tensile tests identify epidermis and hypodermis as the main structural elements of sweet cherry skin. *AoB Plants* **6**, plu019. https://doi.org/10.1093/aobpla/plu019 (2014).
12. Brüggenwirth, M. & Knoche, M. Cell wall swelling, fracture mode, and the mechanical properties of cherry fruit skins are closely related. *Planta* **245**, 765–777. https://doi.org/10.1007/s00425-016-2639-7 (2017).
13. Celus, M., Kyomugasho, C., Van Loey, A. M., Grauwet, T. & Hendrickx, M. E. Influence of pectin structural properties on interactions with divalent cations and its associated functionalities. *Compr. Rev. Food Sci. Food Saf.* **17**, 1576–1594. https://doi.org/10.1111/1541-4337.12394 (2018).
14. Grant, G. T., Morris, E. R., Rees, D. A., Smith, P. J. C. & Thom, D. Biological interactions between polysaccharides and divalent cations: The egg-box model. *FEBS Lett.* **32**, 195–198. https://doi.org/10.1016/0014-5793(73)80770-7 (1973).
15. Braccini, I. & Pérez, S. Molecular basis of Ca^{2+}-induced gelation in alginates and pectins: The egg-box model revisited. *Biomacromolecules* **2**, 1089–1096. https://doi.org/10.1021/bm010008g (2001).
16. Jarvis, M. C. The proportion of calcium-bound pectin in plant cell walls. *Planta* **154**, 344–346. https://doi.org/10.1007/BF00393913 (1982).
17. Jarvis, M. C. Structure and properties of pectin gels in plant cell walls. *Plant Cell Environ.* **7**, 153–164. https://doi.org/10.1111/1365-3040.ep11614586 (1984).
18. Baydoun, E. A. H. & Brett, C. T. The effect of pH on the binding of calcium to pea epicotyl cell walls and its implications for the control of cell extension. *J. Exp. Bot.* **35**, 1820–1831. https://doi.org/10.1093/jxb/35.12.1820 (1984).
19. Fry, S. C. Cross-linking of matrix polymers in the growing cell walls of angiosperms. *Annu. Rev. Plant Phys. Plant Mol. Biol.* **37**, 165–186. https://doi.org/10.1146/annurev.pp.37.060186.001121 (1986).
20. Willats, W. G. T. *et al.* Modulation of the degree and pattern of methyl-esterification of pectic homogalacturonan in plant cell walls: Implications for pectin methyl esterase action, matrix properties, and cell adhesion. *J. Biol. Chem.* **276**, 19404–19413. https://doi.org/10.1074/jbc.M011242200 (2001).
21. Basanta, M. F., de Escalada Plá, M. F., Stortz, C. A. & Rojas, A. M. Chemical and functional properties of cell wall polymers from two cherry varieties at two developmental stages. *Carbohydr. Polym.* **92**, 830–841. https://doi.org/10.1016/j.carbpol.2012.09.091 (2013).
22. Murayama, D. *et al.* Effects of calcium concentration in potato tuber cells on the formation of cross-links between pectin molecules by Ca^{2+}. *Am. J. Potato Res.* **94**, 524–533. https://doi.org/10.1007/s12230-017-9589-x (2017).
23. Martins, V. *et al.* Vineyard calcium sprays induce changes in grape berry skin, firmness, cell wall composition and expression of cell wall-related genes. *Plant Physiol. Biochem.* **150**, 49–55. https://doi.org/10.1016/j.plaphy.2020.02.033 (2020).
24. Schumann, C., Winkler, A., Brüggenwirth, M., Köpcke, K. & Knoche, M. Crack initiation and propagation in sweet cherry skin: A simple chain reaction causes the crack to "run". *PLoS One* **14**, e0219794. https://doi.org/10.1371/journal.pone.0219794 (2019).
25. Marry, M. *et al.* Cell-cell adhesion in fresh sugar-beet root parenchyma requires both pectin esters and calcium cross-links. *Physiol. Plant.* **126**, 243–256. https://doi.org/10.1111/j.1399-3054.2006.00591.x (2006).
26. Schumann, C. & Knoche, M. Swelling of cell walls in mature sweet cherry fruit: Factors and mechanisms. *Planta* **251**, 65. https://doi.org/10.1007/s00425-020-03352-y (2020).

27. Schumann, C., Schlegel, H. J., Grimm, E., Knoche, M. & Lang, A. Water potential and its components in developing sweet cherry. *J. Am. Soc. Hortic. Sci.* **139**, 349–355. https://doi.org/10.21273/JASHS.139.4.349 (2014).
28. Grimm, E. & Knoche, M. Sweet cherry skin has a less negative osmotic potential than the flesh. *J. Am. Soc. Hortic. Sci.* **140**, 472–479. https://doi.org/10.21273/JASHS.140.5.472 (2015).
29. Grimm, E., Pflugfelder, D., van Dusschoten, D., Winkler, A. & Knoche, M. Physical rupture of the xylem in developing sweet cherry fruit causes progressive decline in xylem sap inflow rate. *Planta* **246**, 659–672. https://doi.org/10.1007/s00425-017-2719-3 (2017).
30. Winkler, A., Fiedler, B. & Knoche, M. Calcium physiology of sweet cherry fruits. *Trees* **34**, 1157–1167. https://doi.org/10.1007/s00468-020-01986-9 (2020).
31. Grimm, E. *et al.* Localized bursting of mesocarp cells triggers catastrophic fruit cracking. *Hortic. Res.* https://doi.org/10.1038/s41438-019-0161-3 (2019).
32. Herrmann, K. *Inhaltsstoffe von Obst und Gemüse* (Ulmer, 2001).
33. Ralet, M. C., Dronnet, V., Buchholt, H. C. & Thibault, J. F. Enzymatically and chemically de-esterified lime pectins: Characterisation, polyelectrolyte behaviour and calcium binding properties. *Carbohydr. Res.* **336**, 117–125. https://doi.org/10.1016/S0008-6215(01)00248-8 (2001).
34. Ralet, M. C., Crepeau, M. J., Buchholt, H. C. & Thibault, J. F. Polyelectrolyte behaviour and calcium binding properties of sugar beet pectins differing in their degrees of methylation and acetylation. *Biochem. Eng. J.* **16**, 191–201. https://doi.org/10.1016/S1369-703x(03)00037-8 (2003).
35. Weichert, H. *et al.* Studies on water transport through the sweet cherry fruit surface: VIII. Effect of selected cations on water uptake and fruit cracking. *J. Am. Soc. Hortic. Sci.* **129**, 781–788. https://doi.org/10.21273/JASHS.129.6.0781 (2004).
36. Winkler, A. & Knoche, M. Calcium uptake through skins of sweet cherry fruit: Effects of different calcium salts and surfactants. *Sci. Hortic.* https://doi.org/10.1016/j.scienta.2020.109761 (2021).
37. Winkler, A. & Knoche, M. Penetration of sweet cherry skin by 45Ca-salts: Pathways and factors. *Sci. Rep.* https://doi.org/10.1038/s41598-021-90727-0 (2021).
38. Christensen, J. V. Cracking in cherries V. The influence of some salts and chemicals on cracking. *Frukt og Baer Oslo* 37–47 (1972).
39. Sozzi, G. O., Greve, L. C., Prody, G. A. & Labavitch, J. M. Gibberellic acid, synthetic auxins, and ethylene differentially modulate alpha-L-arabinofuranosidase activities in antisense 1-aminocyclopropane-1-carboxylic acid synthase tomato pericarp discs. *Plant Physiol.* **129**, 1330–1340. https://doi.org/10.1104/pp.001180 (2002).

Acknowledgements
We thank Simon Sitzenstock for technical support and Dr. Alexander Lang for useful discussion and helpful comments on an earlier version of this manuscript. We also thank the Deutsche Forschungsgemeinschaft (DFG, grant KN 402/14-1) for funding this study.

Author contributions
M.K., C.S. and A.W. planned and conducted all experiments and wrote the manuscript. All authors reviewed the manuscript.

Funding
Open Access funding enabled and organized by Projekt DEAL. Deutsche Forschungsgemeinschaft (DFG, grant KN 402/14-1).

Competing interests
The authors declare no competing interests.

Additional information
Correspondence and requests for materials should be addressed to M.K.

Reprints and permissions information is available at www.nature.com/reprints.

Publisher's note Springer Nature remains neutral with regard to jurisdictional claims in published maps and institutional affiliations.

4 Allgemeine Diskussion

Aus den Ergebnissen dieser Arbeit gehen folgende wichtige Erkenntnisse hervor:

1) Makrorisse entstehen aus Mikrorissen, indem nach dem Absterben von Zellen im Bereich des Mikrorisses, dem damit einhergehenden Turgorverlust und der stattfindenden Zellwandquellung, zunächst Epidermiszellen schizogen entlang ihrer Zellwände auseinanderreißen. Da auf der Rissoberfläche vor allem Pektine vorliegen, ist von einem Versagen der Mittellamelle auszugehen (Kapitel 3.1)
2) Zellwandquellung ist ein physikalischer, vollständig reversibler Prozess, welcher mit Hilfe verschiedener Methoden quantifiziert werden kann (Kapitel 3.2). Dabei lässt sich die Ausgangsdicke der Zellwand sowohl im lebenden als auch im toten Gewebeverband nach Plasmolyse durch Deplasmolyse (Kapitel 3.2), durch Zugabe von Calcium (Kapitel 3.4) oder Ethanol (Kapitel 3.2) wiederherstellen. Auch an extrahierten Zellwänden kann die Ausgangsquellung durch die Applikation eines entsprechenden Gegendrucks oder durch Zugabe von Ethanol (Kapitel 3.2) oder Calcium (Kapitel 3.4) wiederhergestellt werden. Lediglich die Quellung, die durch niedrige pH-Werte verursacht wird, ist nicht umkehrbar (Kapitel 3.4).
3) Zellwandquellung wird in turgeszenten Zellen durch den Turgor unterdrückt. Es kommt nur dann zur Volumenzunahme der Zellwände, wenn der Turgor zerstört wird. Dies geschieht durch Absterben der Zellen oder durch Plasmolyse. Gleiches gilt für extrahierte Zellwände, welche in der Quellungszelle eine druckabhängige Quellung zeigen. Experimentell konnte so ermittelt werden, dass ein Druck von etwa 12 kPa ausreicht, um Quellung zu verhindern. Dieser Druck entspricht der Größenordnung des Turgors (Kapitel 3.1 und 3.2)
4) Die Quellungsfähigkeit der Zellwände nimmt vor allem in Phase I und II der Fruchtentwicklung zu und verändert sich anschließend nur noch wenig. Dabei sind Pektine die quellenden Zellwandbestandteile. Unter ihnen findet die stärkste Quellung in den Fraktionen der salzsäurelöslichen Pektine (HSP) und der

natriumhydroxidlöslichen Pektine (OHP) statt. Der Quellungsdruck ändert sich nicht über die Fruchtentwicklung und ist für alle Zellwandbestandteile bei Reife gleich niedrig (Kapitel 3.3)

5) Durch Ca^{2+} und andere mehrwertige Kationen kann die Quellung von Zellwänden verhindert werden. Die Wirkung von Ca^{2+} auf die Quellung ist reversibel. Zellwände können durch Ca entquollen werden. Die Extraktion von Ca durch Chelatoren oder niedrige pH-Werte führt zu einer erhöhten Quellung. (Kapitel 3.4)

Die beschriebenen Erkenntnisschwerpunkte werden in den vorangehenden Kapiteln ausführlich im Kontext der veröffentlichten Literatur diskutiert. Daher widmet sich die nachfolgende Diskussion folgenden Punkten: (1) Vergleich der angewendeten Methoden zur Untersuchung der Zellwandquellung, (2) Ergänzung des Reißverschlussmodells mit den Ergebnissen dieser Arbeit und (3) Auswirkungen der Ergebnisse auf die obstbauliche Praxis, die Züchtung neuer Sorten und die notwendige weitere Forschung.

4.1 Vergleich der angewendeten Methoden zur Untersuchung der Zellwandquellung

Um die vorliegenden Ergebnisse vergleichen und einordnen zu können, soll in diesem Abschnitt auf die Vor- und Nachteile folgender Methoden vergleichend eingegangen werden: (1) Lichtmikroskopische Untersuchung von Epidermissegmenten (ES), (2) Untersuchung extrahierter Zellwände und (3) Untersuchung von Rissen mit Hilfe monoklonaler Antikörper (mABs).

4.1.1 Lichtmikroskopische Untersuchungen von ES

Viele der dieser Arbeit zu Grunde liegenden Ergebnisse beruhen auf der lichtmikroskopischen Untersuchung der Quellung von Zellwänden *in vivo*. Die Methode der lichtmikroskopischen

Untersuchung von epidermalen Zellwänden bietet einige wichtige Vorteile. (1) Die Untersuchungen sind im lebenden Gewebe *in vivo* möglich. Zellwände quellen ausschließlich, wenn in den benachbarten Zellen kein Turgor mehr vorhanden ist (Brüggenwirth et al., 2017; Schlegel et al., 2018; Schumann und Knoche, 2020 (Kapitel 3.2)). Dabei ist das Ausmaß der Zellwandquellung gleich, egal ob lebende Zellen plasmolysieren oder Zellen durch verschiedene Einflüsse abgetötet werden (Schumann und Knoche, 2020 (Kapitel 3.2)) (2) Die Zellwand bleibt in ihrer ursprünglichen Form unverändert. Es kommt nicht zur Veränderung der räumlichen Anordnung der Polymerketten. Somit bleiben die für die Quellung notwendigen Hohlräume (Redgwell et al., 1997) in ihrem ursprünglichen Zustand erhalten. Zudem ist davon auszugehen, dass enzymatische Veränderungen der Zellwand während der Messung der Quellung keine Rolle spielen, da der Endzustand der Quellung („Gleichgewichtsquellung“) bereits nach etwa 5 h erreicht ist und es anschließend nicht mehr zur Änderung der Zellwanddicke kommt (Schumann und Knoche, 2020 (Kapitel 3.2)). (3) Die Messungen werden im mechanisch relevanten Gewebe, der Fruchthaut, durchgeführt. Untersuchungen von Brüggenwirth et al. (2014) zeigten, dass lediglich Epidermis und Hypodermis für die mechanische Stabilität der Fruchthaut verantwortlich sind. Weder die Kutikula noch das Mesokarp haben einen signifikanten Einfluss auf die mechanischen Eigenschaften. (4) Positionsabhängige Untersuchungen sind einfach umsetzbar. Für die meisten Untersuchungen wurden ES aus der äquatorialen Ebene entnommen. Es konnte jedoch gezeigt werden, dass die Zellwandquellung auf der Kirsche von der Stielgrube zum Narbenende einem Gradienten unterliegt (Schumann und Knoche, 2020 (Kapitel 3.2)). Für vergleichende Experimente ist es wichtig, dass die Entnahmeposition der ES identisch gehalten wird. In weiteren Versuchen können positionsabhängige Untersuchungen genutzt werden, um Korrelationen der Zellwandquellung mit der Risshäufigkeit oder einem Calciumgradienten innerhalb der Frucht genauer zu betrachten. (5) Die Mikroskopie von Bruchkanten von Makrorissen erlaubt über die Betrachtung des Versagensmodus Rückschlüsse auf die Wechselwirkung zwischen Zellwandquellung und Zelladhäsion (Schumann et al., 2019 (Kapitel 3.1)). (6) Es können verbundene Stichproben innerhalb eines

ES durchgeführt werden. Dafür eignen sich mehrphasige Experimente. Im lebenden Gewebe kann unter anderem durch Plasmolyse und Deplasmolyse innerhalb eines ES der Turgor entfernt bzw. wiederhergestellt und somit Aussagen über die Reversibilität der Quellung erlangt werden. Auch weitere Faktoren können in mehrphasigen Experimenten auf ihre Reversibilität getestet werden. (7) Die Methode ist kostengünstig. Es werden lediglich ein Mikroskop mit Kamera und entsprechender Analysesoftware sowie frische Kirschen benötigt.

Allerdings hat die lichtmikroskopische Untersuchung an ES auch einige Nachteile. (1) Die Mikroskopie ist an das Vorhandensein frischer (reifer) Kirschen gebunden. Damit begrenzt sich das experimentelle Zeitfenster auf wenige Wochen im Jahr. Um dieses Zeitfenster zu verlängern, können verschiedene Sorten, Gewächshaus und Freilandproduktion oder off-season Kirschen von der Südhalbkugel verwendet werden (Schumann und Knoche, 2020 (Kapitel 3.2)). Bei Letzteren stehen oft keine Informationen über das Produktionsverfahren zur Verfügung. (2) Beim Schneiden der ES kommt es zur Entspannung des Gewebes (Grimm et al., 2012). Das führt dazu, dass sich die ES zusammenziehen. Somit verkleinert sich nicht nur die Fläche des Präparates, sondern auch die Fläche der einzelnen Zellen. Auch die Zellwand zieht sich zusammen und ist folglich dicker. Der Prozess der Entspannung ist allerdings, mit einer Halbwertszeit von rund 2 Minuten, sehr schnell (Grimm et al., 2012) und bereits vollendet, wenn das Präparat unter dem Mikroskop liegt. Bei der Betrachtung kommt es zur Überschätzung der Zellwanddicke *in vivo.* In den vorliegenden Studien wird die Zellwandquellung allerdings ausschließlich als Dickenzunahme, also als Differenz der Dicke der gequollenen Zellwand zum Ursprungszustand betrachtet. Die generellen Aussagen über die Zellwandquellung bleiben damit unberührt, da lediglich davon auszugehen ist, dass das Maß an Dickenzunahme geringfügig unterschätzt wird, die relativen Unterschiede dagegen von einer Entspannung unabhängig sind. (3) Durch das Schneiden der ES tritt Zellsaft aus. Es kann vor allem durch die im Zellsaft vorkommende Äpfelsäure zu Artefakten bei der Zellwandquellung kommen. Es ist daher wichtig, den pH-Wert der Inkubationslösung während des Versuchs durch Pufferzugabe (hier 3 ml mit 10 mM MES pro ES) zu kontrollieren. Dass dies erfolgreich gelang, belegten Messungen des pH-Wertes. Dieser blieb über einen Zeitraum

von 48 h konstant. Der Einfluss des ausgetretenen Saftes ist daher zu vernachlässigen. (4) Es sind keine Aussagen über die Stoffklassen möglich, die für die Quellung verantwortlich sind. Durch die Anwendung verschiedener Behandlungen, wie die Zugabe von Calcium Salzen oder Chelatoren, kann lediglich indirekt und in Verbindung mit Literaturdaten zu anderen Früchten auf die Rolle des Pektins als quellende Zellwandfraktion geschlossen werden. (5) Es kann nicht zwischen der Quellung der Primärwand und der Mittellamelle unterschieden werden. (6) Untersuchungen der Hypodermis bzw. von Mesokarpzellwänden mit der gleichen Methode sind technisch kaum umsetzbar.

4.1.2 Untersuchungen an extrahierten Zellwänden

Bisherige Daten zu Hydratationseigenschaften von Zellwänden wurden überwiegend *in vitro* an extrahierten Zellwänden erhoben, da dies ein gängiges standardisiertes Verfahren zur Ermittlung der Quellung in den Lebensmittelwissenschaften darstellt (Larrauri, 1999). Die Untersuchungen für die vorliegende Arbeit wurden am Alkohol unlöslichen Rückstand (alcohol insoluble residue (AIR)) der Zellwand durchgeführt. Auch die *in vitro* Untersuchungen an extrahierten Zellwänden haben einige Vorteile. (1) Es ist ein hoher Durchsatz an Experimenten möglich, da die Versuche unabhängig vom Vorhandensein frischer Kirschen durchgeführt werden können. (2) AIR kann sequentiell in Fraktionen unterteilt werden. Rückschlüsse auf die für die Quellung verantwortliche(n) Fraktionen sind somit möglich. (3) Der Quellungsdruck ist quantifizierbar.

Als nachteilig sind die folgenden Punkte zu betrachten. (1) Es gibt kein einheitliches Extraktionsverfahren. In der Literatur werden verschiedene Verfahren zur Extraktion von Zellwänden beschrieben (Renard, 2005). Dabei kommt es, je nach verwendetem Extraktionsmittel, zu Veränderungen der Zellwand im Vergleich zum nativen Zustand. Zu den potentiellen Veränderungen zählen: das Auswaschen leicht löslicher Pektine (Huber, 1991, Renard, 2005), das Aufbrechen kovalenter Bindungen (Bock et al., 1977), die Veränderung

des Veresterungsgrades (Jarvis, 1991), eine veränderte verbleibende Enzymaktivität (Brummell, 2006) und die Auswaschung von Kationen wie Calcium (Huber, 1991). Alle diese Veränderungen beeinflussen das Quellungsvermögen des Zellwandextraktes. (2) Bei der Extraktion kommt es zur Veränderung der räumlichen Struktur der Zellwand. Zellwände quellen durch die Einlagerung von Wasser in Poren, welche durch das Herauslösen von Pektinen freigeworden sind (Redgwell et al., 1997). Durch die Zellwandextraktion wird erheblich in die räumliche Struktur und die Anordnung der Polysaccharide eingegriffen. Das Netzwerk aus Pektinen, Hemicellulosen und Zellulosefibrillen wird gestört und es entstehen vergrößerte Hohlräume. Das *in vitro* Quellungspotential wird dadurch erhöht (Kunzek et al., 2002). Diese Diskrepanz zeigt sich auch in den für diese Arbeit erhobenen Daten. So quellen extrahierte Zellwände *in vitro* gemittelt über 12 Sorten um das 4,3fache ihres Ausgangsvolumens und damit doppelt so stark wie dieselben Sorten *in vivo* in der Mikroskopie (Schumann, unveröffentlichte Daten). (3) Durch die Extraktion der Zellwände und die Zerstörung des Gewebeverbandes ist keine Aussage über Auswirkungen der Quellung auf die Zelladhäsion möglich (4) Genaue orts- oder gewebeaufgelöste Untersuchungen sind nicht möglich. Es ist zwar möglich Mesokarp frei von Exokarp zu gewinnen. Allerdings ist es nicht möglich, das Exokarp rückstandslos vom Mesokarp zu trennen. So handelt es sich bei der Fruchthautfraktion daher lediglich um eine Exokarp-angereicherte Fraktion (Alkio et al., 2012). Positionsabhängige Experimente, um unter anderem Gradienten innerhalb der Frucht zu erkennen, sind durch die Menge an AIR, die für Quellungsexperimente benötigt werden, ungenau. (5) Es ist nicht möglich die Primärwand unabhängig von der Mittellamelle zu extrahieren (Zamil und Geitmann, 2017) und separat deren Quellung zu untersuchen (6) Es ist nicht möglich mit verbundenen Stichproben zu arbeiten. Mehrphasige Experimente beschränken sich auf Untersuchungen zum Quellungsdruck. Untersuchungen zu SC, WHC und WRC sind nicht reversibel. AIR, welcher einer Quellung unterzogen wurde, kann nicht rückgetrocknet und wiederverwendet werden. (7) Die Herstellung des AIR ist durch den hohen Verbrauch an Lösungsmitteln teuer.

4.1.3 Untersuchungen mit Hilfe von monoklonalen Antikörpern

Untersuchungen mit mABs sind mikroskopische Untersuchungen, so dass die in 4.1.1 erwähnten Vor- und Nachteile weitgehend auch hier gelten. Das Anfärben von Zellwänden mit mABs bietet zusätzlich folgende Vorteile: (1) Die Strukturidentifikation am Versagensort ist mit der Färbetechnik möglich. Durch die spezifische Bindung der mABs an bestimmte Epitope kann eine Aussage über die an der Rissoberfläche vorkommenden Zellwandbestandteile getroffen werden. In Verbindung mit dem Fluoreszensmarker gibt es nur dann eine Farbreaktion mit dem jeweiligen Antikörper, wenn das entsprechende Epitop, also der jeweilige Zellwandbestandteil, an der Rissoberfläche vorliegt. (2) Durch das Anfärben mit mABs wird eine sehr hohe räumliche Auflösung erreicht. In Versuchen mit Ultradünnschnitten ist das eine der wenigen Methoden, in denen die Mittellamelle unabhängig von der Primärwand betrachtet werden kann.

Als nachteilig sind die folgenden Punkte zu betrachten: (1) Nach der Färbeprozedur sind keine Aussagen über den Quellungszustand der Zellwand mehr möglich. Dieser muss in weiteren Versuchen separat und parallel bestimmt werden (2) Für Aussagen zur Strukturidentifikation an der Rissoberfläche sind frische, reife Kirschen notwendig. Dadurch ist die experimentelle Phase im Jahr auf wenige Wochen begrenzt. (3) Die Antikörper sind teuer. Im Gegensatz zu den üblichen Versuchen mit Ultradünnschnitten, bei denen nur wenige Tropfen Antikörperlösung verwendet werden, sind zum Anfärben von Rissoberflächen deutlich höhere Volumina und somit Antikörpermengen notwendig.

4.1.4 Fazit

Alle drei Methoden sind dazu geeignet, die Zellwand, deren Quellung sowie die Auswirkungen auf die Zelladhäsion genauer zu charakterisieren. Durch die hohe örtliche Auflösung im mechanisch relevanten Gewebe ist die lichtmikroskopische Untersuchung den anderen Methoden vorzuziehen. Dies ist jedoch an das Vorhandensein frischer Kirschen gebunden und nur saisonal möglich. Eine in weiten Strecken hohe Korrelation zwischen *in vivo* und *in vitro*

Untersuchungen an AIR erlaubt es, den experimentellen Durchsatz zu steigern und die Saison zu verlängern. Zudem zeigt die gute Korrelation, dass die gewählte Extraktionsmethode des AIR geeignet ist, um die lichtmikroskopischen Untersuchungen mit Quellungsexperimenten zu SC, WHC und WRC zu ergänzen. Das zusätzliche Anfärben mit mABs kann die rein quantitativen Aussagen über die Zellwandquellung durch die Lichtmikroskopie um eine räumlich hoch aufgelöste Strukturidentifikation von spezifischen Zellwandepitopen ergänzen. Entwicklungsabhängige Aussagen über die chemische Veränderung der extrahierten Zellwände können durch die Verwendung von mABs gut lokalisiert werden. Insgesamt ergibt das Zusammenspiel aller drei Methoden ein wirkungsvolles Werkzeug für die Weiterentwicklung des Reißverschlussmodells, um den Schritt der Zellwandquellung besser verstehen und manipulieren zu können.

4.2 Ergänzung des Reißverschlussmodells

Ausgangspunkt der vorliegenden Arbeit war das Reißverschlussmodell zur Erklärung des Platzens von Kirschfrüchten (siehe Kapitel 2.2). In diesem Modell gilt die Zellwandquellung als eine zentrale Ursache des Versagens, wodurch es zum Aufreißen der Mikrorisse und zur Entwicklung und Verlängerung makroskopisch sichtbarer Risse kommt. Im folgenden Kapitel soll es darum gehen, wie die Erkenntnisse dieser Arbeit das bestehende Modell präzisieren können (Schematisch in Abb. 2).

Experimentelle Nachweise in Bezug auf die einzelnen Ereignisse im Reißverschlussmodell liefert die vorliegende Arbeit bezüglich (1) der Schwächung der Zellwand durch Zellwandquellung und dem sich dadurch ergebenden Verlust der Zelladhäsion (Kapitel 3.1); (2) dem zugrundeliegenden Mechanismus der Quellung (Kapitel 3.2) und (3) der Wirkung der Absenkung des pH-Wertes im Apoplasten und der Calciumextraktion (Kapitel 3.4).

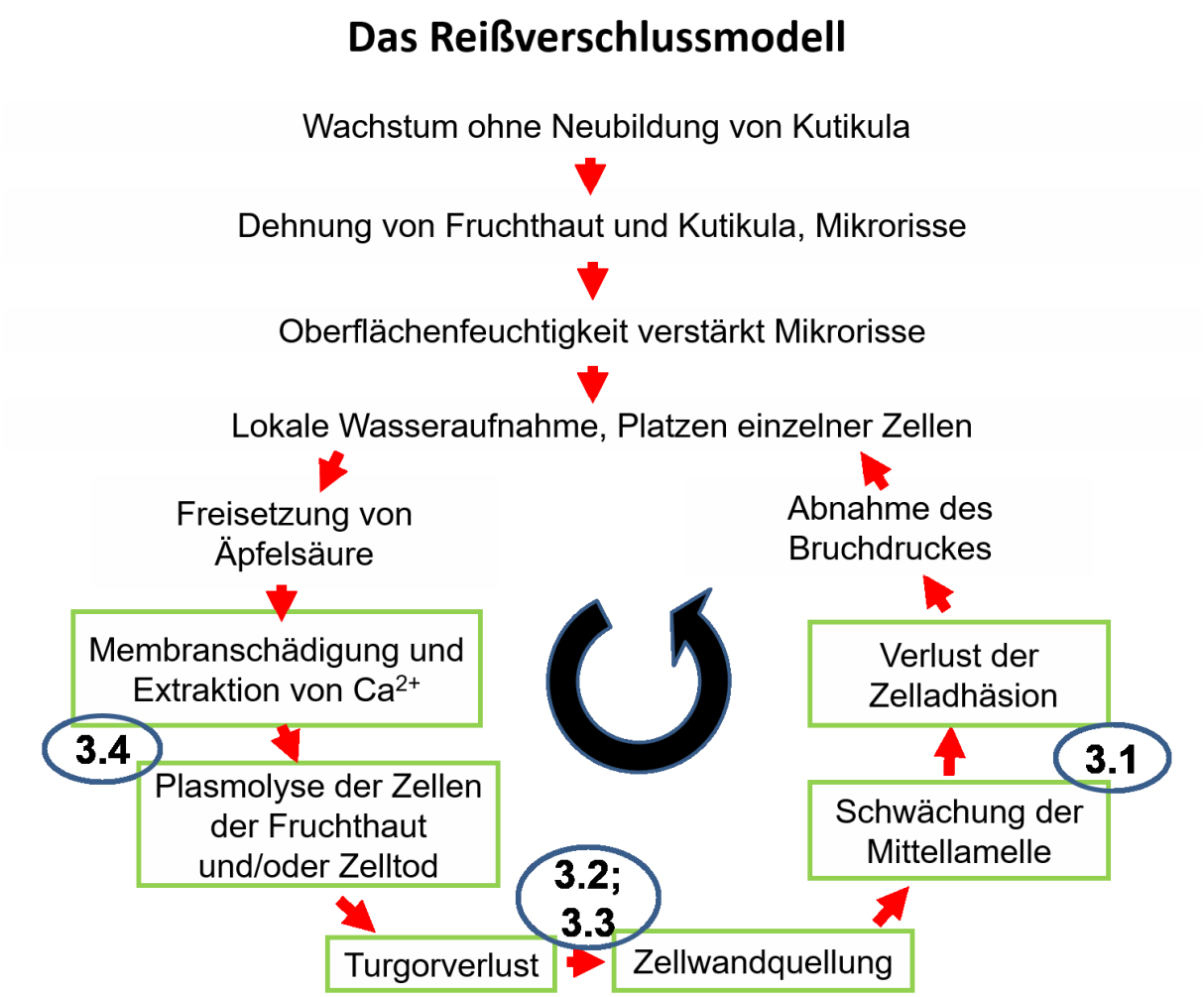

Abb. 2 Schematische Darstellung der Abfolge von Ereignissen, die nach dem Reißverschlussmodell zum makroskopisch sichtbaren Platzen der Kirsche führen. (verändert nach Schumann et al., 2020, Kapitel 3.1). Grün markiert sind Ereignisse, die in der vorliegenden Arbeit genauer untersucht wurden. Nummern in den blauen Kreisen entsprechen dem Kapitel dieser Arbeit, in dem das jeweilige Ereignis betrachtet wird.

4.2.1 Schwächung der Zellwand und Verlust der Zelladhäsion

Brüggenwirth und Knoche (2017) konnten mit Hilfe von biaxialen Zugtests nachweisen, dass gequollene Zellwände mechanisch schwächer sind als ungequollene Zellwände. Dabei ist der Bruchdruck negativ mit der Zellwanddicke von Epidermiszellen korreliert. Je mehr die Zellwände quellen und an Zellwanddicke durch Wassereinlagerung zunehmen, desto eher geben sie der vorherrschenden Belastung durch Dehnung der Fruchthaut nach und reißen schizogen, d.h. entlang der Zellwände. Die vorliegende Arbeit konnte dies bestätigen und zeigt

an Risskannten überwiegend schizogene Risse zwischen zwei Zellen (Kapitel 3.1). Darüber hinaus konnte mit Hilfe von mABs gezeigt werden, dass gering veresterte Pektine an der Rissoberfläche exponiert sind. Sowohl der hohe Anteil an schizogenen Rissen als auch das Vorliegen der Pektine an der Rissoberfläche deuten darauf hin, dass die Pektinmittellamelle die strukturelle Schwachstelle in der Zellwand darstellt. Quillt diese, sinkt die Zelladhäsion.

4.2.2 Mechanismus der Quellung

Grimm und Knoche (2015) zeigten, dass die Zellwand an Dicke durch Wassereinlagerung zunimmt, wenn benachbarte Zellen plasmolysieren. Und zwar stärker, wenn beide Nachbarzellen plasmolysiert vorliegen, als wenn die Plasmolyse nur eine der beiden Nachbarzellen betrifft. Auch Schlegel et al. (2018) belegten, dass es zwischen zwei toten, nicht turgeszenten Zellen zur Dickenzunahme der Zellwand kommt. In Kapitel (3.1) dieser Arbeit konnte gezeigt werden, dass entlang eines Risses von kurz vor der Rissspitze bis hin zum tiefen Riss bis ins Mesokarp die Zellwanddicke antiklinaler Zellwände eng negativ mit der Anzahl an lebenden Zellen korreliert war. Ebenso konnte gezeigt werden, dass die Zellwände unabhängig von der Ursache des Turgorverlustes quellen (Kapitel 3.2). Der Quellungsdruck, der durch die Zellwand aufgebracht wird, ist gering. Er liegt mit etwa 12 kPa (Kapitel 3.2) im Bereich des niedrigen Turgors reifer Früchte (Knoche et al., 2014; Schumann et al., 2014). Der Turgorverlust ist somit eine unmittelbare Voraussetzung für das Quellen von Zellwänden.

Zudem konnte der Mechanismus der Zellwandquellung in der vorliegenden Arbeit genauer beschrieben werden (Kapitel 3.2). Bei der Hydratation handelt es sich um einen rein physikalischen Vorgang. Dieser ist in der Regel vollständig reversibel. Faktoren, die die Quellung fördern (niedriger pH, Chelatoren, oder fortschreitende Fruchtentwicklung) oder reduzieren (Ca oder andere mehrwertige Kationen), wurden identifiziert. In entwicklungsabhängigen Quellungsversuchen wurden schwach in der Zellwand verankerte Pektine als die hauptsächlich quellende Zellwandfraktion identifiziert (Kapitel 3.3).

4.2.3 Sinkender pH im Apoplasten und Calciumextraktion führen zur Zellwandquellung

Winkler et al. (2015) zeigten in Immersionstest, dass niedrige pH-Werte zu einer erhöhten Platzanfälligkeit von Kirschen führen, wohingegen hohe pH-Werte Platzen reduzieren. Diese Beobachtung wird auf die Schwächung von Zellwänden durch niedrige pH-Werte zurückgeführt. Dies geschieht nicht nur von außen, sondern vielmehr durch das Platzen von Mesokarpzellen in Folge einer lokalen Wasseraufnahme und das anschließende Entlassen des Symplasten in den Apoplasten im Inneren der Kirsche. Dabei wird der Apoplast einer Säurekonzentration an Äpfelsäure von 70 mM ausgesetzt (Herrmann, 2001; Winkler et al., 2015). In der vorliegenden Arbeit konnte die pH Abhängigkeit der Zellwandquellung bestätigt werden. Je niedriger der pH-Wert, desto mehr quillt die Zellwand. Es konnte gezeigt werden, dass es eine Wechselwirkung zwischen dem pH-Wert und der Calciumkonzentration gibt (Kapitel 3.4). Wahrscheinlich kommt es einerseits zur Calciumextraktion durch hohe Protonenkonzentration, da beide Kationen um negative Bindungsplätze an den Säuregruppen der Galakturonsäureeinheiten konkurrieren. Zudem liegen diese Säuregruppen bei niedrigem pH zunehmend in undissoziierter Form vor. Das heißt, dass zudem weniger Bindungsplätze vorhanden sind. Durch die Bindung des nur noch einwertigen Protons, fehlt die intermolekulare Vernetzung der Pektine, sie quellen und werden mechanisch instabiler. Überdies konnte gezeigt werden, dass eine Quellung, hervorgerufen durch einen niedrigen pH, irreversibel ist.

4.2.4 Fazit

Das bestehende Reißverschlussmodell konnte in den Punkten die Zellwandquellung betreffend, erweitert und spezifiziert werden. Vor allem im Bereich der Strukturidentifikation am Versagensort und hinsichtlich der hauptsächlich quellenden Fraktion (Pektine) konnten experimentelle Nachweise geliefert werden. Die Beschreibung des Mechanismus der Zellwandquellung und der Einfluss eines niedrigen pH und der Interaktion mit dem

zellwandvernetzenden Calcium sind wichtige Punkte, die langfristig in der obstbaulichen Praxis Erfolge bezüglich der Platzreduktion versprechen.

4.3 Auswirkungen der Ergebnisse auf die obstbauliche Praxis, Züchtung und notwendige weitere Forschung

Potenzielle Anwendungen der Ergebnisse ergeben sich in bestehenden Anlagen für die Entwicklung und Optimierung von Kulturmaßnahmen sowie in zukünftig zu erstellenden Anlagen für die Entwicklung neuer Genotypen. Beide Aspekte werden nachfolgend behandelt.

4.3.1 Calcium Applikationen in der obstbaulichen Praxis

Die Ergebnisse dieser Arbeit zeigen, dass Calciumsalze, neben einer Reihe anderer mehrwertiger Kationen, Zellwandquellung verringern können (Kapitel 3.4). Durch intermolekulare Verbindungen zwischen den HG Molekülen (siehe „egg-box“ Kapitel 2.3), wird die Zellwand stabiler. Die Zelladhäsion wird stärker und kann der Dehnung in der Fruchthaut besser standhalten. Der Effekt eines sinkenden pHs im Apoplasten durch das Austreten von Äpfelsäure nach dem Platzen von Mesokarpzellen, der zur verstärkten Zellwandquellung führt, kann durch die Stabilisierung der Zellwand durch Calcium abgepuffert werden (Kapitel 3.4). Da die Zellwandquellung nach dem Reißverschlussmodell zu den hauptsächlichen Ursachen der Ausweitung eines Mikrorisses zum Makroriss gehört, sollte eine Reduktion des Platzens durch Calciumapplikationen stattfinden. Zum Einfluss von Calciumsalzen auf das Platzen von Kirschen wurde kürzlich ein Review veröffentlicht (Winkler und Knoche, 2019). Dabei wurde herausgestellt, dass Calciumsalze zwar in Immersionstest die Platzhäufigkeit konsistent und signifikant reduzieren können, dass jedoch Spritzapplikationen zu uneinheitlichen Ergebnissen hinsichtlich des Platzens führen. Es ist zu beachten, dass Calcium als zweiwertiges Kation nur schlechte Penetrationseigenschaften durch eine intakte Kutikula aufweist (Schönherr und Bukovac, 1973). Bei Immersionstests von reifen Kirschen kommt es vermutlich zur Penetration

des Calciums direkt durch vorhandene Mikrorisse, an welchen die Barrierefunktion der Kutikula gestört ist. Bei Spritzapplikationen hingegen ist nicht gesichert, an welcher Stelle die Tröpfchen die Kirsche erreichen und ob eine Penetration durch Mikrorisse stattfinden kann (Knoche et al., 2022). Gelangt Calcium durch Mikrorisse in die Zellwand der Epidermis, dient es der Stabilisierung der Fruchthaut durch verminderte Zellwandquellung direkt am mechanisch relevanten Rückgrat der Kirsche (Brüggenwirth et al., 2014). Dagegen dürfte die Penetration durch die Kutikula die Konzentration von Ca im Zellwandraum nur unwesentlich erhöhen. Ziel weiterer Untersuchungen sollte es sein, die Spritzapplikationen so zu gestalten, dass Calcium effektiv an den Mikrorissen ankommt und aufgenommen werden kann. Dann kann Calcium als eine wirkungsvolle und kostengünstige Möglichkeit zur Reduktion von ökonomischen Verlusten durch das Platzen von Kirschen dienen. Potentielle Ansatzpunkte wären Applikationen auf eine nasse Fruchtoberfläche. D.h., Applikationen während oder unmittelbar nach Niederschlägen sowie der Einsatz von Formulierungen mit nicht-phytotoxischen Silikontensiden, die zur Filmbildung in der Lage sind (Knoche, 1994).

4.3.2 Züchtung platzfester Sorten

In der vorliegenden Arbeit konnte gezeigt werden, dass Unterschiede im Quellungsverhalten zwischen den Sorten bestehen (Kapitel 3.2). Auch ist bekannt, dass sich Sorten hinsichtlich ihrer Platzempfindlichkeit unterscheiden (Kapitel 3.1; Christensen, 1996). Allerdings konnte bisher keine signifikante Korrelation zwischen dem Ausmaß der Zellwandquellung und der Platzfestigkeit einer Sorte festgestellt werden (Schumann, unveröffentlichte Daten). Dazu ist folgendes anzumerken: (1) Die Untersuchungen der Zellwandquellung und der Platzfestigkeit wurden bislang nicht am selben Batch von Früchten durchgeführt. Bei der Zellwandquellung gibt es zwischen den Sorten und den Jahren eine signifikante Korrelation (Kapitel 3.2). Allerdings variieren die Ergebnisse zur Platzanfälligkeit in Immersionstest nach Christensen (1972) zwischen einzelnen Anbaujahren (Christensen 1996). Ein Aspekt zukünftiger Untersuchungen sollte es sein, Zellwandquellung und Platzanfälligkeit von Sorten an

demselben Batch zu bestimmen. (2) Nach dem Reißverschlussmodell bedingen nicht nur die mechanischen Eigenschaften der Zellwand die Platzanfälligkeit von Sorten, sondern auch Faktoren, die den Wasserein- und -ausfluss bestimmen (Knoche und Winkler, 2019). Dazu gehören unter anderem: die Anfälligkeit für Mikrorisse; das Wasserpotential der Kirsche bzw. der äußeren Zellschichten, das die treibende Kraft der Wasseraufnahme bestimmt, und die Wasserdurchlässigkeit der Kutikula durch polare Poren (Beyer et al., 2005; Weichert und Knoche, 2006).

Insgesamt ist es vielversprechend durch die Züchtung platzfester Sorten eine für den Anbauer kostengünstige und umweltfreundliche Alternative zu schaffen, um ökonomische Verluste zu minimieren. Die mechanische Stabilisierung der Zellwand kann dazu dienen dieses Ziel zu erreichen. Züchterische Bemühungen sollten daher in Richtung der Manipulation der Zellwand und des darin für die Zelladhäsion verantwortlichen Pektins gehen.

4.3.3 Fazit

Die in der vorliegenden Arbeit gewonnen Erkenntnisse können sowohl auf der Produzentenseite als auch auf der Züchterseite wichtige Fortschritte hinsichtlich der Reduktion der wirtschaftlichen Einbußen durch Platzverluste bringen. In der obstbaulichen Praxis ist es denkbar mit Calciumapplikationen zu arbeiten. Auch auf züchterischer Seite können die Erkenntnisse genutzt werden, um platzfeste Sorten mit stabileren Zellwänden zu züchten. In der weiteren Forschung sind dazu unter anderem Untersuchungen hinsichtlich einer gezielten Applikation von Calciumsalzen und einer Korrelation zwischen der sortenspezifischen Zellwandquellung und der Platzfestigkeit notwendig.

5 Referenzen

Alkio, M., Jonas, U., Sprink, T., van Nocker, S. und Knoche, M. (2012) Identification of putative candidate genes involved in cuticle formation in *Prunus avium* (sweet cherry) fruit. *Annals of Botany* 110, 101-112

Balbontín, C., Ayala, H., Bastías, R.M., Tapia, G., Ellena, M., Torres, C., Yuri, J.A., Quero-García, J., Ríos, J.C., und Silva, H. (2013) Cracking in sweet cherries: A comprehensive review from a physiological, molecular, and genomic perspective. *Chilean Journal of Agricultural Research* 73, 66-72

Basanta, M.F., de Escalada Plá M.F., Stortz, C.A. und Rojas, A.M. (2013) Chemical and functional properties of cell wall polymers from two cherry varieties at two developmental stages. *Carbohydrate Polymers* 92, 830-841

Basanta, M., Ponce, N.M.A., Salum, M.L., Raffo, M.D., Vicente, A.R., Erra-Balsells, R. und Stortz, C.A. (2014) Compositional changes in cell wall polysaccharides from five sweet cherry (*Prunus avium* L.) cultivars during on tree ripening. *Journal of Agricultural and Food Chemistry 62*, 12418-12427

Batisse, C., Fils-Lycaon, F. und Buret, M. (1994) Pectin changes in ripening cherry fruit. *Journal of Food Science* 59, 389-393

Batisse, C., Buret, M. und Coulomb, P.J. (1996) Biochemical Differences in Cell Wall of Cherry Fruit between Soft and Crisp Fruit. Journal of Agricultural and Food Chemistry 44, 453-457

Becker, T., Grimm, E. und Knoche, M. (2012) Substantial water uptake into detached grape berries occurs through the stem surface. *Australian Journal of Grape and Wine Research* 18, 109-114

Beyer, M., Lau, S., und Knoche, M. (2005) Studies on water transport through the sweet cherry fruit surface: IX. Comparing permeability in water uptake and transpiration. *Planta* 220, 474-485

Bidhendi, A.J. und Geitmann, A. (2016) Relating the mechanics of the primary plant cell wall to morphogenesis. *Journal of Experimental Botany* 67, 449–461

Bock, W., Anger, H., Kohn, R., Malovikova, A., Dongowski, G. und Friebe, R. (1977) Charakterisierung mechanolytisch abgebauter Pektinpräparate. *Die Angewandte Makromolekulare Chemie* 64, 133-146

Børve, J. und Stensvand, A. (2003) Use of a plastic rain shield reduces fruit decay and need for fungicides in sweet cherry. *Plant Disease* 87, 523-528

Børve, J., Sekse, L. und Stensvand, A. (2000) Cuticular fractures promote postharvest fruit rot in sweet cherries. *Plant Disease* 84, 1180-1184.

Brinkmann, T., Kuhnke, F., Grimm, E. und Knoche, M. (2022) Sweet cherry flesh cells burst in non-random clusters along minor veins. *Planta* 255, 100

Brummell, D.A. (2006) Cell wall disassembly in ripening fruit. *Functional Plant Biology* 33, 103-119

Brüggenwirth, M., Fricke, H. und Knoche, M. (2014) Biaxial tensile tests identify epidermis and hypodermis as the main structural elements of sweet cherry skin. *AoB Plants* 6

Brüggenwirth, M. und Knoche, M. (2016) Mechanical properties of skins of sweet cherry fruit of differing susceptibilities to cracking. *Journal of the American society for horticultural science* 141, 162-168

Brüggenwirth, M., und Knoche, M. (2017) Cell wall swelling, fracture mode, and the mechanical properties of cherry fruit skins are closely related. *Planta* 245, 765-777

Caffall, K.H. und Mohnen, D. (2009) The structure, function, and biosynthesis of plant cell wall pectic polysaccharides. *Carbohydrate Research* 344, 1879–1900

Cantu, D., Vicente, A.R., Greve, L.C., Dewey, F.M., Bennett, A.B., Labawitch, J.M. und Powell, A.L.T. (2008) The intersection between cell wall disassembly, ripening, and fruit susceptibility to *Botrytis cinerea*. *Proceedings of the National Academy of Sciences of the United States of America* 105, 859–864

Carpita, N.C. und Gibeaut, D.M. (1993) Structural models of primary cell walls in flowering plants: consistency of molecular structure with the physical properties of the walls during growth. *The plant journal* 3, 1-30

Choi, C., Toivonen, P., Wiersma, P.A. und Kappel, F. (2002) Differences in levels of pectic substances and firmness in fruit from six sweet cherry genotypes. *Journal of the American Pomological Society* 56, 197-201

Christensen, J.V. (1972) Cracking in cherries III. Determination of cracking susceptibility. *Acta Agriculturae Scandinavica* 22, 128-136

Christensen, J.V. (1996) Rain-induced cracking of sweet cherries: Its causes and prevention. In: Webster, A.D. und Looney, N.E. (eds.). *Cherries: Crop physiology, production and uses*. CAB International, Wallingford, UK, pp. 297-327.

Cline, J.A., Meland, M., Sekse, L. und Webster, A.D. (1995) Rain Cracking of Sweet Cherries: II. Influence of Rain Covers and Rootstocks on Cracking and Fruit Quality. *Acta Agriculturae Scandinavica, Section B — Soil & Plant Science* 45, 224-230

Considine, J.A. und Kriedemann, P.E. (1972) Fruit splitting in grapes. Determination of the critical turgor pressure. *Australian Journal of Agricultural Research* 23, 17-24

Cosgrove, D.J. (1999) Enzymes and other agents that enhance cell wall extensibility. *Annual Review of Plant Physiology and Plant Molecular Biology* 50, 391–417

Cosgrove, D.J. (2000) Expansive growth of plant cell walls. *Plant Physiology and Biochemistry* 38, 109–124

Cosgrove, D.J. (2005) Growth of the Plant Cell Wall. *Nature Reviews Molecular Cell Biology* 6, 850-861

Cosgrove, D.J. (2022) Building an extensible cell wall. *Plant Physiology* 189, 1246-1277

Cosgrove, D.J. und Jarvis, M.C. (2012) Comparative structure and biomechanics of plant primary and secondary cell walls. *Frontiers in Plant Science* 3, 1-6

Fügel, R., Carle, R. und Schieber, A. (2004) A novel approach to quality and authenticity control of fruit products using fractionation and characterisation of cell wall polysaccharides. *Food Chemistry* 87, 141–150

Fügel, R., Schieber, A. und Carle, R. (2006) Determination of the fruit content of cherry fruit preparations by gravimetric quantification of hemicellulose. *Food Chemistry* 95, 163–168

Glenn, G.M. und Poovaiah, B.W. (1989) Cuticular properties and postharvest calcium applications influence cracking of sweet cherries. *Journal of the American Society for Horticultural Science* 114, 781-788

Grimm, E. und Knoche, M. (2015) Sweet cherry skin has a less negative osmotic potential than the flesh. *Journal of the American Society for Horticultural Science* 140, 472-479

Grimm, E., Peschel, S., Becker, T. und Knoche, M. (2012) Stress and strain in the sweet cherry fruit skin. *Journal of the American Society for Horticultural Science* 137, 383-390

Grimm, E., Peschel, S. und Knoche, M. (2013) Mottling on sweet cherry fruit is caused by exocarp strain. *Journal of the American Society for Horticultural Science* 138, 18-23

Grimm, E., Pflugfelder, D., van Dusschoten, D., Winkler, A. und Knoche, M. (2017) Physical rupture of the xylem in developing sweet cherry fruit causes progressive decline in xylem sap inflow rate. *Planta* 246, 659-672

Herrmann, K. (2001) Inhaltsstoffe von Obst und Gemüse. Ulmer, Stuttgart, Germany

Huber, D.J. (1991) Acidified phenol alters tomato cell wall pectin solubility and calcium content. *Phytochemistry* 30, 2523-2527

Ishii, T., Matsunaga, T., Pellerin, P., O'Neill, M.A., Darvill, A. und Albersheim, P. (1999) The plant cell wall polysaccharide rhamnogalacturonan II self-assembles into a covalently cross-linked dimer. *Journal of Biological Chemistry* 274, 13098–13104

Jarvis, M.C. (1991) Control of thickness of collenchyma cell walls by pectins. *Planta* 187, 218-220

Jarvis, M.C. (2011) Plant cell walls: Supramolecular assemblies. *Food Hydrocolloids* 24, 257-262

Jarvis, M.C., Briggs, S.P.H. und Knox, J.P. (2003) Intercellular adhesion and cell separation in plants. *Plant, Cell and Environment* 26, 977–989

Khadivi-Khub, A. (2015) Physiological and genetic factors influencing fruit cracking. *Acta Physiologiae Plantarum* 37, 1718

Khanal, B.P., Grimm, E. und Knoche, M. (2011) Fruit growth, cuticle deposition, water uptake, and fruit cracking in jostaberry, gosseberry, and black currant. *Scientia Horticulturae* 128, 289-296

Knoche, M. (1994) Organosilicone surfactants: Performance in agricultural spray application. A review. *Weed Research* 34, 221-239

Knoche, M., Beyer, M., Peschel, S., Oparlakov, B. und Bukovac, M.J. (2004) Changes in strain and deposition of cuticle in developing sweet cherry fruit. *Physiologia Plantarum* 120, 667-677

Knoche, M., Grimm, E., and Schlegel, H.J. (2014) Mature sweet cherries have low turgor. *Journal of the American Society for Horticultural Science* 139, 3-12

Knoche, M. und Lang, A. (2017) Ongoing Growth Challenges Fruit Skin Integrity. *Critical Reviews in Plant Sciences* 36, 190-215

Knoche, M., Peschel, S., und Hinz, M. (2002) Studies on water transport through the sweet cherry fruit surface: III. Conductance of the cuticle in relation to fruit size. *Physiologia Plantarum* 114, 414-421

Knoche, M. und Peschel, S. (2006) Water on the surface aggravates microscopic cracking of the sweet cherry fruit cuticle. *Journal of the American Society for Horticultural Science* 131, 192-200

Knoche, M. und Winkler, A. (2017) Rain-induced cracking of sweet cherries. In: Quero-Garcia, J., Iezzoni, A., Pulawska, J. und Lang, G. (eds.). *Cherries: Botany, Production and uses*. CAB International, Wallingford, UK, pp.140-165

Knoche, M. Winkler, A. und Lang, A. (2022) The unzipping of sweet cherry fruit skin and strategies to prevent it. *Italus Hortus* 29, 1-13

Kobayashi, M., Matoh, T. und Azuma, J. (1996) Two chains of rhamnogalacturonan II are cross-linked by borate-diol ester bonds in higher plant cell walls. *Plant Physiology* 110, 1017–1020

Kohn, R. und Kovac, P. (1978) Dissociation constants of D-galacturonic and D-glucuronic acid and their O-methyl derivatives. *Chemicke Zvesti* 32, 478-485

Kondo, S. und Danjo, C. (2001) Cell wall Polysaccharide Metabolism during fruit development in sweet cherry 'Satohnishiki' as affected by gibberellic acid. *Journal of the Japanese Society for Horticultural Science* 70, 178-184

Kunzek, H., Müller, S., Vetter, S. und Godeck, R. (2002) The significance of physico chemical properties of plant cell wall materials for the development of innovative food products. *European Food Research and Technology* 214, 361–376

Lahaye, M., Tabi, W., Le Bot, L., Delaire, M., Orsel, M., Campony, J.A., Garcia, J.Q. und Le Gall, S. (2021) Comparison of cell wall chemical evolution during the development of fruit of two contrasting quality from two members of the Rosaceae family: Apple and sweet cherry. *Plant Physiology and Biochemistry* 168, 93-104

Larrauri, J.A. (1999) New approaches in the preparation of high dietary fiber powders from fruit by-products. *Trends in food Science & Technology* 10, 3-8

Lilleland, O. und Newsome, L. (1934) A growth study of the cherry fruit. *Proceedings of the American Society for Horticultural Science* 32, 291-299

Looney, N.E. (1985) Benefits of calcium sprays below expectations in B.C. tests. *Goodfruit Grower* 36, 7-8.

Matas A.J., Cobb E., Paolillo D.J. und Niklas K.J. (2004) Crack resistance in cherry tomato fruit correlates with cuticular membrane thickness. *HortScience* 39, 1354–1358

McNeil M., Darvill A.G., Fry S.C. und Albersheim P. (1984) Structure and function of the primary cell walls of plants. *Annual Review of Biochemistry* 53, 625–663

Measham, P.F., Bound, S.A., Gracie, A.J., and Wilson, S.J. (2009) Incidence and type of cracking in sweet cherry (Prunus avium L.) are affected by genotype and season. *Crop and Pasture Science* 60, 1002-1008

Milad R.E. und Shackel K.A. (1992) Water relations of fruit end cracking in french prune (*Prunus domestica* L. cv. French). *Journal of the American Society for Horticultural Science* 117, 824–828.

Mohnen, D. (1999) Biosynthesis of pectins and galactomannans. In: Barton, D., Nakanishi, K. und Meth-Cohn, O. (eds.). *Comprehensive Natural Products Chemistry*. Elsevier Science, Amsterdam, NL, pp. 497–527

Mohnen, D. (2008) Pectin structure and biosynthesis. *Current Opinion in Plant Biology* 11, 266–277

Morris, E.R., Powell, D.A., Gidley, M.J. und Rees, D.A. (1982) Conformations and interactions of pectins: I. Polymorphism between gel and solid states of calcium polygalacturonate. *Journal of molecular biology* 155, 507-516

Niklas, K.J. (1992) Plant biomechanics—an engineering approach to plant form and function. *University of Chicago Press*, Chicago

O'Neill, M.A., Ishii, T., Albersheim, P. und Darvill, A.G. (2004) Rhamnogalacturonan II: structure and function of a borate cross-linked cell wall pectic polysaccharide. *Annual Review of Plant Biology* 55, 109–139

Olmstead, J.W., Iezzoni, A.F. und Whiting, M.D. (2007) Genotypic differences in sweet cherry fruit size are primarily a function of cell number. *Journal of the American Society for Horticultural Science* 132, 697–703

Pelloux, L., Rustérucci, C. und Mellerowicz, E.J. (2008) New insights into pectin methylesterase structure and function. *Trends in Plant Science* 12, 267-277

Peschel, S. und Knoche, M. (2005) Characterization of microcracks in the cuticle of developing sweet cherry fruit. *Journal of the American Society for Horticultural Science* 130, 487-495.

Peschel, S., Franke, R., Schreiber, L. und Knoche, M. (2007) Composition of the cuticle of developing sweet cherry fruit. *Phytochemistry* 68, 1017-1025

Peschel, S. und Knoche, M. (2012) Studies on Water Transport through the Sweet Cherry Fruit Surface: XII. Variation in Cuticle Properties among Cultivars. *Journal of the American Society for Horticultural Science* 137, 367-375

Powell, D.A., Morris, E.R., Gidley, M.J. und Rees, D.A. (1982) Conformations and interactions of pectins: II. Influence of residue sequence on chain association in calcium pectate gels. *Journal of molecular biology* 155, 517-531

Raghavendra, N.S., Rastogi, N.K., Raghavarao, K.S.M.S und Tharanathan, R.N. (2004) Dietary fiber from coconut residue: effects of different treatments and particle size on the hydration properties. *European Food Research and Technology* 218, 563-567

Redgwell, R.J., MacRae E., Hallett, I., Fischer, M., Perry, J. und Harker, R. (1997) In vivo and in vitro swelling of cell walls during fruit ripening. *Planta* 203, 162-173

Renard, C.M.G.C. (2005) Variability in cell wall preparations: quantification and comparison of common methods. *Carbohydrate Polymers* 60, 515-522

Schlegel, H.J., Grimm, E., Winkler, A. und Knoche, M. (2018) Orange peel disorder in sweet cherry: Mechanism and triggers. *Postharvest Biology and Technology* 137, 119-128

Schönherr, J. und Bukovac, M.J. (1973) Ion exchange properties of isolated tomato fruit cuticular membrane: Exchange capacity, nature of fixed charges and cation selectivity. *Planta* 109, 73-93

Schols, H.A. und Voragen, A.G.J. (1996) Complex pectins: structure elucidation using enzymes. In: Visser, J. und Voragen, A.G.J. (eds.). *Pectins and Pectinases*, Elsevier Science, Amsterdam, NL, pp. 3–19

Sekse, L. (1995) Fruit cracking in sweet cherries (*Prunus avium* L.). Some physiological aspects - A mini review. *Scientia Horticulturae* 63, 135-141

Sekse, L. (1998) Fruit cracking mechanisms in sweet cherries (*Prunus avium* L.) – A review. *Acta Horticulturae* 468, 637-648

Sekse, L. (2008) Fruit cracking in sweet cherries - Some recent advances. *Acta Horticulturae* 795, 615-623

Sekse, L., Bjerke, K.L., und Vangdal, E. (2005) Fruit cracking in sweet cherries – An integrated approach. *Acta Horticulturae* 667, 471-474

Shomer, I., Frenkel, H. und Polinger, C. (1991) The existence of a diffuse electric double layer at cellulose fibril surfaces and its role in the swelling mechanism of parenchyma plant cell walls. *Carbohydrate Polymers* 16, 199–210

Simon, G. (2006) Review on rain induced fruit cracking of sweet cherries (*Prunus avium* L.), its causes and the possibilities of prevention. *International Journal of Horticultural Science* 12, 27-35

Sozzi, G.O., Greve, L.C., Prody, G.A. und Labavitch, J.M. (2002) Gibberellic acid, synthetic auxins, and ethylene differentially modulate α-L-arabinofuranosidase activities in antisense 1-aminocyclopropane-1-carboxylic acid synthase tomato pericarp discs. *Plant Physiology* 129, 1330–1340

Thomidis, T. und Exadaktylou, E. (2013) Effect of a plastic rain shield on fruit cracking and cherry diseases in Greek orchards. *Crop Protection* 52, 125-129

Tukey, H.B. (1934) Growth of the embryo, seed, and pericarp of the sour cherry (*Prunus cerasus*) in relation to season of fruit ripening. *Proceedings of the American Society for Horticultural Science* 31, 125-144

Tukey, H.B. und Young, J.O. (1939) Histological Study of the Developing Fruit of the Sour Cherry. Botanical Gazette 100, 723-749

Vetter, S. und Kunzek, H. (2003) The influence of suspension solution conditions on the rehydration of apple cell wall material. *European Food Research and Technology* 216, 39–45

Wang X., Wilson L. und Cosgrove D.J. (2020) Pectin methylesterase selectively softens the onion epidermal wall yet reduces acid-induced creep. *Journal of Experimental Botany* 71, 2629–2640

Weichert, H und Knoche, M. (2006): Studies on water transport through the sweet cherry fruit surface: 10. Evidence for polar pathways across the exocarp. *Journal of Agricultural and Food Chemistry* 54, 3951-3958

Willats, W.G.T, McCartney, L., Mackie, W. und Knox, J.P. (2001a) Pectin: cell biology and prospects for functional analysis. *Plant Molecular Biology* 47, 9–27

Willats, W.G.T., Orfila, C., Limberg, G., Buchholt, H.C., van Alebeek, GJ.W.M., Voragen, A.G.J., Marcus, S.E., Christensen, T.M.I.E, Mikkelsen, J.D., Murray, B.S. und Knox, J.P. (2001b) Modulation of the degree and pattern of methyl-esterification of pectic homogalacturonan in plant cell walls: implications for pectin methyl esterase action, matrix properties, and cell adhesion. Journal of Biological Chemistry 276, 19404-19413

Winkler, A., Ossenbrink, M., and Knoche, M. (2015) Malic acid promotes cracking of sweet cherry fruit. *Journal of the American Society for Horticultural Science* 140, 280-287

Winkler, A. und Knoche, M. (2019) Calcium and the physiology of sweet cherries: A review. *Scientia Horticulturae* 245, 107-115

Winkler, A., Peschel, S., Kohrs, K., and Knoche, M. (2016) Rain cracking in sweet cherries is not due to excess water uptake but to localized skin phenomena. *Journal of the American Society for Horticultural Science* 141, 653-660

Yamaguchi, M., Sato, I., Takase, K., Watanabe, A., und Ishiguro, M. (2004) Differences and yearly variation in number and size of mesocarp cells in sweet cherry (*Prunus avium* L.) cultivars and related species. *Journal of the Japanese Society for Horticultural Science* 73, 12-18

Zamil, M.S. und Geitmann, A. (2017) The middle lamella – more than a glue. *Physical Biology* 14 015004

Zdunek, A., Gancarz, M., Cybulska, J., Ranachowski, Z. und Zgórska, K. (2008) Turgor and temperature effect on fracture properties of potato tuber (*Solanum tuberosum* cv. Irga). *International Agrophysics* 22, 89-97

Zhang, Y., Yu, J., Wang, X., Durachko, D.M., Zhang, S. und Cosgrove D.J. (2021) Molecular insights into the complex mechanics of plant epidermal cell walls. *Science* 372, 706–711

Danksagung

Im Anschluss an diese Arbeit möchte ich mich bei einer Reihe an Personen bedanken, die mich in den letzten Jahren begleitet und unterstützt haben und ohne die die Fertigstellung der Arbeit nicht möglich gewesen wäre.

Einen besonderen Dank möchte ich meinem Erstbetreuer Herrn **Prof. Dr. Moritz Knoche** für die kontinuierliche Unterstützung meiner Forschung und der Dissertation aussprechen. Jederzeit stand seine Tür offen für alle Fragen und Probleme. Zudem bin ich äußerst dankbar dafür, dass er sich nie über die Ausfälle durch die vier Elternzeiten beklagt hat. Ich hatte immer das Gefühl volle Unterstützung und Rückendeckung durch ihn und das Institut zu erfahren.

Frau **Prof. Dr. Traud Winkelmann** danke ich für die Übernahme des Korreferates dieser Arbeit und Frau **Prof. Dr. Jutta Papenbrock** für die Übernahme des Vorsitzes der Prüfungskommission.

Für die sprachlichen Korrekturen sowie die hilfreichen inhaltlichen Kommentare an den Manuskripten danke ich Herrn **Dr. Alexander Lang**.

Ich danke dem **Hochschulbüro für Chancenvielfalt**, welches mir für die Fertigstellung der Arbeit eine Promotionsabschlussförderung gewährte und mich so finanziell unterstützte.

Während der gesamten Zeit am Standort in Herrenhausen habe ich mich mit den Kollegen immer sehr wohl gefühlt und möchte mich bei allen für das angenehme Arbeitsklima und die vielen netten Gespräche bedanken. Vielen Dank an **Dr. Martin Brüggenwirth** und **Dr. Andreas Winkler**, an **Dr. Eckhard Grimm** und **Dr. Bishnu Khanal**, an **Sylvia Janning** und **Friederike Schröder**. Bei **Simon Sitzenstock** bedanke ich mich zusätzlich für all die übernommenen Zellwandextraktionen und Messungen an der Quellungszelle. Vielen

Dank auch an die Kollegen aus Ruthe **Herrn Peter Grimm-Wetzel**, **Herrn Marcel Pastwa** und **Frau Hana Weiß**, die über das ganze Jahr dafür Sorge getragen haben, dass in der Saison immer genügend frische Kirschen pünktlich und für mich unkompliziert ins Labor geliefert wurden.

Zuletzt gilt mein herzlicher Dank meiner Familie. Sowohl meinen Eltern **Ute Schumann** und **Jürgen Schumann**, die immer sehr viel Wert auf eine gute Bildung gelegt haben und nie meinen Entscheidungen im Weg standen, als auch meinem Mann **Christoph Schumann** und meinen Kindern **Clara, Lilly, Bruno** und **Enno**. Sie alle waren immer sehr geduldig mit mir und haben mich in stressigen Zeiten ausgehalten. **Christoph**, ich danke Dir für all deine tatkräftige und bedingungslose Unterstützung zu Hause, deine Wertschätzung meiner Arbeit und deine vielen aufmunternden Worte, wenn ich nicht mehr wusste, wie ich alles unter einen Hut bekommen soll! Ich hab euch lieb! Dankeschön!

Lebenslauf

Name:	Schumann, Christine
Geburtsdatum und –ort:	08.05.1987, Pirna (Sachsen)
Staatsangehörigkeit:	Deutschland

Ausbildung und beruflicher Werdegang

01/2015 – heute	Promotion am Institut für Gartenbauliche Produktionssysteme (Abteilung: Obstbau) der Leibniz Universität Hannover unterbrochen durch vier Elternzeiten: 11/1016 - 12/2017, 07/2018 - 12/2019, 08/2020 - 02/2022 und 08/2022 – 12/2023
06/2014 – 12/2014	Sachbearbeiterin, Referat Landwirtschaft im Sächsischen Landesamt für Landwirtschaft, Umwelt und Geologie
10/2010 – 04/2013	Studium der Gartenbauwissenschaften (M.Sc.) an der Leibniz Universität Hannover, Masterarbeit: Das Wasserpotential sich entwickelnder Süßkirschenfrüchte
10/2009 – 09/2010	Jahrespraktikum in der Fairtrade zertifizierten Rosenfarm Red Lands Roses in Ruiro, Kenia
10/2006 – 09/2009	Studium der Gartenbauwissenschaften (B.Sc.) an der Leibniz Universität Hannover, Bachelorarbeit: Olfaktorische Orientierung herbivorer Blütentripse
08/2005 – 07/2006	Freiwilliges ökologisches Jahr im Nationalparkzentrum Sächsische Schweiz
08/1997 – 06/2005	Allgemeines Abitur, Friedrich Schiller Gymnasium Pirna
08/1993 – 07/1997	Grundschule Lohmen

Publikationsliste

Schumann, C., Schlegel, H.J., Grimm, E., Knoche, M. und Lang, A. (2014) Water potential and its components in developing sweet cherry. *Journal of the American Society for Horticultural Science* 139, 349-355.

Schumann, C., Winkler, A., Brüggenwirth, M., Köpcke, K. und Knoche, M. (2019) Crack initiation and propagation in sweet cherry skin: A simple chain reaction causes the crack to 'run'. *Plos One* 14(7), e0219794

Schumann, C. und Knoche M. (2020) Swelling of cell walls in mature sweet cherry fruit: factors and mechanisms. *Planta* 251, 65

Schumann, C., Sitzenstock, S., Erz, L. und Knoche, M. (2020) Decreased deposition and increased swelling of cell walls contribute to increased cracking susceptibility of developing sweet cherry fruit. *Planta* 252, 96

Schumann, C., Winkler, A. und Knoche, M. (2022) Calcium decreases cell wall swelling in sweet cherry fruit. *Scientific reports* 12, 16496